UCLA
UCLA Electronic Theses and Dissertations

Title
Development, anatomy, and function of prefrontal circuits in threat avoidance

Permalink
https://escholarship.org/uc/item/51r566z7

Author
Klune, Cassandra Bernadette Lindsay

Publication Date
2023

Peer reviewed|Thesis/dissertation

eScholarship.org Powered by the California Digital Library
University of California

UNIVERSITY OF CALIFORNIA

Los Angeles

Development, anatomy, and function of prefrontal circuits in threat avoidance

A dissertation submitted in partial satisfaction of the

requirements for the degree Doctor of Philosophy in

Neuroscience

by

Cassandra Bernadette Lindsay Klune

2023

© Copyright by

Cassandra Bernadette Lindsay Klune

2023

ABSTRACT OF THE DISSERTATION

Development, anatomy, and function of prefrontal circuits in threat avoidance

by

Cassandra Bernadette Lindsay Klune

Doctor of Philosophy in Neuroscience

University of California, Los Angeles, 2023

Professor Laura Anne Wilke, Chair

Threat avoidance is a key survival behavior that keeps animals away from harm. However, threat avoidance must be balanced with other behaviors important for survival and well-being, including feeding and social interaction. Excessive avoidance, especially in the absence of threat, is a hallmark symptom of numerous psychiatric disorders including OCD, depression, phobias, and anxiety disorders. Many of these disorders arise early in life. Understanding the neural circuit basis of threat avoidance across development and in adulthood is necessary to understand how these circuits may be perturbed to contribute to psychiatric disease.

Output circuits from the medial prefrontal cortex (mPFC) control both innate and learned threat avoidance behaviors. Two unique features of mPFC – its prolonged development and intricate connectivity – may make it particularly well suited to regulate adaptive responses to a dynamic environment. Compared to other brain regions, mPFC undergoes an extended maturation that lasts into early adulthood. The demands for threat avoidance change with developmental stage and the prolonged maturation of mPFC may support dynamic circuit

changes that contribute to age-specific avoidance strategies. However, we do not understand how the mPFC circuits underlying threat avoidance mature and contribute to behavior in early life. Second, mPFC output circuits are anatomically complex and display a high degree of collateralization. Collateralization of mPFC projections may be a mechanism to precisely coordinate activity in multiple downstream regions to produce behavior, however, complex connectivity patterns have yet to be linked with the behavioral contributions of mPFC circuits.

This thesis elucidates how the circuit maturation and connectivity of mPFC shapes threat avoidance behavior. Using optogenetics, fiber photometry, viral circuit mapping, and slice electrophysiology, this thesis provides convergent evidence that prefrontal projections to the basolateral amygdala and nucleus accumbens change their function throughout early life to shape age-specific avoidance phenotypes. This thesis also reveals the brain wide connectivity patterns of mPFC neurons defined by their projections to the ventral tegmental area, nucleus accumbens, and contralateral mPFC in adult mice. Differential roles of each of these projection classes in learned and innate avoidance were also discovered. Finally, this thesis presents two new user-friendly analysis pipelines to quantify brain wide axonal projections and labelled cell bodies allowing others to continue to probe circuit function together with complex anatomy. The circuits and maturational processes uncovered may be key sites of disruption that lead to psychiatric disease and potential targets for therapeutic intervention.

The dissertation of Cassandra Bernadette Lindsay Klune is approved.

Kate Wassum

Thomas J O'Dell

Weizhe Hong

Laura Anne Wilke, Committee Chair

University of California Los Angeles

2023

Dedicated to my parents,

Barb and Harold Klune

Table of Contents

List of Figures

List of Tables

Acknowledgements

Graduate school has been one of the most enriching and challenging periods of my life. I could not have attained this degree without the support of my mentors, lab mates, family, and friends.

First, I would like to thank my advisor, Dr. Laura DeNardo. I am always inspired by her boundless ambition, rigorous work-ethic, and vibrant energy. Despite the challenges of the last few years, Laura has consistently been a thoughtful and considerate mentor. She has always valued my ideas, encouraged me to take on challenges, and supported my goals. I admire Laura as both the amazing scientist and kindhearted person that she is. The lessons she has taught me will stay with me throughout my career. I would also like to thank the members of my committee, Dr. Kate Wassum, Dr. Weizhe Hong, and Dr. Tom O'Dell. Their expert guidance and thoughtful feedback have been integral to shaping this thesis and myself as a scientist.

I have been fortunate to share the projects in this thesis with many talented collaborators. Thank you to Caitlin Goodpaster for her resourcefulness and unrelenting dedication that made our developmental project flourish. Thank you to Michael Gongwer whose incredible work ethic and creativity helped our circuit mapping project grow in new and exciting ways. I am very grateful for Benita Jin's keen ideas and perspectives that shaped our review article into an insightful piece. I would also like to thank Dr. Zachary Zeidler for his generous assistance and guidance, as well as Christopher Gabriel and Sara Blagburn-Blanco for being kind and supportive lab mates. Rita Chen and Timothy Andrade are both bright undergraduate scientists whose work in our lab, and on the projects in this thesis, are greatly appreciated.

Beyond our lab, I am grateful to many members of UCLA's scientific community who have enriched my time in grad school. Dr. Scott Wilke and the members of the Wilke lab have made our weekly lab meetings valuable and thought provoking. The DeBiase lab has been a wonderful and inspiring group of people to work alongside of. Setting up our lab would have been tremendously more difficult without the generous expertise of members of the Portera-

Cailliau lab. The NSIDP program administration, particularly Jenny Lee and Felix Schweizer, have provided extensive guidance and support throughout every stage of my graduate career. My friends and fellow members of my cohort have been consistent sources and comfort and happiness. I would specifically like to thank Talia Oughourlian and Kwaku Addo-Osafo for all the laughter and encouragement you've given me.

My deepest appreciation goes to my family, whose unwavering love and support has provided continual motivation throughout this journey. Thank you to my parents, Barbara and Harold Klune, who taught me the value of education and instilled within me the confidence to pursue my goals. Their integrity, dedication, and perseverance continually motivate me. Thank you to my brother, Christopher Klune, who inspires me with his earnest dedication to his work and care for those around him. Finally, I would like to thank my best friend and partner, Mitchell Prostebby. His genuine curiosity and excitement for neuroscience reminds me why I fell in love in with science. His kindness and encouragement have kept me afloat over the past 5 years.

Permissions

Chapter 2 is a version of Klune, C. B., Jin, B., & DeNardo, L. A. (2021). Linking mPFC circuit maturation to the developmental regulation of emotional memory and cognitive flexibility. ELife, 10, e64567. https://doi.org/10.7554/eLife.64567

Author Contributions: L.A.D., C.B.K., and B.J., conceptualized the paper. L.A.D., C.B.K., and B.J., wrote and edited the manuscript.

Chapter 3 is in preparation for publication.

Author Contributions: L.A.D., C.B.K., and C.M.G designed the research. C.B.K. and C.M.G performed stereotaxic surgery, behavioral experiements, optogenetics experiemnts and fiber photometry. M.W.G. performed slice electrophysiology, C.B.K., C.M.G, C.G, M.W.G., L.A.D.,

and R.C. performed data analysis. C.B.K., C.M.G., R.C., N.J. and T.A. performed histology. C.B.K., C.M.G. and L.A.D. wrote the manuscript.

Chapter 4 is a version of Gongwer, M. W., Klune, C. B., Couto, J., Jin, B., Enos, A. S., Chen, R., Friedmann, D., & DeNardo, L. A. (2023). Brain-wide projections and differential encoding of prefrontal neuronal classes underlying learned and innate threat avoidance. The Journal of Neuroscience, JN-RM-0697-23. https://doi.org/10.1523/JNEUROSCI.0697-23.2023. *Author Contributions:* C.B.K., M.W.G. and L.A.D. designed the research; C.B.K. performed the stereotaxic AAV injections and PMA fiber photometry; C.B.K. and B.J. performed tissue clearing; C.B.K., M.W.G., and B.J. performed imaging and data analysis; D.F. and M.W.G. wrote DeepTraCE and DeepCOUNT code; J.C. ported the pipeline to python and wrote the jupyter examples; C.B.K., R.C., M.W.G., and A.S.E. performed histology and image analysis, A.S.E. and M.W.G. performed EZM fiber photometry; C.B.K., M.W.G. and L.A.D. wrote the manuscript.

Funding

This work was funded by K01MH116264 (L.A.D.), 1R01MH127214-01A1 (L.A.D.), a Whitehall Foundation Research Grant (L.A.D), a Klingenstein-Simons Foundation Grant (L.A.D.), a NARSAD Young Investigator Award (L.A.D.), a Fay/Frank Seed Grant (L.A.D.), and an NSERC Postgraduate Fellowship (C.B.K.)

Vita

Education

University of California Los Angeles
PhD Candidate, Neuroscience Interdepartmental Ph.D. Program 2018-present

University of Calgary
Bachelor of Science with Honours in Neuroscience, Distinction 2014-2018

Awards and Honors

NSERC Postgraduate Doctoral Scholarship 2020-2023
Graduate Student's Association Presidential Service Award 2021
Brain Research Institute Travel Award 2022,2023
Brain Research Institute Society for Neuroscience Travel Award 2022

Selected Publications

Gongwer, M. W.*, **Klune, C. B.*,** Couto, J., Jin, B., Enos, A. S., Chen, R., Friedmann, D., & DeNardo, L. A. (2023). Brain-wide projections and differential encoding of prefrontal neuronal classes underlying learned and innate threat avoidance. The Journal of Neuroscience, JN-RM-0697-23. https://doi.org/10.1523/JNEUROSCI.0697-23.2023

Klune, C. B.*, Jin, B.*, & DeNardo, L. A. (2021). Linking mPFC circuit maturation to the developmental regulation of emotional memory and cognitive flexibility. ELife, 10, e64567. https://doi.org/10.7554/eLife.64567

Selected Talks

Klune, C. B. Prefrontal-Amygdala Circuit Maturation and its Role in Adaptive Threat Avoidance. The Amygdala Function in Emotion, Cognition and Disease Gordon Research Conference, July 12, 2023, Barcelona, Spain

Klune, C. B. Development of medial prefrontal cortex circuitry and its role in the maturation of avoidance behavior. Integrative Center for Learning and Memory – Young Investigator Lecture Series, June 9, 2023, Los Angeles, California

Klune, C. B. Development of medial prefrontal cortex circuitry and its role in the maturation of avoidance behavior. UCLA Physiology Trainee Seminar Series, April 28, 2022, Los Angeles, California

Klune C. B. Mapping the brain-wide axonal projection patterns of anatomically-defined prefrontal neurons, UCLA Synapse to Circuit Seminar Series, April 8, 2022, Los Angeles, California

Chapter 1: General Introduction

Survival and wellbeing rely on the ability to adaptively respond to threats. Threat avoidance is an evolutionarily conserved response that prevents animals from entering or remaining in threatening situations. However, excessive avoidance is a hallmark symptom of multiple psychiatric disorders including phobias, anxiety disorders, and depression (Cervin et al., 2020; Delgado et al., 2009; Gillan et al., 2014; Ironside et al., 2020; Maner and Schmidt, 2006; Rudaz et al., 2017). As a convergence point of symptomology across numerous mental illnesses, the neural mechanisms underlying avoidance behavior are of critical interest to understand disease pathogenesis. Understanding the circuit mechanisms that control threat avoidance behavior will provide a foundation to understand how they may become disrupted and provide potential targets for therapeutic intervention.

mPFC circuits are critical regulators of threat avoidance behavior (Diehl et al., 2020; Loewke et al., 2021). However, two unique aspects of mPFC circuity have precluded us from a holistic understanding of how mPFC circuit function influences threat avoidance throughout life. First, mPFC undergoes a uniquely protracted period of maturation lasting into early adulthood (Shepard et al., 2017; Du et al., 2018; Bouamrane et al., 2017; Klune et al., 2021). The demands for threat avoidance change with developmental stage as young animals leave parental care and establish independence. However, the developmental trajectories of most mPFC output circuits are unknown and we have almost no data on how circuit maturation shapes behavioral changes throughout early life. Second, mPFC projection neurons innervate many downstream regions and have recently been shown to display extensive collateralization patterns (Gao et al., 2022). We do not understand the full connectivity of mPFC projections that are functionally relevant to avoidance or how collateralization may facilitate top-down control over networks of projection targets. The overarching goal of this thesis is to address these two gaps in knowledge. My research advances our understanding of how mPFC circuitry regulates

avoidance behaviors throughout postnatal development, and how the unique connectivity and function of specific mPFC cell classes support threat avoidance in the adult brain.

Threat avoidance as a survival mechanism

Animals display a variety of behavioral responses to threat. Leading theories in the field predict that the selection of a threat response relies on the imminence of the threat stimulus (Fanselow, 2018). As opposed to escape – the act of fleeing once contacted – threat avoidance prevents contact with a perceived or predicted threat stimulus (Krypotos et al., 2015; LeDoux et al., 2017). Therefore, threat avoidance is conserved across species as a key behavior that supports survival and wellbeing.

To avoid harm endured by trial and error, some avoidance responses are innate. For example, rodents display innate avoidance to bright open spaces which heighten the risk of predation (Costall et al., 1989; Kulesskaya et al., 2014; La-Vu et al., 2020). However, adaptive threat responding must also allow animals to cater behavior to a changing environment. Experience can shape avoidance behavior through associative learning processes (Krypotos et al., 2015). Contexts and cues that have previously been paired with threat can drive avoidance responses (Solomon and Wynne, 1953; Herrnstein, 1969; Moscarello et al., 2013; Bravo-Rivera et al., 2014). Innate avoidance responses are often species-specific, however, across species, animals can acquire threat avoidance responses through learning (Solomon and Wynne, 1953; Herrnstein, 1969; Bolles 1970; Delgado et al., 2009; Yue et al., 2004).

Threat avoidance across the lifespan

The demand for avoidance behavior changes throughout the lifespan. Infants are completely reliant on parental caregivers to protect them from threats. In rodents, infants approach rather than avoid an odor that has been paired with a painful stimulus (Sullivan et al., 1986). This may be due to an association between pain and handling by their mother. Indeed,

infant mice also approach odor paired with a tube of warm water, reminiscent of their mother's presence (Meyer et al., 2016). Other species also display robust attachment to caregivers who inflict pain during infancy (Maestripieri et al., 1999; Stanley, 1962). While a suppression of avoidance to painful stimuli may be beneficial in infancy to ensure proximity to a caregiver, a similar approach would be dangerous in later life. Mice leave the nest of their caregivers around postnatal day (P)21 and must develop individualized strategies to respond to threat. While there is limited evidence of how specific learned avoidance responses change from the juvenile period onward, multiple lines of evidence suggest that age-dependent phenotypes are present.

First, associative threat memory, a component of learned avoidance, is developmentally regulated. In mice, infants begin to form contextual fear memories from P14 onwards, just two days after they open their eyes (Akers et al., 2012). However, in comparison to adult threat memories, these associations are rapidly forgotten and last only a few days (Akers et al., 2012; Guskjolen et al., 2018). By P30, these memories can be retained for weeks (Akers et al., 2012). Variable phenotypes of fear-expression have been reported in adolescence. Patwell et al., (2011) found that expression of contextual fear was dramatically reduced between P29 and P33. However, others have found that P30 mice showed similar levels of freezing to adults (Akers et al., 2012). Adolescent threat responding may be particularly sensitive to genetic and environmental differences that result in the variability seen across labs. Given that associative threat memory is a key component of learned avoidance, this evidence suggests that expression and persistence of learned avoidance behaviors may change over the course of early life and be sensitive to environmental conditions.

The second line of evidence supporting the developmental regulation of learned avoidance is the risky exploration displayed by adolescents across species. In the wild, adolescent animals tend to stray farther from their homes and areas of safety (Hinke et al., 2020; Warkentin et al., 1999). As a result, adolescence is often a period of high mortality and a bottleneck for survival (Overskaug et al., 1999; Cox et al., 2020). In laboratory assays,

adolescent rats show greater exploration of bright and open settings that are typically aversive (Lynn and Brown, 2009). Levels of sensation-seeking, a trait associated with risky behaviors such as drug use, peak in adolescence in humans (Romer and Hennessy, 2007). The opposing nature of risky exploration and threat avoidance, suggests that adolescence may be a period of reduced threat avoidance. This may be an evolutionary mechanism that drives animals to leave parental care and establish independence.

These lines of evidence suggest that forming a holistic understanding of threat avoidance behavior requires careful consideration of developmental stage. Changing environmental circumstances and age-dependent demands shape the level of avoidance that is adaptive in a particular period of life.

Avoidance in psychiatric disease

Avoiding threats often means forgoing other behaviors that are important for survival and wellbeing. Therefore, the potential harm reduction of avoidance behaviors must be balanced with the sacrifice of other opportunities. When avoidance becomes excessive, particularly in the absence of threat or threat predictive stimuli, it can become pathological. Patients with obsessive compulsive disorder (OCD) show exacerbated threat avoidance responses in comparison to healthy controls (Gillan et al, 2014). Depressed patients express more desire to engage in avoidance behaviors than healthy controls, and the extent of avoidance displayed is positively correlated with depression severity (Aldao et al., 2010; Moulds et al., 2007; Dickson and MacLeod, 2006). Perhaps most notably, avoidance patterns are a central feature of anxiety disorders. Broadly, risk avoidance is correlated with trait anxiety (Maner and Schmidt, 2006). More specific avoidance behaviors characterize individual anxiety disorders. For example, avoiding interactions with others is a defining feature of social anxiety disorder while agoraphobia is frequently characterized by avoidance of venturing beyond one's home (Arnaudova et al., 2017). The median age of onset for anxiety disorders is 17 years old with

40% of patients being diagnosed before the age of 14 (Solmi et al., 2022). The median age of onset for all mental disorders is 18. The timing of onset suggests that neuronal perturbations in early life and adolescence may be key contributors to the development of mental illness.

In both anxiety and depression, avoidance as a form of coping has been posited to worsen the severity of other symptoms (Trew, 2011; Arnaudova et al., 2017; Lovibond et al., 2009). Avoidance can prevent individuals from learning safety associations therefore serving to maintain and potentially exacerbate distress related to a stimulus. More broadly, avoidance can keep individuals from experiences that may elevate mood. Therefore, elevated avoidance behavior not only manifests as a symptom of psychiatric illness but may, in some cases, drive the progression of disease.

Rodent models offer many advantages for causal manipulation and detailed study in neuroscience. However, psychiatric diseases are notoriously difficult to model in rodents, with certain symptoms profiles being impossible to induce and measure (Nestler and Hyman, 2013). Rather than attempting to model complex illnesses, it can be valuable to focus on measurable, disease-relevant behaviors that are displayed across species. Threat avoidance is evolutionarily conserved and recruits similar brain regions in both humans and rodents (Bravo-Rivera et al., 2014; 2015; Tottenham and Galvan, 2016). Therefore, the study of threat avoidance can allow us to harness the advantages of rodent models to elucidate the pathogenesis of psychiatric illness. Understanding the neural circuitry underlying avoidance in rodents provides a foundation to understand how similar processes may go awry in patients with psychiatric illnesses.

Modeling Avoidance in a Laboratory Setting

The aversion of rodents to bright open spaces has been used for over a century as a way of assessing innate avoidance. Early studies, characterizing innate rodent behaviors noted the phenomena of thigmotaxis – the avoidance of the center of an open chamber and the

tendency to stay by the walls (Hunter, 1917; Craig, 1919). Over the years, thigmotaxic behavior in the open field assay has become a well-used measure of innate avoidance and anxiety-like behavior (Simon et al., 1994; Lezak et al., 2017). Based on the same innate aversion of bright, open spaces, the elevated plus maze measures time spent in two open arms versus time spent in arms two enclosed arms of equal size which afford shelter and shadows (Pellow, 1986). The elevated zero maze utilizes a similar design, replacing the "plus" shape with a circular design to rid the assay of the difficult to interpret center area (Shepard et al, 1994). In addition to mice showing robust avoidance of the center or open arm portions, entries into these aversive sites are correlated with each other and with increases in corticosterone (Frye et al., 2000; File et al., 1994). Further, time spent in open areas can be modulated by the administration of anxiolytic and anxiogenic drugs suggesting the neural processes mediating innate avoidance in these assays are of interest with respect to psychiatric disease (Pellow, 1986; Shepard et al, 1994; Walf and Frye, 2013).

Conditioned avoidance has been studied in laboratories since the 1930s (Culler and Mettler, 1934; Schlosberg, 1937). Most studies to date have used two-way shuttle avoidance assay to model avoidance in rodents (Mowrer and Lamoreaux, 1946; Moscarello and LeDoux, 2013, Ramirez et al., 2015; Krypotos, 2015). In this assay, rodents are placed in a two-chamber arena and, upon presentation of a tone, must shuttle to the opposite side to avoid a mild shock stimulus. At a random interval, the tone is presented again, and the rodent must shuttle back to the previous side of the box. In this assay, both sides of the chamber are capable of sock administration and the shock is elicited on whichever side of the chamber the animal is on at the presentation of the tone. Therefore, this assay ensures that rodents engage in active avoidance strategy. However, when considered in the context of real-world events, this task has some limitations. There is no "safe-space" in two-way shuttle avoidance. In real-world scenarios, animals often avoid threats in places that they perceive as safe and that are specifically not associated with threat. Further, in most variations of two-way shuttle avoidance, shuttling to the

other side of the box terminates the threat predictive tone. While this may accelerate learning by immediately reinforcing the shuttle response, it is not an accurate representation of the level of control that animals have of their surroundings.

Recent years have seen a rise in the use of platform mediated avoidance (PMA) assays (Bravo-Rivera et al., 2014; 2015; Diehl et al., 2018; 2020; Rodriguez-Romaguera et al., 2016; Rosas-Vidal et al., 2018; Martínez-Rivera et al., 2019). In PMA, a plexiglass platform covers 25% of the shock-grid floor in a standard fear conditioning chamber. Upon presentation of a tone, rodents learn to enter onto the safety platform to avoid a mild foot shock. Unlike two-way avoidance assays, PMA provides the subject with a safe place, and successfully avoiding foot shocks does not terminate the threat-predictive cue (Diehl et al., 2019). These aspects of PMA have been argued to make it more applicable to real-world scenarios involving threat avoidance (Diehl et al., 2019).

Role of mPFC in avoidance behavior

As with many other complex behaviors, the medial prefrontal cortex (mPFC) plays an important role in facilitating avoidance behavior (Moscarello and LeDoux, 2013; Bravo-Rivera et al., 2014; Diehl et al., 2018). In the elevated plus maze, mPFC activity differentiates between time spent in open and closed arms, and inactivation with muscimol increases time spent in open arms (Shah et al., 2004; Adhikari et al., 2011). Using fiber photometry, Loewke et al. (2021) showed that prefrontal projection neurons targeting the dorsal medial striatum (DMS) increase their activity during open arm visits. Optogenetic excitation of these neurons increased time in open arms of an elevated zero maze, indicating a causal role of mPFC-DMS projection neurons in suppressing innate avoidance (Loewke et al., 2021).

mPFC also regulates the expression of learned avoidance, specifically through interactions with the nucleus accumbens (NAc), and the amygdala (Moscarello and LeDoux, 2013; Bravo-Rivera et al., 2014; 2015; Diehl et al., 2018). In learned avoidance paradigms, the

threat is paired with a tone that takes on predictive value. The amygdala mediates associative learning between predictive stimuli and threat (Goosens and Maren, 2001; Maren, 2005; Gründemann and Lüthi; 2015; Grewe et al., 2017). In classical conditioning, this association results in rodents displaying freezing responses to the tone (Goosens and Maren, 2001; Gründemann and Lüthi; 2015). However, in avoidance paradigms the adaptive response is to avoid, not to freeze. mPFC projections to the amygdala are thought to inhibit freezing responses to allow for avoidance behavior (Moscarello and LeDoux, 2013). The NAc receives projections from both the mPFC and BLA (Ding et al., 2001; Ramirez et al., 2015; Diehl et al., 2020). Evidence suggests that these pathways work antagonistically to one another with BLA→NAc neurons promoting avoidance and mPFC→NAc neuron activity reducing avoidance (Ramirez et al., 2015; Diehl et al., 2020). mPFC→NAc neurons have been hypothesized to reduce levels of threat avoidance by synapsing onto inhibitory interneurons in NAc that dampen the activity of NAc output neurons (Diehl et al., 2019). NAc output is thought to gate the execution of avoidance behavior through connections with the substantia nigra pars reticulata (Hormigo et al., 2016). Thus, mPFC exerts top-down control over the BLA and NAc to bias behavior towards avoidance when it is appropriate. The NAc appears to serve as an important integration center of mPFC and BLA signals to gate the execution of avoidance responses. Importantly, there is evidence that mPFC, NAc, and BLA are also modulators of active avoidance in humans (Delgado et al., 2009; Boeke et al., 2018).

Organization of mPFC Circuits

The ability of mPFC to coordinate so many complex functions is a result of its vast and physically complex circuitry. mPFC sends projections to various downstream targets including cortical association areas, striatum, midline thalamus, ventral tegmental area (VTA), claustrum, amygdala, hypothalamus, and midbrain (Gabbott et al. 2005; Vertes, 2004; DeNardo et al 2015, 2019). Similarly, the mPFC receives distributed inputs from other cortical areas, thalamus,

neuromodulatory hubs such as the VTA and locus coeruleus, ventral hippocampus, and amygdala, among other regions (Hoover & Vertes, 2007; Riga et al., 2014). This vast interconnectedness allows mPFC to coordinate many higher order cognitive processes. Inputs from sensory cortices can be integrated with learned and emotional information from limbic centers and and biased in a state-dependent manner by neuromodulator dynamics. Then, mPFC can act through its output pathways to guide activity in downstream regions to promote adaptive behavioral responses.

mPFC controls complex behaviors that involve the coordinated activity of multiple brain regions (Herry and Johansen, 2014; Tovote et al., 2015; Xu et al, 2021; Otis et al., 2017). However, most investigations of the role of prefrontal circuits in behavior have examined one pathway at a time (Riga et al., 2014). The recent publication of a single-neuron projectome of prefrontal cortex has illuminated the remarkable complexity of prefrontal projection neurons (Gao et al., 2022). Almost all identified classes of prefrontal projection neurons send axon collaterals to 5–10 target regions. Collateralization has been proposed as an understudied mechanism through which synchronous or asynchronous patterns of brain activity emerge and contribute to cognitive states (Rockland, 2018). Studies which link connectivity patterns with the functional roles of projection neurons are needed to fully understand how mPFC controls downstream regions on a network basis to produce behavior.

Development of mPFC

Like other brain regions, mPFC development begins during embryogenesis with morphogen gradients controlling the expression of transcription factors that create regional boundaries, direct neuronal migration, and facilitate cell-type specification (Schubert et al., 2015). While mPFC circuits begin assembly during embryogenesis, maturation and refinement of mPFC circuits extend into adulthood. Interneuron maturation and assembly of local micro-circuitry extends from the early postnatal period, through adolescence and into early adulthood in rodents

(Shepard et al., 2017; Du et al., 2018; Bouamrane et al., 2017). Afferent neuromodulatory axons also continue to innervate mPFC into early adulthood (Niwa et al., 2010; Reynolds et al., 2018). These phenomena contribute to dynamic changes in spine density throughout adolescence in mPFC (Kolb et al., 2012; Shapiro et al., 2017; Kroon et al., 2019). The continued ontogenesis of mPFC during into early adulthood allow these circuits to be heavily influenced by early life experience (Kolb et al., 2012).

Relative to local synaptic development within mPFC, far less is known about the neurodevelopmental trajectory of mPFC long-range connectivity. A detailed study focusing of mPFC→BLA projection neurons showed that mPFC axons innervate the BLA around P10, axon density increases until P30, and then pruning and refinement occur into adulthood (Arruda-Carvalho et al., 2017). This suggests that mPFC projection neurons follow suit in the prolonged maturation of local mPFC circuitry. However, aside from mPFC→BLA neurons, almost nothing is known about the synaptic development of mPFC long-range projections. Approaching mPFC development through a circuit specific lens is important as particular classes of mPFC output neurons have been linked to individual behaviors (Riga et al., 2014; Otis et al., 2017; Diehl et al., 2020). Thus, understanding how mPFC-dependent behaviors emerge throughout the developmental period, and how they may be disrupted necessitates a circuit-specific understanding of mPFC development.

While the ongoing maturation and refinement of mPFC circuitry allows sufficient time for environmental factors to shape emergence of complex, adaptive behaviors, this prolonged period renders mPFC circuitry uniquely vulnerable to disruption. Even in comparison to other cortical areas, whose circuit assembly is experience dependent, mPFC development is extends further into early life (Petanjek et al., 2011; Drzeweicki et al., 2016; Elston et al., 2009; Kolb et al., 2012). This may account for why dysfunction of mPFC and its circuitry has been observed in a host of neuropsychiatric and neurodevelopmental disorders including depression, anxiety, schizophrenia and autism (Kolb et al., 2012; Pirone et al., 2018; Hare and Duman, 2020; Ironside et al., 2020;

Knowland and Lim, 2018; Luthi and Luscher, 2014; Park et al., 2016). Defining the critical developmental milestones in mPFC circuit assembly will allow us to define periods wherein circuit disruption may lead to the pathogenies of psychiatric and neurodevelopmental diseases.

Chapter 2: Linking mPFC circuit maturation to the developmental regulation of emotional memory and cognitive flexibility

ABSTRACT

The medial prefrontal cortex (mPFC) and its abundant connections with other brain regions play key roles in memory, cognition, decision making, social behaviors, and mood. Dysfunction in mPFC is implicated in psychiatric disorders in which these behaviors go awry. The prolonged maturation of mPFC likely enables complex behaviors to emerge, but also increases their vulnerability to disruption. Many foundational studies have characterized either mPFC synaptic or behavioral development without establishing connections between them. Here, we review this rich body of literature, aligning major events in mPFC development with the maturation of complex behaviors. We focus on emotional memory and cognitive flexibility, and highlight new work linking mPFC circuit disruption to alterations of these behaviors in disease models. We advance new hypotheses about the causal connections between mPFC synaptic development and behavioral maturation and propose research strategies to establish an integrated understanding of neural architecture and behavioral repertoires.

mPFC circuits: prolonged maturation and targets for early intervention

In the rodent, the medial prefrontal cortex (mPFC) comprises the anterior cingulate cortex (ACC), the prelimbic cortex (PL), and the infralimbic cortex (IL), which each have distinct connectivity and functional properties. As a whole, they are densely interconnected with other cortical association areas, the limbic system, midline thalamic nuclei, and an array of midbrain and brainstem nuclei with unique behavioral functions. Through these diverse inputs and outputs, mPFC plays a key role in decision making, memory, social interactions, mood, and cognition (Kolb and Nonneman, 1978; Kolb et al., 1974; Nonneman et al., 1974). In this review, we focus on cognitive flexibility and emotional learning and memory in both the aversive and

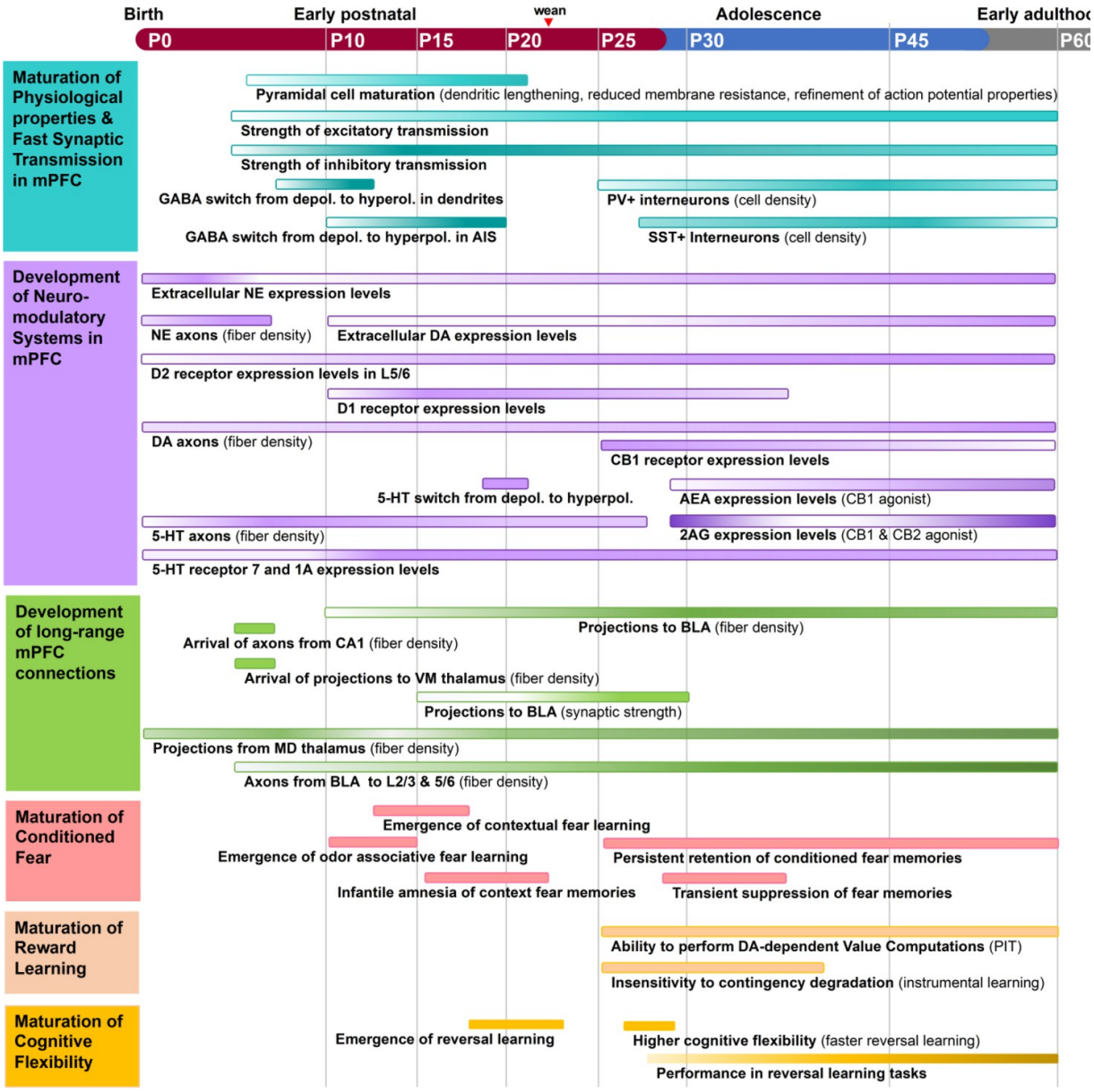

Figure 2-1. Timeline of major events during rodent medial prefrontal cortex (mPFC) development. The structural and functional organization of mPFC circuitry is largely established in early postnatal development and then refines into early adulthood. Adolescence is marked by enhanced bidirectional innervation of mPFC, amygdala, and neuromodulatory centers. Inhibitory neurotransmission increases from P15–P60, with major changes in the excitatory/inhibitory ratio of synaptic transmission in adolescence. Aspects of mPFC circuit development align with the maturation of cognitive behaviors. The ability to perform reversal learning and contextual fear learning emerges just prior to adolescence and remains highly malleable until at least mid-adolescence. Each process is represented as a colored bar, with the gradient of color intensity (low to high) marking initiation, peak, and decline of the process where applicable. Of note, bars representing the magnitude of axonal innervation usually begin at the earliest point reported in the literature, but do not remove the possibility of earlier innervation.

appetitive domains. Like many mPFC-dependent functions, the encoding and expression of

emotional memories, as well as cognitive flexibility, are developmentally regulated, emerging, and maturing during early life and adolescence when the prefrontal cortex is still developing (Kalsbeek et al., 1988; Van Eden and Uylings, 1985; Lewis, 1997; Kolb et al., 2012).

From birth until early adulthood, mPFC cells and circuits undergo changes in their physiological properties and the strength of connectivity with distant brain regions including limbic and neuromodulatory centers (Kolb et al., 2012; Figure 1). This prolonged period of development may be necessary because establishing complex behaviors requires an extended interaction with the environment. However, it opens a long window during which mPFC is vulnerable to disruption. Indeed, numerous mPFC-dependent behaviors are altered in neuropsychiatric disorders that emerge during childhood and adolescence including anxiety disorders, impulse control disorders, depression, schizophrenia, and autism spectrum disorder (ASD) (Schubert et al., 2015). Although mPFC dysfunction is strongly implicated in these diseases, we are only beginning to understand the mechanisms that drive the milestones in mPFC neurodevelopment and support the maturation of adaptive behaviors.

Below we discuss converging cross-species evidence from genetic, neuroanatomical, and neurophysiological studies that reveal continuous remodeling of mPFC cells, synapses, and circuits throughout healthy development, with dramatic changes occurring from the end of the juvenile period through adolescence. We focus on the rodent brain because it is a genetically tractable system that can establish causal links between circuits and behavior. We highlight new research, presenting it chronologically according to rodent development. In the juvenile period, mPFC neurons undergo increases in excitability and synaptic strengthening while long-range connections form and oscillatory rhythms emerge. We postulate that these changes may underlie developmental changes in the ability to form long-term fear memories. In adolescence, we focus on the maturation of inhibitory and neuromodulatory circuits. During adolescence, dramatic increases in mPFC synaptic inhibition align with behavioral changes in conditioned fear, reward learning, and reversal learning. At the same time, the staggered maturation of the

monoamine and endocannabinoid (EC) systems shapes mPFC development in ways we are just beginning to understand. We consider how these processes may be causally related. New research on key disease-relevant genes underscores mPFC inhibitory microcircuits, neuromodulatory systems, and long-range connectivity as some of the most vulnerable elements of developing mPFC circuits. This new work highlights an urgent need to refine our understanding of the mechanisms governing mPFC circuit assembly and to establish causal links between the maturation of mPFC circuits and behavior.

We define postnatal day (P)0–P27 as the juvenile period, P28–P48 as adolescence, and P49–P60 as young adulthood. Each period is marked by milestones in behaviors, sexual maturity, and the structure and function of mPFC cells and circuits (Callaghan et al., 2019Piekarski et al., 2017a; Agoglia et al., 2017; Brust et al., 2015). Others have defined the adolescent period in rat as P28–P42 based on behaviors such as increased risk-taking and social play, inclusion of peak growth spurts, and the emergence from the parental nest in the wild (Spear, 2000). Still, this age range is noted as conservative and its margins can significantly vary per individual and sex. For example, female rats become sexually mature between P32– and P34, but male rats typically mature much later at P45–P48 (Lewis et al., 2002). Studies on fear learning, addiction, reward, and social behaviors define adolescence from as young as P28 to as old as P60, though they center on the range of P28–P48 (Hefner and Holmes, 2007; Adriani et al., 2004; Simon and Moghaddam, 2015; Bell, 2018). Adulthood is generally considered to begin between P60 and P70 in rats (McCutcheon et al., 2009). We integrated this literature to establish our definitions for rats and mice.

By aligning key events during mPFC development with transition points during the maturation of complex behaviors, this review highlights missing links between genes, circuits, and behaviors. We propose that the maturation of the component parts of mPFC circuitry subserves the ontogeny of complex behaviors, with the behavioral functions of mPFC updating during transitions between critical windows of development. We put forth novel hypotheses that

can be tested by using cutting-edge viral-genetic tools to link circuit-level and behavioral changes in the developing brain. New research that addresses these questions could ultimately pinpoint developmental vulnerabilities in mPFC circuits that give rise to pathological states.

The juvenile period: P0–P27

From birth until the week after weaning (P27), neurons in the rodent mPFC undergo a series of remarkable anatomical and physiological transformations while long-range projections establish their connectivity with distant targets. Patterns of oscillatory activity, which can indicate the coordinated activity of mPFC with distal brain regions and can facilitate long-range information transfer, begin to appear. In this section, we align these milestones with evidence that mPFC becomes required for the expression of conditioned fear at the end of the juvenile period. We propose that the juvenile development of mPFC's long-range connections, particularly those with the basolateral amygdala (BLA), is necessary for mPFC's ability to regulate conditioned fear. Furthermore, the immaturity of mPFC and its connections may contribute to the rapid forgetting of contextual fear memories that is observed prior to P24. Reward learning studies in juvenile rodents are scarce, likely because of challenges related to food restriction and operant training in young animals. As a result, this section will focus on how the development of mPFC in the juvenile period facilitates fear learning and memory.

During early postnatal development, pyramidal cells within the mPFC show morphological and functional changes characteristic of synapse development and maturation. During the first month of life, pyramidal cells in layer (L)3 and L5 in the mouse mPFC undergo dendritic lengthening and increases in spine density (Kroon et al., 2019). The pyramidal cell growth in mPFC is accompanied by increases in the speed and amplitude of action potentials and decreased input resistance consistent with increases in ion channel density (Kroon et al., 2019). Between P17 and P24, markers of excitatory and inhibitory synapse maturation significantly increase in rat mPFC (Jia et al., 2018). In general, juvenile (P24–P28) pyramidal

neurons in mPFC of mice have more dendritic spines and show more spine turnover than in adults (P64–P68) (Johnson et al., 2016). Thus, juvenile development is characterized by a robust period of synaptogenesis as well as synaptic pruning and refinement (Figure 1). For an in-depth review about changes in dendritic spines and synapse numbers during the juvenile period and adolescence, see Delevich et al., 2018.

During the first two postnatal weeks, mPFC neurons ramp up their spontaneous firing rates significantly (Brockmann et al., 2011). At P17, rats display significantly higher levels of the immediate early genes (IEG) *Arc*, *c-Fos,* and *Zif268* compared to P24 (Jia et al., 2018). IEGs are expressed rapidly in response to cellular events such as depolarization and are often used as markers of neuronal activity (Minatohara et al., 2015). In adults, basal levels of expression are low but IEGs are transiently induced in response to external stimuli (Minatohara et al., 2015). Thus, the increased IEG expression in early life may reflect immature regulatory mechanisms that eventually control neuronal activity in the adult brain including local inhibition and neuromodulation.

Throughout development, there is a gradual yet specific transition in the ratio of excitatory to inhibitory synaptic inputs per cortical layer. This layer specificity is already evident within the first postnatal month. By the second postnatal week, L3 pyramidal neurons exhibit more excitatory than inhibitory spontaneous synaptic events while L5 pyramidal neurons exhibit roughly equal amounts of each (Kroon et al., 2019). While these laminar differences persist until P30, it is not known to what extent they remain in adulthood. Given that mPFC layers have unique inputs and outputs (Gabbott et al., 2005; DeNardo et al., 2015) and display differential receptor expression (Radnikow and Feldmeyer, 2018), layer-specific differences may indeed persist into adulthood. Such spatiotemporal differences could ultimately establish discrete subcircuits that permit the mPFC to partake in several complex behaviors in a multifaceted manner. Further studies need to be done to elucidate the mechanisms of local mPFC circuit assembly in development.

In addition, oscillatory rhythms, which are critical for precise information flow between regions, begin to emerge in the mPFC as early as the first postnatal week. As early as P3, the rodent mPFC exhibits intermittent spindle-shaped field oscillations that are slower (mostly theta frequency), smaller, and less frequent than their counterparts in sensory cortices (Brockmann et al., 2011). By P5, short periods of low gamma frequency oscillation emerge superimposed on top of these spindles (Brockmann et al., 2011). Around P10, continuous oscillations emerge with theta as their dominant frequency. These changes occur along a slower developmental trajectory than in sensory cortices. Theta oscillations are dominant in mPFC-hippocampal communications in the adult brain, and mPFC oscillatory activities show strong coherence with

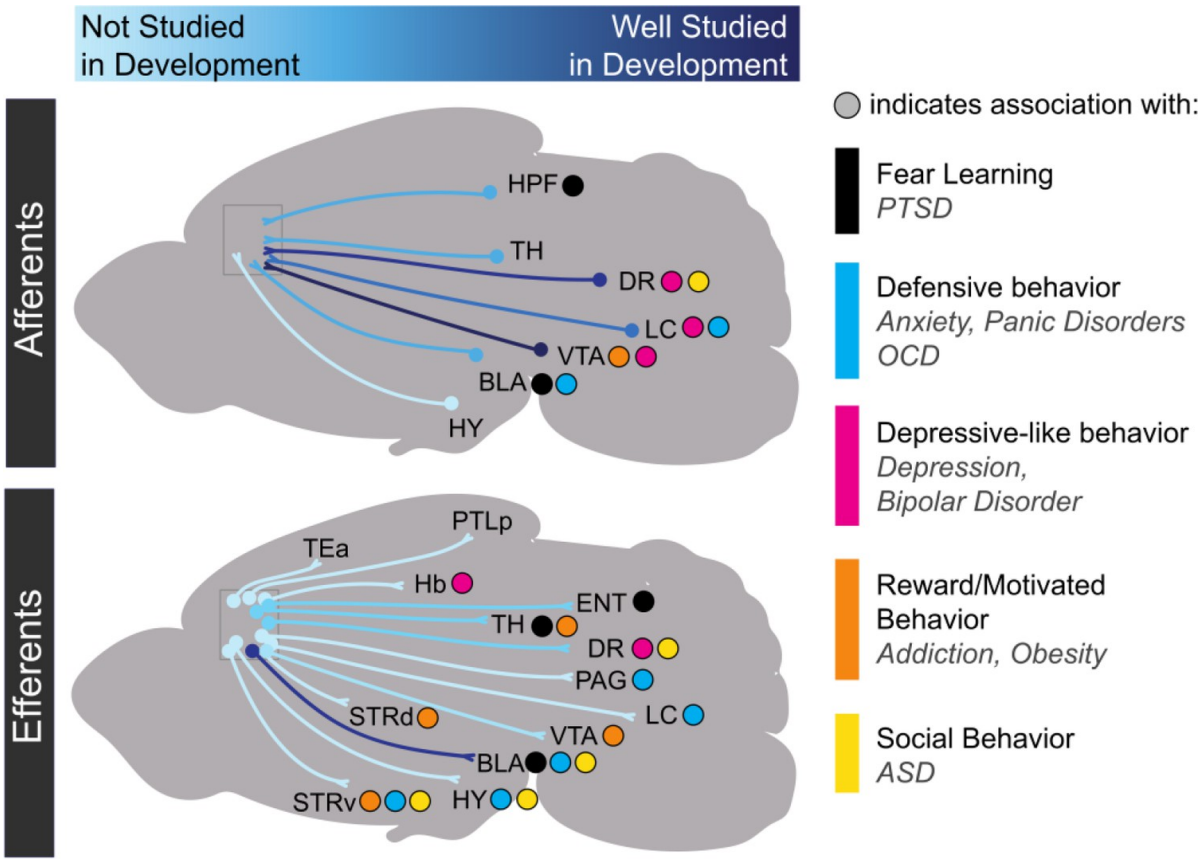

Figure 2-2. Progress in research on the development of medial prefrontal cortex long-range connectivity. Light blue indicates that a particular projection has not been studied in development while dark blue indicates that it has been relatively well-studied. Dots indicate behavioral repertoires and diseases associated with particular connections. HPF: hippocampal formation; TH: thalamus; DR: dorsal raphe nucleus; VTA: ventral tegmental area; LC: locus coeruleus; BLA: basolateral amygdala; HY: hypothalamus; TEa: temporal association area; PTLp: posterior parietal association area; Hb: habenula; ENT: entorhinal cortex; PAG: periaqueductal gray; STRd: dorsal striatum; STRv: ventral striatum.

hippocampal theta even in the first postnatal weeks. Interestingly, Granger causality analyses revealed that the hippocampus was a stronger driver of mPFC activity compared to vice versa, but only in the youngest animals studied (P6–P9) (Brockmann et al., 2011). This suggests that initially the hippocampus entrains network's activity in mPFC and that strengthening of descending influence from the mPFC to the hippocampus occurs later. In both humans and rodents, prefrontal theta is important in memory processes including working memory, fear memory, and reward memory (Backus et al., 2016; Lesting et al., 2013; Courtin et al., 2014; Hyman, 2010; Nishida et al., 2009).

Long-range synaptic connections, which support oscillatory rhythms in mPFC, form and strengthen throughout the early postnatal period. By P7, mPFC axons begin to innervate ventromedial (VM) thalamus (Hartung et al., 2016). mPFC axons begin to innervate the BLA around P10 and continue to increase in density until P30 (Arruda-Carvalho et al., 2017). mPFC sends projections to the lateral entorhinal cortex after P7 (Hartung et al., 2016). Afferent axons targeting mPFC arrive along a similar time course. By P16, amygdalar axons have begun to innervate L2 and L5 of mPFC in the PL and IL subregions (Cunningham et al., 2002). By P7, axons from the hippocampus, VM thalamus, and lateral entorhinal cortex have also reached PL where they play a critical role in the development of oscillatory activity (Hartung et al., 2016). Axons from mediodorsal (MD) thalamus are present by P1, decrease their density at P13, and then increase innervation into adulthood (Ferguson and Gao, 2014). Still, most studies of synaptic connectivity in developing mPFC long-range circuits have been purely anatomical or are lacking altogether. As such, there are a tremendous number of future directions in which researchers can examine the developmental time course and mechanisms of synapse formation between mPFC and long-range targets (Figure 2).

mPFC connections with limbic centers and thalamic nuclei play key roles in a number of adaptive, disease-relevant behaviors including the expression of conditioned fear. It is thus likely that synaptic maturation in these pathways is necessary for the maturation of these

behavioral functions. Changes in mPFC long-range connectivity with the BLA, which is essential for the learning and retrieval of emotional memories (LeDoux, 2009), may play a key role in the developmental regulation of long-lasting fear memories. Like humans, rodents exhibit infantile amnesia, meaning that memories formed early in life are short lasting, while those formed later in life persist (Ramsaran et al., 2019). This phenomenon has been modeled in rodents with contextual fear conditioning (CFC) (Akers et al., 2012; Akers et al., 2014) and inhibitory

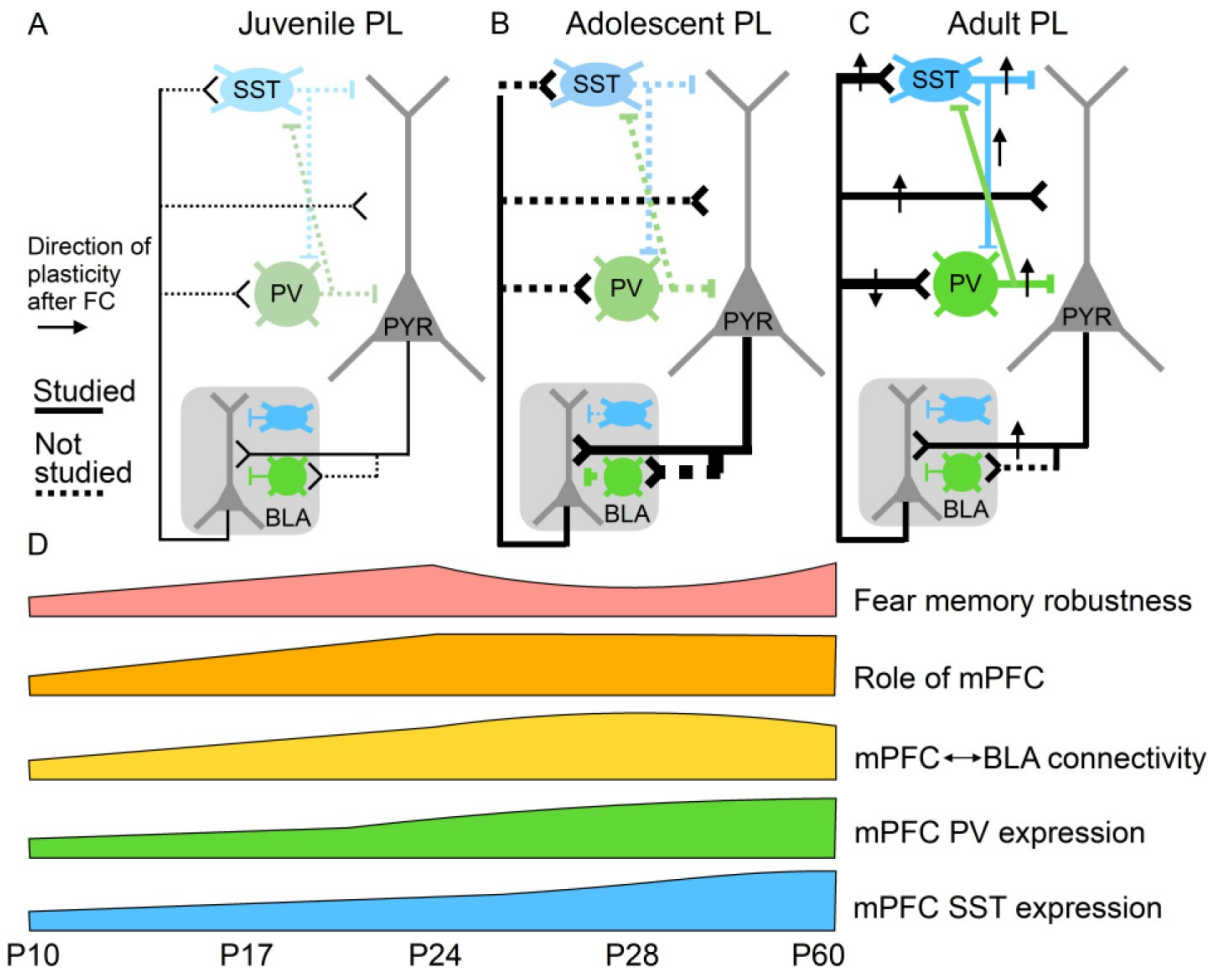

Figure 2-3. Potential relationships between prelimbic cortex-basolateral amygdala (PL–BLA) circuit assembly and the development of persistent fearful memories. (A) During juvenile period, weak connections between PL and BLA may contribute to infantile amnesia. (B) During adolescence, BLA axons continue to innervate PL, and there is a major increase in feed-forward inhibition in the PL projection to the BLA. In addition, parvalbumin-positive and somatostatin inhibitory interneurons, which are known to receive direct synaptic input from BLA, undergo physiological changes. Changes in inhibitory dynamics may contribute to the temporary suppression of fearful memories during adolescence. (C) In the adult, when fearful memories are robust and long-lasting, PL–BLA circuitry has stabilized in its mature form, with a slight refinement in the strength of the descending projection from PL to BLA, and the ascending projection from BLA to PL exhibiting stronger connections onto local interneurons than onto pyramidal cells.

avoidance learning (IA) (Travaglia et al., 2016). In both tasks, rodents trained before the third postnatal week undergo rapid forgetting of learned fearful associations within a week. In contrast, rodents trained in the fourth postnatal week exhibit lasting memories of fearful associations (Akers et al., 2012; Akers et al., 2014; Travaglia et al., 2016). Although the causal role of the mPFC has not been explored in depth during CFC and IA in development, there is evidence that the expression of cued fear prior to P23 can occur independently of mPFC signaling (Li et al., 2012). P24 thus seems to be a turning point in the synaptic development of mPFC connections with the BLA, in the involvement of mPFC in associative fear memories, and in the development of persistent fearful memories, suggesting that these processes may be causally linked (Figure 3).

Importantly, in neuropsychiatric disorders, environmental disruptions and genetic mutations occurring in development may disrupt the early stages of wiring in mPFC inhibitory microcircuits and long-range connectivity. There is a rich body of literature demonstrating that early experience shapes mPFC cells and circuits and the behaviors that rely on them. These studies have been reviewed extensively elsewhere (Kolb et al., 2012; McEwen and Morrison, 2013; Nussenbaum and Hartley, 2019). There remain many open questions about the developmental time course and molecular mechanisms that control mPFC circuit assembly at juvenile stages, and the maturation of mPFC-dependent behaviors during the juvenile period is just beginning to be understood. Establishing links between neural and behavioral processes early in development will ultimately inform our understanding of early stages of disease progression, allowing for development of preventative interventions. Later, we discuss how mutations in disease risk genes cause convergent phenotypes in mPFC inhibitory circuits and long-range connectivity and regulate the organization of neuromodulatory systems, underscoring these circuit elements as some of the most vulnerable during disease progression. In the concluding paragraphs, we discuss how new studies can bridge the gaps between circuit maturation and juvenile behaviors using viral-genetic approaches.

The adolescent period: P28–P48

Adolescence is a key period of maturation for fear and reward learning-related behaviors and cognitive flexibility in which animals employ unique behavioral strategies compared to their adult counterparts. Both human and rodent adolescents display heightened novelty-seeking and risk-taking that can broaden the repertoire of neural and behavioral states and, in doing so, assist individuals as they transition to independence from parental caretakers (Spear, 2000). Throughout the adolescent period, rodents gain the ability to form long-term fear memories, begin to display operant goal-directed behaviors, and improve their performance in tasks that require cognitive flexibility. In this section, we focus on three key aspects of development that likely underlie the maturation of these behaviors: (1) the development of inhibitory neurotransmission in mPFC, (2) the development of the monoamine neuromodulatory systems in mPFC, and (3) the development of the EC system in mPFC. Major developmental milestones in each of these areas are discussed and aligned with behavioral changes, while the lack of causal links and gaps in mechanistic understanding is highlighted.

Development of inhibitory neurotransmission

mPFC inhibitory interneurons undergo robust developmental changes in the adolescent period and are critical for the encoding and expression of fear memories in adulthood. During adolescence, the maturation of inhibitory circuits in mPFC may thus drive changes in fear memory expression. Here, we propose that changes in the number of parvalbumin-positive (PV+) and somatostatin-positive (SST+) cells during adolescence represent changing circuit dynamics that are responsible for the suppression of fear expression between P29 and P35. Further, the sex differences and pubertal influence over PV neuron development may underlie the increased fear of generalization displayed specifically in males (Figure 3 and Figure 4).

Throughout adolescence, inhibitory neurotransmission in mPFC becomes more prominent as inhibitory interneurons develop, assemble into local microcircuits, and refine the dynamics of pyramidal cell activity. After P15, the balance of excitatory to inhibitory inputs onto

pyramidal neurons progresses towards greater inhibition (Bouamrane et al., 2016). This coincides with maturation of all the major inhibitory interneuron groups within mPFC including PV, SST, and calretinin (CR) neurons. These changes in inhibition may explain reductions in the basal expression of IEGs between P25 and adulthood (Jia et al., 2018).

Interestingly, PV development differs between the sexes in certain species. In mice, only males show significant increases in PV+ cell density from postnatal weeks 4 to 6 (Du et al., 2018). In rats, both sexes show increased PV+ cell density from P20 to P40 (Holland et al., 2014). Nonetheless, sex is thought to be an important factor in the development of PV neurons in mPFC. Indeed, manipulations that disrupt PV neuron development have sex-specific effects.

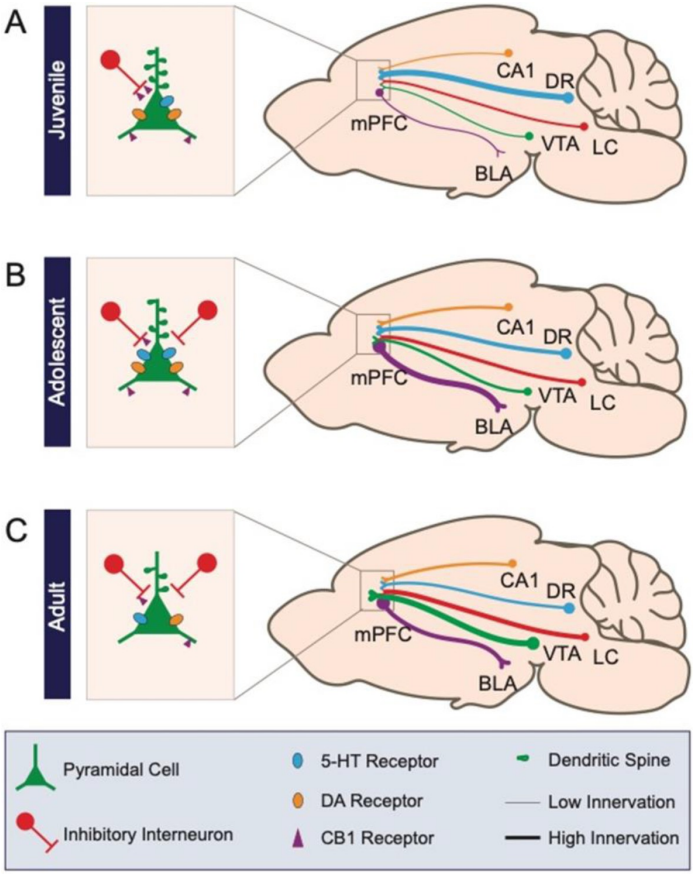

Figure 2-4. Schematic of prefrontal cellular and circuit changes throughout development. (A) The juvenile period is characterized by low-density anatomical connections and elevated spine density. (B) During adolescence, long-range connectivity strengthens along with local inhibitory circuits in medial prefrontal cortex. (C) In the adult, aspects of circuitry refine, including the density of dendritic spines and neuromodulatory receptors. Long-range axonal innervation density continues to increase between some regions. Numbers CA1: CA1 region of the hippocampus; DR: dorsal raphe nucleus; VTA: ventral tegmental area; LC: locus coeruleus; BLA: basolateral amygdala.

Reducing the levels of brain-derived neurotrophic factor decreases PV protein expression specifically in males (Du et al., 2018). Female rats exposed to early life stress show decreased PV levels and social deficits earlier than male rats (Holland et al., 2014). Maternal separation also altered the perineuronal nets of PV interneurons in mPFC in a sex-dependent manner (Gildawie et al., 2020). These sex differences are particularly important given that PV+ interneuron numbers (or PV expression) are reduced in neurodevelopmental disorders including ASD, which has a greater preponderance in males (Rapanelli et al., 2017).

These sex-specific findings are also consistent with evidence that pubertal onset and hormone regulation are important influential factors in mPFC interneuron development. Prepubertal gonadectomy in female mice prevents the peri-pubertal increase in inhibitory neurotransmission in the ACC (Piekarski et al., 2017b). Further prepubertal treatment with estradiol and progesterone advanced puberty and inhibitory neurotransmission development (Piekarski et al., 2017b). Together, these studies indicate that sex, pubertal onset, and hormone regulation are important determinants of mPFC development of inhibitory neurotransmission and circuitry.

Despite this, PV expression increases over adolescence in both male and female mice (Du et al., 2018; Caballero et al., 2014). PV interneurons in the cortex are known for their characteristic fast spiking, making them critical modulators of microcircuit function through feed-forward and feed-back inhibition (Hu et al., 2014). PV, a calcium-binding protein, modulates firing rate by regulating intracellular calcium concentrations (Hu et al., 2014). The adolescent increase in PV is consistent with evidence that PV interneurons do not develop their fast-spiking properties in mice until after weaning (Miyamae et al., 2017). If the increase in PV+ expression in adolescence is disrupted, deficits in mPFC gamma-amino butyric acid (GABA)-ergic neurotransmission last into adulthood (Caballero et al., 2020). This defines the upregulation of PV protein in mPFC during adolescence as an important factor that sculpts the local circuit dynamics with lasting effects.

Other classes of interneurons also undergo major developmental changes during adolescence. In contrast to PV, CR, another calcium binding protein that marks a class of non-fast-spiking interneurons, shows decreasing expression throughout adolescence (Du et al., 2018; Caballero et al., 2014). SST protein levels increase over adolescence in females (Du et al., 2018). In males, protein levels stay the same but the number of SST-expressing cells undergoes developmental changes (Du et al., 2018). Together, these findings show that both number of mPFC interneurons expressing PV, SST, or CR and their functional properties change robustly during adolescence albeit with distinct patterns (Figure 1 and Figure 4).

Physiological changes during the development of pyramidal cells are also a critical factor in the maturation of GABAergic transmission. Early in development, intracellular chloride concentration is high such that GABAA receptor activation is initially depolarizing (Rinetti-Vargas et al., 2017). As chloride concentration decreases with age, GABA switches to having a hyperpolarizing effect (Rinetti-Vargas et al., 2017). In prefrontal pyramidal neurons, the time course during which GABAA activation becomes hyperpolarizing differs between the dendrites and the axon initial segment (AIS) (Rinetti-Vargas et al., 2017). In dendrites, the switch to hyperpolarization occurs around P10. In the AIS, however, the timing of this switch is prolonged into adolescence (Rinetti-Vargas et al., 2017). The differential effect of GABAA activation contributes to the distinct developmental profiles of inhibitory circuits as specific classes of GABAergic cells target particular subcellular compartments of pyramidal cells. For example, chandelier cells, a subtype of PV interneurons, synapse specifically onto the AIS where they can control action potential generation and potentially synchronize the output of nearby cells (Somogyi et al., 1982). Thus, different interneuron types are able to mature their functional connections with mPFC pyramidal cells along distinct timelines. Further examination of the distinct trajectories along which inhibitory microcircuits develop is needed.

The differing developmental patterns of these interneuron classes are pertinent in understanding the maturation of mPFC-dependent behaviors. Specific interneuron classes play

distinct roles in modulating behavior, particularly learned fear, which is developmentally regulated. For example, phasic inhibition of prefrontal PV interneurons is required for the expression of conditioned fear. Through PV neuron-mediated inhibition, prefrontal projection neurons are disinhibited to facilitate fear expression behavior (Courtin et al., 2014). Plasticity in mPFC SST neurons is essential to encode fear memories, and, through synapses onto PV interneurons, mPFC SST neurons modulate the behavioral expression of conditioned fear (Cummings and Clem, 2020; Figure 3).

The regulatory roles of mPFC interneurons in facilitating fear encoding and expression suggest that the maturation of these neurons is a key event in the developmental regulation of conditioned fear. Interestingly, there is evidence that contextual fear memories are temporarily suppressed between P29 and P35. Mice trained at P29 could not express conditioned fear 24 hr later, but did express conditioned fear 13 days later (Pattwell et al., 2011). This suggests that during early adolescence fear encoding remains intact, but fear expression is inhibited. Given that both PV and SST interneurons within mPFC are necessary for fear expression in the adult (Courtin et al., 2014; Cummings and Clem, 2020), the dynamic changes in protein level, cell morphology, and cell density that occur in these interneuron populations through early adolescence may underlie developmental changes in fear memory retrieval. These changes in interneuron populations are likely to interact with developing long-range connections from key regions including the BLA to influence fear memory retrieval. While strengthening of bidirectional connectivity between mPFC and BLA from P10 to P24 may support the ability of rodents to form persistent fearful memories after weaning, dramatic strengthening of inhibitory transmission in mPFC-BLA circuitry may temporarily disrupt fear memory retrieval in adolescence (Figure 3).

The sex differences observed in PV interneuron development may contribute to sex differences in CFC and fear generalization that emerge during development. Males display greater fear generalization to a novel context following CFC depending on the developmental

stage (Colon et al., 2018). This phenotype emerges at P37 for generalization displayed 1 day after training and P33 for generalization displayed 2 weeks after training (Colon et al., 2018). In adults, male rodents have been reported to display greater freezing following CFC than females (Wiltgen et al., 2001; Maren et al., 1994). While this increased freezing has not been reported at adolescent timepoints, linear regression analyses of CFC from P24 to P60 suggest that males display an upward trend of fear expression with age while females display a downward trend (Colon et al., 2018). This suggests that the sex differences observed in adulthood with regards to contextual fear expression may slowly develop through adolescence. These phenotypes may result from the increased PV+ cell density observed throughout adolescence in males but not females (Du et al., 2018).

The development of interneuron populations and inhibitory neurotransmission may also be a key event in the development of cognitively guided behaviors such as reversal learning. In reversal learning tasks, rodents must update their response behaviors when the rules required to receive a food reward are changed. Thus, this behavior relies on persistent motivation for reward, the ability to encode reward memories, and cognitive flexibility. Reversal learning is highly dependent on the orbitofrontal cortex (Groman et al., 2019), and while some reversal tasks have been shown to be insensitive to mPFC inactivation (Floresco et al., 2008; Bissonette et al., 2008), others have resulted in deficits (Kosaki and Watanabe, 2012; Li and Shao, 1998). It has been suggested that mPFC may be important for reversal learning tasks that require greater attentional processes (e.g., difficult discriminanda, visuospatial components) (Bussey et al., 1997; Izquierdo et al., 2017).

The ability of rodents to succeed in reversal learning tasks is developmentally regulated. Juvenile rodents (P26–P27) have been shown to perform well on a four-choice discrimination reversal learning task, learning faster than adults. The performance of both juveniles and adults was reduced following lesions to the dorsomedial frontal cortex (i.e., ACC) (Johnson and Wilbrecht, 2011). The onset of puberty (~P30) appears to disrupt this behavior, leading to worse

performance as an adult. Prepubertal hormone treatment used to mimic early pubertal onset reduces the rate reversal learning (Piekarski et al., 2017b). Importantly, mice were able to learn the initial reward association and showed deficits only after the rule switch. Prepubertal hormone treatment was the same manipulation that, as discussed earlier, increased prefrontal inhibitory neurotransmission, linking these two phenomena. This suggests that the onset of puberty and increased inhibitory neurotransmission transiently disrupts the regulation of reward memory to promote adaptive responding. From P30 onward, reversal learning performance steadily increases. While this may be related to refinement of inhibitory circuitry in mPFC, developmental changes in the orbitofrontal cortex are also likely critical to this behavioral change (Moin Afshar et al., 2020). Notably, the rate at which reversal learning was acquired during adolescence predicted performance on the task in adulthood (Moin Afshar et al., 2020). This suggests that developmental processes influencing reversal learning in adolescence may have long-term behavioral effects (Figure 1).

A major persisting gap in our knowledge of the development of inhibitory interneurons and their role in cognitive and emotional behaviors stems from a lack of understanding from a circuit perspective. GABAergic neurons in mPFC receive monosynaptic connections from various long-range inputs; however, when these connections form and how this affects interneuron development is not understood (Sun et al., 2019; Ährlund-Richter et al., 2019). Further, it has been documented that mPFC sends long-range GABAergic projections to subcortical targets but their development also remain uncharacterized (Lee et al., 2014). Given the unique behavioral contributions of different classes of interneurons, mapping out the unique spatiotemporal trajectory of their synaptic development within mPFC microcircuits and performing targeted manipulations of interneuron function during behavior will significantly advance our understanding of how the synaptic development of mPFC inhibitory interneurons shapes maturing behaviors.

Development of mPFC neuromodulation

The classical neuromodulators dopamine (DA), serotonin (5-hydroxytryptamine [5-HT]), and norepinephrine (NE) are collectively known as monoamine neurotransmitters. These transmitters are released by groups of neurons located in the ventral tegmental area (VTA) and substantia nigra, the raphe nuclei, and the locus coeruleus (LC), respectively. Neurons in these regions send dense projections to the mPFC, where they release neurotransmitter into the synaptic cleft and into the extracellular space outside the synapse. Upon binding to their respective receptors, they can up- or downregulate the membrane potential in target neurons.

In the upcoming sections, we bring together evidence indicating there is an interdependence between the development of the monoamine systems and discuss work relating these developmental processes to the maturation of cognitive function and emotional learning and memory. The 5-HT system develops early and contributes to the structural development of mPFC while providing a necessary foundation for maturation of the DA system. Given the role of mPFC DA in defensive responses, fear learning, and instrumental reward behavior in adulthood, the increase in mPFC DA during adolescence may underlie the maturation of these behaviors. Because the monoamines are linked to many behaviors that are dysregulated in psychiatric disease, the interdependence of their development may explain, in part, the wide variety of phenotypes and genetic mechanisms associated with disease. Thus, mPFC monoaminergic development may present a convergent target for novel therapies for psychiatric illness.

Maturation of the DA system in mPFC

DA fibers from the VTA heavily innervate the mPFC, where they regulate reward learning, fear conditioning, defensive behaviors, and cognitive control (Reynolds et al., 2018; Vander Weele et al., 2018). DA inputs are already detectable in mPFC at birth and have been observed in L2–L6 by P6 (Kalsbeek et al., 1988). Axonal density of these fibers

significantly increases throughout the adolescent period and into early adulthood (Naneix et al., 2012; Willing et al., 2017; Figure 4), with VTA DA axons growing through the nucleus accumbens on their way to mPFC (Reynolds et al., 2018). The magnitude of this innervation is dependent on the disrupted in colorectal cancer (DCC)/Netrin-1 axon guidance system and is vulnerable to disruption through early life drug exposure and psychiatric disease (Reynolds et al., 2018; Manitt et al., 2013; Reynolds et al., 2015). The adolescent maturation of DA axons in mPFC is consistent with the increase in extracellular DA levels in mPFC from P30 to P60 (Niwa et al., 2010). The density of DA receptors increases in the first two postnatal weeks and then declines thereafter (Leslie et al., 1991; Tarazi and Baldessarini, 2000). This decline stabilizes in early adolescence and is maintained into adulthood (Pokinko et al., 2017; Figure 1). The percentage of DA type 2 receptor (D2R)-expressing neurons within PL neuronal ensembles dramatically increases until the fourth postnatal week and remains constant between P30 and P60 (Yu et al., 2019). Importantly, changes in DA receptor levels throughout adolescence are sexually divergent, with females showing a higher D1R/D2R ratio by early adulthood (Cullity et al., 2019). Early life perturbation, including social defeat and stress (Hill et al., 2014; Watt et al., 2014), is also known to disrupt DA receptor levels.

In adulthood, DA in the mPFC plays a crucial role in regulating responses to aversive stimuli and facilitating fear memory. In mice, DA is released in mPFC during the aversive experience of a tail pinch and biases behavior towards defensive reactions (Vander Weele et al., 2018). This suggests that the development of mPFC DA dynamics may play an integral role in the maturation of defensive behaviors. Throughout adolescence, mPFC becomes increasingly involved in the regulation of innate fear responses. At P14, mPFC is not responsive to innate fear (Chan et al., 2011). By P26, PL is responsive to fearful stimuli but not required for fear behavior (Chan et al., 2011). By mid-adolescence (P38–P42), PL regulates freezing behavior for innate fears (Chan et al., 2011). Importantly, mPFC regulation of innate fear modifies neuronal activity in the ventral periaqueductal gray (PAG). DA release in adult mPFC

has been shown to enhance signals in neurons projecting from mPFC to the dorsal PAG (Vander Weele et al., 2018). It remains unclear when this response develops and how it may contribute to the mPFC-PAG activity dynamics in response to aversive stimuli throughout development.

In addition to innate fear, mPFC DA modulates fear learning. D1 and D4 receptors work antagonistically to encode aversive signals during associative fear learning (Lauzon et al., 2009). DA dynamics also play a role in the persistence of fear memories. D1R and D5R activation in mPFC is required for the retention of fear memories over the course of a week (Gonzalez et al., 2014). This is supported by evidence that, depending on the magnitude of DA release in mPFC, it is possible to predict the accuracy of performance on a memory-guided delayed response task (Phillips et al., 2004). At P15, contextual fear memory lasts only 14 hr, but by P30, these fear memories can last at least 28 days (Akers et al., 2012). The adolescent maturation of DA dynamics and receptor densities likely contributes to the emergence of persistent fearful memories during the same period.

mPFC DA also modulates reward-motivated behaviors. While these tasks can be difficult to test in young rodents, it is known that instrumental behavior for food reward changes throughout the adolescent period (Naneix et al., 2012). While adolescent rats learn to lever press for a food reward similarly to adults, they show deficits in altering their behavior following contingency degradation. That is, when an action is no longer required for a reward, adolescent rats continue to perform this action, while adult rats decrease their responding in comparison to another instrumental response required to receive a distinct food reward. However, adolescent rats are still sensitive to reward devaluation and perform Pavlovian to instrumental transfer similarly to adult rats (Naneix et al., 2012; Figure 1). Similar to what has been observed with reversal learning, adolescent rats appear to be able to form associative reward memories but demonstrate impairments in updating these memories.

The maturation of this operant behavior parallels the development of DA axon innervation of mPFC. Importantly, while DA dynamics in the dorsal striatum and nucleus accumbens are also key to reward-learning, innervation by DA axons in these regions does not undergo robust increases during adolescence as occurs in mPFC (Naneix et al., 2012). This poises the development of DA neurotransmission in mPFC as a key event to regulate the maturation of particular aspects of motivated behaviors.

Maturation of the 5-HT system in mPFC

The role of 5-HT neuromodulation during mPFC development is vast, modulating cellular, circuit, and behavioral development. The 5-HT transporter (5-HTT) directs early morphogenic processes that produce the laminar and cytoarchitectonic structure of mPFC. 5-HTT knockout (KO) mice display increased dendritic branching in mPFC pyramidal cells, decreased number of reelin expressing cells, and changes in morphogen expression that alter cytoarchitectonic development (Wellman et al., 2007; Garcia et al., 2019). The effect of 5-HT release on mPFC pyramidal cells also changes throughout development. Administration of 5-HT to mPFC induces depolarization of L5 pyramidal neurons in pups younger than P19, but shifts to a hyperpolarizing effect commencing during the third postnatal week (Béïque et al., 2004). This progression is due to an age-dependent coordination of depolarizing 5HT7 and 5HT2A receptors and hyperpolarizing 5HT1A receptors. 5HT7 and 5HT1A receptors significantly increase during the second postnatal week and then decrease to adult-like expression levels throughout adolescence (Soiza-Reilly et al., 2019; Goodfellow et al., 2009).

As in the DA system, afferent innervation of mPFC by serotonergic axons is developmentally regulated. A recent study utilizing whole brain mapping of serotonergic axons throughout development in mice observed a distinct temporal innervation pattern of mPFC. In contrast to subcortical targets of serotonergic axons, which displayed gradual increases in innervation throughout the postnatal period, 5-HT-positive axons peaked in mPFC at P7 (Garcia

et al., 2019; Maddaloni et al., 2017; Figure 4). Genetic and environmental factors control 5-HT axonal innervation in mPFC. Deleting the cell adhesion protein-encoding gene *Cadherin-13* (*Cdh13*) from embryogenesis positively regulates 5-HT axonal innervation in mPFC (Forero et al., 2017), and early life experiences can modify serotonergic signaling in mPFC (Ohta et al., 2014). As one of the first neuromodulatory systems to develop in mPFC, 5-HT afferents might be uniquely sensitive to the earliest postnatal experiences and are likely to influence a number of subsequent processes during mPFC development. Indeed, the period of peak innervation falls within what has been suggested as a critical period of mPFC 5-HT signaling. Blockade of the 5-HTT between P2 and P11 in mice results in impaired fear extinction in adulthood (Rebello et al., 2014). This manipulation also resulted in dendritic hypertrophy and reduced excitability of pyramidal neurons in IL, the mPFC subregion known to promote extinction (Rebello et al., 2014). Conversely in PL, which promotes fear expression, pyramidal cells became more excitable (Rebello et al., 2014). This exemplifies how early postnatal 5-HT levels modify mPFC cellular properties to influence behavior throughout the lifespan. It is important to note that the critical period of P2–P11 was established in the 129S6/SvEvTac mouse line, which are known to have higher levels of anxiety compared with outbred mice (Rodgers et al., 2002). This may indicate that blockade of 5-HTT converges with other genetic vulnerabilities to produce the behavioral phenotype seen in adulthood.

A study utilizing 5-HTT KO rats found similar evidence that fear extinction in adults was impaired and extended their behavioral investigation to preadolescent (P24) and adolescent (P35) timepoints. Interestingly, they found that while preadolescent rats also displayed impaired fear extinction, adolescent rats showed typical extinction learning (Schipper et al., 2019). This suggests that particular processes occurring in adolescence, perhaps transient states of circuit maturation or synaptic plasticity, temporarily relieve the inhibited fear extinction induced by the absence of 5-HTT. This further illustrates the complex processes that underlie mPFC-

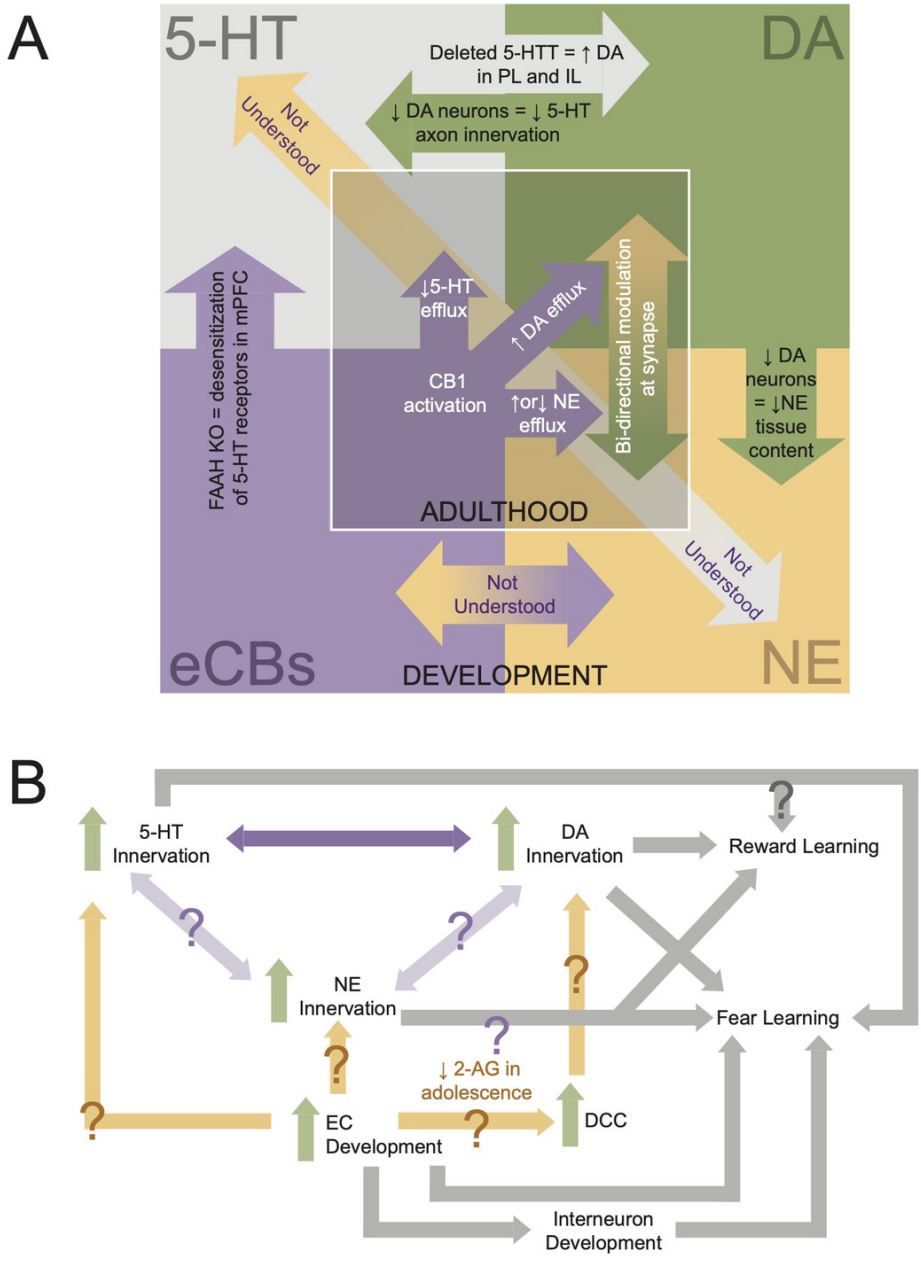

Figure 2-5. Interdependencies during neuromodulatory system development. (A) Schematic showing known interactions between neuromodulatory systems in medial prefrontal cortex (mPFC). Inner square displays phenomena shown in adults, while the outer square displays developmental interactions. (B) Flowchart of how development of mPFC neuromodulations converges to give rise to behavior. Arrows with question marks indicate unstudied interactions.

dependent behaviors and how the interplay between serotonergic development and other aspects of mPFC development converges to regulate behavioral phenotypes.

The development of 5-HT and DA systems is highly interconnected. Administration of 6-hydroxydopamine (6-OHDA), which selectively lesions DA neurons, decreases 5-HT innervation of mPFC (Cunningham et al., 2005). Conversely, deleting the 5-HT transporter selectively increases DA innervation in the IL and PL regions of mPFC and decreases DA innervation in the ACC (Garcia et al., 2019; Figure 5). Thus, 5-HT neuromodulation in mPFC plays a critical role in orchestrating mPFC function from early cellular development to shaping neural circuits to guide behavior. Not only can aberrations to the 5-HT system impair fear extinction, as discussed above, but through interaction with DA development, may also affect reward learning and other aspects of fear learning. The mechanisms by which 5-HT and DA development intersect in mPFC require further attention.

Maturation of the NE system in mPFC

NE axons, originating from the LC, innervate the frontal cortex during embryogenesis and reach adult levels by P6 (Levitt and Moore, 1979). Between P0 and P2, there is a sharp increase in NE tissue content that lowers by P4 and then steadily increases into adulthood (Levitt and Moore, 1979; Figure 4). Like the 5-HT system, there is evidence that the NE system interacts with the DA system in mPFC. Depletion of mPFC DA via local infusion of 6-OHDA from P12–P14 reduced NE content in mPFC tissue in rats aged P30–P65 (Boyce and Finlay, 2009). However, the same study found that DA depletion did not significantly affect NE release in response to a stressful tail pinch (Boyce and Finlay, 2009). Given the prolonged periods of both NE and DA development in mPFC, more studies are needed to determine when and how the DA and NE systems influence one another during mPFC development. Further, our understanding of the interaction between 5-HT and NE in the developing mPFC is entirely lacking (Figure 5). This is despite evidence that these systems are highly intertwined. For example, mice lacking the NE transporter show NE uptake and release by 5-HT terminals in mPFC (Vizi et al., 2004). With the recent development and refinement of intersectional tools for

circuit mapping (Fenno, 2020), it is now possible to simultaneously visualize and manipulate different classes of neuromodulatory neurons that project to mPFC within a single brain. These sorts of approaches will be key to determining how interactions between neuromodulatory systems shape mPFC development (Figure 5).

In adults, the release of NE in mPFC plays an important role in the responses to both appetitive and aversive cues. mPFC NE is released in response to both natural and drug reward as well as reward predictive cues (Mingote et al., 2004; Ventura et al., 2008; Ventura et al., 2003; Ventura et al., 2005). The magnitude of NE release is related to the salience of the reward, and thus, NE may serve as a salience signal (Ventura et al., 2008). Consistent with this, NE release in mPFC is required for food-seeking behavior in the presence of potentially harmful consequences (Latagliata et al., 2010). Conditioned release of NE is also observed in response to aversive stimuli and aversive predictive cues (Ventura et al., 2008; Feenstra et al., 1999). This suggests that the development of NE innervation of mPFC may shape the maturation of responses to appetitive and aversive stimuli and that highly salient events during early life may alter the responsiveness of this system. Indeed, unstable maternal care induces prefrontal NE release and results in increased sensitivity to aversive stimuli in adulthood (Ventura et al., 2013). In the future, studies that manipulate NE dynamics in the developing mPFC will be necessary to determine whether NE signaling drives the maturation of reward- or punishment-driven adaptive behaviors.

Adolescent changes in the mPFC EC system

Fear, stress, and anxiety are modulated by EC signaling within mPFC (Lin et al., 2009; Hill et al., 2011; Fogaça et al., 2012). Impairments in the EC system are observed in a host of psychiatric illnesses including anxiety and depression (Parolaro et al., 2010) . The adolescent period, when many psychiatric illnesses arise, is marked by robust changes in EC signaling. It has been proposed that developmental dynamics in EC signaling may regulate the

emergence of fearful and anxious behaviors (Lee et al., 2016). With evidence emerging that EC receptors may play an essential role in circuit development, we outline how the EC system may influence mPFC circuit assembly. We further discuss how genetic mutations associated with the EC system affect mPFC interneuron development, long-range axonal projections, and conditioned fear.

The EC system, which predominantly consists of two inhibitory g-protein coupled receptors (GPCRs; CB1 and CB2) and two ligands (anandamide [AEA] and 2-arachidonoylglycerol [2-AG]), contributes to the balance of excitatory/inhibitory (E/I) synaptic transmission within the mPFC. AEA is a partial agonist of the CB1 receptor while 2-AG is an agonist for both CB1 and CB2 receptors. Serving as a retrograde mechanism to inhibit neurotransmission, EC signaling regulates neuronal excitability.

Adolescence marks a period of dynamic changes in EC signaling within mPFC and other brain regions. In rats, AEA levels in mPFC increase throughout adolescence while levels of 2-AG follow a U-shaped pattern, decreasing from early to mid-adolescence and then increasing from mid- to late adolescence (Ellgren et al., 2008). CB1 receptor expression levels peak around P25, decrease from early to mid-adolescence, and then plateau in late adolescence (Ellgren et al., 2008). Higher expression of CB1 receptors in juveniles coincided with greater CB1-mediated presynaptic inhibition (Heng et al., 2011). Thus, the EC system is likely to be a prime regulator of neuronal excitability prior to the maturation of inhibitory connectivity in mPFC.

Additionally, the EC system stands poised to orchestrate mPFC synapse and circuit development. EC signaling is crucial during the embryonic period for proliferation and specification of pyramidal cell progenitors (Mulder et al., 2008). The CB1 receptor can also act as an axonal guidance cue; however, the role of CB1 in orchestrating mPFC-specific axon guidance is not well understood (Berghuis et al., 2007). Studies conducted in CB1 KO mice have shown that CB1 is required for healthy mPFC development, particularly interneuron development. The loss of CB1 receptors results in decreased levels of the PV protein in PFC

(Fitzgerald et al., 2011). Further, altered spatial distribution of D2 receptors and reduced mitochondrial number are observed in PV cells in PFC as a result of CB1 KO (Fitzgerald et al., 2012a). However, because these studies were conducted in mice that lack CB1 throughout their lifetime, we lack an understanding of how ECs alter mPFC function through particular phases of development.

Given the robust changes in concentrations of ECs and their receptors throughout adolescence, it is likely that the adolescent period represents a critical window in which disruption to EC signaling may cause mPFC development to go awry. In support of this, exposure to a CB1 agonist, WIN55,212-2, for a 5-day period during mid (P35–P40) or late (P40–P45) adolescence, resulted in reduced GABAergic transmission in mPFC lasting into adulthood (Cass et al., 2014). Similarly, exposure to tetrahydrocannabinol (THC), the CB1 agonist and psychoactive component of marijuana, during adolescence (P35–P45) caused decreased expression of GAD67, the GABA synthesizing enzyme, and increased pyramidal cell firing in mPFC in adulthood (Renard et al., 2017). Given the necessity of mPFC inhibitory neurotransmission in the expression of conditioned fear, these manipulations may have lifelong behavioral consequences.

EC signaling may also be a key influence over development of the DA system in mPFC. CB1 receptors are colocalized at the same GABAergic terminals as D2 receptors and dopaminergic modulation of EC signaling can result in long-term synaptic depression (Chiu et al., 2010). In retinal cultures, CB1 and CB2 receptors have also been shown to modulate axon guidance through interactions with the DCC/Netrin-1 system (Argaw et al., 2011; Duff et al., 2013). Given that the DCC/Netrin-1 guidance system is critical for development of DA axons in mPFC, if interactions between the EC and DCC/Netrin-1 systems also occur in mPFC, EC activity may influence the extent of dopaminergic innervation. For example, as 2-AG and anandamide levels increase in adolescence, changes in CB1 and CB2 activity may in turn alter DCC expression to promote DA axon innervation and branching. This could support increased

and sustained DA innervation of mPFC in adolescence (Figure 5). For a detailed review of the interactions between the EC and DA systems within mPFC, see Fitzgerald et al., 2012b.

The enzyme, fatty acid amide hydrolase (FAAH), regulates levels of AEA, thus modulating CB1 receptor signaling. Mutant mice with reduced FAAH protein levels show increased mPFC axonal innervation of the BLA (Dincheva et al., 2015; Gee et al., 2016). Importantly this phenotype emerges in adolescence as increased axon fiber density is observed in mice at P45 and P75 but not P23 (Gee et al., 2016). Behaviorally, these FAAH-mutated mice show decreased anxiety-like behavior and enhanced fear extinction learning. These findings have been recapitulated in humans with those that express the FAAH A385 allele displaying increased mPFC-amygdala functional connectivity and lower anxiety in adolescence (Dincheva et al., 2015; Gee et al., 2016). Thus, EC signaling regulates structural and functional connectivity of mPFC with important consequences for fear and anxiety-related behaviors.

In adults, EC signaling plays a role in modulating mPFC-dependent behaviors. Levels of ECs modulate conditioned fear. CB1 antagonism increases conditioned freezing while CB2 antagonism decreases this behavior (Llorente-Berzal et al., 2015). Further, inhibiting AEA degradation decreases freezing while inhibiting 2-AG degradation promotes the freezing response (Llorente-Berzal et al., 2015). This suggests that anandamide and 2-AG have opposing influences over the fear response. Importantly, these pharmacological manipulations were given systemically, and it is not known whether mPFC is involved in the effects seen. However, other work has specifically pointed to mPFC ECs in regulating fearful behaviors. mPFC CB1 antagonism disrupts fear extinction (Lin et al., 2009). Inducing hypofunction in N-methyl-D-aspartate receptors (NMDAR) early in life disrupts EC-dependent long-term depression of synapses in mPFC and results in deficits in specifying between fear memories (Lovelace et al., 2014). CB1 receptor activity in BLA neurons that project to mPFC is necessary for associative fear learning (Tan et al., 2010). Thus, EC actions in mPFC and its long-range connections, including with the BLA, contribute to fear learning.

While multiple lines of evidence point to EC signaling as a critical aspect of mPFC development, further work is needed to understand how ECs and their receptors specifically orchestrate mPFC development. CB1 receptor expression changes throughout adolescence and EC signaling are intertwined with monoamine neuromodulatory and inhibitory transmission, which develop along a similar timescale (Figure 1). CB1 receptors likely make important contributions to mPFC pyramidal cell development and axon guidance over long periods of development. Further, the robust changes in concentration of ECs and receptor density over the adolescent period are likely to shape interneuron development and the maturation of fear learning and memory, but causal links are still lacking.

Finally, there is still much to learn about developmental interactions between the EC system and the monoamine neuromodulatory systems in mPFC (Figure 5). Particularly, the developmental interactions between ECs and the 5-HT and NE systems are not well understood. However, it is known that mPFC EC action in adulthood modulates the efflux of 5-HT and NE (Reyes et al., 2012; Morilak, 2012; McLaughlin et al., 2012; Haj-Dahmane and Shen, 2011). For example, a CB1 agonist can either increase or decrease NE efflux in mPFC depending on whether or not a rat was in a state of stress (Reyes et al., 2012). Therefore, the convergence of neuromodulatory development may be a point of vulnerability for experience to disrupt development (Figure 5). Investigating the developmental interactions between neuromodulators is complex. However, by beginning with large-scale manipulations such as receptor and transporter KO lines, and then refining our understanding with cell-type-specific manipulation (e.g., optogenetics or chemogenetics), and receptor manipulation (e.g., pharmacology), we can begin to disentangle these interactions. Notably, understanding how neuromodulatory systems interact in mPFC also requires a more complete developmental understanding of its descending projections to the LC, dorsal raphe, and VTA as modulation of these projection neurons may alter activity in neurons projecting back to mPFC (Figure 2).

Genetic control of mPFC circuit organization and function

mPFC dysfunction is central to the etiology of neuropsychiatric disorders in which cognitive and emotional behaviors go awry. These include addiction (Hiser and Koenigs, 2018), depression, anxiety (Farrell et al., 2013), ASD, and schizophrenia (Schubert et al., 2015), diseases that all have strong genetic contributions. The prolonged maturation of the developing mPFC permits great regulatory control but also enhances vulnerability to genetic and environmental insults. Up to 50% of these mental conditions emerge by adolescence, with molecular and cellular changes manifesting prior to onset of psychiatric disorders (Shapiro et al., 2017). Studies of cross-species translation in a developmental context have shown that both humans and rodents converge in aspects of mPFC maturation and alignment of critical periods of plasticity (Kolb et al., 2012; Callaghan et al., 2019). Mouse models of schizophrenia and ASD have identified altered expression of signaling molecules and changes in inhibitory circuits that produce abnormal E/I balance and mispositioning of cortical layers and axons in the mPFC (Shapiro et al., 2017; Stoya et al., 2014; Schofield et al., 2011). Taken together, these results provide evidence linking neural signatures of vulnerability to changes in mPFC neurobiology and the behavioral process that rely on those circuits.

Here, we will highlight a series of recent studies that used mouse models to explore the mechanisms of disease progression. We discuss how the genes *Cntnap2, Shank3, Disc1,* and *Dlx5/6* produce overlapping phenotypes in aspects of mPFC synaptic development, which we discussed in previous sections. Specifically, we highlight studies that link developmental changes in inhibitory microcircuit organization and function or long-range synaptic connectivity to cognitive disruptions (Table 1). We also highlight recent work that has identified genetic regulators of DA and 5-HT systems in mPFC. We further postulate about how these developmental circuit disruptions may lead to deficits in regulation of conditioned fear, reward learning, and cognitive flexibility that are observed in neuropsychiatric disorders.

Genetic regulation of mPFC inhibitory connectivity and emergent circuit functions

Inhibitory neurotransmission shapes the dynamic routing of information through the neocortex (Isaacson and Scanziani, 2011). Growing evidence shows that inhibitory signaling in mPFC undergoes late-stage changes, including dramatic decreases in the E/I balance in mPFC circuits during adolescence. This prolonged period of change likely renders interneurons in mPFC circuits particularly vulnerable to disruption. Indeed, E/I imbalance is considered a pathophysiological mechanism and interneuron dysfunction has been linked to changes in cognition associated with neuropsychiatric diseases that emerge during adolescence, including schizophrenia, impulse control disorders, attention-deficit disorder (ADHD), and ASD (Sohal and Rubenstein, 2019). Elucidating the genetic programs that control the development of mPFC inhibitory interneurons is critical to understand how inhibition shapes the maturation of mPFC-dependent behaviors in health and disease. Here, we discuss several recent studies that reveal convergent roles for *Dlx5/6, Disc1,* and *Cntnap2* in regulating mPFC interneuron physiology and circuit function.

Oscillatory activity can enhance communication between specific brain regions during cognitive tasks. Gamma rhythms driven by PV interneurons are thought to play key roles in cognition and emotional learning (Uhlhaas and Singer, 2010; Cauli et al., 1997; Kawaguchi, 1997; Cardin et al., 2009; Sohal et al., 2009; Fenton et al., 2016). While increased gamma oscillations in PFC have been observed during tasks that require cognitive flexibility, altered gamma oscillations in PFC may be associated with neuropsychiatric disorders including schizophrenia, in which patients exhibit deficits in cognitive flexibility (Green, 2006), impaired fear extinction, and difficulties learning safety cues (Holt et al., 2012). Postmortem analyses have revealed abnormalities in median ganglion eminence (MGE)-derived interneurons, including reduction in the expression of PV and GAD67, a synthetic enzyme for GABA (Volk and Lewis, 2013).

The *Dlx1–6* genes encode a family of homeobox transcription factors that play critical roles in the development of MGE-derived cortical GABAergic interneurons. While *Dlx6* may have limited expression in adult cortical neurons, *Dlx5* is expressed in PV, SST, CR, and neuropeptide Y (NPY) cells in superficial cortical layers, and predominantly in PV cells in deep cortical layers (Wang et al., 2010). *Dlx5/6-/-* KOs have reduced numbers of cortical PV cells and increased dendritic branching in the PV cells that remain (Wang et al., 2010).
In *Dlx5/6+/-* heterozygous mice, alterations in the properties of mPFC PV interneurons arise in early adulthood, beginning around P63. In these mice, PV interneurons have abnormal physiological properties, including wider action potentials, higher input resistance, and slower membrane time constants (Cho et al., 2015a). These changes result in reductions in the amplitude of gamma frequency-induced inhibitory postsynaptic currents in connected mPFC pyramidal neurons. At the same age, *Dlx5/6+/-* mice exhibit heightened anxiety and deficits in a rule-shift task that requires cognitive flexibility. Importantly, *Dlx*5/6+/- mice exhibit deficits in task-related gamma frequency power and task performance that can be rescued by pharmacological augmentation of mPFC interneuron function (Cho et al., 2015a). Together, these studies link mutations in *Dlx5* and *Dlx6,* key genes that regulate mPFC interneuron development, to alterations in gamma oscillations that underlie deficits in cognitive flexibility. These mechanisms may contribute to post-adolescent onset of cognitive changes in schizophrenia as well as aberrations in fear and reward learning (Cho et al., 2020).

Though *Dlx5* and *Dlx6* have not been linked to specific disorders, *Disc1 (disrupted-in schizophrenia-1)* and *Cntnap2* have similar functions in cortical interneurons. DISC1 is a scaffolding protein that interacts with numerous synaptic proteins and enzymes to regulate diverse processes including cortical development and synapse formation (Brandon and Sawa, 2011). A translocation in *DISC1* was reported in a Scottish pedigree as a rare but penetrant risk factor for several mental illnesses including schizophrenia, depression, and bipolar disorder

			Phenotypes		
Gene	**Protein function**	**Cell types**	**Cellular**	**Circuit**	**Behavior**
CNTNAP2	Axonal transmembrane protein	PYR, INs	Reduced spine density, reduced excitatory and inhibitory synaptic input to PYR cells	Altered phase modulated spiking to delta and theta rhythms, reduced long-range cortico-cortical connectivity, and reduced local connectivity	Repetitive behaviors and cognitive inflexibility
Disc1	Intracellular scaffold	PYR, INs, glia	Reduced PV expression, change in Pr in INs, and reduced inhibitory input to PYR cells	Reduced feed-forward inhibition in thalamocortical circuits and elevated E/I ratio	Impairments in working memory, latent inhibition, and pre-pulse inhibition, and increased immobility in forced swim test
Dlx5/6	Transcription factor	MGE INs	Deficits in IN migration and reduced IN number	Altered gamma rhythms	Anxiety and congnitive inflexibility
Shank3	Excitatory synaptic scaffold	PYR	Reduced dendritic complexity, reduced spine density and PSD length, and reduced excitatory synaptic transmission	Reduced frontostriatal connectivity, reduced local and long-range cortical connectivity, and reduced prefrontal gray matter	Social deficits, anxiety, and repetitive behaviors

Table 2-1. Summary of phenotypes in four mouse models. PYR: pyramidal cell; IN: interneuron; MGE: median ganglionic eminence; Pr: release probability; PSD: postsynaptic density; E/I: excitatory/inhibitory.

(Millar et al., 2000). Several mouse models of *Disc1* have reductions in PV expression in prefrontal cortex (Niwa et al., 2010; Hikida et al., 2007; Shen et al., 2008; Ibi et al., 2010; Ayhan et al., 2011; Lee et al., 2013) and exhibit impairments in multiple cognitive domains (Niwa et al., 2010; Brandon and Sawa, 2011; Lee et al., 2013; Koike et al., 2006; Clapcote et al., 2007; Li et al., 2007; Kvajo et al., 2008). Until recently, however, the function of *Disc1* in regulating mPFC inhibitory connectivity and circuit function remained unexplored.

Using mice that are heterozygous for the *Disc1* locus impairment (LI) allele, recent work revealed that *Disc1* regulates the connectivity between mPFC pyramidal cells and PV interneurons. Beginning as early as P15, mPFC L2/3 pyramidal cells exhibit reduced inhibitory synaptic input that likely results from reductions in release probability in PV interneurons. These changes have consequences for circuit function, causing a significant decrease in the strength of feed-forward inhibition in the MD thalamus–mPFC pathway (Delevich et al., 2020), one of the most prominent sources of input to the mPFC (DeNardo et al., 2015). The authors also

observed elevations in the E/I ratio in mPFC pyramidal neurons (Delevich et al., 2020), a property that is hypothesized to be associated with the pathobiology of neuropsychiatric diseases (Sohal and Rubenstein, 2019; Yizhar et al., 2011). Phenotypic analyses of *Disc1* mutant mice have revealed deficits in cognition (Clapcote et al., 2007). Further, *Disc1* has been shown to interact with cannabis exposure to induce deficits in learned fear, indicating possible vulnerability in the interaction between inhibitory neurotransmission and the EC system (Ballinger et al., 2015). Given the importance of mPFC inhibitory circuit function in these behavioral functions, the identified changes in inhibitory circuits may affect both cognitive and emotive functions.

Cntnap2 encodes Caspr2, a member of the neurexin family of cell adhesion molecules that is expressed widely throughout the brain in development and in adulthood (Poliak et al., 1999). Mutations in *Cntnap2* are implicated in a human disorder characterized by cognitive and emotional deficits including schizophrenia, obsesive compulsive disorder (OCD), ADHD, and ASD (Strauss et al., 2006; Alarcón et al., 2008; Arking et al., 2008; Bakkaloglu et al., 2008; Peñagarikano et al., 2011). Like *Dlx5/6+/-* mice, *Cntnap2* KO mice exhibit changes in the physiological properties of PV cells in addition to reductions in the total number of PV-, NPY-, and CR-positive interneurons (Peñagarikano et al., 2011). PV cells lacking *Cntnap2* have wider spikes, slower membrane time constants, greater adaptation, and more depolarized membrane potentials compared to controls (Vogt et al., 2018). These data suggest that *Cntnap2* may regulate the properties of voltage-dependent sodium and/or potassium channels that mediate action potentials and repolarization in PV interneurons (Vogt et al., 2018).

Consistent with the reduction in the number of cortical interneurons, *Cntnap2-/-* L2/3 pyramidal cells in mPFC receive fewer inhibitory synaptic inputs than their wildtype counterparts. As *Cntnap2-/-* mice navigate a virtual environment, interneurons exhibit elevated firing rates during both locomotion and immobility. In addition, *Cntnap2* deletion causes reductions in interneuron phase locking to the local field potential (LFP) in delta (4 Hz) and theta

(4–8 Hz) frequency ranges and *Cntnap2-/-* units tended to fire later in the LFP cycle (Lazaro et al., 2019). Delta oscillations in mPFC have been shown to entrain the amygdala during fear expression (Fujisawa and Buzsáki, 2011), and theta oscillations are associated with signaling safety in fear conditioned animals (Likhtik et al., 2014). Thus, alterations in phase locking of mPFC neurons may give rise to cognitive and affective behavioral dysfunction observed in the *Cntnap2* mouse model (Lazaro et al., 2019).

Based on these studies, PV interneurons and their emergent circuit functions appear to be some of the most vulnerable elements in mPFC circuitry. In several mouse models that exhibit overlapping cognitive deficits, alterations in the physiology and connectivity of mPFC inhibitory interneurons emerge around adolescence. Taken together with work showing that mPFC interneurons undergo major changes in their physiology and circuit functions during adolescence, these studies suggest that the processes that regulate interneuron development during adolescence may be particularly vulnerable to genetic insults. Perturbations to these processes are likely to be determining factors during disease progression. Using floxed alleles and cell-type-specific cre-driver lines, future research can perform spatiotemporally targeted manipulations in mPFC interneurons to refine our understanding of how and when circuit-level deficits contribute to behavioral deficits in cognitive and emotive domains.

Genetic regulation of excitatory connectivity in mPFC

Cntnap2 also regulates excitatory connectivity and the physiological properties of mPFC pyramidal cells in a manner that converges with other disease risk genes including *Shank3.* In L5 pyramidal cells, *Cntnap2* deletion causes a reduction in action potential frequency and input resistance specifically in subcortical projection neurons (Brumback et al., 2018). In L2/3, *Cntnap2-/-* pyramidal cells exhibit decreases in the strength and number of excitatory synaptic inputs (Lazaro et al., 2019).

In contrast to *Cntnap2,* which is expressed broadly across cell types, the expression of *Shank3* in the PFC is most prevalent in pyramidal cells, with limited expression in GABAergic interneurons, and no apparent expression in glial cells (Guo et al., 2019). *Shank3* encodes an excitatory postsynaptic scaffolding protein that interacts with a variety of postsynaptic density proteins to control dendritic spine morphology and synaptic function (Naisbitt et al., 1999; Sala et al., 2001; Monteiro and Feng, 2017). *Shank3* is also associated with ASD (Durand et al., 2007) as well as with schizophrenia and Phelan–McDermid syndrome, in which patients exhibit ASD-like behaviors including intellectual disability (Phelan and McDermid, 2012). Recent work examined the consequences of *Shank3* deletion in the ACC.

The ACC is implicated in an array of cognitive functions, including decision making, motivation, cost-benefit analyses, and social behaviors (Apps et al., 2016; Chang et al., 2013). *Shank3* KO mice exhibit numerous structural deficits in ACC pyramidal neurons including reductions in dendritic complexity, spine density, and in the length and thickness of postsynaptic densities (Guo et al., 2019). *Shank3* KO neurons also exhibit reductions in both the frequency and amplitude of miniature excitatory postsynaptic currents, consistent with reductions in both the number and strength of excitatory synapses. The decrease in synaptic strength can be attributed to deficits in α-amino-3-hydroxy-5-methyl-4-isoxazole propionic acid receptor-mediated current, while currents through NMDARs were unaffected. Importantly, these deficits can be rescued by targeted delivery of Shank3 to ACC in the adult brain, indicating that Shank3 acts cell autonomously to maintain the strength and number of excitatory synapses in adulthood (Guo et al., 2019).

In addition to regulating local connectivity within prefrontal areas, both *Cntnap2* and *Shank3* KO mice exhibit reductions in prefrontal long-range connectivity. In *Cntnap2-/-* mice, decreases in local and long-range functional connectivity are apparent across prefrontal subregions, but these changes are most robust in the cingulate cortex. Regions that exhibit hypoconnectivity with prefrontal areas include the parietal areas, temporal

association areas, and hippocampus (Liska et al., 2018). Similarly, *Shank3B-/-* homozygous KOs exhibit deficits in local prefrontal connectivity and in long-range connectivity with the retrosplenial (RSP) cortex, ACC, and the striatum. PFC and RSP represent key nodes in the default-mode-network (DMN). In *Shank3B-/-* mice, PFC was more disconnected from the DMN. In both mutants, effects were specific to the PFC and motor and sensory networks did not show significant changes in connectivity (Liska et al., 2018).

Cntnap2 and *Shank3* KO mice exhibit social deficits and motor stereotypies characteristic of ASD and other disorders. However, given their influence over mPFC structural development, synapse formation, and long-range connectivity, both *Cntnap2* and *Shank3* also stand poised to be critical genetic regulators of both fear and reward learning. However, their role in the development of these behaviors is poorly understood. Future investigations may look to these genes as sites of vulnerability in the maturation of cognitive and emotional behaviors controlled by mPFC.

In distinct mouse models, disruptions in inhibitory signaling, synchrony, and long-range connectivity emerge as key points of convergence. These circuit-level signatures may represent important targets for new interventions designed to prevent or ameliorate the symptoms of neuropsychiatric disorders. To date, most studies of genetic mechanisms of mPFC circuit assembly have used whole-animal KOs, in some cases crossing them to transgenic lines that allow them to perform cell-type-specific investigations. These approaches have revealed specific deficits in PV-pyramidal synapses in *Disc1-L1* and *Dlx5/6* mutants. However, given that in these studies the genetic manipulations affected cells across the brain beginning from embryonic development, there are limitations in our understanding of the mechanisms of action and their timing. In the future, studies that use spatially and temporally controlled strategies to manipulate gene expression will provide necessary insights into the cellular and molecular mechanisms underlying the onset of human neuropsychiatric disorders.

Genetic regulation of mPFC neuromodulatory systems

Dysfunction of the neuromodulatory systems in mPFC is associated with neuropsychiatric diseases in which emotional learning and cognitive flexibility are compromised. Thus, the genes that control the developmental wiring of mPFC neuromodulatory systems may play a critical role in the pathogenesis of such diseases. Dysfunction in mPFC DA signaling has been implicated in schizophrenia (Rao et al., 2019; Howes et al., 2017) and depression (Han and Nestler, 2017). As previously discussed, DA axonal innervation of mPFC dramatically increases throughout the adolescent period and is dependent on DCC/Netrin-1 signaling. *Dcc* knockdown mice show enhanced DA innervation of mPFC and enhanced cognitive flexibility in adulthood (Manitt et al., 2013). This suggests that an increase in DCC expression may cause deficits in cognitive flexibility and contribute to disease phenotypes. Indeed, the rs2270954 polymorphism of the *Dcc* gene was found to be associated with schizophrenia (Grant et al., 2012).

5-HT innervation of mPFC has been associated with *Cdh13*. Mice deficient in *Cdh13* display increased innervation of mPFC compared to control mice (Forero et al., 2017; Forero et al., 2020). Behaviorally, fear extinction is disrupted in male *Cdh13* KO mice but not females. This suggests a sex-dependent mechanism through which *Cdh13* deficiency modulates emotional memory. Importantly, *Cdh13* also directs development in other brain areas such as the hippocampus (Rivero et al., 2015). Thus, further research is needed to understand how the role of *Cdh13* specifically in mPFC may lead to the behavioral impairments seen in *Cdh13* KO mice. This is of great importance given that mutations in *Cdh13* have been associated with a vast number of neuropsychiatric disorders including ADHD (Rivero et al., 2013), depression (Edwards et al., 2012), schizophrenia (Otsuka et al., 2015; Børglum et al., 2014), and bipolar disorder (Cho et al., 2015b).

Future directions: tackling mPFC complexity in development

The recent circuit analyses in mouse models of neuropsychiatric disorders underscore how mPFC inhibitory microcircuits, neuromodulatory systems, and long-range connectivity – circuit elements that undergo dramatic changes throughout juvenile and adolescent development (Figure 1) – are some of the most vulnerable elements in disease progression. Based on this work, there is an urgent need to refine our understanding of the links between these aspects of mPFC neurodevelopment and maturing behaviors. Uncovering the time course and regulatory mechanisms guiding the assembly of mPFC circuits will refine our understanding of which developmental milestones have profound effects on mPFC function and how they come about. This knowledge will be key to understanding the neural basis of behavioral transitions during development and can inform targeted manipulations of mPFC circuit elements to directly test their behavioral functions at distinct developmental stages. For instance, during the juvenile period, new work can test whether the strengthening of long-range mPFC connections with regions including the BLA contributes to mPFC's increasing role in fear and reward learning and a developmental switch from short- to long-lasting fear memories (Figure 1 and Figure 3). In adolescence, targeted manipulations of inhibitory and neuromodulatory cell types can test whether strengthening synaptic inhibition and refinement of mPFC neuromodulation are required for the maturation of reward learning, conditioned fear, and cognitive flexibility (Figure 1 and Figure 4). Establishing links between neurodevelopment and behavior is an essential first step to understanding how and when early insults transform these processes and can inform new interventional strategies to slow or prevent disease progression.

With the explosion of viral and genetic approaches over the last 10 years, we have tools in hand to manipulate these developmental processes with unprecedented specificity and resolution (Luo et al., 2018). Thereby, we can directly link the maturation of cells and circuits to the maturation of complex behaviors. The emergent hypotheses we put forth in this review can be tested using viral-genetic approaches to (1) define causal links between specific aspects of

cellular and circuit development and cognitive and emotive functions, (2) understand how the developmental processes we describe are contingent on one another, and (3) discover the molecular and cellular programs that control the maturation of mPFC connectivity. Genes that wire specific mPFC synaptic connections can form the basis of new genetic tools to target developing circuit elements with increasing precision.

Developmental changes in the expression of emotional memories and cognitive flexibility may rely on developmental milestones within mPFC inhibitory microcircuits. Around the same time that mPFC inhibitory interneurons undergo changes in the expression of key signaling proteins (e.g., PV and SST) and mPFC inhibitory synaptic currents strengthen dramatically, animals exhibit temporary deficits in fear memory retrieval, increases in fear memory generalization, decreased performance in reversal learning, and insensitivity to reward contingency degradation. Thereafter, as inhibitory circuitry is refined, fear memory becomes robust and persistent, reward learning becomes sensitive to contingency degradation, and performance improves in reversal learning tasks (Figure 1). This suggests that precise inhibitory control over the timing or levels of mPFC activity is necessary for mature forms of cognitive and emotive behavior to emerge. It is unclear whether connections between mPFC interneurons and distinct classes of pyramidal cells uniquely control the maturation of these different behavioral functions, or whether there is a common mechanism governing the observed changes in each behavioral domain. Determining whether this is the case will require a more detailed understanding of synaptic development between classes of mPFC interneurons and pyramidal cells and new research that performs targeted manipulations of activity, connectivity, and synaptic function in different mPFC neuronal types during behavior in developing animals.

Conceptually similar approaches can also be applied to determine how the developing DA, 5-HT, and NE systems shape the maturation of emotional memory and cognitive flexibility. For instance, increased innervation of DA axons in mPFC may promote the maturation of defensive behaviors (i.e., freezing), the retention of fear memory, and instrumental learning,

while 5-HT signaling in adolescence may be critical for the development of fear extinction. The development of NE signaling dynamics may promote the attribution of salience and learned associations to reward and fear cues. Addressing these questions will require a more detailed understanding of how neuromodulation shapes both behavior and the underlying neural signaling at different stages of development. We can leverage transgenic tools for activity dependent genetic labeling (DeNardo and Luo, 2017) to capture behaviorally activated neurons in the developing brain and then assess their behavioral functions at later times using invasive methods such as Ca2+ imaging. By performing developmental activity-based tagging with concurrent manipulations of neuromodulatory signaling, we may be able to determine how neuromodulation shapes the neural basis of behavior at juvenile and adolescent stages.

Proper assembly of mPFC circuits requires temporally precise orchestration of multiple interdependent systems. From birth through adolescence, the DA, NE, 5-HT, and EC systems influence each other's development in ways we are only beginning to understand (Figure 5). As the 5-HT system is one of the earliest to form connections, it might have particularly strong influence over the maturation of the other monoamine systems as they innervate mPFC. Global manipulations of 5-HT signaling during specific developmental windows cause concurrent changes in DA levels in mPFC and impair fear extinction in adulthood. To test whether these interactions occur locally within mPFC, new research could combine viral tracing with genetic deletion of the 5-HT synthetic enzyme tryptophan hydroxylase 2, *Tph2*. By disrupting 5-HT signaling specifically in projections to mPFC during development, new research can ask whether DA signaling is reduced in a corresponding way. Using intersectional genetic strategies to simultaneously visualize 5-HT and DA axons in mPFC within a single brain can further reveal how disruptions in 5-HT signaling impact the development of both systems. As EC signaling has been shown to regulate DA receptors levels and to interact with Dcc/Netrin-1 signaling to promote axon guidance in the retina, it may regulate development of DA axons in mPFC. The neuromodulatory systems are exquisitely sensitive to early occurring environmental changes

and genetic mutations that have lasting behavioral consequences. Because of this, understanding how their development is intertwined may help to explain the spectrum of behavioral phenotypes associated with neuropsychiatric disorders.

Precise wiring of mPFC long-range connections is essential for mPFC function in adulthood, but our understanding of the timeline along which specific pathways mature and how circuit maturation shapes behavior is lacking. In the case of fear learning and memory, mPFC circuits known to play a role in the adult brain may also underlie the developmental regulation of fearful memories. Bidirectional connectivity between mPFC and BLA increases dramatically during the fourth postnatal week. At the same time, fear memories become robust and long-lasting. As such, the developmental strengthening of mPFC-BLA connectivity may be essential to establish prefrontal control of the expression of conditioned fear. To test whether these processes are causally linked, new research can determine whether increasing activity in the mPFC-BLA pathway during fear learning and memory in juvenile development enhances the ability to form long-lasting memories. Interestingly, reward learning and cognitive flexibility mature along a similar timeline (Figure 1) and deficits in long-range connectivity are hallmarks of psychiatric disease (Table 1). Thus, enhanced regulatory control that comes with the maturation of mPFC long-range synaptic connectivity may have broad affects, allowing mature forms of numerous cognitive and emotional behaviors to emerge.

Importantly, the development of many mPFC connections that play key roles in the regulation of emotional memory and cognition, including connections with the medial entorhinal cortex and midline thalamic nuclei, has not been carefully examined in development (Figure 2). In the case of conditioned fear, research that explores the anatomical and functional maturation of these connections, both in naive animals and in those that have undergone fear conditioning in juvenile stages when fear memories are short-lived, can link developmental changes in synaptic function to age-dependent differences in fear memory robustness. Arruda-Carvalho et al. provide an elegant example of how to describe the structural and functional maturation of an

mPFC pathway using channelrhodopsin (ChR2)-assisted circuit mapping (Arruda-Carvalho et al., 2017). With this approach, in which mPFC axons are transduced with ChR2 and light-evoked postsynaptic currents are recorded in target cells in a downstream region of interest, we can understand precisely when long-range mPFC synaptic connections form and functionally mature, and how they respond to learning. Given that individual mPFC pathways have been linked to distinct behavioral functions, synaptic connections that mature along different developmental timelines may regulate maturing behaviors during distinct developmental windows. This information will be important for understanding windows of vulnerability during disease progression.

As we gain a more detailed understanding of when particular mPFC connections form and mature, we can begin to investigate the underlying molecular mechanisms. Extracellular signals can be important modulators of synapse development. For instance, the innervation of BLA by mPFC axons is modulated by levels of ECs. As discussed, manipulations to the EC system only affect mPFC→BLA neurons at the beginning of adolescence, suggesting a specific temporal window in which EC signaling may direct mPFC circuit maturation. To hone-in on the precise temporal dynamics with which the EC system acts on mPFC circuitry, conditional KOs or pharmacological manipulations of EC signaling can be performed at discrete time points throughout the developmental period. Further, the EC system may modulate the extent of innervation in other mPFC target regions. Future studies can look at how manipulations in EC levels affect the extent of axon innervation in other mPFC target regions important for fear and reward learning and cognition, including thalamic nuclei and striatal regions.

In addition to external influences from neuromodulatory signals, genes encoding synaptic organizer proteins may also play a critical role in wiring mPFC connections. For instance, *Cdh8* is expressed selectively in mPFC neurons that project to the striatum. Given its role in target selection and synaptic plasticity in the retina and hippocampus, *Cdh8* may specifically regulate wiring of mPFC-striatal synapses. *Cdh13* regulates the development of 5-

HT axons in mPFC, and the guidance cues Dcc/Netrin-1 regulate wiring of DA fibers in mPFC, though it remains unclear whether Cdh13 and Dcc/Netrin-1 exclusively regulate 5-HT and DA axons in mPFC, or if their function extends to other pathways as well. If *Cdh8*, *Cdh13*, and *Dcc/Netrin-1* indeed play specific roles in wiring frontostriatal, serotonergic, and dopaminergic connectivity, respectively, we can then leverage them as tools to manipulate those pathways and measure the impact on developing behaviors.

As *Cdh8*, *Cdh13,* and *Dcc/Netrin-1* have been linked to ASD, depression, and schizophrenia, investigating their role in wiring the healthy brain can provide important clues about how mPFC circuitry is perturbed in disease.

Major hurdles in developmental circuit mapping stem from the challenge of precise stereotaxic targeting in small developing brains. Now, researchers often rely on brute-force approaches to target specific regions in early postnatal development. Wiring specificity genes like *Cdh8*, whose differential expression patterns in the nervous system allow them to regulate the formation and maturation of specific classes of synapses, could eventually form the basis of new cre-driver lines. New transgenic lines that provide genetic access to particular classes of developing mPFC neurons can ease our reliance on precise stereotaxic targeting in early postnatal stages. In combination with floxed alleles, optogenetics, chemogenetics, and genetically encoded Ca2+ indicators, new cre-driver lines that provide access to particular developing circuit elements will allow us to link the assembly of mPFC circuits to maturing behaviors with unprecedented specificity.

Chapter 3: Prefrontal circuit mechanisms driving developmental changes in safety-seeking behaviors

ABSTRACT

Survival in nature depends critically on safety-seeking behavioral strategies that become encoded in neuronal circuits. Throughout the animal kingdom, distinctive behavioral repertoires emerge over development. Juveniles gradually abandon the protection of caregivers and adolescents embrace risky exploration that affords independence and autonomy. As adolescents become adults, behavior refocuses on self-preservation. However, how developing neural circuits program these behavioral transitions remains unknown. In adults, the medial prefrontal cortex (mPFC) encodes threat predictive cues and dynamically controls threat-avoiding behavior through projections to limbic centers including the basolateral amygdala (BLA) and nucleus accumbens (NAc). While these regions undergo a prolonged maturation, we lack mechanistic links between frontolimbic circuit function and behavior across development. Here we show that threat avoidance behavior is developmentally regulated in mice; juveniles have weak memories of threats, adolescents explore more than they avoid threats, and adults have persistent, high levels of threat avoidance. We used fiber photometry, in vivo optogenetics, synaptic physiology, and viral circuit tracing to monitor and manipulate activity in the developing brain, establishing direct causal links between mPFC circuit activity and the distinctive behavioral strategies of juveniles, adolescents and adults. We found that while mPFC output to the BLA promotes avoidance behavior during adulthood, these circuits are functionally immature in juveniles and activating them impedes avoidance. During adolescence, when demands shift, maturing mPFC-BLA connections are eclipsed by mPFC-NAc activity, biasing behavior towards risky exploration. Our studies reveal that frontolimbic circuit elements mature at different rates

and require delicate coordination to produce developmentally appropriate behaviors. By revealing these developmental trajectories, we establish a foundation for understanding how they can be perturbed during their protracted maturation. Pathways linking mPFC to the BLA and NAc represent key loci for understanding and repairing dysfunctional behaviors associated with mood and anxiety disorders.

INTRODUCTION

The universal process of growing up requires that individuals adapt their behaviors to meet developmental milestones. As animals leave the protection of caregivers, they must balance safety-seeking with exploratory behaviors that allow them to establish nuanced behavioral responses to a dynamic environment. Doing so requires that as the animals gain experience, learned behaviors become encoded in neuronal circuits. Across the animal kingdom, conserved transitions in threat-avoiding behaviors have been observed throughout early life. Juveniles typically rely on caregivers for protection, but in many species, including frogs, penguins, and humans, adolescents engage in risky exploration while adults seek safety (Warkentin et al., 1999; Hinke et al, 2020, Tymula ey al., 2021; Spear et al., 2000; Laviola et al., 2003; Overskaug et al., 1999). As of yet, we do not understand how neuronal circuit maturation progresses to promote these behavioral transitions.

In adults, the mPFC encodes threats and guides threat avoidance behavior through top-down control of subcortical regions including the BLA and NAc (Bravo-Rivera et al., 2014; Diehl et al., 2018; 2020). mPFC undergoes a prolonged development that lasts until early adulthood, rendering it uniquely vulnerable to genetic or environmental insults throughout early life (Arruda-Carvalho et al., 2017; Drzewiecki et al., 2016; Kroon et al., 2019; Kolb et al., 2012). mPFC dysfunction underlies anxiety disorders, obsessive compulsive disorder, and depression – diseases characterized by excessive avoidance that tend to arise in adolescence (Arnaudova et

al., 2017; Cervin et al., 2020; Gillan et al., 2014; Ironside et al., 2020; Maner and Schmidt, 2006; Rudaz et al., 2017; Solmi et al., 2022). Understanding the trajectory of mPFC circuit development and establishing mechanistic links between circuit maturation and milestones in threat avoidance behavior is critical for preventing and treating these psychiatric illnesses.

Here, we reveal transitions in learned threat avoidance behavior between juvenile, adolescent, and adult mice and link these with differential activity patterns in mPFC, NAc, and BLA. We uncover drastic differences in the function of prefrontal circuits by age which, together with differential rates of synaptic development in mPFC-NAc and mPFC-BLA pathways, jointly determine age-specific behavioral responses to threat.

METHODS

Subjects

Female and male C57B16/J mice (JAX Stock No. 000664) were group housed (2–5 per cage). Infant mice were housed with their mothers and weaned at postnatal day 21. Mice were kept on a 12 hr light cycle (lights on 7am-7pm) in a temperature and humidity controlled room. Food and water were available ad libitum. All procedures followed animal care guidelines approved by the University of California, Los Angeles Chancellor's Animal Research Committee.

Behavioral Assays

Platform-mediated avoidance

Mice were handled for 3 days preceding the behavioral testing procedure. The conditioning chamber consisted of an 18 x 30 cm cage with a grid floor wired to a scrambled shock generator (Lafayette Instruments). The chamber was surrounded by a custom-built acoustic chamber and scented with 50% Windex. A thin acrylic platform (1.3 cm thick) covered 25% of the floor. Two small weigh boats filled with vanilla, almond or coconut extract were placed beneath the floor to encourage exploration of the chamber by the mice. During training on P23,

P35 or in adulthood, mice were presented with three baseline 30s 4 kHz tones (CS), followed by nine presentations of the CS that co-terminated with a 2 s foot shock (0.13mA). The following day, mice were presented with six CS in the absence of shocks to probe ability to retrieve and express avoidance memory. Tones were separated by a randomized interval lengths that ranged from 80 to 150 seconds. Non-shocked control mice underwent identical procedures except foot shocks were omitted.

Open-field Test

Mice were acclimated to the testing room for 10 minutes, and then placed in a plastic arena (50 x 50 x 40 cm). Locomotor activity and time spent in the center of the arena were recorded during a 10 minute test using the video-tracking system BioViewer. Using the tracking system, the arena was divided into two zones, the center (25% of the total area) and periphery (75% of the total area). Time spent in each zone as well as total distance traveled was recorded.

Shock Sensitivity To assess the minimum foot-shock intensity required to elicit a behavioral response (vocalization, scurry or dart), naive P23, P35 and adult mice were placed in the same operant conditioning chamber as in PMA, but without the platform. Mice were exposed to a series of foot shocks, beginning at 0.02 mA and increased at 0.02 intervals until 0.20mA. The amplitude of the foot-shock at which a given mouse first vocalized, scurried and darted was recorded. Vocalization was defined as the emittance of an audible sound. Scurry was defined as rapid stepping with the absence of jumping. Dart was defined as a high velocity, horizontal jump.

Real-time place preference

To determine if optogenetic manipulation of PL→NAc or PL→BLA projections impacted behavior beyond PMA, RTPP tests were performed the day following PMA retrieval for all optogenetic experiments. Following connection to the blue (stimulation; 473 nm; 15 Hz; SLOC Lasers, Shanghai, China) or red light (inhibition; 590 nm; 0 Hz; SLOC Lasers) laser, the mice

were spaced in a place preference chamber for 20 min. For the first 10 min baseline period, mice were allowed to freely explore the apparatus and BioViewer software was used to track movement and determine which half of the chamber they preferred. This was used to determine which half of the chamber would receive laser stimulation or inhibition. For the following 10 min laser light was delivered on the preferred side of the chamber (PL→NAc inhibition and PL→BLA stimulation) or the non-preferred side (PL→NAc stimulation or PL→BLA inhibition). Results were calculated as percent change from baseline (test-baseline/baseline x 100).

Optogenetic manipulation of PL→NAc and PL→BLA projections during PMA

Surgery

Juvenile cohorts (trained at P23) underwent viral injections at P9, adolescent cohorts (trained at P35) underwent viral injections at P19, and adult cohorts (trained or perfused after P60) underwent viral injections on or after P46. Mice were induced in 5% isoflurane in oxygen until loss of righting reflex and transferred to a stereotaxic apparatus. For P9 and P19 mice, the stereotax fitted with an attachment for developing mice including a small bite bar and developmental ear bars. A nonsteroidal anti-inflammatory agent was administered pre- and postoperatively to minimize pain and discomfort. The mouse's head was shaved and prepped with three scrubs of alternating betadine and then 70% ethanol. Following a small skin incision, a dental drill was used to drill through the skull above the target. In P9 animals a 27-gauge syringe was used to poke a small hole in the skull. A syringe pump (Kopf, 693A) with a Hamilton syringe was used for pressure injections. For stimulation experiments, mice were bilaterally infused with adeno-associated virus (AAV) expressing either the excitatory opsin channelrhodopsin (AAV8-Ef1a-FAS-ChR2(H134)-mCherry-WPRE-pA, Addgene plasmid 37090, custom AAV produced from Janelia Virus Service). For inhibition experiments, mice were bilaterally infused with an AAV expressing the red-shifted inhibitory opsin Jaws (AAV5-hSyn-Jaws-KGC-GFP-ER2, Addgene #65014). Control mice were infused with a red fluorescent protein (AAV1-CAG-tdTomato,

Addgene #59462). Viral injection volume was scaled by age with 200nL injected at P9, 300nL injected at P19 and 700nL injected in adults. Virus was infused bilaterally at a rate 75nL/min into the PL (AP: +1.8; M: ±0.4; DV: -2.3mm). The syringe was left in the brain for 5-10 min following viral infusion in adult and adolescent mice. In juvenile mice the syringe was left in the brain for 2-5 minutes to decrease surgery time as mice were more sensitive to anesthesia. At P9 and P19, this coordinate was scaled based on the bregma-lamda distance using Neurostar StereoDrive Software (Neurostar GmbH, Tübingen, Germany). After recovery, P9 mice were returned to their home cage with their mother. All other ages the animals were housed with littermates.

Approximately 4 days prior to PMA training (10 days after viral infusion), juvenile and adolescent mice underwent an additional stereotaxic surgery to implant bilateral optical fibers. This was done to accommodate for skull growth during viral expression. Adult mice received fiber implants 1 week prior ro PMA training. 200 um optical fibers (Braintech) were bilaterally implanted in the NAc (AP: +1.3; M: ±0.1; DV: -4.7mm) or BLA (AP: -1.6; M: ±3.0; DV: -4.3mm) and secured with Metabond (Parkell, NY, USA) to allow stimulation or inhibition of PL terminals in each of these areas.

Optogenetic manipulation during PMA

Prior to all experiments mice were habituated to optic tether (200 um, 0.22 NA, Doric Lenses, Quebec, Canada). No optogenetic manipulation occurred during PMA training. For mice injected with ChR2, during the retrieval day, PL projections to either the NAc or BLA were photo-excited with a blue laser (473 nm; 15 Hz; SLOC Lasers) controlled by the behaviourDEPOT fear conditioning experimenter MATLAB app (Gabriel et al., 2022), during each of the six 30s tone presentations. The light power delivered, as measured through an optic fiber pre-implant, was set to output 10mW of light. For mice injected with Jaws, during the retrieval day, PL projections to either the NAc or BLA were photo-inhibited with constant red light laser (590 nm; SLOC Lasers). The light power delivered, as measured through an optic fiber pre-implant, was set to output 7.5mW of light.

Fiber photometry recordings during PMA

Surgery

Separate cohorts of each age were used to record bulk activity in PL, BLA or NAc. Mice were infused with AAV expressing the genetically encoded calcium indicator GCaMP6s (AAV9-GCaMP6s-WPRE-SV40, Addgene #100844). Virus (300 nL for all ages) was injected into either PL (AP: +1.8; M: ±0.4; DV: -2.3mm), NAc (AP: +1.3; M: ±0.1; DV: -4.7mm) or BLA (AP: -1.6; M: ±3.0; DV: -4.5mm). Infusions were done at a rate of 75nl/min and syringes left in place for 2-10 min, depending on the age. Similar to optogenetic experiments, optic fiber implants occurred in a separate surgery 4 days prior to PMA training. At this time the fiberoptic cannula (400um, 0.66 NA, Doric Lenses) was unilaterally implanted into the PL, NAc or BLA to allow for subsequent imaging of GCaMP fluorescence in cell bodies of each region.

Recordings during PMA

Fiber photometry was used to image bulk calcium activity in PL, NAc, and BLA neurons throughout PMA training and retrieval. Animals were habituated to the optical tether one day prior to recordings. During PMA training and retrieval we simultaneously imaged GCaMP6s and control fluorescence in each region using a commercial fiber photometry system and companion Synapse software controlling an RZ10x lock-in amplifier (Tucker Davis Technologies Inc., Alachua, FL). Two excitation wavelengths (465 and 405 nm) were modulated at 211 and 566Hz and filtered and combined by a fluorescence mini cube (Doric Lenses, Quebec, Canada). The combined excitation light was delivered via a 400 um core, 0.37 NA, low-fluorescence patch cord (Doric Lenses, Quebec, Canada) to an implanted optical fiber (fiber core diameter: 400 um; Doric Lenses). GCaMP6s emission fluorescence was collected through the mini cube and caused onto a femtowatt photoreceiver (Newport, Model 2151, gain set to DC LOW). LED power was set such that 80 and 20 units of light were received by the system for the 465 nm and 405 nm channel, respectively. Fluorescence was sampled at 1017 Hz, and demodulated by the processor. Time stamps for tone experiment start, finish and each tone onset were collected using TTLs sent from

a custom MATLAB experiment designer (MathWorks, Natick, MA). Signals were saved using Synapse software and exported to MATLAB for analysis.

Ex vivo electrophysiology

Surgery and Fear Conditioning

To optogenetically stimulate PL axons in the BLA and NAc, we injected 100nL of AAV8-Syn-ChR2(H134R)-GFP (Addgene #58880) into right PL using techniques described above. Surgeries were performed 12-16 days prior to recording. For BLA recordings, naive and fear-conditioned animals were recorded on the same day using age- and sex-matched littermate controls. Fear conditioning was performed by delivering 6 20-second tones (4 kHz, 75 dB) co-terminating with a 2-second 0.5mA footshock. A randomized interval between 90 and 120 seconds separated each tone. Naive animals remained in their home cage. Recordings were performed the day after fear conditioning.

Acute Brain Slice Preparation

To prepare acute brain slices, mice were anesthetized with isoflurane and transcardially perfused with ice-cold slicing ACSF solution containing (in mM) 2.5 KCl, 1 NaH_2PO_4, 26.2 $NaHCO_3$, 4 $MgCl_2$, 11 Glucose, 210.3 Sucrose, 0.5 $CaCl_2$, and 0.5 Na-Ascorbate (bubbled with 95% O_2 / 5% CO_2). The brain was rapidly dissected, and 300μm (BLA) or 230μm (NAc) sections were obtained from the hemisphere ipsilateral to the injection site using a Leica VT1200S vibratome. Slices were transferred to normal ACSF containing 125 NaCl, 2.5 KCl, 26.2 $NaHCO_3$, 1 NaH_2PO_4, 2 $MgCl_2$, 11 Glucose, and 2 $CaCl_2$ (bubbled with 95% O_2 / 5% CO_2) and held at 34°C for 35-40 minutes. Slices were then allowed to cool to room temperature. Slices containing PL were also collected to verify the injection site.

Slice Electrophysiology

Recordings were performed at room temperature in normal ACSF. BLA and NAc were identified using white matter tracts and PL axon fluorescence. Cells were visualized under infrared-differential interference contrast through a 40x objective. Voltage clamp experiments

were performed using borosilicate pipettes (5-7MΩ) filled with internal solution containing 117 CsMS, 20 HEPES, 0.4 EGTA, 2.8 NaCl, 5 TEA-Cl, 4 Na_2-ATP, and 0.4 Na-GTP, adjusted to pH 7.3 using CsOH (280-290mOsm). In some NAc recordings, 1mM QX-314 was also included. Excitatory currents from mPFC terminal stimulation were obtained by holding neurons at -70mV and delivering 0.1ms (BLA) or 0.5ms (NAc) of 5-30mW blue (~470nm) light through the 40x objective using a CoolLED pE-300Ultra light source. Inhibitory currents were recorded in the same way but holding neurons at 0mV. Data were collected using a Multiclamp 700B amplifier and Digidata 1440A digitizer (Axon Instruments) with pClamp 10 (Molecular Devices). Recordings were sampled at 10kHz and filtered at 2kHz. Series resistance and input resistance were monitored throughout the experiment by measuring the capacitive transient and steady-state deflection in response to a 5mV test pulse, respectively. Series resistance was <25MΩ, did not change more than 20% throughout a session, and was not compensated. Data were analyzed in Python. Analysis was based on the average of 10 sweeps. Currents were analyzed relative to the baseline holding current. EPSCs and IPSCs were quantified by measuring the peak response when cells were voltage clamped at -70mV and 0mV, respectively. In some cases, a clear polysynaptic peak was present in the excitatory current after the initial monosynaptic peak. In these cases, the minimum value of the initial monosynaptic peak was used as the excitatory current. For comparisons of peak current values across conditions, analyses were restricted to cells with 15-30mW stimulation intensity. Statistical outliers were excluded via Grubbs' test (alpha 0.01). The EPSC peak value was divided by the IPSC peak value for each cell to calculate the E/I ratio.

Viral strategy to visualize synaptic innervation of NAc and BLA

Surgery

To visualize synaptic boutons from PL axons in the BLA and NAc we utilized a newly developed viral construct, (pAAV-hSyn-FLEx-loxP-Synaptophysin-mGreenLantern-T2A-GAP43-mScarlet, Schwarz Lab, St. Jude). AAV (serotype 2/9) was synthesized by the St. Jude Children's

Research Hospital Vector Development and Production Core to a final titer of 4.9x10^12. When in the presence of Cre, axons will express the red fluorescent protein mScarlet, and boutons the green fluorescent protein mGreenLantern. Stereotaxic surgeries were performed similarly to previous experiments, except the virus was delivered iontophoretically using glass micropipettes whose outside tip diameter measured 10-30um. A mixture of AAV-Syn-mGap-43-mScarlet and a AAV-Cre (AAV8-Ef1a-mCherry-IRES-Cre) was infused at a ratio of 3:1. A positive 5 uA, 7-second alternating injection current was delivered for 10 min (Stoelting Co.) to infuse the virus mixture and left in place for 2-10 min following infusion. The virus was allowed to express for 2 weeks and then brain perfused for analysis.

Histology

Following the behavioral experiments, mice were deeply anesthetized in a chamber filled with Isoflurane and transcardinally perfused with phosphate buffered saline (PBS), followed by 4% paraformaldehyde (PFA). Brains were removed and post-fixed in 4% PFA overnight, placed into 30% sucrose solution, then sectioned into 60um slices using a cryostat and stored in PBS or cryoprotectant. Images were acquired at 10x with a Leica STELLARIS confocal microscope or at 5x on a Leica DM6 B scanning microscope.

GFP immunofluorescence was used to confirm expression of GCaMP6s in cell bodies and Jaws expression in PL axons terminals. Floating coronal sections were washed 3 times in 1x PBS for 30 min and then blocked for 2hr at room temperature in a solution of 10% normal goat serum and 0.3% Triton X-100 dissolved in PBS. Sections were then washed 3 times in PBS for 15 min and incubated in 3% serum blocking solution containing chicken anti-GFP polyclonal antibody (1:2000; Aves Labs, Davis, CA) with gentle agitation at 4℃ overnight. Sections were next rinsed 3 times in PBS for 30 min and incubated with donkey anti-chicken IgY, AlexaFluor 488 conjugate (1:500; Jackson ImmunoResearch, West Grove, PA) in 0.5% serum blocking solution at room temperature for 2 hr. Sections were washed a final 2 times in PBS for 10 min.

RFP immunofluorescence was used to confirm expression of ChR2-mCherry, as well as mCherry and tdTomato control viruses in PL axon terminals. Floating coronal sections were washed 3 times in 1x PBS for 30 min and then blocked for 2hr at room temperature in a solution of 10% normal donkey serum and 0.3% Triton X-100 dissolved in PBS. Sections were then washed 3 times in PBS for 15 min and incubated in 3% serum blocking solution containing rabbit anti-RFP polyclonal antibody (1:2000; Rockland Immunochemicals, Pottstown, PA) with gentle agitation at 4℃ overnight. Sections were next rinsed 3 times in PBS for 30 min and incubated with donkey anti-rabbit IgY, Cyanine Cy3 conjugate (1:500; Jackson ImmunoResearch, West Grove, PA) in 0.5% serum blocking solution at room temperature for 2 hr. Sections were washed a final 2 times in PBS for 10 min.

RFP and GFP immunofluorescence were used to amplify expression of GAP43-mScarlet and Synaptobrevin-mGreenLantern for visualization. Staining procedures were as described above. Samples were imaged on a 63x on a Leica STELLARIS confocal microscope. Confocal z-stacks were analyzed in three dimensions (3D) using Imaris software (Oxford Instruments). First, we rendered a 3D surface of the mScarlet+ axons and masked out any red or green fluorescence outside the surface. Then we trained a filament classifier to detect fluorescent axons and measured the total summed length of all axonal segments in the region of interest. Next, we generated surfaces around the green fluorescent synaptic puncta. Surfaces were filtered based on the red fluorescence intensity – boutons were only counted if they were located within top 50% brightest axon fluorescence intensity.

Data analysis

Behavioral analysis

High resolution videos of PMA were collected at 50 Hz using Chameleon3 USB cameras (Teledyne FLIR) Point tracking of videos were performed in DeepLabCut and behavior analyzed using behaviorDEPOT. Custom MATLAB code was used to quantify time on platform, latency to enter the platform, freezing,

Fiber Photometry

Data were pre-processed using a custom-written pipeline in MATLAB. Prior to analysis the signal was downsampled by 10x. Using the polyfit function, the isosbestic signal was fit to the 465nm signal and this curve was subtracted from the 465nm channel. To align fiber photometry and behavioral data a lookup table was generated using linear interpolation between each TTL pulse to identify which behavior frame lines up with each photometry frame. Z scores were calculated using a baseline period of -5 to 0 seconds relative to tone onset for tone-aligned responses (i.e. tone and shock responses), -20 to -15 seconds relative to epoch onset for platform-related behaviors (i.e. platform entries and exits) and -2 to 0 seconds relative to epoch onset for freezing bouts. The average of all traces for an individual animal was calculated and used for analysis. To generate plots, each animal's average trace was smoothed by averaging values from every 0.5 seconds and the mean ±SEM of smoothed traces across animals was displayed. Area under the curve (AUC) values were calculated from the average trace for each individual animal.

Statistical analysis

All statistical tests were performed in GraphPad Prism.

RESULTS

Developmental changes in threat avoidance behavior

Mice exhibit developmental changes in the retention and expression of conditioned fear but it is unclear to what extent their threat avoidance behavior changes as animals mature (Akers et al., 2012; Pattwell et al., 2011). To examine this, we trained juvenile, adolescent, and adult mice in platform mediated avoidance (PMA; Figure 3-1a–c). In PMA, a conditioned tone prompts mice to enter a safety platform to avoid a mild foot shock. Mice in all age groups learned PMA, increasing their fraction of successful trials and time spent on the safety platform – decreasing

their latency to enter the platform, and showing modest increases in conditioned freezing over the course of training (Figure 3-1d).

The next day, we tested their learned avoidance behavior in a retrieval session. We presented conditioned tones in the absence of foot shocks and observed age-specific behavioral repertoires (Figure 3-1e). During presentations of threatening tones, adults had persistent, high

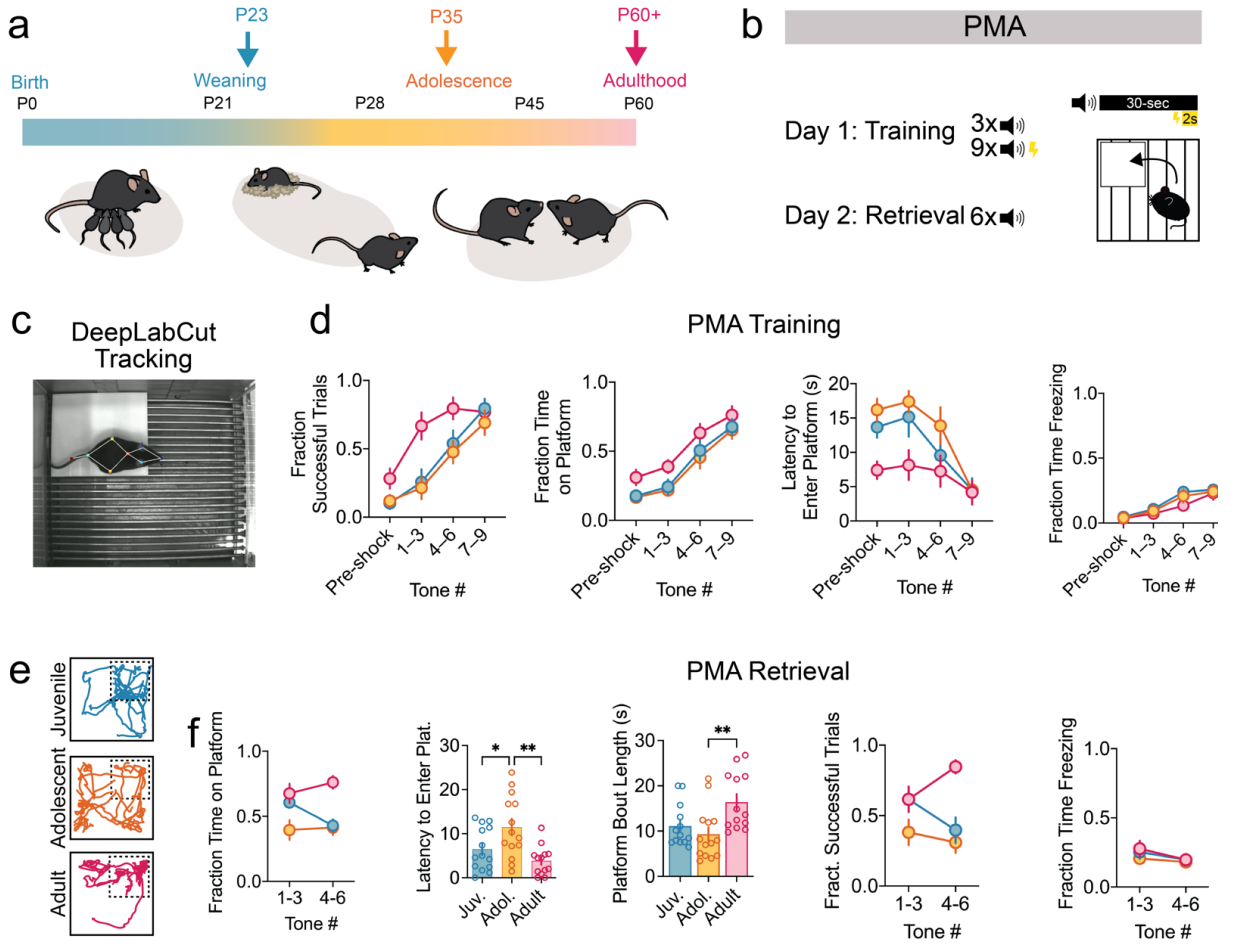

Figure 3-1. Learned avoidance behavior is developmentally regulated. (A) Selection of ages for study. (B) PMA protocol. (C) Keypoint tracking using DeepLabCut. (D) Behavioral performance during PMA training (Successful trials: $F_{trial}(2.6,96.5) = 36.47$, $P<0.0001$; $F_{age}(2,37)=8.01$; $P=0.0013$; Time on Platform: $F_{trial}(2.4,88.9) = 60.45$, $P<0.0001$; $F_{age}(2,37)=4.31$; $P=0.021$; Latency: $F_{trial}(2.67,98.85) = 18.75$, $P<0.0001$; $F_{age}(2,37)=4.91$; $P=0.013$; Freezing: $F_{trial}(1.94,71.74) = 34.89$, $P<0.0001$; $F_{age}(2,37)=0.68$; $P=0.51$, 2-way ANOVA with post hoc Tukey test, Juvenile N=13, Adolescent N=14, Adult N=13). (E) Representative examples of mouse trajectory maps during a PMA retrieval session. (F) Behavioral performance during PMA retrieval (Successful trials: $F_{trial}(4.04, 147.9) = 0.36$, $P=0.84$; $F_{age}(2,37)=9.85$; $P=0.0004$, Mixed-Effects Analysis; Time on Platform: $F_{trial}(1,37) = 0.42$, $P=0.52$; $F_{age}(2,37)=10.26$; $P=0.0003$, 2-way ANOVA with post hoc Tukey test; Latency: $F(2,38) = 7.13$, $P=0.0024$, One-way ANOVA with post hoc Tukey test; Bout Duration: $F(2,38) = 5.74$, $P=0.0067$, One-way ANOVA with post hoc Tukey test; Freezing: $F_{trial}(1,34) =6.59$, $P=0.015$; $F_{age}(2,34)=0.35$; $P=0.71$, 2-way ANOVA with post hoc Tukey test, Juvenile N=13, Adolescent N=14, Adult N=13).
Data represent mean ± standard error of the mean (s.e.m.), *p<0.05, **p<0.01.

levels of PMA, adolescents had low levels of PMA, and juveniles initially showed adult-like levels of PMA that decreased by the second half of the retrieval session (Figure 3-1f). These differences in PMA levels could be attributed to developmental differences in the latency to enter the platform and in platform bout length. Compared to adults and juveniles, adolescents took longer to enter the safety platform following tone onset. Both juveniles and adolescents had shorter platform bout lengths – they tended to leave the platform soon after stepping on (Figure 3-1g,h).

We next performed a series of control experiments to confirm that behavioral differences in PMA reflected developmental changes in learned threat avoidance behavior. Shock sensitivity levels and distance traveled in the conditioning chamber were similar across age groups (Figure 3-2a,b). Adults spent significantly more time exploring the center of an open field compared to younger mice, suggesting that their robust PMA is not due to increased anxiety-like behavior (Figure 3-2c). For each age group, non-shocked control mice spent significantly less time on the

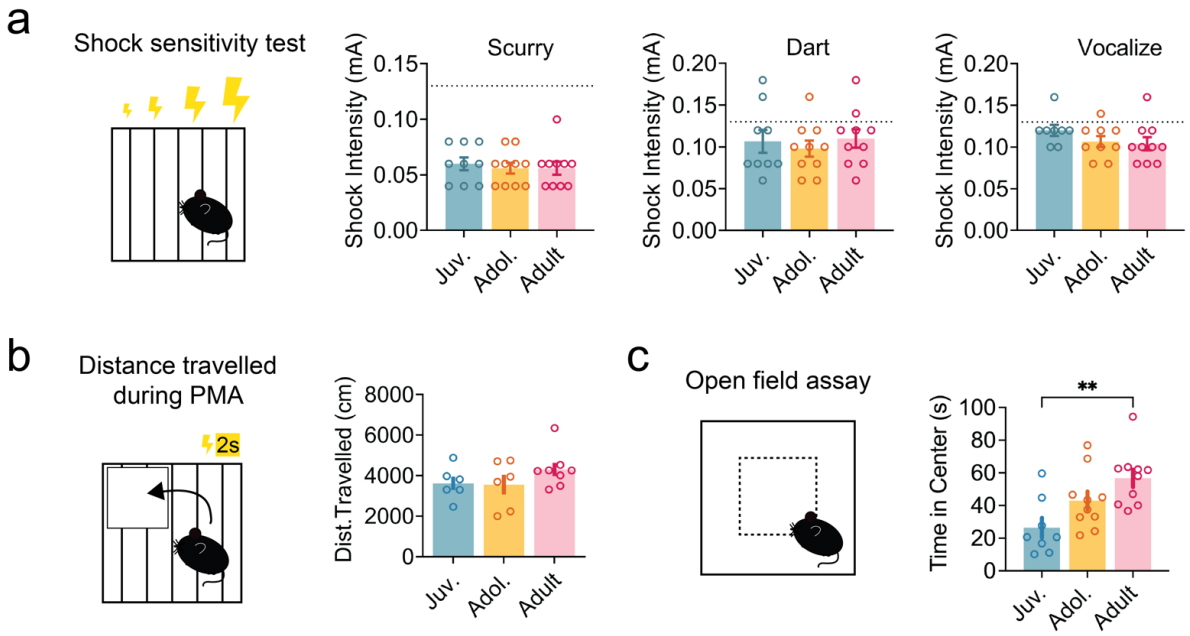

Figure 3-2. Shock thresholds in juvenile, adolescent, and adult mice. (A) Summary data of behavioral responses to progressive increases in shock intensity (Scurry: F(2,26)=0.17, P=0.85; Dart: F(2,26)=0.31, P=0.74; Vocalize: F(2,24)=1.37, P=0.27; One-way ANOVA with post hoc Tukey test; Juvenile N=9, Adolescent N=10, Adult N=10 mice). (B) Summary data of distance traveled during PMA training (F(2,12)=1.29, P=0.3,One-way ANOVA with post hoc Tukey test; Juvenile N=6, Adolescent N=6, Adult N=8 mice). (C) Summary data of time in the center of an open field (F(2,25)=6.74, P=0.005,One-way ANOVA with post hoc Tukey test; Juvenile N=8, Adolescent N=10, Adult N=10 mice). Data represent mean ± s.e.m., **p<0.01.

platform and had fewer 'successful trials', meaning they did not tend to be on the platform in the last two seconds on the tone when the shock would occur during training (Figure 3-3). These data suggest that observed differences in PMA reflect developmental changes in learned threat responses rather than changes in shock sensitivity, locomotion, innate anxiety levels, or a natural preference for being on the platform.

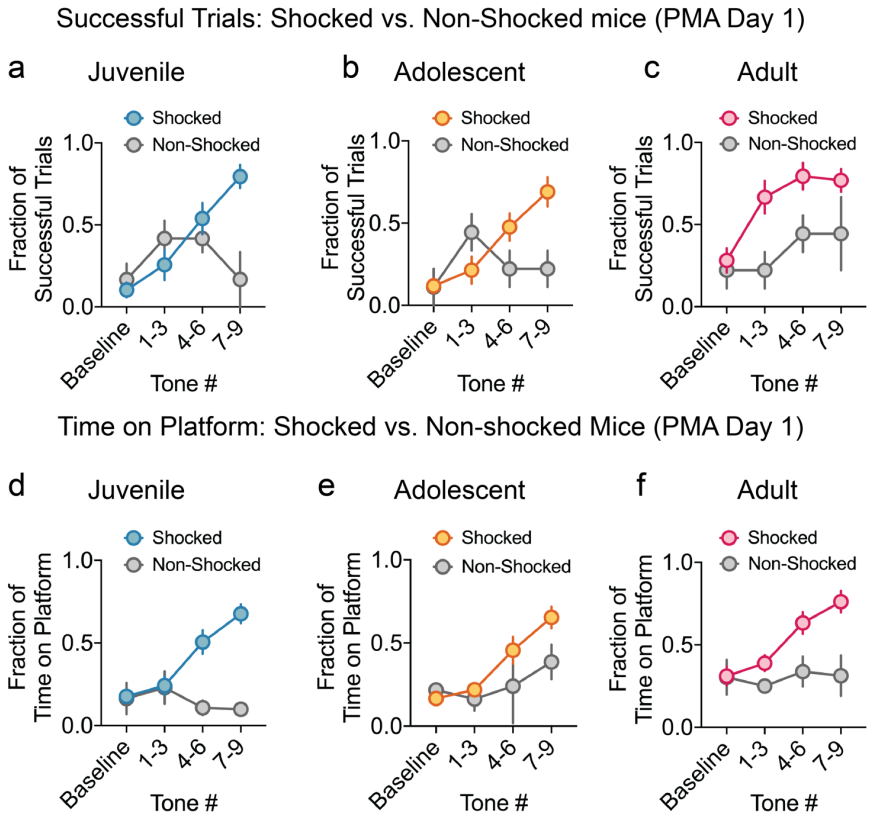

Figure 3-3. Behavior in non-shocked control mice. (A-C) Comparing successful trials during PMA Day 1 for shocked vs.non-shocked control mice. (A) Summary data of successful trials for juvenile mice (Successful trial: $F_{trial}(3,45)=3.0$, $P=0.04$, $F_{shock}(1,15)=1.5$, $P=0.24$, $F_{int}(3,45)=3.32$, $P=0.028$; Two-way ANOVA with post hoc Sidak test; N=4 non-shocked mice, N=13 shocked mice). (B) Summary data of successful trials for adolescent mice (Successful trial: $F_{trial}(3,45)=4.41$, $P=0.008$, $F_{shock}(1,15)=2.51$, $P=0.13$, $F_{int}(3,45)=5.12$, $P=0.004$; Two-way ANOVA with post hoc Sidak test; N=3 non-shocked mice, N=14 shocked mice). (C) Summary data of successful trials for adult mice (Successful trial: $F_{trial}(3,48)=7.25$, $P=0.0004$, $F_{shock}(1,16)=7.65$, $P=0.014$, $F_{int}(3,48)=2.05$, $P=0.12$; Two-way ANOVA with post hoc Sidak test; N=5 non-shocked mice, N=13 shocked mice). (D-F) Comparing time on platform during PMA Day 1 for shocked vs.non-shocked control mice. (D) Summary data of time on platform for juvenile mice (Successful trial: $F_{trial}(3,45)=4.17$, $P=0.012$, $F_{shock}(1,15)=11.16$, $P=0.0045$, $F_{int}(3,45)=9.65$, $P<0.0001$; Two-way ANOVA with post hoc Sidak test; N=4 non-shocked mice, N=13 shocked mice). (E) Summary data of time on platform for adolescent mice (Successful trial: $F_{trial}(3,45)=5.67$, $P=0.002$, $F_{shock}(1,15)=2.46$, $P=0.14$, $F_{int}(3,45)=1.23$, $P=0.31$; Two-way ANOVA with post hoc Sidak test; N=3 non-shocked mice, N=14 shocked mice). (F) Summary data of time on platform for adult mice (Successful trial: $F_{trial}(3,48)=8.78$, $P<0.0001$, $F_{shock}(1,16)=9.17$, $P=0.008$, $F_{int}(3,48)=4.93$, $P=0.005$; Two-way ANOVA with post hoc Sidak test; N=5 non-shocked mice, N=13 shocked mice). Data represent mean ± s.e.m.

To determine if age-dependent changes in PMA during retrieval reflected developmental differences in the rate of fear extinction, we examined 'successful trials' during the retrieval session. Adults increased their number of successful trials from ~50% to 100% across the retrieval session. Juveniles began the session with adult-like levels of successful trials, but decreased over time, suggesting that extinction of the threat avoidance memory may contribute to their decrease in PMA. Adolescents already had few successful trials from the beginning of the retrieval session (Figure. 3-1i). In a cohort of mice, we performed a second retrieval test 3 weeks after training. While adults had persistent, high levels of PMA, juveniles showed a modest decrease and adolescents showed a modest increase in PMA levels compared to their 1-day retrieval test,

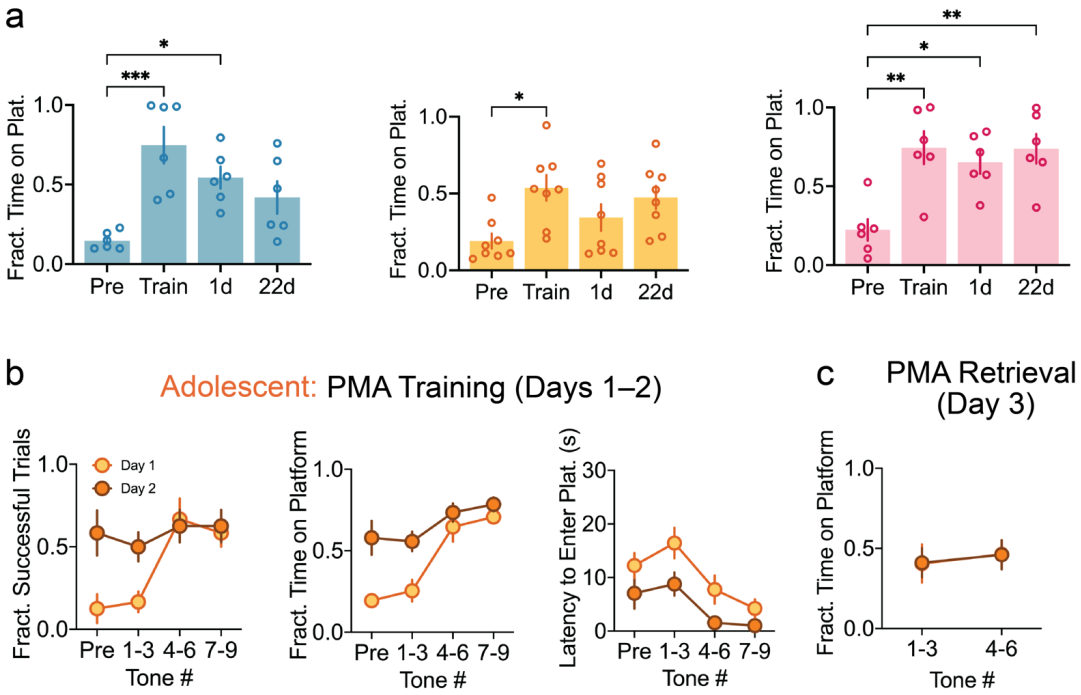

Figure 3-4. Behavioral effects of extended training. (A) Time spent on platform during baseline 1-3 tones of training, at the end of training, during the 1 day retrieval session and 22 days following training in juveniles $F(3,20)=4.764$, $P=0.0006$,One-way ANOVA with post hoc Tukey test; N=6), adolescents $F(3,28)=0.0153$, $P=0.0153$,One-way ANOVA with post hoc Tukey test; N=8) and adults $F(3,20)=0.4059$, $P=0.0008$,One-way ANOVA with post hoc Tukey test; N=6) mice. (B-C) Effects of a second day of PMA training in adolescent mice. (B) Summary data of behavior during PMA training days 1 and 2 (Successful trial: $F_{trial}(3,42)=6.8$, $P=0.0007$, $F_{day}(1,14)=4.6$, $P=0.049$, $F_{int}(3,42)=3.5$, $P=0.02$; Time on Platform: $F_{trial}(2.6,36.5)=19.7$, $P=0.0007$, $F_{day}(1,14)=12.96$, $P=0.003$, $F_{int}(3,42)=3.37$, $P=0.03$; Latency: $F_{trial}(3,42)=0.48$, $P=0.7$, $F_{day}(1,14)=7.3$, $P=0.02$, $F_{int}(3,42)=0.48$, $P=0.7$; Two-way ANOVA with post hoc Sidak test; N=8 adolescent mice). (C) Summary data of PMA during retrieval for adolescent mice that received 1 vs. 2 days of training (Time on Platform: $F_{trial}(1,13)=0.58$, $P=0.46$, $F_{training}(1,13)=0.00009$, $P=0.99$; $F_{int}(3,42)=0.003$, $P=0.95$; Two-way ANOVA with post hoc Sidak test; 1 day of training: N=7 mice, 2 days of training: N=8 mice). Data represent mean ± s.e.m, *p<0.05, **p<0.01, ***p<0.001.

suggesting that fear extinction was not likely to determine the low levels of PMA observed in adolescents (Figure 3-4). Conditioned freezing levels were similar across ages, suggesting that developmental differences in PMA reflect differences in conditioned avoidance responses rather than in the strength of the association between the tone and the shock (Figure. 3-1j).

We next sought to determine if the low levels of PMA in adolescents reflected weaker learning. We provided adolescent mice with a second day of training and then tested them in a retrieval session on day 3. Even after two days of training, adolescent mice exhibited low levels of PMA (Figure 3-4b,c). This suggests that in adolescence, low levels of PMA are more likely to be determined by competing behavioral drives or altered consolidation rather than incomplete learning.

Neural dynamics underlying PMA across development

In humans and rodents, the mPFC, BLA, and NAc are key neural substrates for threat avoidance (Bravo-Rivera et al., 2014; Diehl et al., 2020; Boeke et al., 2017; Delgado et al., 2009). In adults, mPFC neurons encode threat-predictive cues, active avoidance behaviors and conditioned freezing. Activity in mPFC is required for active threat avoidance (Bravo-Rivera et al., 2014; Diehl et al., 2020; Capuzzo and Floresco, 2020). BLA encodes learned threat associations and is required for the expression of active avoidance behavior (Choi et al., 2010). NAc gates the expression of threat avoidance behavior through its outputs to midbrain centers (Floresco, 2015; Gale et al., 2004; Nonaka et al., 2014; Ramirez et al., 2015). But when and how these brain regions encode threat-predictive cues or threat-induced behaviors across development is poorly understood. To test this, we used fiber photometry to measure bulk calcium fluorescence as a proxy for neural activity in juvenile, adolescent, and adult mice.

In PL (Figure 3-5a), during PMA retrieval, mice of all ages had similar increases in PL activity during platform entries (Fig. 3-5b). However, once animals entered the safety platform, PL activity decreased to a greater extent in adults compared to juveniles and adolescents (Figure 3-5b). During threatening cues, adults had significantly higher activity at tone onset compared to

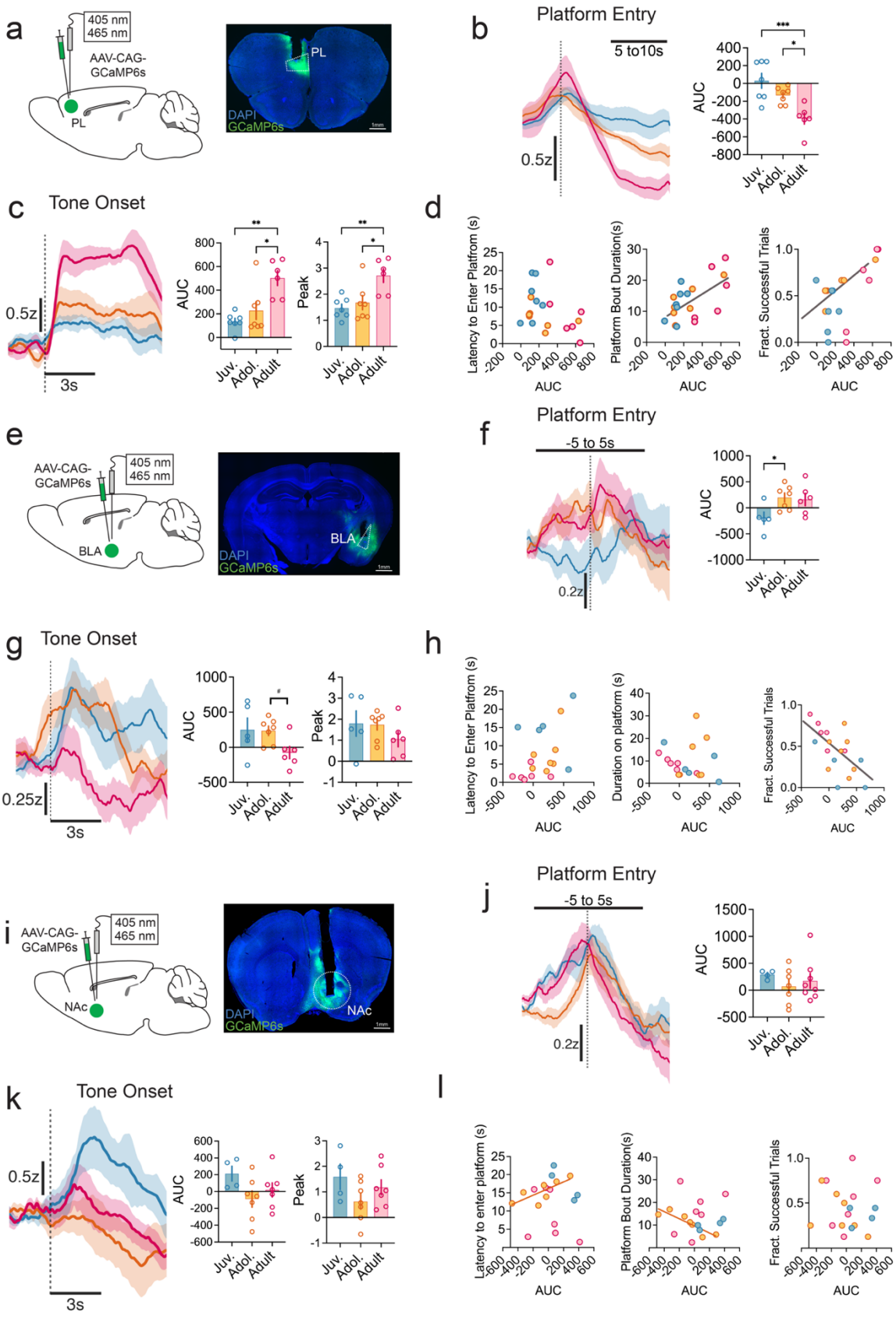
a
405 nm
465 nm
AAV-CAG-
GCaMP6s
PL
DAPI
GCaMP6s
b
Platform Entry
5 to10s
0.5z
AUC
Juv.
Adol.
Adult
c
Tone Onset
0.5z
3s
AUC
Peak
d
Latency to Enter Platfrom (s)
Platform Bout Duration(s)
Fract. Successful Trials
AUC
e
BLA
f
-5 to 5s
0.2z
g
Tone Onset
0.25z
h
Latency to Enter Platfrom (s)
Duration on platform (s)
i
NAc
j
k
l
Latency to enter platform (s)

Figure 3-5. Neural dynamics underlying PMA in PL, BLA and NAc. (A) Left: Schematic of AAV injection and optic fibre implant in PL. Right: Representative image showing GCaMP6s expression in PL neurons and fibre placement. (B) Averaged fluorescence changes (Z-score) surrounding platform entries (dotted line) across the entire retrieval session (9 tones total). Shading reflects between-subjects s.e.m. Quantification of area under the curve (AUC) 5 to 10 seconds after entry across ages: $F(2,17) = 10.66$, $P=0.0010$, One-way ANOVA with post hoc Tukey test. (C) Averaged Z-score in response to tone onset across the retrieval session, only when the animal was off of the platform. Quantification of AUC 3 seconds after tone onset: $F(2,17) = 10.19$, $P=0.0012$, One-way ANOVA with post hoc Tukey test. (D) Linear regression between the AUC during 3 seconds following tone onset and behavior (Latency: $F(1,18) = 2.739$, $P=0.115$, Bout Duration: $F(1,18) = 11.46$, $P=0.0033$, Successful trials: $F(1,18) = 8.99$, $P=0.0077$, Juvenile N=7, Adolescent=7, Adult N=6). (E) Left: Schematic of AAV injection and optic fibre implant in BLA. Right: Representative image showing GCaMP6s expression in BLA neurons and fibre placement. (F) Averaged Z-score surrounding platform entries (dotted line) across the retrieval session . Quantification of AUC 5 seconds before entry to 5 seconds after across ages: $F(2,15) = 3.88$, $P=0.045$, One-way ANOVA with post hoc Tukey test. (G) Averaged Z-score in response to tone onset across the retrieval session, only when the animal was off of the platform. Quantification of AUC 3 seconds after tone onset: $F(2,15) = 3.09$, $P=0.075$, One-way ANOVA with post hoc Tukey test. (H) Linear regression between the AUC during 3 seconds following tone onset and behavior (Latency: $F(1,16) = 3.48$, $P=0.081$, Bout Duration: $F(1,16) = 0.108$, $P=0.747$, Successful trials: $F(1,16) = 10.88$, $P=0.0045$, Juvenile N=4, Adolescent=7, Adult N=6). (I) Left: Schematic of AAV injection and optic fibre implant in NAc. Right: Representative image showing GCaMP6s expression in NAc neurons and fibre placement. Scale bars, 100μm. Data represent mean ± s.e.m, *p<0.05, **p<0.01, ***p<0.001.

juveniles and adolescents (Figure 3-5c). Looking across age groups, the area under the curve (AUC) of the tone response was positively correlated with platform bout duration and successful trials (Figure 3-5d). These data indicate that while PL encodes threat-induced behaviors beginning in juvenile stages, larger PL responses to unconditioned and conditioned stimuli, and more pronounced decreases in activity when the animal enters the safe location, contribute to the elevated levels of threat avoidance observed in adults.

In the BLA (Figure 3-5e), during PMA retrieval, activity in adolescents and adults ramped up during platform entries and then decreased once animals entered the safety platform. On the other hand, in juveniles, BLA activity increased only after they entered the safety platform. (Figure 3-5f). During the tone onset, activity in the BLA was greater in juveniles and adolescents, while adults showed a small onset response followed by a suppression (Figure 3-5g). The AUC of the tone onset response was negatively correlated with successful trials (Figure 3-5h), indicating that following a brief threat signal, low levels of BLA activity facilitate effective avoidance strategies in adults. These data also suggest that opposing BLA activity levels (i.e. high activity in adults vs. low activity in juveniles) facilitate PMA in different developmental stages.

In NAc (Fig. 3-5i), during PMA retrieval, all ages ramped up activity during entries onto the safety platform, and then decreased activity once animals were on the safety platform (Figure 3-5j). Minimal changes in activity at the onset of conditioned tones were observed during training, yet, juveniles had the largest tone onset responses during PMA retrieval (Figure 3-6, Figure 3-5k). In many adolescents, NAc activity decreased after tone onset and this suppression of NAc activity was associated with shorter latencies to enter the platform and shorter bout duration

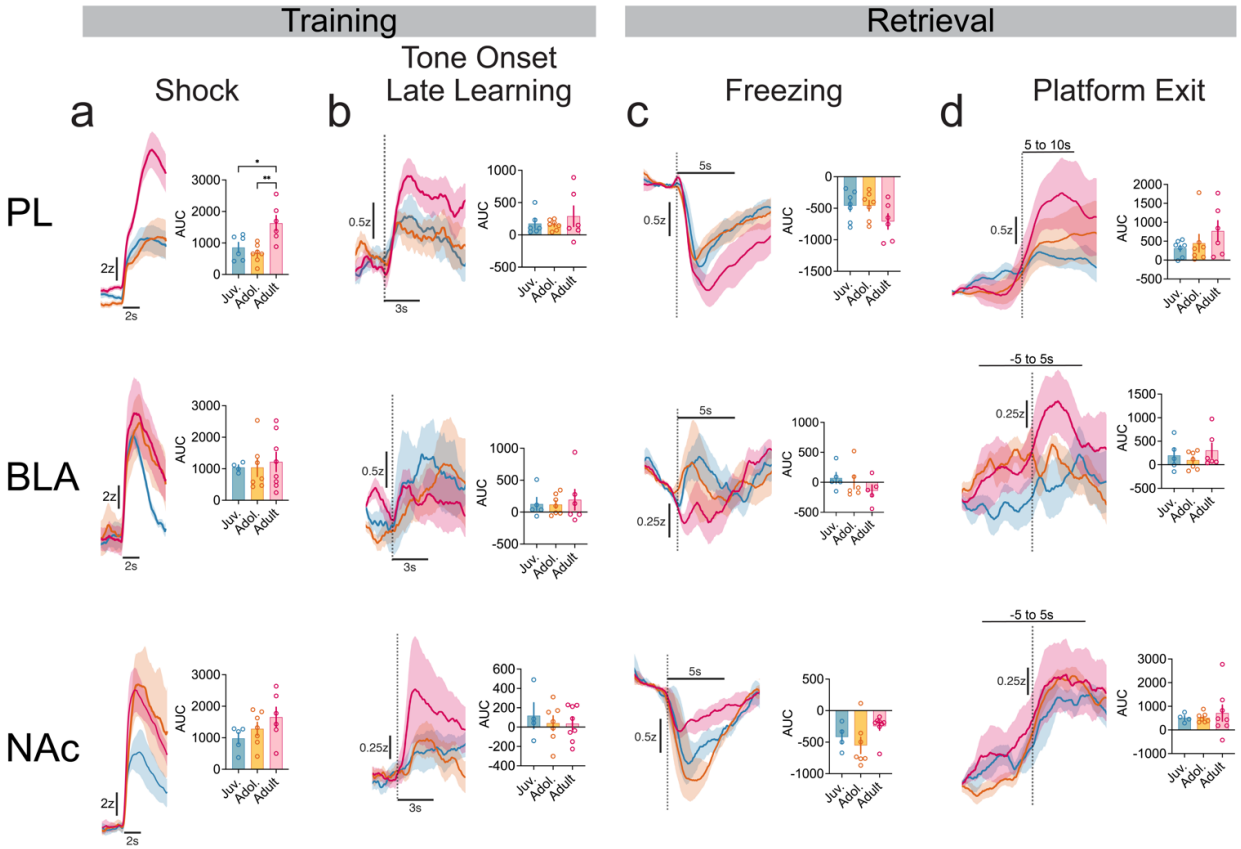

Figure 3-6. Neural dynamics during behavior events of interest. (A) Averaged Z-score in response to shock during training. Quantification of AUC 2 seconds following shock start across ages (PL: $F(2,16) = 8.49$, $P=0.0031$; BLA: $F(2.15)=1.07$, $P=0.208$; NAc: $F(2,16)=1.798$, $P=0.876$, One-way ANOVA with post hoc Tukey test. (B) Averaged Z-score in response to tone onset during tones 10-15 of training. Quantification of AUC 3 seconds following onset across ages (PL: $F(2,16) = 2.065$, $P=0.583$; BLA: $F(2,15)=0.709$, $P=0.876$; NAc: $F(2,16)=0.032$, $P=0.788$, One-way ANOVA with post hoc Tukey test. (C) Averaged Z-score during freezing bouts during retrieval session. Quantification of AUC 5 seconds following bout across ages (PL: $F(2,17) = 0.43$, $P=0.152$; BLA: $F(2,13)=0.077$, $P=0.376$; NAc: $F(2,16)=0.824$, $P=0.106$, One-way ANOVA with post hoc Tukey test. (D) Averaged Z-score during platform exits during retrieval session. Quantification of the difference between AUC 5 seconds after exit and 5 seconds before the exit (PL: $F(2,17) = 0.636$, $P=0.046$; BLA: $F(2,16)=2.083$, $P=0.217$, One-way ANOVA with post hoc Tukey test). Quantification of total AUC from 5 seconds before exit through 5 seconds after NAc: $F(2,15)=0.284$, $P=0.481$, One-way ANOVA with post hoc Tukey test). Data represent mean ± s.e.m, *$p<0.05$, ***$p<0.001$.

(Figure 3-5l). No such relationships between NAc activity and behavior were observed in the other age groups. This suggests that in adolescence, low levels of threat avoidance are encoded in NAc activity.

Manipulations of PL-BLA projections during PMA across development

Others have shown that in adult mice, PL-BLA projection neurons encode conditioned tones and threat avoidance behaviors (Jercog et al., 2021; Kajs et al., 2022), and that activating PL-BLA projections enhances threat avoidance levels (Diehl et al., 2020). Human fMRI studies indicate that there is a developmental switch in PFC-amygdala functional connectivity between childhood and adulthood (Gee et al., 2013). However, the circuit basis for these developmental changes in PFC-BLA connectivity and how they causally affect behavior throughout early life

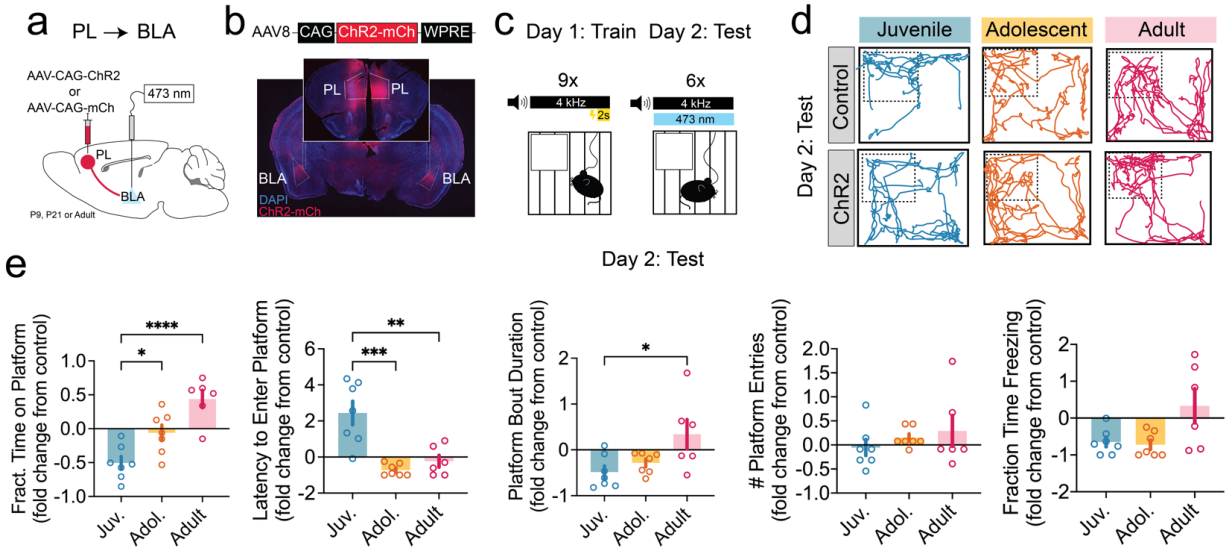

Figure 3-7. Manipulating PL-BLA during PMA across development. (A) Schematic of AAV injection into PL and optic fibre implant over BLA. (B) Representative image showing ChR2-mCherry expression in PL neurons and axon terminals in BLA. (C) Protocol for stimulating PL-BLA axonal projections during PMA. (D) Representative mouse trajectory maps during tones in the retrieval test with PL-BLA activation. (E) Summary data for behavior with PL-BLA stimulation during PMA retrieval (Time on Platform: $F(2,17) = 16.78$, $P<0.0001$; Latency: $F(2,17)=15.61$, $P=0.0001$; Bout Duration: $F(2,17)=4.74$, $P=0.02$; Entries: $F(2,17)=0.74$, $P=0.49$; Freezing: $F(2,17)=4.78$, $P=0.02$; One-way ANOVA with post hoc Tukey test, Juvenile N=8 control, N=7 ChR2, Adolescent N=7 control, N=7 ChR2, Adult N=7 control, N=6 ChR2).Data represent mean ± s.e.m, *p<0.05, **p<0.01, ***p<0.001.

remain unknown. We used optogenetics to investigate how the PL-BLA pathway influences threat avoidance across development.

We hypothesized that elevating activity in the PL-BLA pathway could increase PMA levels in juvenile and adolescent mice. To test this, we injected AAV-ChR2 or an AAV-mCherry control virus into PL and implanted bilateral optic fibres above BLA (Figure 3-7a,b). Two weeks after the viral injection, we trained juvenile, adolescent or adult mice in PMA without optogenetic stimulation. Then, during the retrieval session, we paired tone presentations with blue laser pulses (50 ms, 15 Hz, 10mA) to activate PL axon terminals in BLA while recording animal behavior (Figure 3-7c,d). All mice learned PMA (Figure 3-8a).

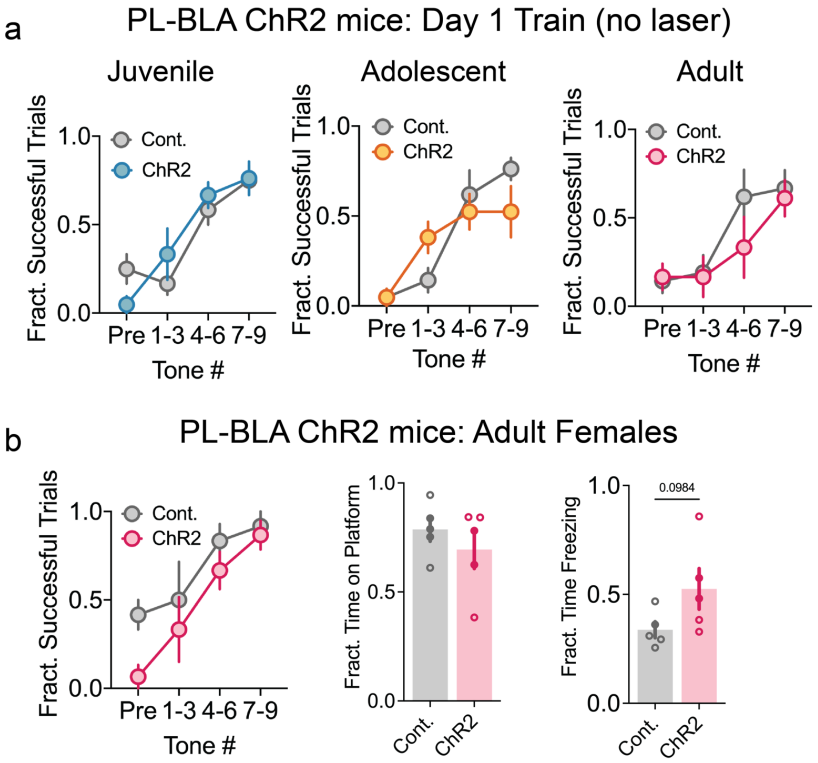

Figure 3-8. Training day behavioral data for PL-BLA ChR2 and JAWS mice. (A) Fraction of successful trials during PMA training (laser off) for juvenile, adolescent for PL-BLA ChR2 stimulation experiments (Juvenile: $F_{trial}(3,39)=22.28$, $P<0.0001$; $F_{virus}(1,13)=0.06$, $P=0.82$; $F_{int}(3,39)=1.64$, $P=0.2$, Cont. N=8, ChR2: N=7; Adolescent: $F_{trial}(2.4,29)=17.65$, $P<0.0001$; $F_{virus}(1,12)=0.14$, $P=0.72$; $F_{int}(3,39)=2.3$, $P=0.09$, Cont. N=7, ChR2: N=7; Adult: $F_{trial}(1.6,17.8)=17.84$, $P=0.006$; $F_{virus}(1,11)=1.57$, $P=0.24$; $F_{int}(3,33)=0.6$, $P=0.59$, Cont. N=7, ChR2: N=6; 2-way ANOVA with Sidak multiple comparisons test). (B) Summary data for female adults for PL-BLA ChR2 stimulation experiments ($F_{trial}(1.570,10.99) = 11.25$, $P=0.0033$, $F_{Virus}(1,7)=4.481$, $P=0.0720$, Two-way ANOVA; Time on platform: $P=0.3978$; Freezing: $P=0.0984$, Cont. N=5, ChR2: N=5, Unpaired T-test). Data represent mean ± s.e.m.

To compare the effects of optogenetic stimulation on PMA across development, we quantified how much time mice spent on the platform during presentations of the tone, the latency to enter the platform after tone onset, the number of platform entries per tone, and the platform bout duration. To compare across ages, for each measurement, we normalized the values for the ChR2 group to the mean of the age-matched control group and plotted the fold change. Consistent with previous studies, we found that activating the PL-BLA pathway in adults increased PMA, increasing time spent on the platform and decreasing the latency to enter the platform (Fig 3e). Of note, we only observed these effects in adult males. We did not observe further increases in PMA in female mice, which may have been due to a ceiling effect (Figure 3-8b). We did not observe sex differences in juveniles or adults, so grouped the sexes for those analyses.

Surprisingly, in juveniles, activating the PL-BLA pathway decreased the amount of time mice spent on the platform, increased the latency to enter the platform, and decreased the number of platform entries per tone and platform bout duration (Figure 3-7e). We observed an intermediate phenotype in adolescents. Similar to what we observed in adults, activating PL-BLA during presentations of the tone in adolescents decreased their latency to enter the platform and slightly increased the number of platform entries per tone. However, this manipulation also decreased the platform bout duration. So even though adolescent mice entered the safety

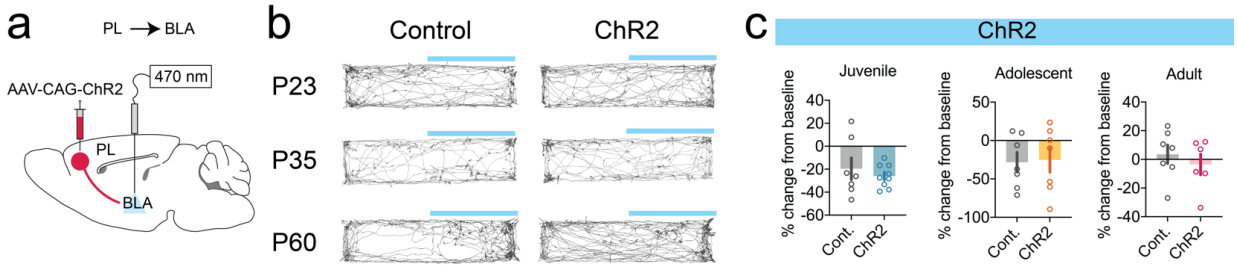

Figure 3-9. Real time place preference for PL-BLA ChR2 and JAWS mice. (A) Schematic of AAV-ChR2 injection into PL and optic fibre implant over BLA. (B) Representative mouse trajectory maps during RTPP forwith PL-BLA stimulation for control and ChR2-expressing mice. (C) Summary data of percent change from baseline occupancy in laser-paired chamber for PL-BLA ChR2 stimulation experiments (Juvenile: P=0.84, Cont. N=7, ChR2: N=9; Adolescent: P=0.80, Cont. N=7, ChR2: N=7; Adult: P=0.45, Cont. N=7, ChR2: N=6; Mann-Whitney U Test). Data represent mean ± s.e.m.

platform with shorter latency than controls, they left the platform more quickly. As a result, activating PL-BLA in adolescents had no net effect on time spent on the platform compared to age-matched controls (Figure 3-7e). We did not observe differences between ChR2-expressing mice and controls in real time place aversion assay (Figure 3-9), suggesting that the activation of the PL-BLA pathway was not innately aversive at any age.

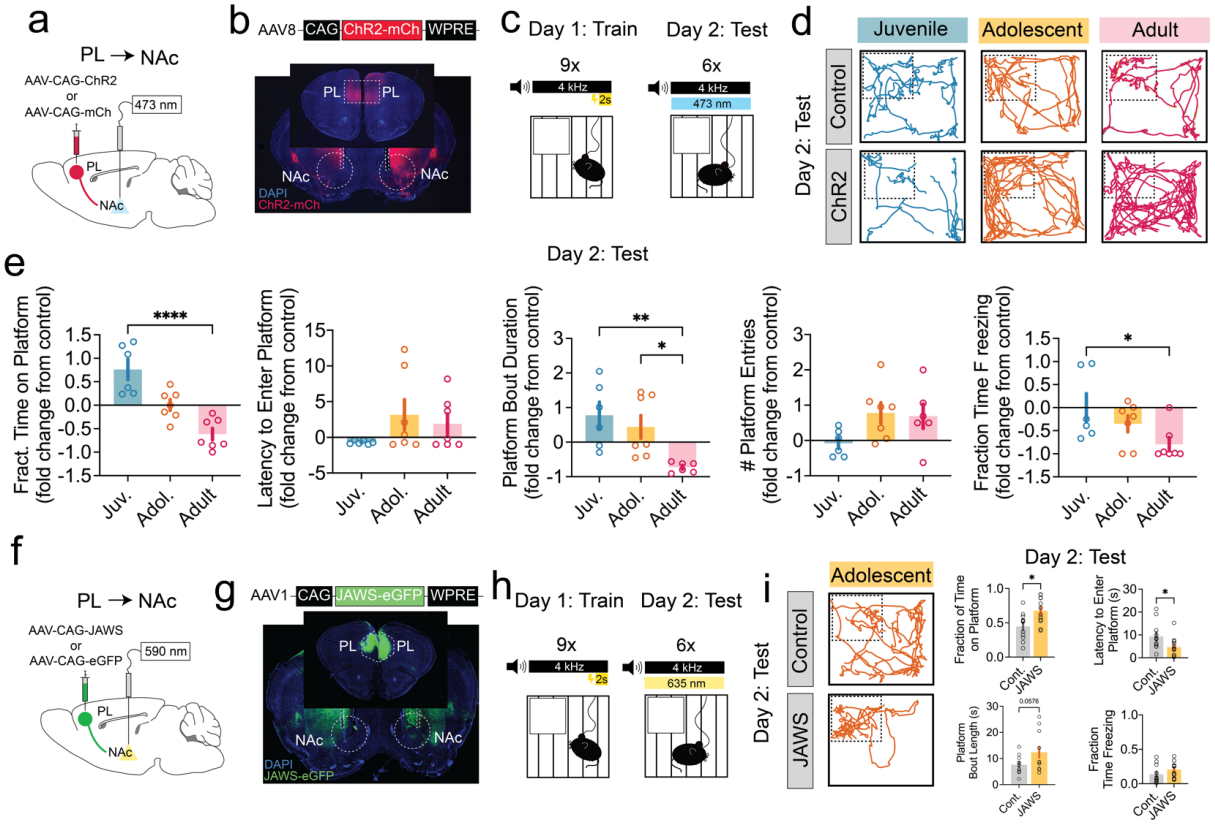

Figure 3-10. Manipulating PL-NAc during PMA across development. (A) Schematic of AAV injection into PL and optic fibre implant over NAc. (B) Representative image showing ChR2-mCherry expression in PL neurons and axon terminals in NAc. (C) Protocol for stimulating PL-NAc axonal projections during PMA. (D) Representative mouse trajectory maps during tones in the retrieval test with PL-NAc activation. (E) Summary data for behavior during PMA retrieval with PL-NAc axon terminal stimulation (Time on Platform: $F(2,17)=20.17$, $P<0.0001$; Latency: $F(2,17)=1.56$, $P=0.24$; Bout Duration: $F(2,16)=6.66$, $P=0.0079$; Entries: $F(2,16)=2.92$, $P=0.07$; Freezing: $F(2,17)=3.59$, $P=0.05$; One-way ANOVA with post hoc Tukey test, Juvenile N=10 control, N=7 ChR2, Adolescent N=6 control, N=7 ChR2, Adult N=6 control, N=7 ChR2). (F) Schematic of AAV-JAWS injection into PL and optic fiber implant over NAc. (G) Representative image showing JAWS-eGFP expression in PL neurons and axon terminals in NAc. (H) Protocol for PL-NAc axon terminal inhibition during PMA. (I) Representative mouse trajectory maps during tones in the retrieval test with PL-NAc axon terminal inhibition. (J) Summary data for behavior during PMA retrieval (Time on Platform: $P=0.01$; Latency: $P=0.04$, Bout Duration: $P=0.057$, Freezing:$P=0.20$; Welch's two-tailed t-test, N=11 control, N=12 JAWS). Data represent mean ± s.e.m, *p<0.05, **p<0.01, ****p<0.0001.

Manipulations of PL-NAc projections during PMA across development

In contrast to the PL-BLA pathway, activating the PL-NAc projections decreases threat avoidance behaviour in adult rats (Diehl et al., 2020). But their functions in the developing brain are unknown. To investigate this, we used optogenetics to activate PL-NAc projections during PMA in juvenile, adolescent or adult mice. As before, we injected AAV-ChR2 or AAV-mCherry into PL two weeks before PMA training and then implanted optic fibres above NAc 4 days before PMA training. We trained mice in PMA without laser stimulation. During the retrieval session, we paired presentations of the conditioned tone with 15 Hz laser stimulation to activate PL axon terminals in NAc (Fig. 3-10a-c). All groups learned PMA (Extended Data Fig. 4.1a).

To determine the effects of PL-NAc activation during the retrieval session, we again quantified avoidance behaviors and normalized ChR2 mice to age-matched controls. Consistent with previous studies, we found that in adults, activating PL-NAc projections decreased time spent on the platform (Fig. 3-10d). This effect was mainly due to decreases in the platform bout duration, as we observed no changes in the latency to enter the platform or in the number of platform entries (Fig. 3-10e). Taken together with our PL-BLA data (Fig 3-7), these findings point to a

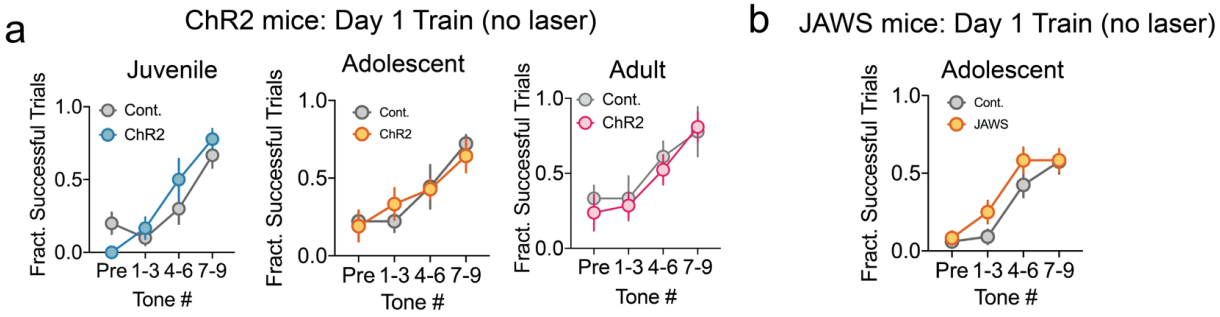

Figure 3-11. Training day behavioral data for PL-NAc ChR2 and JAWS mice. (A) Fraction of successful trials during PMA training (laser off) for juvenile, adolescent for PL-NAc ChR2 stimulation experiments (Juvenile: $F_{trial}(3,42)=20.11$, $P<0.0001$; $F_{virus}(1,14)=0.06$, $P=0.82$; $F_{int}(3,39)=1.64$, $P=0.2$, Cont. N=10, ChR2: N=6; Adolescent: $F_{trial}(1.9,21.8)=11.99$, $P=0.0003$; $F_{virus}(1,11)=0.003$, $P=0.96$; $F_{int}(3,33)=0.44$, $P=0.72$, Cont. N=6, ChR2: N=7; Adult: $F_{trial}(2.1,23.4)=7.55$, $P=0.003$; $F_{virus}(1,11)=0.68$, $P=0.42$; $F_{int}(3,33)=0.11$, $P=0.95$, Cont. N=6, ChR2: N=7; 2-way ANOVA with Sidak multiple comparisons test). (B) Fraction of successful trials during PMA training (laser off) for adolescent PL-NAc JAWS inhibition experiment ($F_{trial}(2.5,53.76)=37.67$, $P<0.0001$; $F_{virus}(1,21)=1.84$, $P=0.19$; $F_{int}(3,63)=1.06$, $P=0.37$, Cont. N=11, JAWS: N=12; 2-way ANOVA with Sidak multiple comparisons test). Data represent mean ± s.e.m.

functional dissociation in which PL-BLA promotes entering and staying on the platform and activating PL-NAc promotes platform exits without affecting entries.

Similar to what we observed with the PL-BLA pathway, activating PL-NAc in juveniles produced opposing behavioral effects compared to adults. Compared to age-matched controls, juveniles spent more time on the platform and entered with shorter latency (Fig. 3-10e). Activating PL-NAc during retrieval had no effect on how much time adolescent mice spent on the safety platform, but we observed mild increases in the latency to enter the platform and in the number of platform entries (Fig 3-10e). However, since they already exhibited low levels of avoidance, we hypothesized that the lack of change in time spent on the platform may be due to a ceiling effect. If the PL-NAc was already highly active during the tone, further activating that pathway may not produce observable behavioral effects. To test this, we used the inhibitory opsin JAWS to silence PL-NAc in adolescent mice during the retrieval session (Figure 3-10f-h, Figure 3-11b). Silencing PL-NAc projections during presentations of the conditioned tone increased the time mice spent on the safety platform by decreasing their latency to enter the platform and mildly increasing platform bout length (Figure 3-10i), Further, we found that activating the PL-NAc pathway produced a place preference in adolescent mice but not in juveniles or adults. These data suggest that during adolescence, elevated activity, and unique rewarding properties in the PL-NAc pathway contributes to lower levels of avoidance in response to threatening cues.

Synaptic development of the PL-BLA and PL-NAc pathways

Synapse density and electrophysiological properties of neurons within mPFC undergo major changes throughout early life (Drzewiecki et al., 2016; Kroon et al., 2019; Delevich et al, 2018). Less is known about synapse maturation in mPFC output circuits. A previous study showed that the PL-BLA pathway undergoes a protracted maturation with axons continuing to elaborate in BLA and synaptic excitation strengthening through adolescence (Arruda-Carvalho et al., 2017). We sought to examine synaptic development in the PL-NAc pathway and how its trajectory aligns with maturation of the PL-BLA pathway. We compared the synaptic density and synaptic strength

in the PL-BLA and PL-NAc pathways across development to understand how they jointly contribute to changes in threat avoidance behaviors.

We first set out to determine how PL axonal and synaptic density in BLA and NAc changes across the ages of interest. We injected into PL a viral vector designed to label presynaptic puncta and axons with bright green and red fluorophores, respectively (Figure 3-13a). Allowing approximately two weeks for viral expression, we then perfused mice at P23, P35 or P60, immunostained brain sections, and imaged axons and putative presynaptic puncta in BLA and NAc using a confocal microscopy (Figure 3-13b). In BLA, PL axon density decreased significantly between adolescence and adulthood and we observed a similar trend in NAc (Figure 3-13c,d). In PL-BLA axons, we observed a small increase in the number of presynaptic boutons per axon length in adults (Figure 3-13d), suggesting that while many PL-BLA axons are pruned throughout adolescence, the remaining axons make additional synaptic contacts.

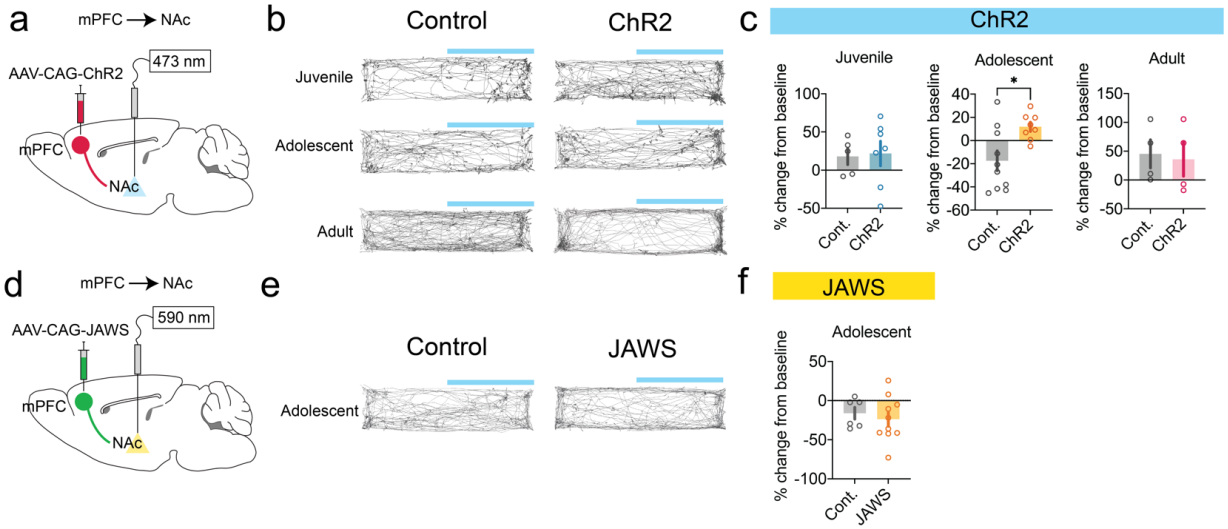

Figure 3-12. Real time place preference for PL-NAc ChR2 and JAWS mice. (A) Schematic of AAV-ChR2 injection into PL and optic fibre implant over NAc. (B) Representative mouse trajectory maps during RTPP forwith PL-NAc stimulation for control and ChR2-expressing mice. (C) Summary data of percent change from baseline occupancy in laser-paired chamber for PL-NAc ChR2 stimulation experiments (Juvenile: P=0.76, Cont. N=5, ChR2: N=7; Adolescent: P=0.02, Cont. N=10, ChR2: N=8; Adult: P=0.66, Cont. N=4, ChR2: N=4; Mann-Whitney U Test). (D) Schematic of AAV-JAWS injection into PL and optic fibre implant over BLA. (E) Representative mouse trajectory maps during RTPP forwith PL-BLA inhibition for control and JAWS-expressing mice. (F) Summary data of percent change from baseline occupancy in laser-paired chamber for PL-NAc JAWS inhibition experiment (Adolescent: P=0.37, Cont. N=6, ChR2: N=10; Mann-Whitney U Test). Data represent mean ± s.e.m, *p<0.05.

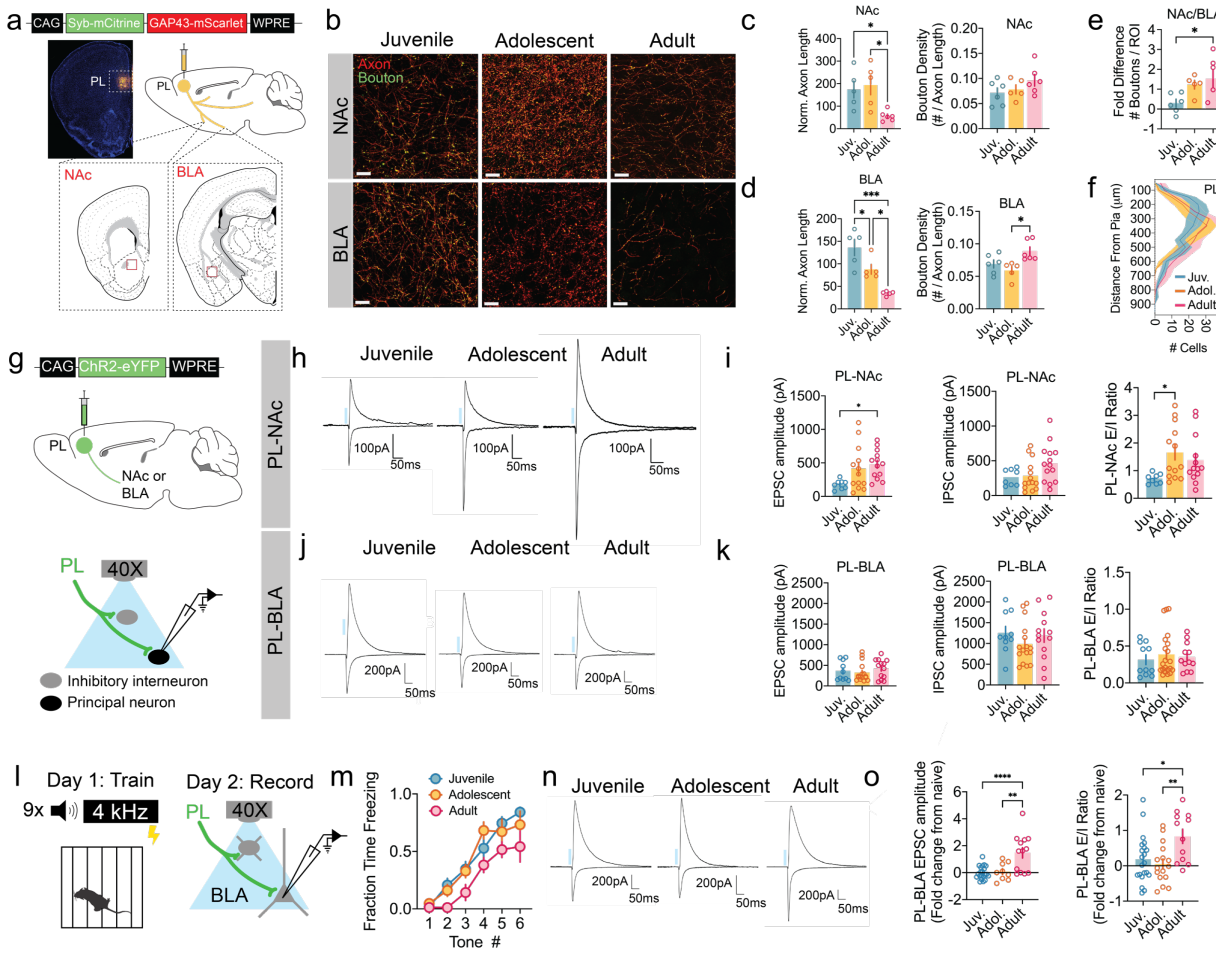

Figure 3-13. Synaptic development of PL-NAc and PL-BLA pathways. (A) Schematic of AAV-CONVERGed injection into PL and patch clamp recording configuration. (B) Representative images of axons and Syb puncta in BLA and NAc.(C) Summary data of axon and bouton density in NAc in juvenile, adolescent and adult mice (Axon Density: $F(2,14) = 2.437$, $P=0.1237$ Bouton Density: $F(2,14) = 1.607$, $P=0.2354$; One-way ANOVA). (D) Summary data of axon and bouton density in BLA in juvenile, adolescent and adult mice (Axon Density: $F(2,14) = 10.48$, $P=0.0017$; Bouton Density: $F(2,14) = 05.791$, $P=0.0147$; One-way ANOVA). (E) Fold difference in number of boutons per each ROI between NAc and BLA ($F(2,14) = 4.097$, $P=0.0398$; One-way ANOVA; Juvenile N=6 mice, Adolescent N=5 mice, Adult N=6 mice). (F) Quantification of fluorescence across PL layers of injection site ($F_{distanc}(19,280)=105.8$, $P<0.0001$, $F_{age}(2,280)=1.43e-03$, >0.99, Two-way ANOVA). (G) Schematic of AAV-ChR2 injection into PL and patch clamp recording configuration. (H) Representative PL-evoked EPSCs (V_m=70mV) and IPSCs (V_m=0mV) recorded in NAc medium spiny neurons in juvenile, adolescent and adult mice. (I) Summary data of PL-evoked synaptic currents in NAc across development (EPSC: $F(2,31)=3.84$, $P=0.03$; IPSC: $F(2,33)=2.92$, $P=0.07$; E/I ratio: $F(2,31)=3.33$, $P=0.049$; One-way ANOVA with post hoc Tukey test; Juvenile N=8 cells from 5 mice; Adolescent N=14 cells from 4 mice; Adult N=14 cells from 4 mice). (J) Representative PL-evoked EPSCs (V_m=70mV) and IPSCs (V_m=0mV) recorded in BLA pyramidal neurons in juvenile, adolescent and adult mice. (K) Summary data of PL-evoked synaptic currents in BLA pyramidal cells across development (EPSC: $F(2,36)=0.66$, $P=0.52$; IPSC: $F(2,36)=0.94$, $P=0.4$; E/I ratio: $F(2,41)=0.29$, $P=0.75$; One-way ANOVA with post hoc Tukey test; Juvenile N=11 cells from 5 mice; Adolescent N=16 cells from 4 mice; Adult N=13 cells from 4 mice). (L) Schematic of fear conditioning followed by patch clamp recording configuration for recording PL-evoked synaptic currents in BLA. (M) Summary data of freezing during fear conditioning ($F_{trial}(5,60)=54.4$, $P<0.0001$; $F_{age}(2,12)=4.7$, $P=0.03$; $F_{int}(10,60)=1.01$, $P=0.45$; Two-way ANOVA; Juvenile N=6 mice; Adolescent N=5 mice; Adult N=4

mice). (N) Representative PL-evoked EPSCs (Vm=70mV) and IPSCs (Vm=0mV) recorded in BLA pyramidal neurons in fear conditioned juvenile, adolescent and adult mice. (O) Summary data of PL-evoked synaptic currents in BLA pyramidal cells across development calculated as fold change from naive (trained/$mean_{naive}$-1) (EPSC: $F(2,40)=12.3$, $P<0.0001$; E/I ratio: $F(2,46)=5.66$, $P=0.006$; One-way ANOVA with post hoc Tukey test; Juvenile N=21 cells from 6 mice; Adolescent N=16 cells from 5 mice; Adult N=13 cells from 4 mice). Data represent mean ± s.e.m, *p<0.05, **p<0.01, ***p<0.001, ****p<0.0001.

To investigate if the relative PL innervation of BLA vs. NAc differs by age, we calculated the fold difference in the bouton density in BLA vs. NAc in individual mice. We found that while juveniles had similar bouton density between the two structures – their fold differences averaged near zero – adolescents and especially adults had greater bouton density in NAc relative to BLA (Figure 3-13e). In PL, neurons that project to BLA are enriched in superficial layers while neurons that project to NAc are spread across layers. We did not observe significant differences in the layer distribution of AAV-transduced PL neurons between age groups (Figure 3-13f), suggesting that a faster rate of pruning in the PL-BLA vs. PL-NAc pathway may contribute to the observed developmental differences in the relative bouton densities.

Next, we used channelrhodopsin-assisted circuit mapping to determine how the strength of synaptic transmission in PL-BLA and PL-NAc pathways changes over development (Petreanu et al., 2007). In naive mice, we injected AAV-ChR2 into PL. Allowing two weeks for viral expression, we then prepared acute brain slices from juvenile, adolescent, or adult mice. We performed whole cell patch clamp recordings from neurons in BLA or NAc, recorded excitatory and inhibitory postsynaptic currents (EPSCs and IPSCs) evoked by optogenetically stimulated invading PL axon terminals (Figure 3-13g). In the PL-NAc pathway, the amplitude of EPSCs increased significantly between P23 and P35 and remained high until P60. On the other hand, the amplitude of IPSCs increased between P35 and P60. As a result, the ratio of excitatory to inhibitory currents (E/I ratio) in the PL-NAc pathway was significantly higher in adolescents and adults compared to juvenile mice (Figure 3-13h,i). In the PL-BLA pathway, we observed modest increases in the amplitude of EPSCs and IPSCs from P35 to P60, but no changes in the E/I ratio

across those ages (Figure 3-13j,k). These data suggest that different rates of synaptic development in the PL-NAc and PL-BLA pathways may contribute to differences in learned avoidance behavior.

Previous studies showed that in adults, cued fear conditioning enhances the E/I ratio in the PL-BLA pathway[40], suggesting that learning reorganizes top-down circuits. We performed a similar experiment to determine if the capacity for such plasticity changes over development. As described above, we injected AAV-ChR2 into PL. Two weeks later, when mice were juveniles, adolescents or adults, we performed auditory fear conditioning. This experimental design ensured that each mouse received the same number of footshocks, which can induce plasticity on their own. The next day, we prepared acute brain slices, performed whole cell patch clamp recordings from BLA principal neurons, and recorded EPCs and IPSCs evoked by optogenetic stimulation of PL axon terminals (Figure 3-13l). Mice of all ages significantly increased their freezing levels during fear conditioning (Figure 3-13m). However, we only observed changes in PL-BLA synaptic strength in adult mice. For each age group, we calculated fold-change in the strength of postsynaptic currents and the E/I ratio compared to naive controls (Figure 3-13k). In adults, but not in juveniles or adolescents, we observed a significant fold increase in EPSC amplitude and in the E/I ratio (Figure 3-13n,o), suggesting that adult-specific circuit-level plasticity in the PL-BLA pathway contributes to their elevated levels of PMA.

DISCUSSION

We find that rather than following a linear trajectory in which threat avoidance becomes continually more robust with age, adolescent mice have lower expression of learned avoidance than both their younger juvenile counterparts and adults. Juveniles reduce their threat avoidance behavior rapidly across a PMA session, suggesting they have weaker threat memories than adults. In the juvenile stage, when individuals rely on caregivers for protection and the mPFC circuitry necessary to contextualize aversive experiences remains immature,

weaker threat memories may actually prevent dysfunctional behaviors from developing. Risky exploration in adolescence is conserved across many species, suggesting it plays a key role in behavioral and brain development. Lower levels of threat avoidance in adolescence may facilitate dispersal from parental care, allow individuals to prioritize other behaviors such as foraging and socializing, and facilitate investigation of potential threats to shape future behaviors. However, how neural circuit maturation enables these developmental transitions was unknown. Here, for the first time, we established direct causal links between the maturation of frontolimbic circuits and developmental changes in threat avoidance behavior. We mapped the relative developmental trajectories of mPFC projections to BLA and NAc and revealed how they jointly determine age-specific behavioral repertoires. Our data suggests that pronounced rearrangements of frontolimbic circuits, as opposed to linear strengthening with age, underlies developmental milestones in threat avoidance behavior.

We were surprised that optogenetically activating PL-BLA and PL-NAc projections had opposite effects in juveniles compared to adults. Previous studies showed that PL-BLA axons prune between late adolescence and adulthood, but the relative development in the PL-NAc pathway was unknown (Arruda-Carvalho et al., 2017; Cressman et al., 2010). Using viral circuit tracing and synaptic physiology, we showed that, in juveniles, PL neurons make many weak synapses in BLA and NAc that are pruned between adolescence and adulthood. In adults, BLA projections to NAc and NAc projections to substantia nigra promote threat avoidance, suggesting that during threatening cues, PL preferentially activates particular classes of BLA and NAc projection neurons to promote avoidance (Ramirez et al., 2015; Hormigo et al., 2016). In juveniles, the initial overproduction of synapses may connect PL axon terminals with many classes of BLA and NAc projection neurons. Optogenetic activation of PL-BLA and PL-NAc projections may therefore cause opposing effects in juveniles compared to adults by exciting BLA and NAc neurons involved in competing behaviors. These results suggest that during threat avoidance in juveniles, a small subset of PL neurons with specific connectivity in BLA and

NAc are weakly activated by threatening cues to promote avoidance, albeit to a lesser extent than in adults. Our fiber photometry recordings support this idea.

Our fiber photometry recordings revealed that in juveniles and adolescents, during threatening cues, PL is weakly activated compared to adults. Also, adults had greater suppression of PL activity following entries onto the safety platform compared to both juveniles and adolescents. Weaker activation during the threatening cues was correlated with shorter platform stays and fewer successful trials, suggesting a causal relationship between PL dynamics and age-specific behavioral repertoires. Maturation of ascending connectivity from BLA may contribute in part to these observed age-specific differences. BLA activity is required for sustained tone responses in PL in adulthood, suggesting a potential role of this reciprocal circuit in PMA (Jercog et al., 2021). While we observed larger, more prolonged tone responses in BLA in juveniles and adolescents compared to adults, more investigation is needed to determine what neuronal classes contribute to this activity. Ascending BLA-PL projection neurons, which are preferentially connected to PL-BLA neurons, may only be weakly activated by threatening cues in juveniles (Little and Cartar; 2013).

In adolescents, a faster pace of synaptic development in the PL-NAc pathway compared to PL-BLA along with functional changes within NAc itself drove lower levels of threat avoidance. Our optogenetics studies revealed that elevated activity in the PL-NAc pathway contributed to lower levels of threat avoidance levels in adolescents. We also found that higher levels of NAc activity during threatening cues was correlated with longer latencies to enter the safety platform and shorter platform stays. We only observed these relationships in adolescents, suggesting NAc activity is a primary driver of adolescent-specific behaviors. Developmental increases in synaptic excitation in the PL-NAc pathway occurred earlier as compared to synaptic excitation in the PL-BLA pathway and compared to synaptic inhibition in the PL-NAc pathway. This relative enhancement of excitatory synaptic connectivity in the PL-NAc pathway may define a key window of development when PL-NAc activity has an outsized influence on

behavior, promoting risky exploration at the expense of threat avoidance. This previously unknown synaptic mechanism may contribute to increased risky behaviors across species (Warkentin et al., 1999; Hinke et al., 2020; Tymula et al., 2012; Laviola et al., 2003).

Important considerations when interpreting this work are that prefrontal projection pathways comprise neurons with heterogeneous molecular identities and axon collateral targeting (Gao et al., 2022). Despite PL-BLA and PL-NAc excitation having opposing effects in our results, there exists a population of PL neurons that projects to both BLA and NAc (Gao et al., 2022). How specific classes of neurons within these pathways contribute to avoidance is not understood. Further, the identity and behavioral relevance of neurons in BLA and NAc that PL terminals synapse onto, and how these connections may reorganize throughout development is an important topic for further research.

In humans and rodents, the juvenile and adolescent periods are sensitive windows when stressors can perturb brain development and threat-induced behaviors (Tottenham and Galvan et al., 2016; Gerhard et al., 2021). In humans, developmental and stress-induced changes in functional connectivity, region volume, and task-dependent dynamics have pointed to PFC, amygdala, and NAc as sensitive regions where external factors may alter activity, contributing to psychiatric diseases (Tottenham and Galvan et al., 2016; Gee et al., 2013; 2016). In rodents, chronic stress occurring in the juvenile and adolescent period leads to later alterations in spine density, interneuron function, and neurotransmission within mPFC, BLA and NAc (Pinzon-Parra et al., 2019; Yuen et al., 2012; Hill et al., 2014; Negron-Oyarzo et al., 2014). However, most studies focus on adult outcomes or use ex-vivo measurements to correlate neuronal and behavioral changes. The lack of studies of the in vivo, causal functions mPFC, BLA and NAc in the developing brain have left a major gap in our understanding of how interactions between these regions produce developmental transitions in threat-induced behaviors. Our findings address this critical gap, delineating the developmental trajectories of PL-BLA and PL-NAc pathways and causally linking their function to age specific avoidance phenotypes. In

understanding the processes by which these circuits mature to control avoidance, we have a foundation to understand how they can become disrupted.

Chapter 4: Brain-wide projections and differential encoding of prefrontal neuronal classes underlying learned and innate threat avoidance

ABSTRACT

To understand how the brain produces behavior, we must elucidate the relationships between neuronal connectivity and function. The medial prefrontal cortex (mPFC) is critical for complex functions including decision-making and mood. mPFC projection neurons collateralize extensively, but the relationships between mPFC neuronal activity and brain-wide connectivity are poorly understood. We performed whole-brain connectivity mapping and fiber photometry to better understand the mPFC circuits that control threat avoidance in male and female mice. Using tissue clearing and light sheet fluorescence microscopy, we mapped the brain-wide axon collaterals of populations of mPFC neurons that project to nucleus accumbens (NAc), ventral tegmental area (VTA), or contralateral mPFC (cmPFC). We present DeepTraCE, for quantifying bulk-labeled axonal projections in images of cleared tissue, and DeepCOUNT, for quantifying cell bodies. Anatomical maps produced with DeepTraCE aligned with known axonal projection patterns and revealed class-specific topographic projections within regions. Using TRAP2 mice and DeepCOUNT, we analyzed whole-brain functional connectivity underlying threat avoidance. PL was the most highly connected node with functional connections to subsets of PL-cPL, PL-NAc and PL-VTA target sites. Using fiber photometry, we found that during threat avoidance, cmPFC and NAc-projectors encoded conditioned stimuli, but only when action was required to avoid threats. mPFC-VTA neurons encoded learned but not innate avoidance behaviors. Together our results present new and optimized approaches for quantitative whole-brain analysis and indicate that anatomically-defined classes of mPFC neurons have specialized roles in threat avoidance.

INTRODUCTION

The medial prefrontal cortex (mPFC) is a vastly interconnected brain region that controls complex functions including memory, decision making, and mood (Euston et al., 2012; Giustino and Maren, 2015; Klune et al., 2021). Through its axonal projections, mPFC exerts top-down control over downstream regions, promoting adaptive responses in dynamic circumstances (Ye et al., 2016; Kim et al., 2017; Murugan et al., 2017; Otis et al., 2017a; Jayachandran et al., 2019; Diehl et al., 2020). While studies have linked individual mPFC projections to discrete behavioral functions (Warden et al., 2012; Riga et al., 2014; DeNardo et al., 2015; Ye et al., 2016; Kim et al., 2017; Murugan et al., 2017; Otis et al., 2017b; Vander Weele et al., 2018; Siciliano et al., 2019; Diehl et al., 2020; Mathis et al., 2021), mPFC neurons are anatomically heterogenous, with extensive axon collaterals (Gao et al., 2022). Many mPFC-dependent behaviors involve coordinated activity in multiple downstream brain regions (Kim et al., 2015). Because of its role in survival behaviors and neuropsychiatric disorders (Euston et al., 2012; Giustino and Maren, 2015; Klune et al., 2021), there is an urgent need to integrate mPFC neuroanatomy with functional studies to understand how classes of mPFC projection neurons contribute to behavior. To address this, we developed new approaches for whole brain circuit mapping. By combining these approaches with fiber photometry, we examine the unique roles of three mPFC cell classes in learned threat avoidance, a survival behavior that is highly relevant to fear and anxiety disorders (Diehl et al., 2019).

Many studies use retrograde viral approaches to manipulate or observe the activity of projection-defined populations (Zhang et al., 2011; Roth, 2016; Dana et al., 2019). In many cases, activation of axon collaterals may inadvertently influence animal behaviors. Interpreting results from such studies therefore requires understanding the full projection patterns of neuronal classes of interest. Traditional studies of axon collaterals established foundational knowledge but have been limited by low-throughput approaches that require predefining collateral targets. These include measuring overlap of retrograde tracers following injections into multiple targets (Gabbott

et al., 2005; Murugan et al., 2017) or recording from source neurons while antidromically stimulating target regions (Ishikawa and Nakamura, 2006; Ishikawa et al., 2008). Serial two-photon tomography and single neuron reconstructions have greatly improved our understanding of prefrontal projection patterns. But these techniques are expensive and computationally- and time-intensive, making them impractical for many labs (Oh et al., 2014; Gao et al., 2022).

Conversely, tissue clearing (Chung et al., 2013; Renier et al., 2016) and light sheet fluorescence microscopy (LSFM) are fast, easy, and affordable and can preserve three dimensional (3D) circuit architecture without the need to align structures. These approaches are useful for comparing projection patterns of genetically-, anatomically- or behaviorally-defined neurons and generating new hypotheses that can be tested using functional methods. To enhance their throughput, we developed DeepTraCE (Deep learning-based Tracing with Combined Enhancement) for quantifying bulk-labeled fluorescent axons and DeepCOUNT for quantifying fluorescently labeled cell bodies. DeepTraCE and DeepCOUNT build on the machine learning-based image segmentation package TrailMap (Friedmann et al., 2020) to form a user-friendly whole-brain analysis pipeline based on tissue clearing and LSFM.

Advances in computer vision allow researchers to train classifiers to detect axons in tissue volumes (Berg et al., 2019; Friedmann et al., 2020). However, axon morphology varies across brain regions causing classifiers to fail (Gao et al., 2022). To overcome this, DeepTraCE combines multiple models that have been separately trained using TrailMap to accurately identify axons with differing appearances. After segmenting the axons using a combination of TrailMap models, DeepTraCE registers the brains to a common coordinate framework and quantifies innervation density by brain region. Similarly, DeepCOUNT uses TrailMap to detect cells and then quantifies cell bodies by brain region.

We used DeepTraCE, DeepCOUNT and fiber photometry to reveal novel insights into mPFC threat avoidance circuits. The prelimbic (PL) subregion of mPFC is integral to both learned and innate threat avoidance (Stern et al., 2010; Bravo-Rivera et al., 2014; Capuzzo and Floresco,

2020). Yet our understanding of the underlying PL circuit mechanisms is incomplete. We focused on PL neurons that project to the contralateral PL (cPL), nucleus accumbens (NAc), or ventral tegmental area (VTA). These neuronal classes have established roles in cognition (Murugan et al., 2017; Lak et al., 2020; Lui et al., 2021) and reward-seeking (Kim et al., 2017; Otis et al., 2017a), but the relationship between their connectivity and function remains poorly understood, especially in aversive learning. Here we mapped their brain-wide collateral projections. DeepTraCE accurately detected axons, outperforming other model combination methods. Using DeepCOUNT, we mapped brain-wide neuronal activation patterns as mice avoided threats and then constructed functional networks, finding that PL was one of the most highly connected nodes. Using fiber photometry, we discovered that projection-defined PL classes have specialized roles in threat avoidance. Further, we demonstrated the utility of combining common techniques like fiber photometry with DeepTraCE and DeepCOUNT to understand the detailed structural and functional connectivity of the cells being studied.

METHODS

Animals

Female and male C57B16/J mice (JAX Stock No. 000664) or TRAP2;Ai14 mice (JAX Stock Nos. 030323 and 007914) were group housed (2–5 per cage) and kept on a 12 hour light cycle (lights on 7am-7pm). All animal procedures followed animal care guidelines approved by the University of California, Los Angeles Chancellor's Animal Research Committee.

Surgery

Mice were induced in 5% isoflurane in oxygen until loss of righting reflex and transferred to a stereotaxic apparatus where they were maintained under 2% isoflurane in oxygen. Mice were warmed with a circulating water heating pad throughout surgery and eye gel was applied to the animal's eyes. The mouse's head was shaved and prepped with three scrubs of alternating betadine and then 70% ethanol. Following a small skin incision, a dental drill was used to drill

through the skulls above the injection targets. A syringe pump (Kopf, 693A) with a hamilton syringe was used for injections. Injections were delivered at a rate 75nL/min and the syringe was left in the brain for 7 minutes following injection. For collateralization mapping, 300uL of AAVrg-Ef1a-mCherry-IRES-Cre-WPRE (Addgene 55632-AAVrg, $1.7x10^{13}$ vg/mL) was injected unilaterally into either left NAc (AP: 1.3, ML: -1.0, DV: 4.7), left VTA (AP: -3.3, ML: 0.4, DV: -4.5), or right PL (AP: 1.8, ML: -0.5, DV: -2.3). 200uL of AAV8-hSyn-DIO-hCHR2(H134R)-EYFP-WPRE ($1.7x10^{13}$ vg/mL) was then injected into left PL (AP: 1.8, ML: -0.4, DV: -2.3). To control for Cre-independent expression of EYFP, control mice received a single injection of 200uL of AAV8-hSyn-DIO-hCHR2(H134R)-EYFP-WPRE into left PL. For fiber photometry from cPL and NAc-projectors, we injected AAVrg- Ef1a-mCherry-IRES-Cre-WPRE (same as above) or AAVrg-EF1a-mCherry-IRES-Flpo-WPRE (Addgene 55634-AAVrg, $1.7x10^{13}$ vg/mL) into either cPL or NAc, and after 2 weeks of expression injected AAV8-EF1a-Con-Foff-2.0-GCamp6m-WPRE into PL (Addgene 137120-AAV8). For recordings from PL-VTA neurons, we injected AAVrg- Ef1a-mCherry-IRES-Cre-WPRE (same as above) into VTA and AAV5-CAG-GCamp6m-WPRE (Addgene 100839-AAV5) into PL. 400uM optic fibers (Doric) were implanted into left PL (AP: 1.8, ML: -0.4, DV: -2.3) and sealed in place using Metabond (Patterson Dental Company, 5533559, 5533492, S371). For topographical mapping of the origin of each projection type, mice were injected with 300uL of cholera toxin subunit B (ThermoFisher, C34775, C34776, C34778) or Fluorogold (SCBT, C223769) at the same coordinates for cPL, NAc and VTA listed above. For pain management mice received 5mg/kg carprofen diluted in 0.9% saline subcutaneously. Mice received one injection during surgery and daily injections for two days following surgery. Samples with mistargeted injection sites were excluded from analysis. Samples with obviously poor antibody penetration or distribution following tissue clearing were also excluded.

Brain Slice Histology and Immunostaining

Mice were transcardially perfused with phosphate-buffered saline (PBS) followed by 4% paraformaldehyde (PFA) in PBS. Brains were dissected, post-fixed in 4% PFA for 12–24h and

placed in 30% sucrose for 24–48 hours. They were then embedded in Optimum Cutting Temperature (OCT, Tissue Tek) and stored at -80°C until sectioning. 60um floating sections were collected into PBS. Sections were washed 3x10min in PBS and then blocked in 0.3% PBST containing 10% normal donkey serum (Jackson Immunoresearch, 17-000-121) for 2h. Sections were then stained with chicken anti-GFP (AVES 1020 at 1:2000), rabbit anti-RFP (Rockland 600-401-379 at 1:2000) or rat anti-CTIP2 (Abcam ab18465, 1:200) in 0.3% PBST containing 3% donkey serum overnight at 4°C. The following day, sections were washed 3x5min in PBS and then stained with secondary antibody (Jackson Immunoresearch Cy2 donkey anti-chicken IgG(H+L) 703-225-155, 1:1000, Cy3 donkey anti-rabbit IgG(H+L) 711-005-152, 1:1000 or Alexa647 donkey anti-rat IgG(H+L) 702-605-150, 1:500) in 0.3% PBST containing 5% donkey serum for 2 hours at room temperature. Sections were then washed 5 min with PBS, 15 min with PBS+DAPI (Thermofisher Scientific, D1306, 1:4000), and then 5 min with PBS. Sections were mounted on glass slides using FluoroMount-G (ThermoFisher, 00-4958-02) and then imaged at 10x with a Leica STELLARIS confocal microscope or at 5x on a Leica DM6 B scanning microscope.

Brain Clearing

Mouse brains were collected and processed based on the published Adipo-Clear protocol (Chi et al., 2018a) with slight modifications. Mice were perfused intracardially with 20mL of PBS (Gibco) followed by 4% paraformaldehyde (PFA, Electron Microscopy Sciences) on ice. Brains were hemisected approximately 1mm past midline and postfixed overnight in 4% PFA at 4°C. The following day, samples were dehydrated with a gradient of methanol (MeOH, Fisher Scientific):B1n buffer (1:1,000 Triton X-100, 2% w/v glycine, 1:10,000 NaOH 10N, 0.02% sodium azide) for 1 hour for each step (20%, 40%, 60%, 80%) on a nutator (VWR). Samples were then washed with 100% MeOH 2x for 1hr each and then incubated in a 2:1 dicholoromethane (DCM):MeOH solution overnight. The following day, two washes of 1hr in 100% DCM were performed followed by three washes of 100% MeOH for 30min, 45min then 1hr. Samples were

bleached for 4 hours in 5:1 H2O2/MeOH buffer. A cascade of MeOH/B1n washes (80%, 60%, 40%, 20%) for 30min each rehydrated the samples followed by a 1h wash in B1n buffer. 5%DMSO/0.3M Glycine/PTxWH permeabilized tissue for one hour and then again for 2h with fresh solution. Samples were washed with PTxwH for 30min and then incubated in fresh PTxwH overnight. The following day two more PTxwH washes lasted 1h then 2h. For axon analysis, samples were incubated in primary GFP antibody (AVES Labs GFP 1020) at 1:2000 in PTxwH shaking at 37°C for 11 days, washed in PTxwH 2x1h and then 2x2h, then for two days with at least one PTxwH change per day while shaken at 37°C. For TRAP2 experiments, samples were incubated in primary RFP antibody (Rockland 600-401-379) at 1:300 in PTxwH shaking at 37°C for 11 days, washed in PTxwH 2x1h and then 2x2h, then for two days with at least one PTxwH change per day while shaken at 37°C. Samples were then incubated in secondary antibody (AlexaFluor 647, ThermoFisher Scientific) for 8 days shaken at 37°C. Samples were washed in PTxwH 2x1h, then 2x2h, then 2 days with at least one PTxwH change per day while shaken at 37°C. Samples were then washed in 1x PBS twice 1x1hr, 2x2hr and then overnight. To dehydrate samples, a gradient of washes in MeOH:H2O (20%, 40%, 60% and 80%) were conducted for 30min each, followed by 3x100% MeOH for 30min, 1h, then 1.5h. Samples were incubated overnight in 2:1 DCM:MeOH on a nutator. The next day, samples were washed in 100% DCM 2x1h each. Samples were then cleared in 100% DBE. DBE was changed after 4h. Samples were stored in DBE in a dark place at room temperature. Imaging took place at least 24h after clearing.

Whole Brain Imaging

Brain samples were imaged on a light-sheet microscope (Ultramicroscope II, LaVision Biotec) equipped with a sCMOS camera (Andor Neo) and a 2x/0.5 NA objective lens (MVPLAPO 2x) equipped with a 6 mm working distance dipping cap. Image stacks were acquired at 0.8x optical zoom using Imspector Microscope v285 controller software. For axons, we imaged using 488-nm (laser power 20%) and 640-nm (laser power 50%) lasers. The samples were scanned with a step-size of 3 µm using the continuous light-sheet scanning method with the included

contrast adaptive algorithm for the 640-nm channel (20 acquisitions per plane), and without horizontal scanning for the 488-nm channel. For TRAP2-Ai14 brains, the 640-nm channel was imaged at 20% laser power without the contrast adaptive algorithm.

Model Training

Light sheet images of fluorescently labeled axons were segmented using the 3D U-net based machine learning pipeline TrailMap (Friedmann et al., 2020). We trained new models for segmentation of cortical axons using inference learning as described in the TrailMap pipeline (https://github.com/AlbertPun/TRAILMAP). Each training dataset included 6–20 hand-labeled image cubes (120x120x100 pixels). Training cubes were selected from a variety of brain regions across 9 different mice. Each brain region was represented across multiple mice. 10-20% of the image cubes were held out for use in model validation. Axons were hand-labeled in 3 or 4 planes from each cube. Where necessary, artifacts (pixels that could be mistakenly interpreted as axons, often bright clumps of antibody near the edge of the brain) were given a separate label. 1-pixel-wide edges of axons were labeled using python to be given less weight in training of the 3D convolutional network, which accounts for slight variability in human annotation patterns.

We performed iterative training “sessions”, with each session having unique training data targeted to the weaknesses of the previous model. Each training session consisted of 5-20 epochs (20-120 steps per epoch). We selected the best model from each session by plotting loss in validation data across epochs. Loss was minimized to prevent overtraining. We used the weights from the best model as the starting point for the next session. Sessions were continued until all visible axons in the desired regions were reliably detected by the model.

We observed differences in axon appearance that likely stem from a combination of the speed-resolution trade-off of light sheet microscopy and the physical properties of the axons. Based on careful visual analysis of axons in different brain regions, we found that most axons were either bright and highly delineated, fuzzy and indistinct, or fell in the middle of these two categories. We therefore predicted that 3 models would best capture the axons in our dataset.

We classified each brain region into one of three groups: delineated, moderately distinguished, or indistinct axons, and we trained models 1, 2, and 3 to segment these types of axons, respectively. This empirical approach of classifying axons into three groups and then combining the models outperformed other model combination methods, as described below.

To train our models, we used the published TrailMap model weights as a starting point. First, 7 training sessions were performed with data from regions assigned to Model 2. The result of the final session was used as Model 2 in the manuscript. To generate Model 1, we used the weights of Model 2 as the starting point. 2 sessions of training were performed using training data from regions assigned to Model 1. To generate Model 3, the weights of Model 2 were used as the starting point and 4 sessions of training were performed using training data from regions assigned to Model 3. In the DeepTraCE software, users can select the number of models they would like to use and assign brain regions accordingly. Or, they can simply use a single model.

The TRAP2-Ai14 model was trained in the same manner. Initial weights were derived from a model that had been trained on fos^{+} cells. From this, 6 sessions of training with 20 steps per epoch and 4-150 epochs per session were performed to generate the TRAP2-Ai14 model based on tdTomato+ TRAPed cells.

Axon Model Validation

We validated our analysis pipeline including image segmentation, scaling and axon thinning by selecting 120x120x100 pixel cubes from regions assigned to the ‘delineated’, ‘moderately distinguished’, and ‘indistinct’ groups in brains that were not included in initial training or validation data sets. Two human experts annotated 2–4 planes from each stack, marking pixels likely to contain axons. In stacks with difficult-to-distinguish axons, such as deep regions, experts used larger brush strokes to label broader groups of pixels likely to contain axons. One-pixel edges were then added to human annotations in python.

The raw image stacks were segmented as explained below. In brief, each stack was segmented with Models 1, 2 and 3 using TrailMap and scaled in ImageJ to a 10um space. Scaled

images were skeletonized in python at 8 different thresholds for binarization, combined in MATLAB, and pixel values were adjusted in ImageJ. Using the same quantification threshold as used in all analyses (number of skeletonized pixels with intensity above 64 divided by total number of pixels in the region), labeling density was calculated in human-annotated “axon-positive” pixels (LP) and “axon-negative” pixels (LN), excluding edges to account for slight variability in human labels. Distinction score was calculated from these values as (LP-LN)/LN+(1-LP). While direct true/false positive and true/false negative rates cannot be calculated due to the axon thinning process, which reduces the number of labeled pixels, LP correlates with the true positive rate, LN correlates with the false positive rate, and 1-LP correlates with the false negative rate. Thus, LP-LN in the numerator will increase distinction score when better separation is obtained between true and false positives, and LN and 1-LP in the denominator will decrease the distinction score if there is a higher rate of false positives or false negatives.

Alternate model combination methods were performed in FIJI. Maximum probability projections between all models were calculated by generating images with maximum pixel values across all models for each cube then processing the cubes for validation as above. Summation of probability maps between models was calculated by adding probability calculated by each model, then dividing by 3 prior to processing the cubes for validation as above. Distinction scores from alternate approaches were compared using repeated measures one-way ANOVA with Dunnett’s multiple comparisons test, comparing individual model selection (DeepTraCE) with each other method. Statistical comparisons of distinguishment scores were performed using GraphPad PRISM.

TRAP2-Ai14 Model Validation

To validate that cell counts produced by DeepCOUNT were accurate, we selected 120x120x100 pixel image cubes from several brain regions across multiple brains not included in the training dataset. Cubes were scaled and processed in the same manner as whole-brain data to produce a raw cell count from each cube. Two human experts then manually counted cells in

each cube. Average counts from the two human experts were then compared to counts produced by DeepCOUNT as shown in Figure 5.

DeepTraCE Analysis Pipeline

Image Segmentation & Registration

Whole-brain image stacks from the 640nm channel from each brain were segmented three times in TrailMap, once each using models 1, 2, and 3. Following segmentation, the 488nm autofluorescence channel and axon segmentations from each model were converted to 8-bit and scaled to 10um resolution in FIJI with scaling values of 0.40625 in the x and y directions and 0.3 in the z direction using a bilinear interpolation algorithm. To improve image registration, each scaled 488nm image was manually rotated in the x, y, and z planes using the TransformJ ImageJ plugin (https://imagescience.org/meijering/software/transformj/) such that the midline blood vessels visible were all visible in the same z plane. The same manual rotation parameters were then applied to the three scaled model segmentation images from the corresponding brain.

The scaled and manually rotated 488nm autofluorescence channel was registered using elastix to the Gubra Lab LSFM atlas average template, which has annotations based on the Allen CCF (Klein et al., 2010; Wang et al., 2020; Perens et al., 2021). The same transformation was applied to the scaled and manually rotated model segmentations using transformix. Image registration quality was manually verified by overlaying the atlas image and the registered 488nm channels in ImageJ. Following segmentation and registration of each model, the transformix images were converted to 8-bit .tif format in ImageJ. When combining multiple probability maps, it is important that minimum and maximum pixel values are comparable between images. Model 1 produced slightly lower maximum probability values compared to the other two models. We corrected for this by brightening segmentations from Model 1 by 34% to match pixel values obtained by the other models prior to combination and thinning. We provide a unified python pipeline for automating these steps in the supporting software repository.

Model Combination & Thinning

Converted segmentations from the three models were then combined by generating a new image in which pixel values in each region were extracted from the model with best performance in that region (Figure 1D). The same regional model assignments were used for all brains in the data set. Regional model assignments are provided in Figure 3-2. Following model combination, axon segmentations were thinned (or 'skeletonized') as described in the TrailMap pipeline (Friedmann et al., 2020). In brief, images were binarized at 8 different thresholds from 20 to 90% of the maximum intensity value using python. Skeletons were combined in MATLAB by summing values from each skeleton. Small objects unlikely to be axons were removed by calculating connected components within the combined skeleton and removing objects less than 90 voxels in size. Combined skeletons with small objects removed were optimized for visualization and quantification using an ImageJ macro that multiplied each pixel value by 17.

Axon Quantification

Regional axon innervation was quantified in MATLAB (Mathworks) by counting the number of skeletonized pixels in each brain region above a threshold (64), then dividing this pixel count by the total number of pixels in a region. This regional pixel count was then divided by the total number of labeled pixels across the brain to normalize for differences in total fluorescence and viral expression. Regions were defined by a collapsed version of the LSFM atlas in which maximum granularity was balanced with the need to account for slight differences in registration which would lead to inaccurate quantification of small brain regions. This atlas was cropped on the anterior and posterior ends to match the amount of tissue visible in our data. Fiber tracts, ventricular systems, cerebellum, and olfactory bulb were excluded from analysis.

All statistical comparisons were performed in MATLAB and GraphPad Prism v9. For comparison of regional axon labeling between cell types, Two-way ANOVA with Tukey's multiple comparison correction was performed on all brain regions. Anterior-posterior axon distributions within regions were calculated in MATLAB by binning the whole-brain image into 100um voxels and calculating the percentage of segmented pixels within each voxel. Voxels falling within a given

region were summed across the medial-lateral and dorsal-ventral axis and normalized for total fluorescence as above. The averaged summation of axon counts from a given cell class was then averaged and plotted along with the standard error of the mean.

Axon Visualization

To visualize axons as shown in Figures 1 and 3, Z-projections of raw light sheet data were created in FIJI by scaling images to a 4.0625um space, virtually reslicing images in the coronal plane, and performing maximum intensity z-projections of 100um depth followed by local contrast enhancement. Axon segmentations were created by overlaying skeletonized and registered axon segmentations from each sample of a cell type in a slightly different color and virtually reslicing in the coronal plane. 3D projections were created in Imaris using a representative sample from each cell type. Dotogram overlays (Figures 2 and 4) were created using MATLAB. Images were binned into 100um voxels and the percentage of segmented pixels within each voxel was calculated. Area of visible dot in the overlay corresponds with the averaged labeling intensity within a voxel across a condition. Outer dots represent the cell type with the highest labeling intensity within that voxel.

Computational Analyses

Hierarchical clustering of regional axon quantifications was performed as described by Kebschull et al.(Kebschull et al., 2020).

DeepCOUNT Analysis Pipeline

Image Segmentation & Registration

Whole-brain image stacks from the 640nm channel from each brain were segmented in TrailMap using the TRAP2-Ai14 trained model. Images were registered using the 488nm autofluorescence channel as described above. Transformed images were converted to 8-bit in ImageJ.

3D Maxima Detection & Single-Pixel Reduction

MATLAB was used to identify 3D maxima of the transformed probability map. Connected component analysis was then used to reduce any maxima that consisted of multiple pixels into a single pixel per cell.

Cell Quantification

Regional TRAPed cell density was quantified in MATLAB (Mathworks) by counting the number of labeled pixels (i.e. cells) in each brain region, then dividing this pixel count by the total number of pixels in a region. This regional pixel count was then divided by the total number of detected cells across the brain to normalize for differences in tamoxifen-induced recombination. Regions were defined in the same way as described for the DeepTraCE pipeline.

Functional Network Construction

In MATLAB, we calculated simple linear correlations between all pairs of brain regions based on the normalized, per area TRAPed cell counts. The nodes and connections in the networks represent brain regions and correlations that survived thresholding using Pearson's $r \geq 0.9$ and $P < 0.05$ as cutoffs. While potentially interesting, we did not consider negative correlations in the current analysis. We used Cytoscape software to visualize and analyze networks. Degree was calculated by counting all the above-threshold connections for a given node. Node size is proportional to degree and lines represent above-threshold correlations.

4-Hydroxytamoxifen Preparation

4-hydroxytamoxifen (4-OHT; Sigma, Cat# H6278) was dissolved at 20 mg/mL in ethanol by shaking at 37°C for 15 min and was then aliquoted and stored at –20°C for up to several weeks. Before use, 4-OHT was redissolved in ethanol by shaking at 37°C for 15 min, a 1:4 mixture of castor oil:sunflower seed oil (Sigma, Cat #s 259853 and S5007) was added to give a final concentration of 10 mg/mL 4-OHT, and the ethanol was evaporated by vacuum under centrifugation. The final 10 mg/mL 4-OHT solutions were always used on the day they were prepared. All injections were delivered intraperitoneally (i.p.).

Behavioral assays

For PMA experiments, mice were placed in an operant chamber with a shock floor. The quarter of the floor furthest from the door of the chamber was covered in a white plexiglass platform. Two odor pods with novel scents (vanilla, almond, coconut, or peanut butter) were placed underneath the part of the shock floor not covered by the platform to promote exploration.

For TRAP2 experiments, on training day, mice received 3 baseline tones (30s, 4000Hz, 75dB) followed by 9 tone-shock pairings (0.13mA shock, 2s, co-terminating), where mice could learn to avoid the shock by entering the safety platform. Tones were separated by a random interval between 80 and 150 seconds. The next day, mice received 6 tones with no shock. Mice were injected with 4-OHT solution immediately following the retrieval session. Non-shock control animals were placed in the operant chamber with no platform for five minutes on day 1, and on day 2 were placed in the operant chamber for five minutes and injected with 4-OHT solution immediately after this session. Brains were harvested 2 weeks after TRAPing for brain clearing, light sheeting imaging, and analysis.

For fiber photometry recordings during PMA, mice received 3 baseline tones on day 1, followed by 12 tone-shock pairings on day 1 and 16 tone-shock pairings on days 2, and 3. For EZM experiments, mice were placed on a custom-built elevated zero maze 24 inches in diameter for 15 minutes. Both assays were recorded using a Point Grey Chameleon3 USB camera (Teledyne FLIR).

Fiber Photometry

Mice were habituated to the operant chamber and optic fiber for at least two days prior to recording. A TDT RZ10x processor in combination with the TDT Synapse software was used to simultaneously record the 405nm isosbestic channel and the 465nm signal channel during behavior. For each mouse, the light output was adjusted such that the 465nm and 405nm channel produced a signal of approximately 80mV as reported by the Synapse software.

Fiber Photometry Analysis

Point-tracking of PMA videos were performed in DeepLabCut (Mathis et al., 2018) and behavior was analyzed using BehaviorDEPOT (Gabriel et al., 2022). Elevated Zero Maze behavioral epochs were annotated manually. Fiber photometry analysis was performed in MATLAB in a modified version of an example provided by TDT. To align fiber photometry and behavioral data, TTL pulses marking the beginning and end of each tone were aligned between the fiber photometry signal and video frames. A lookup table was generated using linear interpolation between each TTL pulse to identify which behavior frame lines up with each photometry frame. For alignment of EZM fiber photometry data, a silent TTL pulse was generated every 30 seconds to be used for alignment in the same manner.

Fiber photometry signal was down-sampled by a factor of 10 prior to analysis. To account for potential movement artifacts and bleaching, the 405nm isosbestic control channel was fit to the 465nm signal using the polyfit function, and this curve was then subtracted from the 465nm signal. Z scores of this signal were calculated using a baseline period of -10 to 0 seconds relative to the tone for tone-aligned responses (i.e. tone and shock responses) and -20 to -15 seconds relative to epoch onset for all other behaviors (i.e. platform entries and exits, closed arm entries and exits, head dips). The average of all traces for an individual animal was calculated and used for analysis. To generate plots, each animal's average trace was smoothed by averaging values from every 0.5 seconds (for time-locked tone and shock responses) or using a moving average of 0.5 seconds (for all other traces), and the mean ± SEM of smoothed traces across animals was displayed. BLA axon collaterals from photometry brains were quantified in 2-D images acquired on a Leica DM6 B scanning fluorescence microscope. We took the ratio of fluorescence intensity in BLA to fluorescence intensity in a nearby background region of cortex that did not contain axons. 1 was subtracted from this value such that 0 represents the absence of axons.

Statistical Analysis

Statistical analysis was performed using GraphPad Prism. For whole-brain analysis of axons, ANOVA examined the influence of neuronal class on projections patterns. We corrected for multiple comparisons using Tukey's post-hoc tests. For analysis of TRAPed cells in key brain regions, we compared PMA animals to controls using student's t-tests. For fiber photometry experiments, ANOVA with Tukey posthoc tests evaluated the influence of neuronal class on observed activity. All correlation analyses between photometry and behavior data or photometry and axon data were performed using a simple linear regression. In Figures 3 and 5, a single principal components analysis was performed that included all animals across groups. First, per area counts were normalized by region volume and total counts per brain (counts of axon-containing pixels or TRAPed cells, respectively). To visualize the whole-brain data in two-dimensional space, principal components analysis was applied to these normalized, per area counts to find the axes that captured the most variance across different brain areas. The per animal data across all brain regions was then projected onto the first two principal components. All computations were performed using MATLAB.

Code Accessibility

Code, instructions and sample data available at https://github.com/DeNardoLab/DeepTraCE and https://github.com/jcouto/DeepTraCE/tree/gui

RESULTS

DeepTraCE Workflow

We developed DeepTraCE, an open-source, end-to-end analysis pipeline for quantifying bulk axonal projection patterns in cleared brains. DeepTraCE takes in raw images of fluorescently labeled axons and then applies TrailMap (Friedmann et al., 2020), a machine learning pipeline that trains a 3D U-net framework to automatically identify axons in cleared tissue (Figure 4-1a).

TrailMap provides a pre-trained model that users can fine tune to fit their samples. However, it

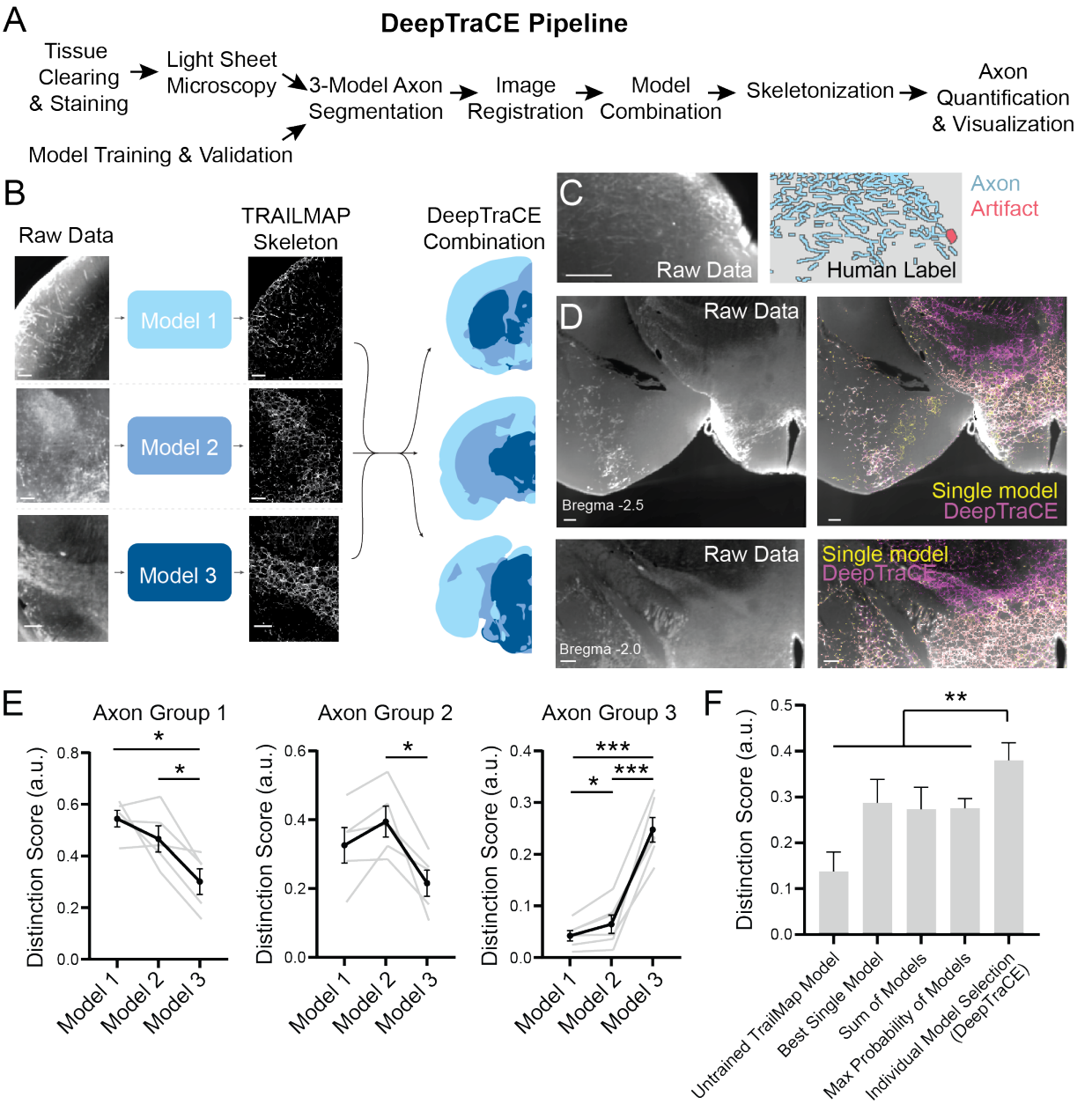

Figure 4-1. DeepTraCE workflow. (A) Overview of DeepTraCE workflow. (B) Demonstration of segmentation using 3 different models followed by model combination**.** (C) Example of human-labeled axons and artifacts for model training**.** (D) Overlay of raw data and axon segmentation using single model or DeepTraCE concatenated models**.** (E) Distinction score produced by models 1, 2, and 3 for images from regions assigned to axon groups 1, 2, and 3. Repeated-measures one-way ANOVA with Benjamini, Krieger and Yekutieli post hoc test (FDR=0.05). (Group 1: F(1.4, 5.5)=8.503, P=0.0257; Group 2: F(1.4, 7.8)=7.753, P=0.0309; Group 3: F(1.2, 6.1)=73.76, P=0.0001). (F) Comparison of DeepTraCE with alternate segmentation and model combination strategies. Repeated measures one-way ANOVA with Benjamini, Krieger and Yekutieli post hoc test (FDR=0.05) (F(2, 33)=14.46, P<0.0001). See Figure 1-1 for detailed statistics. Scale bars, 200um. Descriptive statistics: mean ± SEM. *P<0.05, **P<0.01, ***P<0.001. Distinction score: (LP-LN) / (LN+(1-LP)). LP = axon+ human label. LN = axon- human label.

was challenging to train a model that could sufficiently generalize across the diversity of mPFC axonal structures in all of their target regions; some axons were bright and delineated (e.g. in cortical areas) while others were dense and indistinct (e.g. in the basolateral amygdala and thalamus). To surmount this hurdle, DeepTraCE allows users to combine multiple trained models to optimize axon detection throughout the brain. After importing 3D image stacks, multiple models trained using TrailMap fully segment each brain. DeepTraCE then registers each brain to a standard atlas and generates a new image in which pixel values in each region were extracted from the assigned model. Axons in the resulting images are then thinned to single-pixel width (Friedmann et al., 2020) and the number of axon-containing pixels are quantified for each brain region (Figure 4-1a).

Validation of model combination method

To determine how many models to combine, we examined raw images of fluorescently-labeled axons taken with LSFM. We grouped brain regions into three main categories based on the visual quality of PL axons (e.g. thick and delineated or dense and fuzzy). These categories largely segregated with the physical location of brain regions in tissue volumes (Figure 4-1b). We used TrailMap (Friedmann et al., 2020) to train three separate models that we fine-tuned for each set of regions (Figure 4-1b-d).

To validate the DeepTraCE model assignments, we performed quantitative comparisons of model accuracy in representative brain regions from each category, using human annotations as a reference. Human experts traced pixels containing axons in image stacks from each group of brain regions (Figure 4-1c). We segmented images using each of the three models in addition to the original TrailMap model that was trained on serotonergic axons (Friedmann et al., 2020). We then calculated the resulting axonal labeling density with reference to human labels.

In LSFM of cleared tissue, the size of small fluorescent structures is amplified such that a thin object such as an axon occupies several more pixels in the image than it does in true

biological space. We account for this overrepresentation by thinning segmented axons to a single pixel width (Friedmann et al., 2020). However, because rapid imaging of intact rodent brains requires lower optical resolution, it can be challenging in some regions to hand-label axons with single pixel precision. This caveat to whole-brain light sheet microscopy approach prevents the calculation of “true positive” and “true negative” rates based on human annotation. So, common metrics such as F1 score, precision, and recall do not provide interpretable measures of segmentation accuracy. Instead, we calculated a ‘distinction score’ that measures the density of segmented axons in regions that humans estimated as containing axons vs. not containing axons. If there is a large mismatch between human and computer labels, the distinction score will approach 0. Better overlap with human labels will produce higher distinction scores, but the upper limit is arbitrary due to the axon thinning process, which inherently reduces machine labeling even in human-annotated axon-positive pixels. We empirically observed that well-aligned labels produce values between 0.2 and 0.6 depending on the brain region. When applied to our validation set, Models 1, 2, and 3 produced the highest distinction scores in images from the brain regions assigned to each model (Figure 4-1e).

Previous studies used alternative approaches to overcome the limitations of a single-model approach in whole-brain image segmentation. Some excluded deeper, more densely innervated areas from analysis (Kramer et al., 2021). Others combined probability maps from different segmentation methods by extracting the maximum probability for each pixel (Kebschull et al., 2020). To compare DeepTraCE with these alternative approaches, we calculated the distinction score across all human-annotated images in the validation set using the original TrailMap model that was trained on serotonin neurons, our best-trained single model, the maximum probability between our three models, the sum of probabilities, and the DeepTraCE combined models. DeepTraCE had the highest distinction score (Figure 4-1f), indicating that it performed more accurate axon segmentation from images.

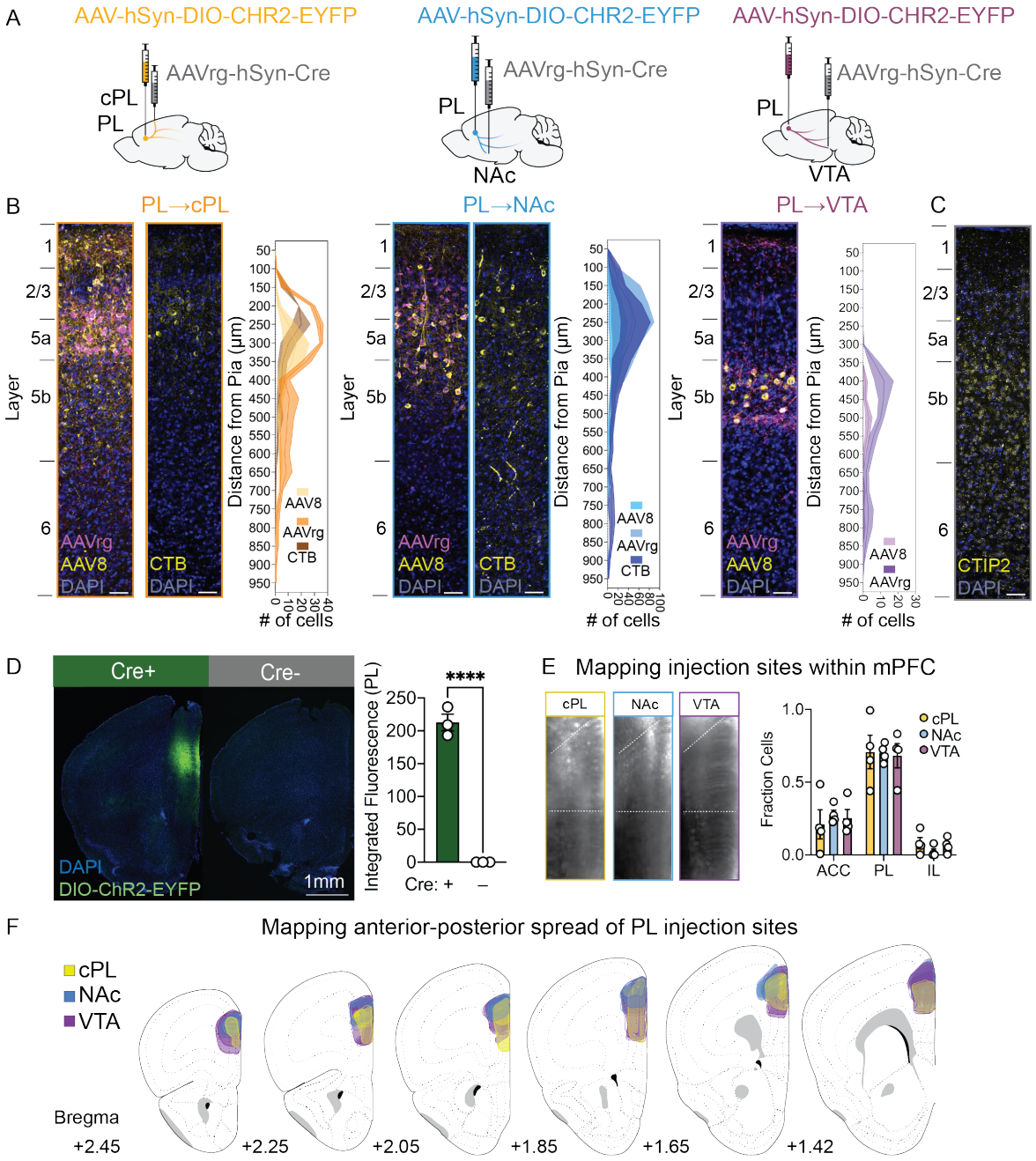

Figure 4-2. Validation of Cre-Dependent Virus and Injection Site Mapping.
(A) Viral injection strategy for targeting projection-defined PL neurons. (B) Layer distributions of PL neurons retrogradely labeled via injections of AAVrg, AAVrg+AAV8, CTB-594, CTB-647, and AAVrg-EGFP in cPL, NAc, and VTA, respectively (cPL: $F_{tracer}(2,6)=4.76$, $P=0.06$; $F_{bin}(2.5,15.3)=20.04$, $P<0.0001$, n=3/group; NAc: $F_{tracer}(2,6)=0.52$, $P=0.62$; $F_{bin}(1.1,6.7)=4.54$, $P=0.07$, n=3/group; VTA: $F_{tracer}(1,4)=203.6$, $P=0.0001$; $F_{bin}(1.7,6.8)=4.28$, $P=0.07$, n=3/group 2-way ANOVA). Scale bars, 100um. (B) Representative stain of layer marker CTIP2 in PL. Scale bars, 100um. (C) Representative coronal sections of brains injected with AAVrg-Cre and AAV-DIO-ChR2-EYPF (left) or AAV-DIO-ChR2-EFYP in the absence of Cre and quantification of fluorescence in PL. (D) Raw fluorescence images from LSFM showing mPFC injection sites for PL-cPL, PL-NAc and PL-VTA collateral mapping experiments. Quantifications show fraction of fluorescently labeled cells detected in ACC, PL and IL (each dot represent 1 mouse, n=4 mice per group). (E) Maps of fluorescently labeled cell bodies across the anterior-posterior axis of mPFC for each cell class. Error bars, S.E.M., ****$P<0.001$, Student's t-test.

Viral circuit mapping and brain clearing strategy

We mapped the brain-wide axon collaterals of PL neurons that project to cPL, NAc or VTA. Our goals were 1) to demonstrate the utility of DeepTraCE and 2) to provide an important anatomical resource for researchers studying mPFC function. Therefore, we used a commonly employed dual-virus approach to fluorescently label populations of PL projection neurons (Schwarz et al., 2015). In contrast to multi-site retrograde tracer injections, this approach allows us to visualize the bulk brain-wide collateralization patterns of each projection-defined class of neurons. We first injected an axon-terminal-transducing adeno-associated virus (Tervo et al., 2016) expressing Cre recombinase (AAVrg-hSyn-Cre) into cPL, NAc, or VTA. Next, into PL, we injected AAV expressing Cre-dependent EYFP-tagged Channelrhodopsin-2 (AAV8-hSyn-DIO-ChR2-EYFP), which traffics efficiently to axons (Figure 4-2a). We used the iDISCO clearing variant, Adipo-Clear (Chi et al., 2018a, 2018b) to immunostain intact brains for EYFP and render the tissue transparent. We then imaged the hemispheres ipsilateral to the PL injection with LSFM (Figure 4-3).

In separate animals, we used confocal microscopy to examine the distribution of retrogradely labeled cell bodies in brain sections (Figure 4-2). Different retrograde tracers can have preferences for particular neuronal types. For instance, while AAVrg favors cortical layer (L)5 over L6, rabies virus has the opposite preference (Sun et al., 2019). Cholera toxin subunit B (CTB) is inefficient for labeling pyramidal tract neurons in L5 (Leow et al., 2022). To assess potential biases in our retrograde labeling method, we analyzed the layer distribution for AAVrg-Cre-mCherry+ cells and the combination of AAVrg-hSyn-Cre-mCherry and AAV8-hSyn-DIO-ChR2-EYFP (assessed based on EYFP fluorescence). As a comparator, we measured the layer distribution of CTB+ cells in PL following injections into cPL and NAc. Consistent with previous reports observing other populations of PT neurons, we did not observe retrogradely labeled PL cells when we injected CTB into the VTA (Leow et al., 2022). We determined layer boundaries based on DAPI nuclear staining in combination with immunostaining for Ctip2, a marker of subcerebral projection neurons located in L5b-6 (Arlotta et al., 2005). Layer boundaries and

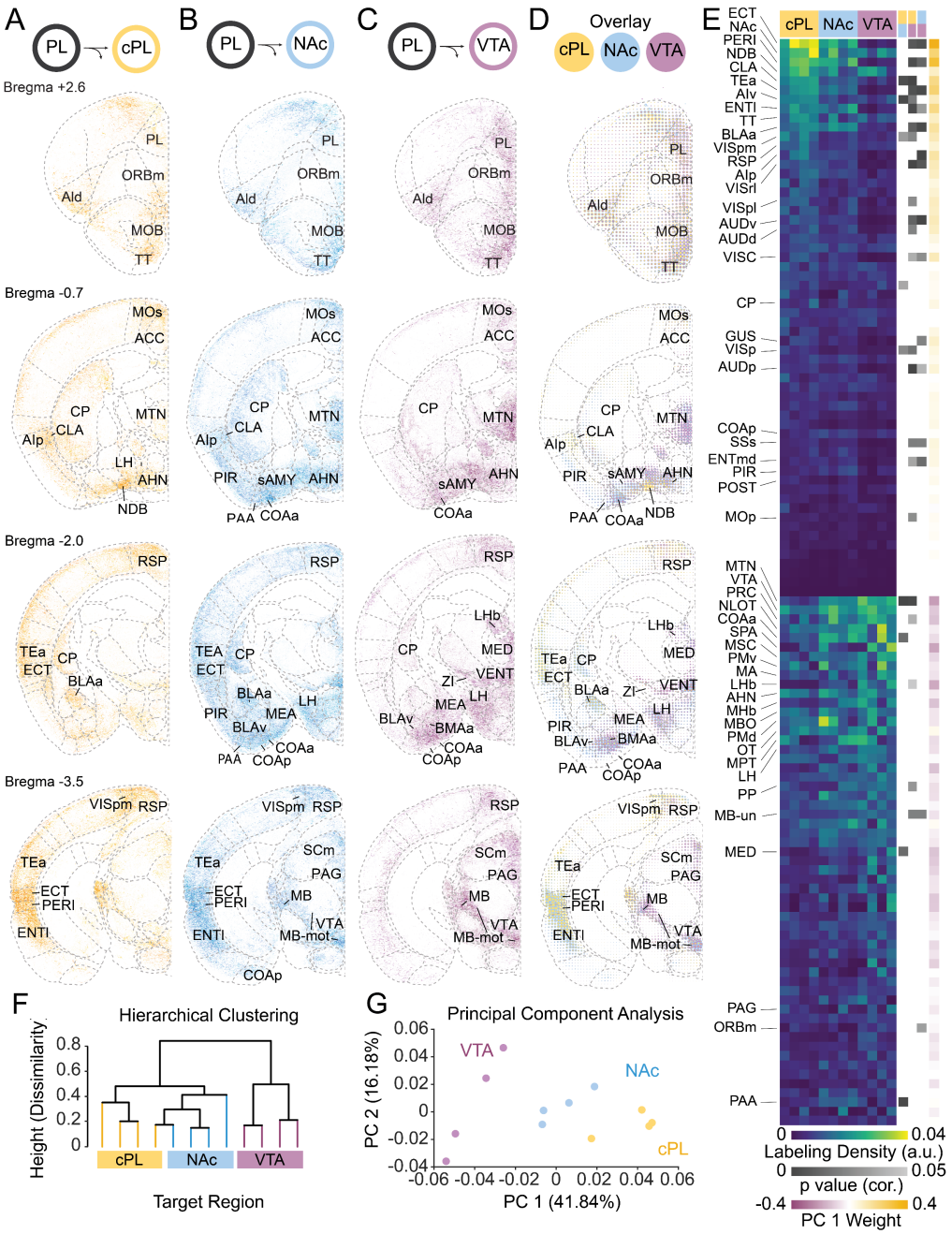

Figure 4-3. Visualization and quantification of brain-wide projection patterns of mPFC
(A–C) DeepTraCE segmentation of single 10um coronal optical sections of thinned axons registered to the standardized brain atlas. Represents 4 overlaid brains from each neuronal class. (D) Dotogram overlay of 3 cell classes. Innervation by cPL-, NAc- and VTA-projecting PL neurons shown in yellow, blue and purple, respectively. (E) Left heatmap: relative labeling density (normalized to region volume and gross label content per brain) across 140 regions defined by the Allen Brain Atlas. Middle heatmap: P values from multiple comparisons of axon innervation density. Right heatmap: Loadings for PC1 (arbitrary PC weight units) (F) Dendrogram of hierarchical clustering of regional axon quantifications from 12 mice, colored by target region. (G) Locations of individual mice projected in principal component (PC) space defined by the first two PCs (arbitrary PC units, cPL, *n*=4; NAc, *n*=4; VTA, *n*=4). Abbreviations: Isoctx, isocortex; OLF, olfactory areas; HPF, hippocampal formation; CTXsp, cortical subplate; CNU, cerebral nuclei; HY, hypothalamus; MB, midbrain; HB, hindbrain. See Tables 1-1, 3-1 and 3-2 for related data.

thicknesses aligned with previous literature (Figure 4-2) (DeNardo et al., 2015; Anastasiades et al., 2019; Anastasiades and Carter, 2021). Consistent with previous findings (McGarry and Carter, 2016; Collins et al., 2018; Anastasiades et al., 2019), PL-cPL and PL-NAc neurons were preferentially located in L2–5a and PL-VTA neurons were restricted to L5b. We found no statistical differences in the distribution of cells labeled with AAVrg alone, AAVrg+AAV8 or CTB (Figure 4-2b,c). As reported previously, we observed few AAVrg-labeled cell bodies in L6 (Sun et al., 2019; Leow et al., 2022). While L6 neurons were likely underrepresented in our datasets, we could still extract meaningful differences between classes. To ensure viral labeling was specific, we confirmed there was no cre-independent expression of our fluorescent constructs (Fig. 4-2d) and that injection sites were centered on PL. Fluorescent labeled neurons were mostly in PL, with some in the anterior cingulate cortex (ACC) (Figure 4-2e,f).

Whole-brain projection patterns of PL-cPL, PL-NAc and PL-VTA neurons

We used DeepTraCE to determine the extent to which PL-cPL, PL-NAc and PL-VTA neurons collateralize to other brain regions. Examination of thin optical sections revealed widespread collateralization for all three classes. Overall, innervation patterns were consistent with reports of general mPFC projection patterns (Gabbott et al., 2005; Anastasiades et al., 2019; DeNardo et al., 2019); mPFC axons were prominent in cortical association areas, striatum, midline thalamus, claustrum, amygdala, hypothalamus and midbrain but largely absent from hippocampus, sensory thalamus, and relatively sparse in primary sensory areas (Figure 4-3a-c).

We generated dotograms (Oh et al., 2014) to visually summarize the inter-class distinctions. To create the dotogram, we averaged axon density across all samples for a given projection class and then overlaid the samples in brain space. Dot color indicates the neuronal class and dot size corresponds to the averaged axonal density within a voxel (Figure 4-3d). Compared to PL-VTA neurons, PL-cPL and PL-NAc neurons more densely innervated cortical areas, especially the temporal association area (TEa), ectorhinal area, and entorhinal cortex. On

the other hand, PL-VTA collaterals preferentially innervated thalamic (TH) and midbrain (MB) regions, a subset of which also received collateral input from PL-NAc neurons. All three subclasses innervated NAc and olfactory tubercle (OT), while PL-NAc neurons were the primary source of collaterals to piriform cortex (PIR).

We next quantified regional innervation densities and plotted them as a heatmap. For each brain, we normalized the number of axon-containing pixels in each region to the total number of axon-containing pixels in the brain. We then sorted regions according to their innervation density by projection classes; regions receiving more PL-cPL collaterals are on top and those receiving more PL-VTA collaterals are in the bottom half of the heatmap (Figure 4-3e). While there was little overlap between projection patterns of PL-cPL and PL-VTA neurons, PL-NAc neurons shared several projection targets with both other classes. Brain-wide statistical comparisons confirmed the presence of 29 significantly differentially innervated brain regions, the most notable of which were in the cortex, subplate, and thalamus (Figure 4-3e).

Because PL-cPL, PL-NAc and PL-VTA projection neurons all collateralize broadly, we wondered if these neuronal classes could be separated based on their whole-brain projection patterns. To test this, we used two dimensionality reduction techniques. We first performed hierarchical clustering, in which Euclidean distance between individual brains based on axonal density in each subregion is marked by a higher branch point on the graph. PL-VTA neurons formed a distinct cluster, while PL-NAc and PL-cPL collaterals formed partially overlapping clusters (Figure 4-3f).

We also used principal component analysis to assess differences in whole-brain projection patterns for each cell class. We plotted the location of each brain along the axes of the first two principal components. While PL-cPL and PL-VTA projection classes could be clearly separated along the first principal component, PL-NAc brains were positioned in between, with some overlap with PL-cPL brains (Figure 4-3g). To assess which projection patterns distinguished the classes, we plotted the weights of each brain region in contribution to the first principal component.

Positively weighted regions generally had the most innervation from PL-cPL collaterals including TEa, PERI, and ECT, and negatively weighted regions were those with most innervation from PL-VTA collaterals, including MTN and midbrain areas (Figure 4-3e). These data show that while cPL and NAc-projectors have substantial overlap, PL-cPL and PL-VTA neurons represent separable classes, distinguished in large part by their collaterals to TEa/PERI/ECT, olfactory and limbic

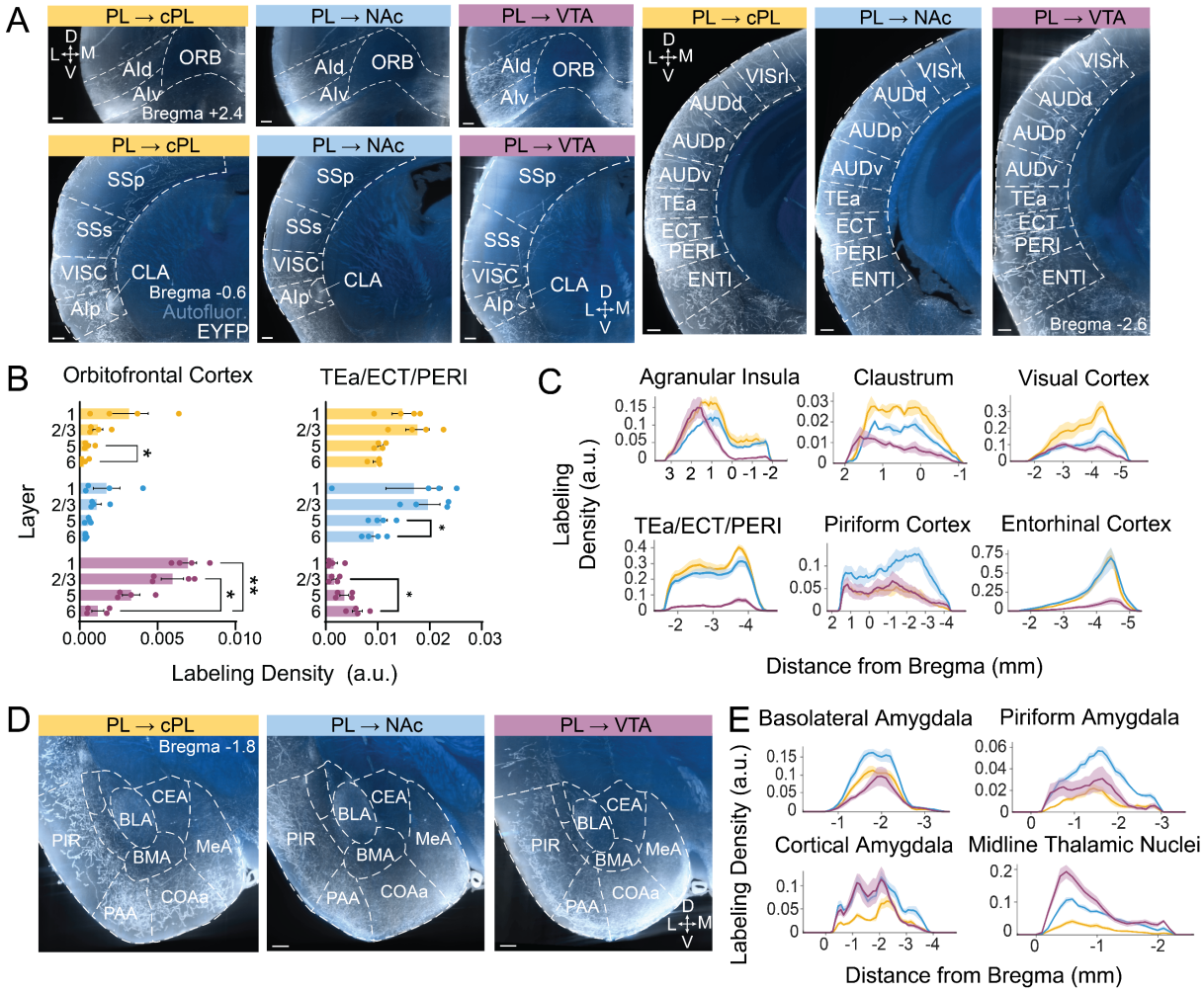

Figure 4-4. Region-specific collateralization patterns of PL-cPL, PL-NAc and PL-VTA neurons
(A) Coronal view of 100um z-projections of raw 640nm (axons, white) and 488nm (autofluorescence, blue) channels from individual brains. Images show class-specific innervation patterns in anterior (left) and posterior (right) cortical areas. (B) Layer distributions of axonal innervation in select cortical target regions. (C) Visualizations of axonal innervation density along the anterior-posterior axis in select regions. (D) Raw images showing axons in the amygdalar complex. (E) Quantification of axonal innervation density along the anterior- posterior axis of a given region. PL-cPL, PL-NAc and PL-VTA neurons coded in yellow, blue and purple, respectively. N=4/group. Descriptive statistics are from 2-way ANOVA with Tukey's post-hoc multiple comparison test. See Table 1-1 and 3-1 for detailed statistics and abbreviations. Error bars: mean ± S.E.M. *P<0.05, **P<0.01.

areas, and thalamus and midbrain, respectively. Together, the innervation patterns we observed

were consistent with bulk projection mapping (Sesack et al., 1989; Vertes, 2004; Oh et al., 2014) and single neuron reconstructions (Winnubst et al., 2019; Gao et al., 2022), indicating that DeepTraCE accurately captured meaningful class-specific distinctions in collateral targeting.

Layer-specific and topographic innervation patterns in the cortex and subplate

Whole-brain analysis of bulk labeled neuronal classes is well-suited for understanding the geometric organization of axonal projections *within* brain regions, which can have important functional implications. The neocortex is organized into layers that contain distinct neuronal types with different morphology, physiology, and connectivity (Harris and Shepherd, 2015; Anastasiades and Carter, 2021). Long-range cortico-cortical axons may innervate superficial or deep layers depending on the hierarchical relationship with the target region (Harris and Shepherd, 2015; Anastasiades and Carter, 2021). Compared to sensory and motor cortices, much less is known about the layer organization of long-range mPFC connectivity, especially for specific projection classes. To investigate this, we plotted PL-cPL, PL-NAc and PL-VTA collateral innervation density across layers in cortical target areas (Figure 4-4a-b). In ORB, all classes preferentially targeted superficial layers (L1, L2/3). In TEa, ECT, and PERI, PL-cPL and PL-NAc collaterals preferentially targeted superficial layers (L1, L2/3) while PL-VTA collaterals targeted the deep layers (L5, L6) (Figure 4-4b). These findings suggest that PL-cPL, PL-NAc and PL-VTA may all participate in feedforward or feedback connectivity depending on the target region.

Many PL target regions contain functional gradients that are orthogonal to layer-defined microcircuits. We therefore investigated whether PL classes project to topographically-defined locations in target regions (Figure 4-4c). Compared to PL-cPL and PL-NAc, PL-VTA collaterals had a tighter distribution in the anterior portion of agranular insula (AI) and claustrum (CLA). Compared to PL-VTA neurons, PL-cPL and PL-NAc collaterals were biased toward posterior visual cortex. PL-NAc collaterals were especially prominent in the posterior PIR. All three classes and similar distributions across entorhinal cortex, preferentially targeting the posterior part.

Interestingly, PIR and AI both contain anatomical and functional gradients (Gehrlach et al., 2020; Poo et al., 2022). Our data suggest that class-specific PL projections may be a determining factor in these gradients.

While all projection classes sent collaterals to the amygdalar complex, amygdalar nuclei were differentially innervated. Notably, the anterior basolateral amygdala (BLAa) was robustly innervated by PL-cPL and PL-NAc neurons, but less so by PL-VTA neurons. Meanwhile, compared to PL-cPL neurons, PL-NAc neurons sent many more collaterals to olfactory amygdalar areas, including anterior cortical amygdalar area (COAa) and piriform amygdalar area (PAA) (Figure 4-4d,e). As PL-NAc collaterals were also more prominent in posterior PIR, which was recently found to play a role in spatial cognition (Poo et al., 2022), PL-NAc neurons may have privileged control over areas dedicated to olfactory processing during cognition and emotional learning.

Whole-Brain Cell Counting Pipeline

The application of computer vision to light sheet data extends beyond axon tracing and can be used to identify signatures of brain function. Expression of IEGs such as c-fos are frequently used as a proxy of neural activity (Sheng and Greenberg, 1990; Franceschini et al., 2020). For instance, recent studies have used tissue clearing, IEG-labeling, and LSFM to screen for changes neuronal activation following experiences with drugs or fear learning (Wheeler et al., 2013; Renier et al., 2016; Vetere et al., 2017; DeNardo et al., 2019). Quantifying IEG-expressing cells on brain-wide scale can serve as means to infer behaviorally-relevant changes in functional connectivity. However, currently available open-source packages for whole-brain cellular quantification can be error prone, especially in regions of particularly dense labeling.

As a companion to DeepTraCE, we developed DeepCOUNT (Deep-learning based Counting of Objects via 3D U-Net pixel Tagging) (Figure 4-5a). We first trained a TrailMap model to recognize fluorescently labeled cell bodies. This produces a probability map of which

pixels are most likely to contain a cell body. After thresholding the images to a desired probability cutoff, they are registered to a standard brain, and DeepCOUNT uses a 3D maxima detection strategy in combination with a connected component analysis to ensure each neuron is represented by a single pixel. This single-pixel output can then be used to obtain regional cell counts across the brain.

We compared DeepCOUNT performance to that of ClearMap (Renier et al., 2016), a commonly used cell detection algorithm designed for tissue clearing and LSFM, and human observers. Two human observers analyzed image volumes from six different brain regions. Cell counts produced with DeepCOUNT were more accurate counts than ClearMap, using human counts as the ground truth (Figure 4-5b,c).

Whole-brain threat avoidance networks

We used DeepCOUNT to map regions and functional connections involved in threat avoidance at a whole-brain level. PL is required for threat avoidance behavior (Bravo-Rivera et al., 2014; Diehl et al., 2018). Previous studies examining c-fos expression following active avoidance behavior analyzed only discrete regions of interest (Nikolaev et al., 1992; Duncan et al., 1996; Bravo-Rivera et al., 2015), some of which are PL target sites. How PL coordinates threat avoidance-related neural activity on a brain-wide scale is not understood. To begin to address this question, we used DeepCOUNT and activity-dependent genetic labeling to map brain-wide neuronal activation following a platform mediated avoidance (PMA) (Bravo-Rivera et al., 2014), a form of learned threat avoidance.

We labeled activated neuronal populations using TRAP2 mice (*Fos*$^{icre\text{-}2A\text{-}ERT2}$), in which the c-fos promoter drives expression of tamoxifen-inducible Cre recombinase. We crossed TRAP2 to the Ai14 Cre reporter line (Madisen et al., 2010; Allen et al., 2017; DeNardo et al., 2019). We then trained the *TRAP2;Ai14* mice in PMA and TRAPed them after a threat

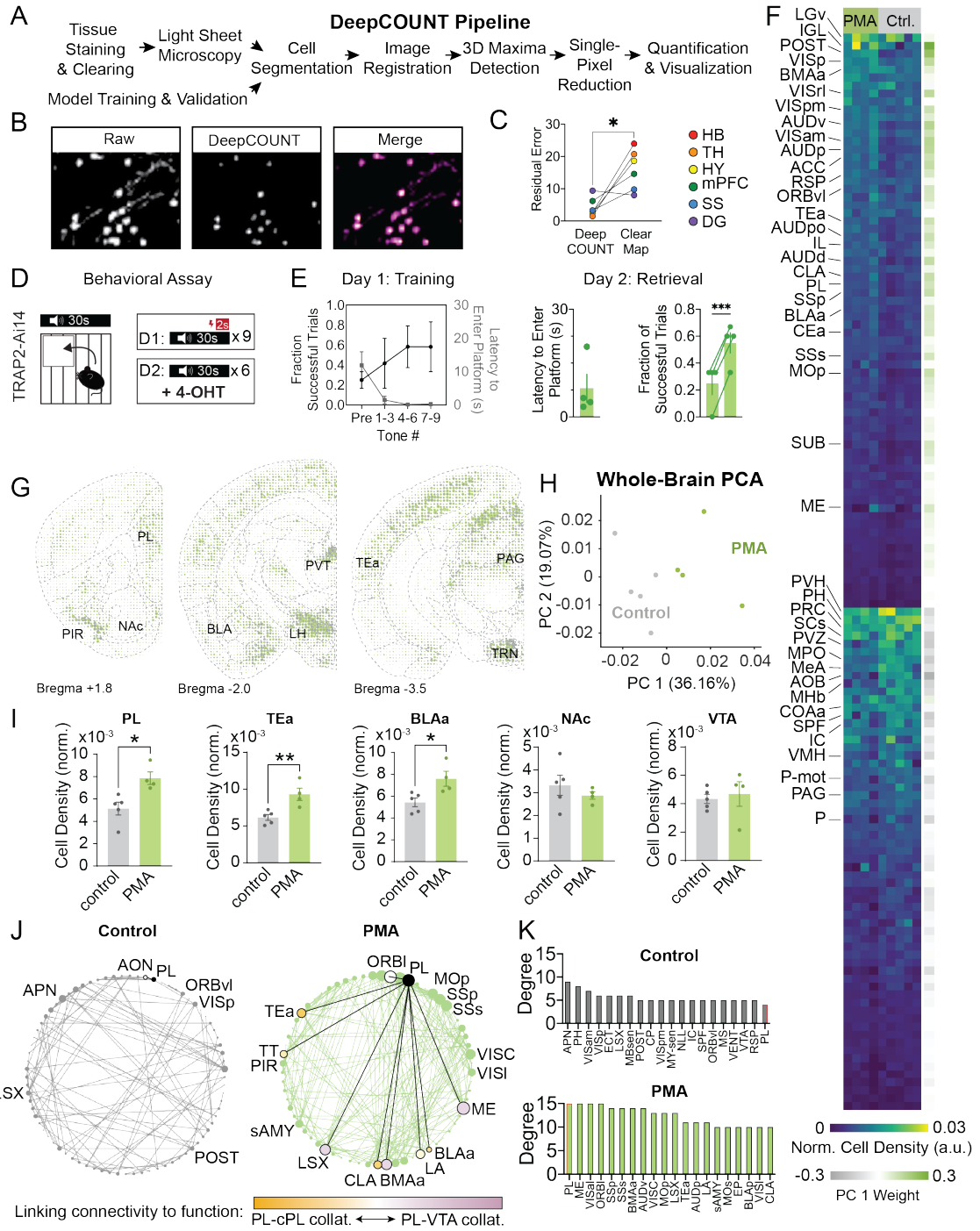

Figure 4-5. Whole-brain IEG mapping of learned avoidance with DeepCOUNT.
(A) Overview of DeepCOUNT workflow (B) Overlay of raw data and axon segmentation using trained cell detection model. (C) Sample cell identification with DeepCOUNT. Comparison of residual error values for DeepCOUNT and ClearMap as compared to human annotations (P=0.022, n=6 brain regions; paired t-test). (D) Overview of platform mediated avoidance assay. TRAP2;Ai14 mice were trained in PMA on day (D)1 and then TRAPed during a retrieval test on D2. (E) Fraction of successful trials increased (F=5.67, P=0.012, n=4, One-way ANOVA) and latency to enter the platform decreased (F=7.21, P=0.005, n=4, One-way ANOVA) across training. On retrieval day, mice entered the platform with an average latency of 7.9 s after tone onset and were more likely to be on the platform at the end of the tone compared to pre-training (P=0.0005, n=4, paired t-test). (F) Left heatmap: relative cell density

(normalized to region volume and gross label content per brain) across 140 regions defined by the Allen Brain Atlas. Right heatmap: Loadings for PC1 (arbitrary PC weight units). (G) Dotogram overlay of control (grey) and PMA (green) conditions. Dots represent the density of TRAPed cells in a given voxel. (H) Locations of individual mice projected in principal component (PC) space defined by the first two PCs (arbitrary PC units, control, *n*=5; PMA, *n*=4). (I) Comparison of TRAPed cell density in 5 brain regions of naïve controls (grey) and PMA-trained mice (green) (Student's t-test; **P*<0.05, ***P*<0.01; control: *n*=5; PMA: *n*=4). (J) Network diagrams for control (left) and PMA-trained (right) mice based on brain wide interregional correlations. Node size is proportional to degree. (K) Degree values for top 20 most connected regions for each condition (PL outlined in red). Error bars, mean ± S.E.M. See Table 5-2 for interregional correlations related to network construction shown in J,K.

avoidance retrieval session by pairing that experience with a tamoxifen injection (Figure 4-5d). In PMA, we defined successful trials as those in which the animal remained on the platform for the last 2 seconds of the tone, when the shock normally occurs. During training, mice significantly increased their fraction of successful trials and decreased their latency to enter the safety platform. On the retrieval day, mice entered the platform with an average latency of 7.9 seconds after tone onset and were more likely to remain on the platform at the end of the tone compared to their pre-training baseline (Figure 4-5e).

We used DeepCOUNT to quantify TRAPed cell density in each brain region and plotted these data as a heatmap in which regions with more TRAPed cells in PMA-trained mice are on top and regions with more TRAPed cells in naïve controls are in the bottom half of the heatmap (Figure 5F). We also plotted the data as a dotogram (Figure 4-5g). Principal component analysis of whole-brain TRAPed cell counts separated PMA-trained and non-shocked control animals along the first principal component (PC1) (Figure 4-5h). PC1 weights revealed that PMA-activated brain regions were biased toward the cortex, hippocampal formation, and cortical subplate (Figure 4-5f). We compared cell counts between PMA and control animals in PL and several key target regions, finding significant increases in the number of TRAPed cells in PL, BLA, and TEa but not in NAc or VTA (Figure 4-5i). Overall, our DeepCOUNT screen identified regions known to be involved in threat avoidance (e.g. PL and BLA). We also identified several regions with unknown roles in threat avoidance (e.g. TEa and postsubiculum (POST) that will be of interest for future functional studies) (Figure 4-5f,g,i).

To relate the organization of PL circuits to their role in threat avoidance, we assessed functional connectivity based on whole-brain TRAPing. We computed inter-regional correlations for groups of PMA-trained and naïve control mice. This allowed us to identify sets of regions where the numbers of TRAPed cells co-varied across mice. Regions that co-vary may constitute elements of a network engaged during learned threat avoidance. We then generated network graphs in which the nodes and connections represent brain regions and correlations that survived thresholding using $r \geq 0.9$ and $P < 0.05$ as cutoffs. In the network plots, node size is proportional to degree, or the number of connections for that node (Figure 4-5j).

To link these findings to our neuroanatomical studies, we examined PL functional connectivity while considering the collateral maps presented in figures 3-4. Our network analysis revealed PL as one of the mostly highly connected nodes in the PMA group (Figure 4-5k). PL was functionally connected to several cortical areas (TEa, ORBl, MOp, SSp, SSs), taenia tecta (TT), the lateral septal complex (LSx), claustrum (CLA), several amygdalar regions (LA, BLAa, BMAa), and the median eminence (ME). Of these regions, CLA, TEa, TT are preferentially innervated by PL-cPL collaterals and LSx is preferentially innervated by PL-VTA collaterals. Compared to PL-VTA, PL-NAc and PL-cPL neurons send denser projections to BLAa. Compared to PL-cPL neurons, PL-NAc and PL-VTA neurons send denser projections to BMAa (Figures 4-3,4-4). To visualize this preferential anatomical innervation on the functional connectivity maps, we colored the PL-connected nodes based on their PCA weight from the analysis shown in Figure 4-3e (Figure 4-5j). These data suggest that all three neuronal classes likely contribute to threat avoidance behavior and that they may act via particular collateral projections.

Fiber Photometry During Platform-Mediated Avoidance

As prelimbic cortex has been implicated in both innate and learned avoidance, we investigated how different PL cell classes contribute to threat avoidance by using fiber

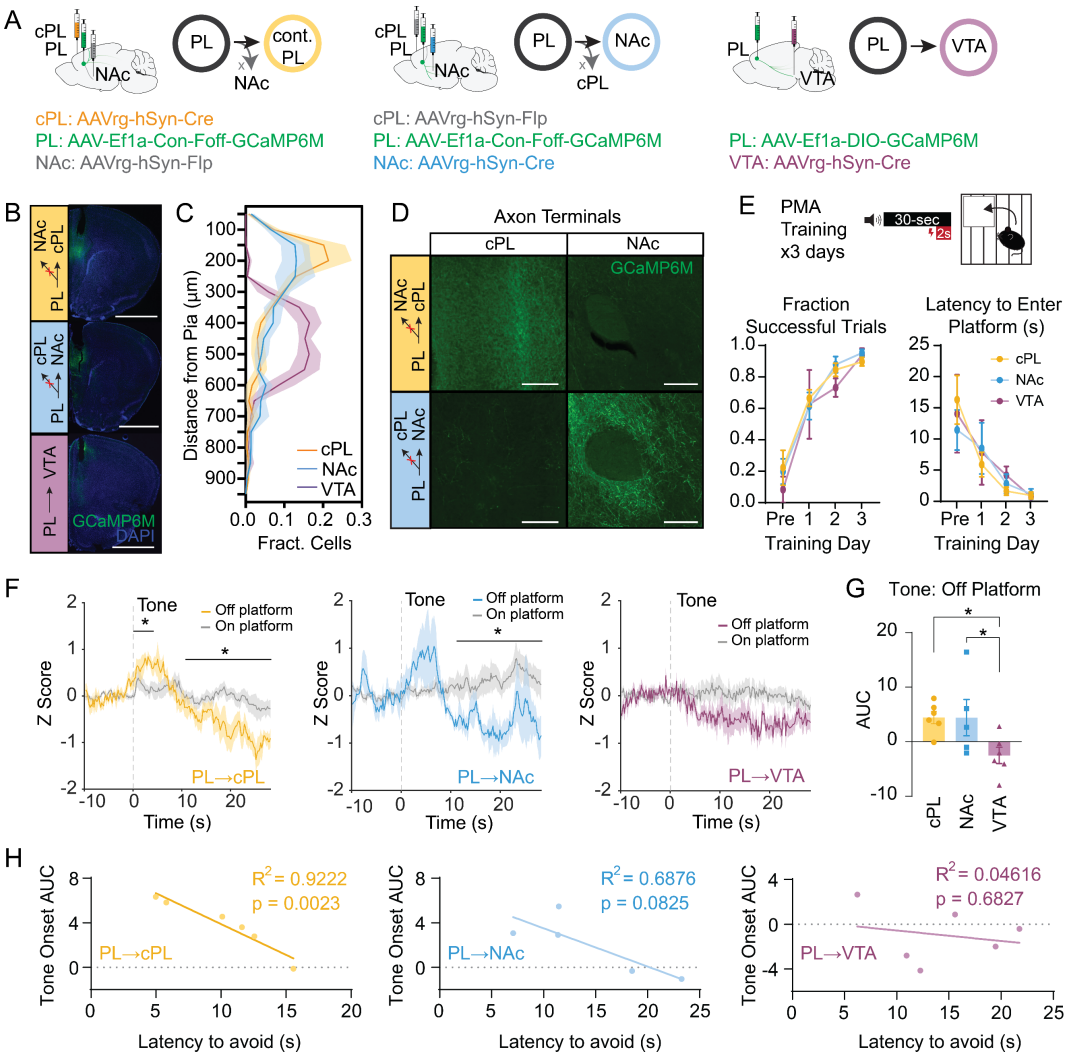

Figure 4-6. Neuronal class-specific activity during threat cues. (A) GCaMP injection strategy. Left: to target cPL-projecting neurons, mice were injected with AAVrg-Cre in cPL and AAVrg-Flp in NAc, and Con-Foff-GCaMP6M in PL. Middle: to target NAc-projecting neurons, mice were injected with AAVrg-Flp in cPL and AAVrg-Cre in NAc, and Con-Foff-GCaMP6M in PL. Right: to target VTA-projecting neurons, mice were injected with AAVrg-Cre in VTA and DIO-GCaMP6M in PL. (B) Representative images of GCaMP expression and fiber placement sites in PL. Scale bar, 1mm. (C) Distribution of cPL-, NAc- and VTA-projecting GCaMP-expressing cells across cortical layers ($F_{bin}(4,54) = 28.3$, $P<0.0001$, $F_{binxclass}(36,234) = 34.09$, $P<0.0001$; cPL: n=6, NAc: n=5, VTA: n =6; 2-way ANOVA). (D) Representative images of axon terminals in cPL and NAc using the intersectional viral targeting strategy shown in A. Scale bars, 100um. (E) Schematic of PMA assay and behavioral performance across sessions. Fraction successful avoids: $F_{day}(2,24) = 65.18$, P<0.0001, $F_{class}(2,14) = 0.58$, P=0.57, $F_{class\ x\ day}(6,36) = 0.43$, P=0.86, two-way ANOVA. Latency to enter platform: $F_{day}(3,36) = 14.27$, P<0.0001, $F_{class}(2,14) = 0.09038$, P=0.91, $F_{class\ x\ day}(6,36) = 0.48$, P=0.82, two-way ANOVA. (F) GCaMP fluorescence in cPL-, NAc-, and VTA-projecting neurons. Signals are aligned to tone onset and separated by whether mouse is on (colored trace) or off (grey trace) the safety platform at the start of the tone. *P<0.05 for student's t-test comparing on vs. off platform activity in a given time window. (G) AUC analysis of Ca^{2+} signal for tone periods (0–10s) when mice were off the platform ($F(2,14) = 4.106$, P=0.04, cPL: n=6, NAc: n=5, VTA: n =6; One-way ANOVA with Tukey post-hoc test. (H) Correlation between AUC during off-platform tone periods (0-10s) and average latency for a mouse to enter the platform. Error bars, mean ± S.E.M.

photometry to record population-level neural activity. Activity in PL-NAc neurons has previously

been shown to reduce learned avoidance responses (Diehl et al., 2020). PL-VTA and PL-cPL neurons have yet to be studied in the context of learned avoidance; however, PL-VTA neurons encode aversive stimuli, and PL-cPL neurons are a strong candidate to mediate the prefrontal hemispheric synchrony observed in spatial avoidance (Vander Weele et al., 2018; Dickson et al., 2022). Further, all three of the populations we mapped have axon collaterals in BLA, a key region in fear and avoidance learning (Arruda-Carvalho and Clem, 2014; Diehl et al., 2020). In addition to revealing insights into the functions of understudied neuronal classes, our populations of choice allow us to dissect the heterogeneity of PL-BLA neurons and their role in avoidance.

Given the high overlap of collateral projection targets for PL-cPL and PL-NAc neurons (Figures 4-3i,j), we further separated these classes using an intersectional viral strategy (Fenno et al., 2020). To record neuronal activity in PL-cPL neurons that do not project to NAc, we injected AAVrg-Cre into cPL and AAVrg-Flp into NAc. We then injected Cre-On Flp-Off GCaMP6M into PL. We switched the Cre and Flp injection sites to record from NAc-projecting neurons that do not project to cPL. To record from VTA-projecting neurons, we injected AAVrg-Cre into VTA and DIO-GCaMP6M into PL (Figure 6A,B). Most $GCaMP^+$ cell bodies from the intersectionally-defined cPL- and NAc-projecting neurons were in superficial layers of PL, while cell bodies from VTA-projecting neurons were restricted to the deeper layers (Figure 4-6c), as expected from our initial layer analysis (Figure 4-2b). We observed few $GCaMP^+$ axon terminals in NAc from the cPL-projecting group, and few $GCaMP^+$ axon terminals in cPL from the NAc-projecting group (Figure 4-6d), suggesting our intersectional strategy was effective in separating these populations.

We recorded from PL while mice performed PMA. We kept the shock active across 3 days of recording, which allowed us to average signals over many trials without extinction occurring. Mice learned quickly, successfully avoiding most shocks and entering the platform with an average latency of 8 seconds after tone onset on the first day of training, with minor

performance improvements across days (Figure 4-6e). We first analyzed responses to the conditioned tone. Interestingly, tone-evoked neural activity distinguished between epochs when mice were off vs. on the safety platform (Figure 4-6f). cPL-projecting neurons had significantly higher activity at the tone onset when the animal was off the platform. As the tone progressed, activity in these neurons gradually decreased. We observed a similar trend in NAc-projecting neurons. In contrast, PL-VTA cells lacked a tone onset response, but did have a gradual decrease in activity during the conditioned tone (Figure 4-6g). These findings suggest neural activity in response to a conditioned stimulus is modulated by whether threat requires action, and that these patterns vary across projection classes.

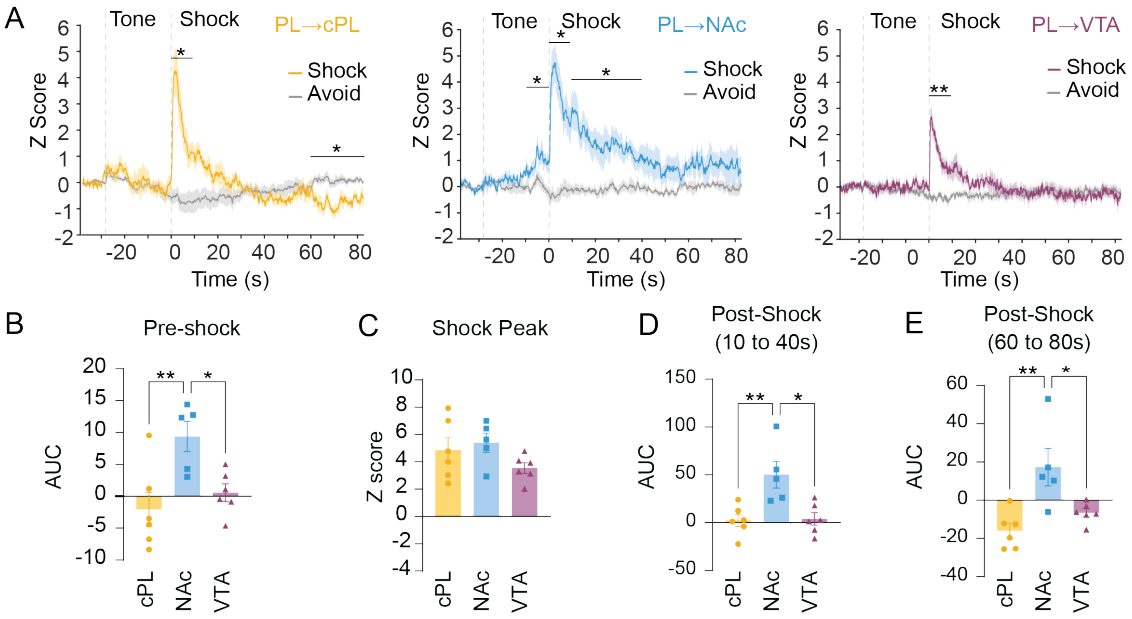

Figure 4-7. Neuronal class-specific activity during aversive stimuli. (A) GCaMP fluorescence in cPL-, NAc- and VTA-projecting PL cells. Signals are aligned to shock onset and separated by whether mouse is on (colored trace) or off (grey trace) the safety platform during the shock period. **P*<0.05, ***P*<0.01 for student's t-test comparing on vs. off platform activity in a given time window. Analysis of Ca^{2+} signals for circa-shock periods: (B) Pre-shock AUC: F(2,14) = 6.97, *P*=0.0079 (C) Shock AUC: F(2,14) = 1.87, *P*=0.19 (D) Post-shock AUC (10–40s): F(2,14) = 8.28, *P*=0.0042 (E) Post-shock AUC (60–80s): F(2,14) = 8.79, *P*=0.0034. For B-C, cPL: *n*=6, NAc: *n*=5, VTA: *n* =6, One-way ANOVA with Tukey post-hoc test. Error bars, mean ± S.E.M.

To determine if the observed tone onset responses related to avoidance behavior, we calculated correlations between the AUC for the first 10 seconds of the tone and the average latency to enter the platform. Activity in the PL-cPL neurons had a tight negative correlation with

the latency to enter the platform. Activity in the PL-NAc neurons also had negative correlation with latency to enter the platform, but it did not reach significance. Activity in PL-VTA neurons had no relationship with the latency to enter the platform (Figure 4-6h). Together, these findings point to PL-cPL projectors as a key neuronal class that links threatening cues to avoidance behavior.

Activity in all classes sharply increased upon foot shock onset (Figure 4-7a). NAc-projecting neurons had significantly higher activity than the other two classes in the ten seconds preceding a shock (Figure 4-7b), consistent with a larger role for those cells in risky exploration. We found no differences in peak shock response between the three classes (Figure 4-7c). Further, while activity in PL-VTA neurons rapidly returned to baseline levels following the foot shock, activity in PL-cPL and PL-NAc neurons had prolonged deviations from baseline for up to a minute after the shock. Activity in NAc-projecting neurons remained elevated above baseline for up to eighty seconds following a foot shock, while activity in cPL-projecting neurons decreased steadily during the same period (Figure 4-7d,e). These data suggest that while all PL classes encode aversive stimuli, prolonged post-shock activity in PL-cPL and PL-NAc neurons may play specialized roles in action-outcome learning.

Prefrontal Neuron Classes Distinguish between Learned and Innate Avoidance

To further classify the effects of aversive learning on neural activity in PL cell classes, we compared their activity during learned vs. innate threat avoidance. Using the same mice from the PMA experiments, we recorded neural activity in the Elevated Zero Maze (EZM), in which two quarters of an elevated ring are protected by walls and the other two quarters are open. Mice innately avoid the open arms of this apparatus, where there is more perceived threat potential.

We compared activity during entries and exits from the safe zone in each assay. In PMA, population activity in all three neuronal classes increased prior to platform entries, an effect that

grew stronger with training (Figure 4-8a). In contrast, only NAc- and cPL-projecting neurons increased their activity prior to entry into the closed arm of the EZM (Figure 4-8b). During exits from the safe zone, a form of risky exploration, all three PL classes had similar increases in

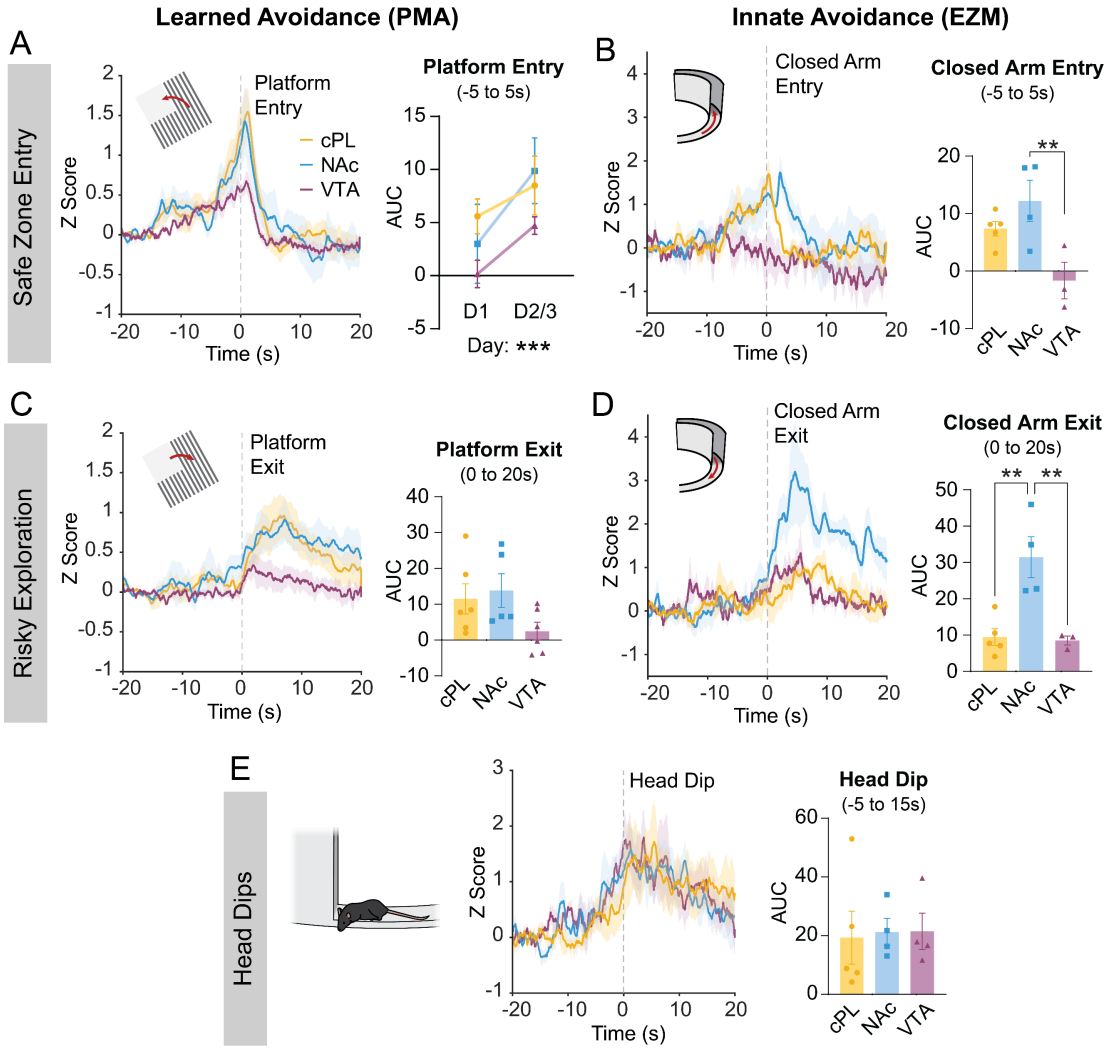

Figure 4-8. Neuronal class-specific activity during learned vs. innate threat avoidance behavior. (A,B) GCaMP fluorescence aligned to safe-zone entry in learned (A) vs. innate (B) avoidance for cPL-projecting (yellow), NAc-projecting (blue) and VTA-projecting (purple) neurons. Inset plots show AUC analysis of Ca^{2+} signal aligned to avoidance (-5–5s). Platform entry AUC increases between training Day (D)1 and D2/3 across cell types. (PMA: $F_{day}(1,14) = 17.59$, P=0.0009, $F_{class}(2,14) = 1.488$, P=0.26, $F_{class\ x\ day}(2,14) = 0.98$, P=0.40, two-way ANOVA; EZM: F(2,9)=6.11, P=0.02; One-way ANOVA with Tukey post-hoc test). (C,D) GCaMP fluorescence aligned to onset of risky exploration in learned (C) vs. innate (D) avoidance for cPL-projecting (yellow), NAc-projecting (blue) and VTA-projecting (purple) neurons. Inset plots show AUC analysis of Ca^{2+} signal aligned to exploration onset (0–20s) (PMA: F(2,14) = 2.43, P=0.12; EPM: F(2,9) = 11.97, P=0.0029, One-way ANOVA with Tukey post-hoc test). (E) Analysis of Ca^{2+} signals during head dips (F(2,10) = 0.64, P=0.55; One-way ANOVA with Tukey post-hoc test.). Error bars, mean ± S.E.M. PMA: cPL n=6, NAc n=5, VTA n=6; EZM: cPL n=5, NAc n=4, VTA n=3.

activity during PMA (Figure 4-8c). In innate avoidance, however, exits from the closed arm were marked by a significantly larger response in NAc-projecting neurons compared to the other two cell populations (Figure 4-8d). Together, these data indicate that aversive learning enhances encoding of avoidance behaviors and engages VTA-projecting neurons to behavioral circuits for threat avoidance. Further, PL-NAc neurons preferentially encode risky exploration.

A concern with comparing fiber photometry recordings across different classes of neurons is that differences in signal between the classes could lead to exaggerated results in one direction. While PL-VTA neurons had lower overall activity during risky exploration of the shock bars and open arm, all three PL classes had similar activity during head dips on the EZM, another form of exploratory behavior (Figure 4-8e). This suggests that PL-VTA neurons did not simply have lower activity than the other classes during behavior, but instead that these differences are specific to situations when animals are navigating the environment.

PL-cPL and PL-NAc activity is correlated with BLA collateral axon density

PL-cPL and PL-NAc neuronal classes both send dense collateral projections to BLA (Figures 4-3e, 4-4e), a key region in fear and avoidance learning and memory (Ledoux, 2000). However, recent single neuron reconstructions revealed that PL-cPL and PL-NAc classes are heterogeneous and contain neurons that do not send collaterals to the BLA (Gao et al., 2022). We took advantage of this heterogeneity to estimate the activity of BLA collaterals, calculating correlations between the activity measured using fiber photometry and the density of GCaMP+ axons in the BLA. To do this, after completing the fiber photometry experiments, we perfused the mice and quantified axonal GCaMP fluorescence in the BLA in 2D brain sections (Figure 4-9a).

In both PL-cPL and PL-NAc classes, we observed a significant positive correlation between tone-onset responses (AUC during first 4 seconds of the tone when mice were off the platform) and the density of GCaMP+ axon collaterals in BLA (Figure 4-9b). On the other hand, we observed no significant relationships between activity and platform entries or exits (Figure 4-

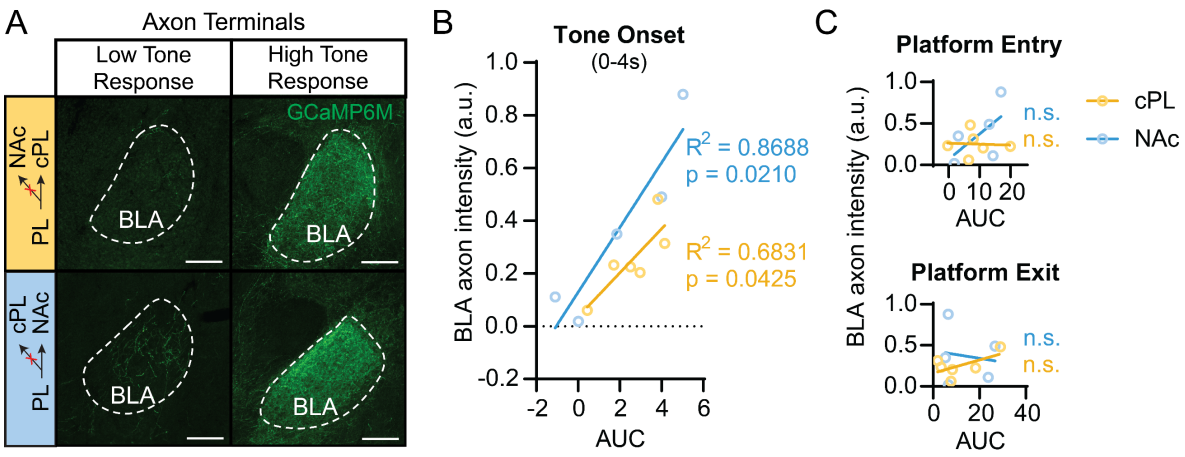

Figure 4-9. Correlation of neural activity and BLA axon collateralization in PL-cPL and PL-NAc populations. (A) Representative images of GCaMP$^+$ axon terminals in BLA of animals with low and high off-platform tone responses. (B) BLA axon intensity is correlated with off-platform tone response (AUC: 0 to 4s). cPL *n*=6, NAc *n*=5. Simple linear regression. (C) BLA axon intensity is not correlated with platform entry responses on Day 2/3 (AUC: -5 to 5s; PL-NAc: R^2=0.38, p=0.27; PL-cPL: R^2=0.003, p=0.92) or platform exit responses (AUC: 0 to 20s; PL-NAc: R^2=0.38, p=0.27; PL-cPL: R^2=0.003, p=0.92). cPL *n*=6, NAc *n*=5. Simple linear regression.

9c). These data suggest that within the PL-NAc and PL-cPL populations, those neurons that collateralize to the BLA drive responses to threatening cues. Importantly, since we used intersectional approaches to separate PL-cPL and PL-NAc neurons, these data also indicate that multiple subclasses of PL-BLA projection neurons encode conditioned cues. Interestingly, for PL-NAc neurons, there was a trend-level correlation between activity during platform entries and BLA collateral axon density. This suggests there may be a subclass of PL neurons that projects to both NAc and BLA and encodes the behavioral action of threat avoidance, but more investigation is needed to confirm this.

DISCUSSION

In this study, we integrated whole-brain mapping with the observation of neural activity to better understand how mPFC controls threat avoidance behavior. We introduce DeepTraCE and DeepCOUNT, open-source analysis pipelines for quantifying bulk axonal projection patterns and cells, respectively. We used DeepTraCE to produce whole brain projection maps of three populations of mPFC projection neurons: PL-cPL, PL-NAc, and PL-VTA. We combined activity-

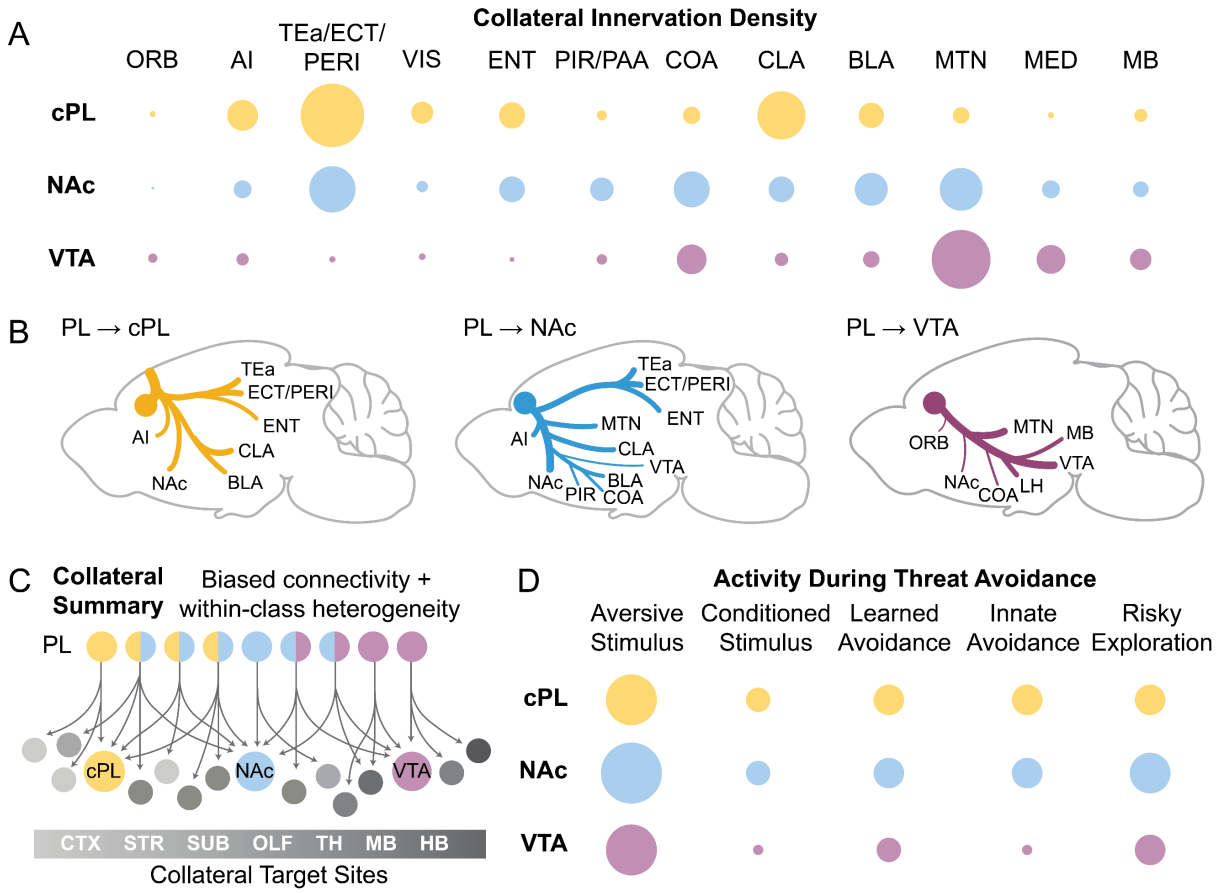

Figure 4-10. Summary of Findings. (A) Visualization of collateralization density in key targets of PL–cPL, PL–NAc, and PL–VTA neurons. Dot radius correlates with average normalized labeling density within a region. (B) Schematic of whole-brain collateralization patterns of PL–cPL, PL–NAc, and PL–VTA neurons. (C) Summary of PL efferent connectivity patterns. (D) Visualization of activity levels in PL–cPL, PL–NAc, and PL–VTA neurons during aspects of threat avoidance. Dot radius correlates with average normalized signal intensity. See Table 1 for abbreviations.

dependent genetic labeling with DeepCOUNT to relate the structural and functional organization of brain-wide networks for threat avoidance. With whole-brain projection maps as a foundation, we used intersectional viral targeting to separate the overlapping populations of PL-cPL and PL-NAc neurons. We then recorded the activity of PL-cPL, PL-NAc and PL-VTA neuronal populations during learned and innate threat avoidance. Our study reveals PL class-specific roles in threat avoidance and demonstrates the utility of DeepTraCE and DeepCOUNT for linking high-throughput neuroanatomy with functional techniques to reveal mechanisms of complex behavior (Figure 4-10).

While we have gained invaluable insights into the complex anatomy of cortical neurons from single neuron reconstructions (Oh et al., 2014; Economo et al., 2018; Gao et al., 2022), the equipment, expertise, and time required to reconstruct individual neurons are out of reach for many labs. Other high-throughput techniques such as MAPseq (Kebschull et al., 2016) provide single cell resolution, but are costly and limited to predefined target regions. While bulk labelling approaches lose granularity, DeepTraCE's high-throughput workflow combined with its reliance on common viral techniques make it a useful tool to tackle many unanswered questions. Mouse Cre-driver lines and floxed alleles can be used with DeepTraCE to analyze the projection patterns of defined neuronal populations and how they can be altered by genetic manipulations. Or, DeepTraCE and DeepCOUNT can be used to define differences in structural and functional connectivity resulting from environmental insults such as chronic stress. With DeepTraCE, in addition to simply quantifying relative densities of axonal projections in target regions, users can assess within-region changes in layer-specific or topographic targeting. This information can guide the design of precisely targeted functional studies.

There are caveats associated with retrograde viruses, brain clearing, and LSFM. AAVrg viruses have been shown to have preferential labelling of corticothalamic (CT) neurons in L5, and biases against CT neurons in L6 (Sun et al., 2019; Leow et al., 2022), while CTB showed the opposite pattern of layer bias (Leow et al., 2022). We observed few AAVrg+ neurons in L6, but some CTB+ neurons (Figure 2B) and may have underestimated the contributions of L6 cells to the population data for PL-cPL and PL-NAc neurons (Gabbott et al., 2005; Anastasiades and Carter, 2021). Also, tissue clearing does not always achieve complete transparency. This issue, together with resolution limits of light sheet microscopes that can visualize intact mouse brains in a timely fashion, can produce blurring of structures deep in the tissue. While estimates of axonal density may be less accurate in deep brain structures, they are likely to be biased to a similar degree for different neuronal classes so are still well-suited for comparing inter-class differences. Finally, like most mapping studies, we visualized axons but not synapses. Therefore, our

DeepTraCE quantifications may also include axons of passage. To mitigate this, our models were trained to exclude major white matter tracts.

Despite these caveats, our brain wide projections maps of PL-cPL, PL-VTA, and PL-NAc neurons aligned with known projection patterns (Sesack et al., 1989; Vertes, 2004; Gabbott et al., 2005; Oh et al., 2014; DeNardo et al., 2019; Winnubst et al., 2019; Gao et al., 2022) – underscoring the accuracy of TrailMap (Friedmann et al., 2020) and DeepTraCE – and revealed unappreciated topographic innervation patterns. Consistent with bulk tracing studies (Sesack et al., 1989; Vertes, 2004; DeNardo et al., 2019), we observed the densest PL projections in association cortices, claustrum, striatum, amygdala, polymodal thalamic nuclei, hypothalamus, and midbrain. These bulk projection patterns are the sum of multiple classes.

mPFC contains intratelencephalic (IT) neurons that project within the cortex and pyramidal tract (PT) neurons that project to subcortical areas. PL-cPL neurons fall in the IT class, PL-VTA neurons are from the PT class, and PL-NAc contain members of both (Anastasiades and Carter, 2021). In line with these classifications and single neuron reconstructions (Winnubst et al., 2019; Anastasiades and Carter, 2021; Gao et al., 2022), we observed that PL-cPL neurons were enriched in superficial layers (L2-5a) and collateralize to other cortical association areas, subplate, and striatum. Consistent with the well-described features of PT neurons (Economo et al., 2018; Anastasiades and Carter, 2021; Gao et al., 2022), we observed retrogradely labeled PL-VTA neurons localized to L5b and collateralize to the thalamus, pons, striatum, and midbrain. PL-NAc neurons collateralized broadly to both IT and PT targets (Anastasiades and Carter, 2021). The diversity of the collateral targets of PL-NAc neurons is supported by single neuron reconstructions that revealed a variety of subclasses targeting only a few structures(Gao et al., 2022). Overall, this excellent alignment between our data and previous work supports the utility of DeepTraCE for capturing meaningful class-specific differences in connectivity in a high-throughput manner.

On a brain wide scale, counts of IEG-expressing cells can reveal behaviorally-relevant activity and functional connectivity (Wheeler et al., 2013; Vetere et al., 2017; DeNardo et al., 2019). Previous studies examining c-fos expression following active avoidance behavior analyzed only discrete regions of interest (Nikolaev et al., 1992; Duncan et al., 1996; Bravo-Rivera et al., 2015). Using DeepCOUNT we recapitulated previous findings of activation in PL, BLA and OFC following PMA and found high numbers of TRAPed cells in understudied regions including POST and TEa (Bravo-Rivera et al., 2015). POST is important for spatial learning, and PL neurons that project there may facilitate learning of the location of the safety platform (Bett et al., 2012, 2013; Peckford et al., 2014). PL projections to TEa may facilitate long-term storage of the avoidance memory, as TEa is necessary for long term retrieval of cued fear (Sacco and Sacchetti, 2010). Functional connectivity analysis revealed the major functional targets of PL. Of these, TEa, CLA, and TT are highly innervated by the collaterals of PL-cPL projection neurons, while LSx and BMAa are more densely innervated by PL-NAc and PL-VTA collaterals. These represent new targets to manipulate in future studies of threat avoidance and highlight how whole brain anatomical and functional maps can be used together to identify novel behaviorally-relevant pathways.

We used fiber photometry to determine how each class of neuron encodes threat avoidance. We found that intersectionally-defined PL-NAc and PL-cPL neurons increased their activity during conditioned tones, but only when mice were off the safety platform, suggesting those populations encode the predictability of threat. In contrast, PL-VTA neurons decreased their activity in response to the threat predictive cue. Single unit recordings haven shown that distinct populations are excited and inhibited by a conditioned tone during PMA (Diehl et al., 2018). Our results indicate that the projection targets we studied may be a factor that separates these populations.

We found that PL-NAc neurons encoded risky exploration. This is consistent with previous work showing that excitation of PL-NAc projections decreases avoidance behaviors (Diehl et al., 2020). However, individual neurons within this projection class have heterogeneous functions. A

subset of mPFC-NAc neurons restrain reward seeking under threat of punishment (Kim et al., 2017). Other work suggests mPFC-NAc neurons that suppress reward seeking preferentially target the NAc shell (Piantadosi et al., 2020). Our AAVrg targeted the NAc core and we likely captured a larger proportion of mPFC-NAc neurons involved in risk engagement rather than suppression. Our observation of PL-NAc neurons resembles the activity patterns seen in mPFC neurons projecting to dorsomedial striatum during avoidance (Loewke et al., 2021; Kajs et al., 2022). Indeed, we observed mPFC-NAc collaterals in the dorsomedial striatum, suggesting these populations overlap.

All three projection classes studied send axon collaterals to the BLA. Bulk stimulation of mPFC-BLA neurons promote avoidance in PMA by reducing the latency to enter the platform following tone onset (Diehl et al., 2020). Further, auditory fear conditioning induces synaptic plasticity in the mPFC-BLA pathway (Arruda-Carvalho and Clem, 2014). We found that within the PL-cPL and PL-NAc classes, the magnitude of the tone onset response correlates with the amount of axon collateral innervation within the BLA. This suggests neurons projecting to BLA are a major driver of the tone onset responses within each population. Single neuron reconstructions showed that mPFC-BLA projection neurons are heterogeneous, including a class with no collateralization (Gao et al., 2022). Our results demonstrate that PL-BLA neurons, which encode threat predictive cues, include neurons collateralizing to NAc and cPL, suggesting synchronized transmission of this signal to multiple downstream regions may facilitate the brain dynamics necessary for learning and/or behavioral responding. Collateralization has been suggested as an understudied mechanism through which synchronous or asynchronous patterns of brain activity emerge and contribute to cognitive states (Rockland, 2018).

PL-cPL connections are important for both hemispheric synchronization and lateralization of mPFC activity. Lateralization has been associated with anxiety-like behavior (Costa et al., 2016) and stress responses in rodents (Sullivan and Gratton, 1999; Stevenson et al., 2008; Lee et al., 2015), and increased mPFC hemispheric synchrony has been associated with spatial

avoidance (Dickson et al., 2022). Our data show that PL-cPL neurons persistently tracked threat, threat predictive cues, and threat avoidance behaviors. In the future, studies manipulating these neurons will be required to understand whether these activity patterns are necessary for learned or innate avoidance.

PL-VTA populations encoded learned but not innate threat avoidance behavior. Associative learning depends on the mPFC to encode predictive cues and on VTA to encode prediction errors (Lak et al., 2020). PL-VTA neurons may regulate the separable actions of these two regions. To our knowledge, we are the first to directly study the role of mPFC-VTA neurons in threat avoidance, however, VTA-mPFC neurons have been shown to respond to aversive stimuli and facilitate associative learning (Gonzalez et al., 2014; Puig et al., 2014; Kim et al., 2016; Vander Weele et al., 2018). mPFC-VTA may form part of a feedback loop influencing aversive learning. Interestingly, PL-VTA neurons showed the greatest collateral innervation of LHb. In gerbils, VTA and LHb have been shown to have opposing effects on acquisition of learned avoidance with stimulation of VTA enhancing avoidance and stimulation of LHb impairing it (Shumake et al., 2010). PL neurons that project to both VTA and LHb may balance the activity within each region to control avoidance responses.

ACC	Anterior Cingulate Cortex
AH	Anterior Hypothalamic Area
AHN	Anterior Hypothalamic Nucleus
AId	Agranular Insula, dorsal part
AIp	Agranular Insula, posterior part
AIv	Agranular Insula, ventral part
ATN	Anterior Group of the dorsal thalamus
AUDd	Dorsal auditory area
AUDp	Primary auditory area
AUDv	Ventral auditory area
BLA	Basolateral amygdala
BLAa	Basolateral amygdala, anterior part
BLAv	Basolateral amygdala, ventral part
BNST	Bed nucleus of the stria terminalis
CLA	Claustrum
cPL	Contralateral prelimbic area
CNU	Cerebral nuclei
COA	Cortical amygdalar area
COAa	Cortical amygdalar area, anterior part
COAp	Cortical amygdalar area, posterior part
CP	Caudate putamen
CTXsp	Cortical subplate
DP	Dorsal peduncular area
ECT	Ectorhinal cortex
ENTl	Entorhinal area, lateral part
ENTm	Entorhinal area, medial part
EP	Endopiriform nucleus
GENd	Geniculate group, dorsal thalamus
GU	Gustatory areas
HB	Hindbrain
HPF	Hippocampal formation
IC	Inferior colliculus
IGL	Intergeniculat leaflet of the lateral geniculate complex
IL	Infralimbic cortex
ILM	Intralaminar nucleus of the dorsal thalamus
Isoctx	Isocortex
LAT	Lateral geniculate nucleus
LGv	Ventral part of the lateral geniculate nucleus
LH	Lateral hypothalamus
LHb	Lateral habenula
MA	Magnocellular Nucleus
MB	Midbrain
MB-un	Midbrain-unlabeled
MBO	Mammillary body
MeA	Medial amygdala
MED	Medial group of the dorsal thalamus
MHb	Medial habenula
MOp	Primary motor area
MOs	Secondary motor area
mPFC	medial prefrontal cortex
MPN	Medial preoptic nucleus
MTN	Midline group of the dorsal thalamus
MY-mot	Medulla, motor related
MY-sen	Medulla, sensory related
NAc	Nucleus accumbens
NDB	Nucleus of the diagonal band
NLOT	Nucleus of the lateral olfactory tract
OLF	Olfactory tract
ORBm	Orbital area, medial part
OT	Olfactory tubercle
P-mot	Pons, motor related
P-Sat	Pons, behavioral state related
P-Sen	Pons, sensory related
PAA	Piriform-amygdalar area
PAG	Periaqueductal grey
PERI	Perirhinal area
PH	Posterior hypothalamic nucleus
PIR	Piriform area
PL	Prelimbic area
POST	Postrhinal area
PP	Peripeduncular nucleus
PPN	Pedunculopontine nucleus
PRC	Precommisural nucleus
PVHd	Paraventricular hypothalamic nucleus, descending division
PVR	Periventricular region
RE	Nucleus of reuniens
RSP	Retrosplenial cortex
RT	Reticular nucleus of the thalamus
sAMY	Striatum-like amygdala
SCm	Superior colliculus, motor related
SCs	Superior colliculus, senosry related
SNr	Substantia nigra, reticular part
SPA	Subparafascicular area
SPF	Subparafascicular nucleus
SSp	Primary somatosensory area
SSs	Secondary somatosensory area
SubG	Subgeniculate nucleus
TEa	Temporal association area
TH	Thalamus
TR	Postpiriform transition area
VENT	Ventral group of the dorsal thalamus
VISC	Visceral area
VISp	Primary visual area
VISpl	Posterolateral visual area
VISpm	Posteromedial visual area
VISrl	Rostrolateral visual area
VTA	Ventral tegmental area
ZI	Zona incerta

Table 4-1. List of Abbreviations

Chapter 5: General Discussion

mPFC is a key brain region that facilitates both innate and learned threat avoidance. mPFC encodes threat and threat predictive stimuli and through its vast output circuitry, biases activity in downstream regions to guide behavior (Adhikari et al., 2011; Bravo-Rivera et al., 2014; 2015; Diehl et al., 2018; 2020; Loewke et al., 2021). Two unique features of mPFC – its protracted development and complex connectivity – may make it particularly well suited to control dynamic responses to a changing environment. Through detailed investigation of these two features, this thesis expands our knowledge of how mPFC circuits work together to regulate threat avoidance throughout the lifespan.

Two prefrontal pathways targeting the BLA and NAc have been shown to bidirectionally control threat avoidance in adult male rats (Diehl et al., 2020). However, their function had never been probed in early life. Chapter 3 of this thesis elucidates the developmental trajectories of PL-BLA and PL-NAc pathways and shows their differential function in threat avoidance behavior by age. These findings provide key insights into how the developing brain reorganizes to produce age-specific behavioral repertoires.

Studies detailing the physical complexity of mPFC circuits have largely done so independent of functional investigations. Chapter 4 links the brain-wide connectivity patterns of three prefrontal projections with their differential responses in learned and innate avoidance behavior. Additionally, whole brain activity mapping revealed understudied prefrontal projections that may be relevant to aspects of threat avoidance behavior. Together, these studies highlight how multiple mPFC projection pathways work in tandem to shape threat avoidance at different ages and across different assays.

The relative maturity of prefrontal pathways shape avoidance in early life

A key finding from Chapter 3 is that PL-BLA and PL-NAc pathways undergo differential timelines of maturation that together coordinate threat avoidance throughout early life. PL

projections have previously been shown to increase axon density in BLA throughout the first weeks of life, peak at P30, and decrease density into adulthood (Arruda-Carvalho et al., 2017). At PL-BLA synapses, the AMPA/NMDA ratio increases between P15 and P30 (Arruda-Carvalho et al., 2017). A reasonable hypothesis based on this data would be that the influence of the PL-BLA pathway during threat avoidance would linearly increase across development. However, our findings reveal that exciting the PL-BLA pathway has opposing effects in the juvenile and adult periods. In adults, optogenetic excitation of PL-BLA projections enhanced avoidance but the same manipulation disrupted avoidance at P23. This suggests that synaptic reorganization of the PL-BLA by age supports differential behavioral repertoires. Moreover, this period of reorganization spanning across adolescence may be a period in which this circuit is uniquely vulnerable to disruption.

Interestingly, excitation the PL-NAc pathway also had differential effects in early life. In adults, excitation of PL-NAc projections reduced avoidance, likely by promoting risky exploration. A role for the PL-NAc pathway in risky exploration in adults is also supported by findings in Chapter 4 that PL-NAc projections increased their activity when mice left the closed arm of the elevated plus maze to explore the open arm. However, in juvenile mice, PL-NAc excitation augmented time on platform. This effect was already reversed by adolescence where excitation no longer supported avoidance and inhibition of PL-NAc projections instead increased avoidance. This suggests that rapid reorganization of PL inputs with local NAc circuitry occurs between the juvenile period and adolescence, whereas PL-BLA circuitry undergoes more gradual changes between the juvenile period and adulthood.

Our electrophysiology data further reveals the nature of the staggered maturation of PL-BLA and PL-NAc pathways. Changes in E/I ratio were observed in the PL-NAc pathway between juvenile and adolescent periods but between adolescent and adult periods in the PL-BLA pathway. Studies investigating developmental changes locally within NAc are limited but also suggest there is rapid maturation from juvenile to adolescent periods. The largest change

in the number of D1 and D2 receptors expressed in NAc occurs before P30 in rats (Teicher et al., 2995). Similarly, a study investigating microglial-mediated pruning of D1 receptors suggested pruning occurs primarily during early adolescence (Kopec et al., 2018). In contrast, BLA undergoes a variety of changes between adolescence and adulthood. The number of neurons and glia in BLA are reduced between P35 and P90 in rats (Rubinow and Juraska, 2009). The number of dendritic branches in neurons also increase between P35 and adulthood (Koss et al., 2013). Together, this evidence supports a rapid maturation of the PL-NAc pathway between the juvenile period and adolescence and a more gradual time course of maturation in the PL-BLA pathway from the juvenile period to adulthood.

The staggard maturation pattern of PL-NAc and PL-BLA neurons may be a key process that shapes early life transitions in threat avoidance. Chapter 3 defined a nonlinear maturation of learned avoidance with adolescent mice displaying lower avoidance than both their younger juvenile counterparts and adults. In adolescents, inactivation of PL-NAc increased avoidance suggesting an high activity in this pathway may contribute to lower avoidance displayed adolescents. By adulthood, the observed increases in the E/I ratio of the PL-BLA pathway may balance this excitation, and other mechanisms may be in place that inhibit the PL-NAc pathways to promote avoidance.

Fiber photometry experiments in Chapter 3 showed that following platform entry, PL activity was suppressed in adult animals to a greater extent than in juveniles and adolescents. This may indicate inhibition of PL-NAc projections to prevent risky exploration and keep mice on the platform. In Chapter 4, our projection specific photometry data show that PL-NAc projectors increased activity at tone onset but then reduced their activity as the tone went on. This further suggests PL may inhibit the PL-NAc population to engage in avoidance. Previous work from Diehl et al., (2018) show that PMA training results in an increase in the number of PL neurons that become inhibited during that tone period and that this inhibitory signaling is required for avoidance (Diehl et al., 2018). Together with our data, it can be hypothesized that PL-NAc

neurons are a key population that are inhibited when animals are in a safe location during threatening cues.

The separable roles of PL-BLA and PL-NAc projections are interesting considering the collateralization patterns uncovered in Chapter 4. PL-NAc neurons, at least in part, collateralize to the BLA. This aligns with previous data using single neuron reconstructions (Gao et al, 2022). Gao et al. characterized a subtype of PL neurons that project predominantly to the BLA, NAc, and pallidum. However, they also characterized a class of PL neurons that project exclusively to BLA, and others that project to BLA and other regions not including NAc. This neuronal heterogeneity within the PL-NAc and PL-BLA pathways is important direction for future research. It is likely subpopulations of these pathways drive aspects of avoidance-related behavior. In Chapter 4, we showed that the magnitude of tone onset response observed in intersectionally-defined PL-NAc neurons correlates with the extent of collateral axon density in BLA. This suggests that the subsets of these population that collateralize to BLA are key drivers of the tone onset response and other neurons in the population may have different patterns of activity. Interestingly, the neurons identified by Gao et al., that projected to both NAc and BLA also innervated numerous other cortical and subcortical regions. These neurons may function in large scale coordination or induce state-like changes that modulate numerous brain regions. Neurons contacting fewer targets may have more specialized roles in discrete aspects of cognition and behavior.

Novel top-down prefrontal pathways in threat avoidance

The data presented in Chapter 4 revealed a previously unknown role PL-VTA projections in distinguishing between innate and learned threat avoidance. PL-NAc and PL-cPL pathways showed similar activity during entry onto the safety platform during PMA and entry into the closed arm in the EZM. By contrast, the PL-VTA pathway was only activated during platform entries in PMA, indicating a specific role in learned avoidance. Further work manipulating this pathway is needed to understand if it plays a causal role in learned avoidance.

In contrast to the PL-VTA pathway, the PL-cPL pathway investigated in Chapter 4 showed response dynamics to multiple task elements of both learned and innate avoidance. PL-cPL neurons persistently tracked threat, threat predictive cues, and threat avoidance behaviors. Broadly, PL-cPL connections control hemispheric synchronization of mPFC activity. Given that lateralization of mPFC activity has been associated with anxiety-like behavior and stress responses in rodents, alterations in the dynamics of these neurons may push avoidance responses into a pathological state (Costa et al., 2016; Sullivan and Gratton, 1999; Stevenson et al., 2008; Lee et al., 2015). The responses of PL-cPL projections to threat and threat cues can serve as a foundation to investigate how they may differ under stress and in disease.

Prefrontal projections to temporal association areas (TEa), piriform cortex (PIR) and claustrum (CLA) may also support threat avoidance. The functional connectivity analyses presented in Chapter 4 revealed that the number of active neurons in PL was highly correlated with the number of active neurons in TEa, PIR, and CLA in mice that performed PMA. TEa has been implicated in the long-term retrieval of cued fear (Sacco et al., 2010). Therefore, PL-TEa projections may facilitate long term storage of avoidance memories. CLA has been implicated in salience processing and behavioral selection under high cognitive demand (Seeley et al., 2007; Smith et al., 2019; White et al., 2020). PL-CLA projections may be recruited in situations where engagement in avoidance requires complex decision making.

Limitations and Future Directions

There are limitations associated with the experiments included within this thesis. Firstly, previous evidence has demonstrated that changes in fluorescence in the striatum measured using fiber photometry reflects primarily non-somatic changes in calcium rather than spiking (Legaria et al., 2022). While it is unclear how this may differ between brain regions, which can have differences in dendritic morphology, it is important to consider this may be the case in other brain regions as well. This is not to say that the information attained from fiber photometry is not useful in the goals of this dissertation. Rather than making claims to implicate somatic

activity in aspects of behavior, our studies were designed to ask how activity in specific regions or in bulk neuronal projections relate to specific factors. In Chapter 3, this factor is age. In Chapter 4, these factors are type of avoidance (innate vs. learned) or the projection target of neurons of interest. Striking differences were observed in all cases. These may be due to differences in the activity of long-range inputs, interneuron function, signal integration, and neuronal activation.

Future experiments may choose to use measures of single neuron activity, such as head mounted miniature microscopes, during threat avoidance assays (Aharoni et al., 2019; Stamatakis et al., 2021; Chen et al., 2022). The recent development of a two-color miniscope could be particularly well suited for understanding how PL balances the activity of PL-BLA and PL-NAc pathways (Aharoni and Hoogland 2019). Differential expression of green- and red-shifted calcium indicators in either PL-BLA or PL-NAc neurons would allow for highly detailed observation of how neurons comprising these projections behave throughout the task (Dana et al., 2016). Observing individual neuron differences within each population could help reveal heterogeneous function within these populations. Finally, analyzing activity of neurons that express both calcium indicators may shed light on how neurons that project to both NAc and BLA contribute to avoidance. Miniscope experiments, however, are not well suited for use in developing mice. Probes that measure single unit recordings, which have been used during PMA in adults, may help to uncover how neuronal dynamics in PL differ by age (Diehl et al., 2018).

A limitation of the PMA assay is that it is difficult to parse apart the engagement of active and passive avoidance strategies. Entries onto the platform are an active avoidance response, however, once on the platform, passive avoidance keeps animals from venturing off. While these specific responses could be isolated during our fiber photometry recordings, our open-loop optogenetic manipulations altered activity throughout the entire tone period where mice may engage in both active and passive avoidance. Therefore, how PL-NAc and PL-BLA

pathways causally drive only active or passive avoidance is not known. Future studies may utilize closed-loop optogenetic designs to inhibit prefrontal projections during behaviorally-locked time periods such as approach of the platform or after entry onto the platform. Another alternative would be to see if the roles of PL-NAc and PL-BLA pathways are similar in the two-way shuttle-box avoidance task which requires an active avoidance response (LeDoux et al., 2017).

Finally, all of the observations and manipulations of PL pathways within this thesis took place at the bulk level. While this yielded informative results, the molecular identities and heterogeneity of neurons comprising these populations is not well understood. From Gao et al., (2022), it is evident that the bulk projections studied include multiple subsets of projection types, however, we do not know how they may differentially contribute to behavior. Further, we do not know the genetic signatures of behaviorally relevant PL neurons which can help inform targeted therapeutics. Mouse cre-driver lines can be used to manipulate and observe the activity of genetically defined populations. Hypotheses of genes of interest can be gleaned from transcriptomic data of PL projection neurons (Gao et al., 2022). Mouse cre-drive lines can also be used with DeepTraCE to understand the bulk projection patterns of genetically defined prefrontal neurons.

Conclusions

Together, the findings of this thesis expand our knowledge of how mPFC circuitry regulates threat avoidance throughout different stages of life. I showed that because of the differential developmental trajectories of PL-NAc and PL-BLA pathways, distinct circuit configurations underlie threat avoidance behavior in different developmental stages. I mapped the brain wide connectivity patterns of PL-cPL, PL-NAc, and PL-VTA neurons and show how these populations differentially encode aspects of learned and innate avoidance in adulthood. Finally, I identified unstudied PL projections that may contribute to avoidance and created open-source analyses pipelines to help other link complex connectivity with behavioral function.

These advances elucidate how prefrontal circuits function throughout life to coordinate avoidance, a necessary foundation to understand how they may be disrupted to lead to psychiatric disease.

References

Adhikari, A., Topiwala, M. A., & Gordon, J. A. (2011). Single Units in the Medial Prefrontal Cortex with Anxiety-Related Firing Patterns Are Preferentially Influenced by Ventral Hippocampal Activity. *Neuron*, *71*(5), 898–910. https://doi.org/10.1016/j.neuron.2011.07.027

Adriani, W., Granstrem, O., Macri, S., Izykenova, G., Dambinova, S., & Laviola, G. (2004). Behavioral and Neurochemical Vulnerability During Adolescence in Mice: Studies with Nicotine. *Neuropsychopharmacology*, *29*(5), 869–878. https://doi.org/10.1038/sj.npp.1300366

Agoglia, A. E., Holstein, S. E., Small, A. T., Spanos, M., Burrus, B. M., & Hodge, C. W. (2017). Comparison of the adolescent and adult mouse prefrontal cortex proteome. *PLOS ONE*, *12*(6), e0178391. https://doi.org/10.1371/journal.pone.0178391

Aharoni, D., & Hoogland, T. M. (2019). Circuit Investigations With Open-Source Miniaturized Microscopes: Past, Present and Future. *Frontiers in Cellular Neuroscience*, *13*, 141. https://doi.org/10.3389/fncel.2019.00141

Ährlund-Richter, S., Xuan, Y., Van Lunteren, J. A., Kim, H., Ortiz, C., Pollak Dorocic, I., Meletis, K., & Carlén, M. (2019). A whole-brain atlas of monosynaptic input targeting four different cell types in the medial prefrontal cortex of the mouse. *Nature Neuroscience*, *22*(4), 657–668. https://doi.org/10.1038/s41593-019-0354-y

Akers, K. G., Arruda-Carvalho, M., Josselyn, S. A., & Frankland, P. W. (2012). Ontogeny of contextual fear memory formation, specificity, and persistence in mice. *Learning & Memory*, *19*(12), 598–604. https://doi.org/10.1101/lm.027581.112

Akers, K. G., Martinez-Canabal, A., Restivo, L., Yiu, A. P., De Cristofaro, A., Hsiang, H.-L. (Liz), Wheeler, A. L., Guskjolen, A., Niibori, Y., Shoji, H., Ohira, K., Richards, B. A., Miyakawa, T., Josselyn, S. A., & Frankland, P. W. (2014). Hippocampal Neurogenesis Regulates Forgetting During Adulthood and Infancy. *Science*, *344*(6184), 598–602. https://doi.org/10.1126/science.1248903

Alarcón, M., Abrahams, B. S., Stone, J. L., Duvall, J. A., Perederiy, J. V., Bomar, J. M., Sebat, J., Wigler, M., Martin, C. L., Ledbetter, D. H., Nelson, S. F., Cantor, R. M., & Geschwind, D. H. (2008). Linkage, Association, and Gene-Expression Analyses Identify CNTNAP2 as an Autism-Susceptibility Gene.

The American Journal of Human Genetics, *82*(1), 150–159. https://doi.org/10.1016/j.ajhg.2007.09.005

Aldao, A., Nolen-Hoeksema, S., & Schweizer, S. (2010). Emotion-regulation strategies across psychopathology: A meta-analytic review. *Clinical Psychology Review*, *30*(2), 217–237. https://doi.org/10.1016/j.cpr.2009.11.004

Allen, W. E., DeNardo, L. A., Chen, M. Z., Liu, C. D., Loh, K. M., Fenno, L. E., Ramakrishnan, C., Deisseroth, K., & Luo, L. (2017). Thirst-associated preoptic neurons encode an aversive motivational drive. *Science*, *357*(6356), 1149–1155. https://doi.org/10.1126/science.aan6747

Anastasiades, P. G., Boada, C., & Carter, A. G. (2019). Cell-Type-Specific D1 Dopamine Receptor Modulation of Projection Neurons and Interneurons in the Prefrontal Cortex. *Cerebral Cortex*, *29*(7), 3224–3242. https://doi.org/10.1093/cercor/bhy299

Anastasiades, P. G., & Carter, A. G. (2021). Circuit organization of the rodent medial prefrontal cortex. *Trends in Neurosciences*, *44*(7), 550–563. https://doi.org/10.1016/j.tins.2021.03.006

Apps, M. A. J., Rushworth, M. F. S., & Chang, S. W. C. (2016). The Anterior Cingulate Gyrus and Social Cognition: Tracking the Motivation of Others. *Neuron*, *90*(4), 692–707. https://doi.org/10.1016/j.neuron.2016.04.018

Argaw, A., Duff, G., Zabouri, N., Cécyre, B., Chainé, N., Cherif, H., Tea, N., Lutz, B., Ptito, M., & Bouchard, J.-F. (2011). Concerted Action of CB1 Cannabinoid Receptor and Deleted in Colorectal Cancer in Axon Guidance. *The Journal of Neuroscience*, *31*(4), 1489–1499. https://doi.org/10.1523/JNEUROSCI.4134-09.2011

Arking, D. E., Cutler, D. J., Brune, C. W., Teslovich, T. M., West, K., Ikeda, M., Rea, A., Guy, M., Lin, S., Cook, E. H., & Chakravarti, A. (2008). A Common Genetic Variant in the Neurexin Superfamily Member CNTNAP2 Increases Familial Risk of Autism. *The American Journal of Human Genetics*, *82*(1), 160–164. https://doi.org/10.1016/j.ajhg.2007.09.015

Arlotta, P., Molyneaux, B. J., Chen, J., Inoue, J., Kominami, R., & Macklis, J. D. (2005). Neuronal Subtype-Specific Genes that Control Corticospinal Motor Neuron Development In Vivo. *Neuron*, *45*(2), 207–221. https://doi.org/10.1016/j.neuron.2004.12.036

Arnaudova, I., Kindt, M., Fanselow, M., & Beckers, T. (2017). Pathways towards the proliferation of avoidance in anxiety and implications for treatment. *Behaviour Research and Therapy*, *96*, 3–13. https://doi.org/10.1016/j.brat.2017.04.004

Arruda-Carvalho, M., & Clem, R. L. (2014). Pathway-Selective Adjustment of Prefrontal-Amygdala Transmission during Fear Encoding. *The Journal of Neuroscience*, *34*(47), 15601–15609. https://doi.org/10.1523/JNEUROSCI.2664-14.2014

Arruda-Carvalho, M., Wu, W.-C., Cummings, K. A., & Clem, R. L. (2017). Optogenetic Examination of Prefrontal-Amygdala Synaptic Development. *The Journal of Neuroscience*, *37*(11), 2976–2985. https://doi.org/10.1523/JNEUROSCI.3097-16.2017

Ayhan, Y., Abazyan, B., Nomura, J., Kim, R., Ladenheim, B., Krasnova, I. N., Sawa, A., Margolis, R. L., Cadet, J. L., Mori, S., Vogel, M. W., Ross, C. A., & Pletnikov, M. V. (2011). Differential effects of prenatal and postnatal expressions of mutant human DISC1 on neurobehavioral phenotypes in transgenic mice: Evidence for neurodevelopmental origin of major psychiatric disorders. *Molecular Psychiatry*, *16*(3), 293–306. https://doi.org/10.1038/mp.2009.144

Backus, A. R., Schoffelen, J.-M., Szebényi, S., Hanslmayr, S., & Doeller, C. F. (2016). Hippocampal-Prefrontal Theta Oscillations Support Memory Integration. *Current Biology*, *26*(4), 450–457. https://doi.org/10.1016/j.cub.2015.12.048

Bakkaloglu, B., O'Roak, B. J., Louvi, A., Gupta, A. R., Abelson, J. F., Morgan, T. M., Chawarska, K., Klin, A., Ercan-Sencicek, A. G., Stillman, A. A., Tanriover, G., Abrahams, B. S., Duvall, J. A., Robbins, E. M., Geschwind, D. H., Biederer, T., Gunel, M., Lifton, R. P., & State, M. W. (2008). Molecular Cytogenetic Analysis and Resequencing of Contactin Associated Protein-Like 2 in Autism Spectrum Disorders. *The American Journal of Human Genetics*, *82*(1), 165–173. https://doi.org/10.1016/j.ajhg.2007.09.017

Ballinger, M. D., Saito, A., Abazyan, B., Taniguchi, Y., Huang, C.-H., Ito, K., Zhu, X., Segal, H., Jaaro-Peled, H., Sawa, A., Mackie, K., Pletnikov, M. V., & Kamiya, A. (2015). Adolescent cannabis exposure interacts with mutant DISC1 to produce impaired adult emotional memory. *Neurobiology of Disease*, *82*, 176–184. https://doi.org/10.1016/j.nbd.2015.06.006

Béïque, J.-C., Campbell, B., Perring, P., Hamblin, M. W., Walker, P., Mladenovic, L., & Andrade, R. (2004). Serotonergic Regulation of Membrane Potential in Developing Rat Prefrontal Cortex: Coordinated Expression of 5-Hydroxytryptamine (5-HT) $_{1A}$, 5-HT $_{2A}$, and 5-HT $_{7}$ Receptors. *The Journal of Neuroscience*, *24*(20), 4807–4817. https://doi.org/10.1523/JNEUROSCI.5113-03.2004

Bell, M. R. (2018). Comparing Postnatal Development of Gonadal Hormones and Associated Social Behaviors in Rats, Mice, and Humans. *Endocrinology*, *159*(7), 2596–2613. https://doi.org/10.1210/en.2018-00220

Berg, S., Kutra, D., Kroeger, T., Straehle, C. N., Kausler, B. X., Haubold, C., Schiegg, M., Ales, J., Beier, T., Rudy, M., Eren, K., Cervantes, J. I., Xu, B., Beuttenmueller, F., Wolny, A., Zhang, C., Koethe, U., Hamprecht, F. A., & Kreshuk, A. (2019). ilastik: Interactive machine learning for (bio)image analysis. *Nature Methods*, *16*(12), 1226–1232. https://doi.org/10.1038/s41592-019-0582-9

Berghuis, P., Rajnicek, A. M., Morozov, Y. M., Ross, R. A., Mulder, J., Urbán, G. M., Monory, K., Marsicano, G., Matteoli, M., Canty, A., Irving, A. J., Katona, I., Yanagawa, Y., Rakic, P., Lutz, B., Mackie, K., & Harkany, T. (2007). Hardwiring the Brain: Endocannabinoids Shape Neuronal Connectivity. *Science*, *316*(5828), 1212–1216. https://doi.org/10.1126/science.1137406

Bett, D., Stevenson, C. H., Shires, K. L., Smith, M. T., Martin, S. J., Dudchenko, P. A., & Wood, E. R. (2013). The Postsubiculum and Spatial Learning: The Role of Postsubicular Synaptic Activity and Synaptic Plasticity in Hippocampal Place Cell, Object, and Object-Location Memory. *The Journal of Neuroscience*, *33*(16), 6928–6943. https://doi.org/10.1523/JNEUROSCI.5476-12.2013

Bissonette, G. B., Martins, G. J., Franz, T. M., Harper, E. S., Schoenbaum, G., & Powell, E. M. (2008). Double Dissociation of the Effects of Medial and Orbital Prefrontal Cortical Lesions on Attentional and Affective Shifts in Mice. *The Journal of Neuroscience*, *28*(44), 11124–11130. https://doi.org/10.1523/JNEUROSCI.2820-08.2008

Boeke, E. A., Moscarello, J. M., LeDoux, J. E., Phelps, E. A., & Hartley, C. A. (2017). Active Avoidance: Neural Mechanisms and Attenuation of Pavlovian Conditioned Responding. *The Journal of Neuroscience*, *37*(18), 4808–4818. https://doi.org/10.1523/JNEUROSCI.3261-16.2017

Bolles, R. C. (1970). Species-specific defense reactions and avoidance learning. *Psychological Review*, *77*(1), 32–48. https://doi.org/10.1037/h0028589

Børglum, A. D., Demontis, D., Grove, J., Pallesen, J., Hollegaard, M. V., Pedersen, C. B., Hedemand, A., Mattheisen, M., Uitterlinden, A., Nyegaard, M., Ørntoft, T., Wiuf, C., Didriksen, M., Nordentoft, M., Nöthen, M. M., Rietschel, M., Ophoff, R. A., Cichon, S., Yolken, R. H., … Mors, O. (2014). Genome-wide study of association and interaction with maternal cytomegalovirus infection suggests new schizophrenia loci. *Molecular Psychiatry*, *19*(3), 325–333. https://doi.org/10.1038/mp.2013.2

Bouamrane, L., Scheyer, A. F., Lassalle, O., Iafrati, J., Thomazeau, A., & Chavis, P. (2017). Reelin-Haploinsufficiency Disrupts the Developmental Trajectory of the E/I Balance in the Prefrontal Cortex. *Frontiers in Cellular Neuroscience*, *10*. https://doi.org/10.3389/fncel.2016.00308

Boyce, P. J., & Finlay, J. M. (2009). Extracellular dopamine and norepinephrine in the developing rat prefrontal cortex: Transient effects of early partial loss of dopamine. *Brain Research Bulletin*, *79*(2), 104–110. https://doi.org/10.1016/j.brainresbull.2009.01.012

Brandon, N. J., & Sawa, A. (2011). Linking neurodevelopmental and synaptic theories of mental illness through DISC1. *Nature Reviews Neuroscience*, *12*(12), 707–722. https://doi.org/10.1038/nrn3120

Bravo-Rivera, C., Roman-Ortiz, C., Brignoni-Perez, E., Sotres-Bayon, F., & Quirk, G. J. (2014). Neural Structures Mediating Expression and Extinction of Platform-Mediated Avoidance. *Journal of Neuroscience*, *34*(29), 9736–9742. https://doi.org/10.1523/JNEUROSCI.0191-14.2014

Bravo-Rivera, C., Roman-Ortiz, C., Montesinos-Cartagena, M., & Quirk, G. J. (2015). Persistent active avoidance correlates with activity in prelimbic cortex and ventral striatum. *Frontiers in Behavioral Neuroscience*, *9*. https://doi.org/10.3389/fnbeh.2015.00184

Brockmann, M. D., Pöschel, B., Cichon, N., & Hanganu-Opatz, I. L. (2011). Coupled Oscillations Mediate Directed Interactions between Prefrontal Cortex and Hippocampus of the Neonatal Rat. *Neuron*, *71*(2), 332–347. https://doi.org/10.1016/j.neuron.2011.05.041

Brumback, A. C., Ellwood, I. T., Kjaerby, C., Iafrati, J., Robinson, S., Lee, A. T., Patel, T., Nagaraj, S., Davatolhagh, F., & Sohal, V. S. (2018). Identifying specific prefrontal neurons that contribute to autism-associated abnormalities in physiology and social behavior. *Molecular Psychiatry*, *23*(10), 2078–2089. https://doi.org/10.1038/mp.2017.213

Brust, V., Schindler, P. M., & Lewejohann, L. (2015). Lifetime development of behavioural phenotype in the house mouse (Mus musculus). *Frontiers in Zoology*, *12*(S1), S17. https://doi.org/10.1186/1742-9994-12-S1-S17

Bussey, T. J., Muir, J. L., Everitt, B. J., & Robbins, T. W. (1997). Triple dissociation of anterior cingulate, posterior cingulate, and medial frontal cortices on visual discrimination tasks using a touchscreen testing procedure for the rat. *Behavioral Neuroscience*, *111*(5), 920–936. https://doi.org/10.1037/0735-7044.111.5.920

Caballero, A., Flores-Barrera, E., Cass, D. K., & Tseng, K. Y. (2014). Differential regulation of parvalbumin and calretinin interneurons in the prefrontal cortex during adolescence. *Brain Structure and Function*, *219*(1), 395–406. https://doi.org/10.1007/s00429-013-0508-8

Caballero, A., Flores-Barrera, E., Thomases, D. R., & Tseng, K. Y. (2020). Downregulation of parvalbumin expression in the prefrontal cortex during adolescence causes enduring prefrontal disinhibition in adulthood. *Neuropsychopharmacology*, *45*(9), 1527–1535. https://doi.org/10.1038/s41386-020-0709-9

Callaghan, B., Meyer, H., Opendak, M., Van Tieghem, M., Harmon, C., Li, A., Lee, F. S., Sullivan, R. M., & Tottenham, N. (2019). Using a Developmental Ecology Framework to Align Fear Neurobiology Across Species. *Annual Review of Clinical Psychology*, *15*(1), 345–369. https://doi.org/10.1146/annurev-clinpsy-050718-095727

Capuzzo, G., & Floresco, S. B. (2020). Prelimbic and Infralimbic Prefrontal Regulation of Active and Inhibitory Avoidance and Reward-Seeking. *The Journal of Neuroscience*, *40*(24), 4773–4787. https://doi.org/10.1523/JNEUROSCI.0414-20.2020

Cardin, J. A., Carlén, M., Meletis, K., Knoblich, U., Zhang, F., Deisseroth, K., Tsai, L.-H., & Moore, C. I. (2009). Driving fast-spiking cells induces gamma rhythm and controls sensory responses. *Nature*, *459*(7247), 663–667. https://doi.org/10.1038/nature08002

Cass, D. K., Flores-Barrera, E., Thomases, D. R., Vital, W. F., Caballero, A., & Tseng, K. Y. (2014). CB1 cannabinoid receptor stimulation during adolescence impairs the maturation of GABA function in the adult rat prefrontal cortex. *Molecular Psychiatry*, *19*(5), 536–543. https://doi.org/10.1038/mp.2014.14

Cauli, B., Audinat, E., Lambolez, B., Angulo, M. C., Ropert, N., Tsuzuki, K., Hestrin, S., & Rossier, J. (1997). Molecular and Physiological Diversity of Cortical Nonpyramidal Cells. *The Journal of Neuroscience*, *17*(10), 3894–3906. https://doi.org/10.1523/JNEUROSCI.17-10-03894.1997

Cervin, M., Perrin, S., Olsson, E., Claesdotter-Knutsson, E., & Lindvall, M. (2020). Incompleteness, harm avoidance, and disgust: A comparison of youth with OCD, anxiety disorders, and no psychiatric disorder. *Journal of Anxiety Disorders*, *69*, 102175. https://doi.org/10.1016/j.janxdis.2019.102175

Chan, T., Kyere, K., Davis, B. R., Shemyakin, A., Kabitzke, P. A., Shair, H. N., Barr, G. A., & Wiedenmayer, C. P. (2011). The Role of the Medial Prefrontal Cortex in Innate Fear Regulation in Infants, Juveniles, and Adolescents. *The Journal of Neuroscience*, *31*(13), 4991–4999. https://doi.org/10.1523/JNEUROSCI.5216-10.2011

Chang, S. W. C., Gariépy, J.-F., & Platt, M. L. (2013). Neuronal reference frames for social decisions in primate frontal cortex. *Nature Neuroscience*, *16*(2), 243–250. https://doi.org/10.1038/nn.3287

Chi, J., Crane, A., Wu, Z., & Cohen, P. (2018). Adipo-Clear: A Tissue Clearing Method for Three-Dimensional Imaging of Adipose Tissue. *Journal of Visualized Experiments*, *137*, 58271. https://doi.org/10.3791/58271

Chi, J., Wu, Z., Choi, C. H. J., Nguyen, L., Tegegne, S., Ackerman, S. E., Crane, A., Marchildon, F., Tessier-Lavigne, M., & Cohen, P. (2018). Three-Dimensional Adipose Tissue Imaging Reveals Regional Variation in Beige Fat Biogenesis and PRDM16-Dependent Sympathetic Neurite Density. *Cell Metabolism*, *27*(1), 226-236.e3. https://doi.org/10.1016/j.cmet.2017.12.011

Chiu, C. Q., Puente, N., Grandes, P., & Castillo, P. E. (2010). Dopaminergic Modulation of Endocannabinoid-Mediated Plasticity at GABAergic Synapses in the Prefrontal Cortex. *The Journal of Neuroscience*, *30*(21), 7236–7248. https://doi.org/10.1523/JNEUROSCI.0736-10.2010

Cho, C.-H., Lee, H.-J., Woo, H. G., Choi, J.-H., Greenwood, T. A., & Kelsoe, J. R. (2015). *CDH13* and *HCRTR2* May Be Associated with Hypersomnia Symptom of Bipolar Depression: A Genome-Wide Functional Enrichment Pathway Analysis. *Psychiatry Investigation*, *12*(3), 402. https://doi.org/10.4306/pi.2015.12.3.402

Cho, K. K. A., Davidson, T. J., Bouvier, G., Marshall, J. D., Schnitzer, M. J., & Sohal, V. S. (2020). Cross-hemispheric gamma synchrony between prefrontal parvalbumin interneurons supports behavioral

adaptation during rule shift learning. *Nature Neuroscience*, *23*(7), 892–902. https://doi.org/10.1038/s41593-020-0647-1

Cho, K. K. A., Hoch, R., Lee, A. T., Patel, T., Rubenstein, J. L. R., & Sohal, V. S. (2015). Gamma Rhythms Link Prefrontal Interneuron Dysfunction with Cognitive Inflexibility in Dlx5/6+/− Mice. *Neuron*, *85*(6), 1332–1343. https://doi.org/10.1016/j.neuron.2015.02.019

Choi, J.-S., Cain, C. K., & LeDoux, J. E. (2010). The role of amygdala nuclei in the expression of auditory signaled two-way active avoidance in rats. *Learning & Memory*, *17*(3), 139–147. https://doi.org/10.1101/lm.1676610

Chung, K., Wallace, J., Kim, S.-Y., Kalyanasundaram, S., Andalman, A. S., Davidson, T. J., Mirzabekov, J. J., Zalocusky, K. A., Mattis, J., Denisin, A. K., Pak, S., Bernstein, H., Ramakrishnan, C., Grosenick, L., Gradinaru, V., & Deisseroth, K. (2013). Structural and molecular interrogation of intact biological systems. *Nature*, *497*(7449), 332–337. https://doi.org/10.1038/nature12107

Clapcote, S. J., Lipina, T. V., Millar, J. K., Mackie, S., Christie, S., Ogawa, F., Lerch, J. P., Trimble, K., Uchiyama, M., Sakuraba, Y., Kaneda, H., Shiroishi, T., Houslay, M. D., Henkelman, R. M., Sled, J. G., Gondo, Y., Porteous, D. J., & Roder, J. C. (2007). Behavioral Phenotypes of Disc1 Missense Mutations in Mice. *Neuron*, *54*(3), 387–402. https://doi.org/10.1016/j.neuron.2007.04.015

Collins, D. P., Anastasiades, P. G., Marlin, J. J., & Carter, A. G. (2018). Reciprocal Circuits Linking the Prefrontal Cortex with Dorsal and Ventral Thalamic Nuclei. *Neuron*, *98*(2), 366-379.e4. https://doi.org/10.1016/j.neuron.2018.03.024

Colon, L., Odynocki, N., Santarelli, A., & Poulos, A. M. (2018). Sexual differentiation of contextual fear responses. *Learning & Memory*, *25*(5), 230–240. https://doi.org/10.1101/lm.047159.117

Costa, N. S., Vicente, M. A., Cipriano, A. C., Miguel, T. T., & Nunes-de-Souza, R. L. (2016). Functional lateralization of the medial prefrontal cortex in the modulation of anxiety in mice: Left or right? *Neuropharmacology*, *108*, 82–90. https://doi.org/10.1016/j.neuropharm.2016.04.011

Costall, B., Jones, B. J., Kelly, M. E., Naylor, R. J., & Tomkins, D. M. (1989). Exploration of mice in a black and white test box: Validation as a model of anxiety. *Pharmacology Biochemistry and Behavior*, *32*(3), 777–785. https://doi.org/10.1016/0091-3057(89)90033-6

Courtin, J., Chaudun, F., Rozeske, R. R., Karalis, N., Gonzalez-Campo, C., Wurtz, H., Abdi, A., Baufreton, J., Bienvenu, T. C. M., & Herry, C. (2014). Prefrontal parvalbumin interneurons shape neuronal activity to drive fear expression. *Nature*, *505*(7481), 92–96. https://doi.org/10.1038/nature12755

Cox, S. L., Authier, M., Orgeret, F., Weimerskirch, H., & Guinet, C. (2020). High mortality rates in a juvenile free-ranging marine predator and links to dive and forage ability. *Ecology and Evolution*, *10*(1), 410–430. https://doi.org/10.1002/ece3.5905

Craig, W. (1919). Tropisms and instinctive activities. *Psychological Bulletin*, *16*(5), 151–159. https://doi.org/10.1037/h0071321

Cressman, V. L., Balaban, J., Steinfeld, S., Shemyakin, A., Graham, P., Parisot, N., & Moore, H. (2010). Prefrontal cortical inputs to the basal amygdala undergo pruning during late adolescence in the rat. *The Journal of Comparative Neurology*, NA-NA. https://doi.org/10.1002/cne.22359

Culler, E., & Mettler, F. A. (1934). Conditioned behavior in a decorticate dog. *Journal of Comparative Psychology*, *18*(3), 291–303. https://doi.org/10.1037/h0072306

Cullity, E. R., Madsen, H. B., Perry, C. J., & Kim, J. H. (2019). Postnatal developmental trajectory of dopamine receptor 1 and 2 expression in cortical and striatal brain regions. *Journal of Comparative Neurology*, *527*(6), 1039–1055. https://doi.org/10.1002/cne.24574

Cummings, K. A., & Clem, R. L. (2020). Prefrontal somatostatin interneurons encode fear memory. *Nature Neuroscience*, *23*(1), 61–74. https://doi.org/10.1038/s41593-019-0552-7

Cunningham, M. G., Bhattacharyya, S., & Benes, F. M. (2002). Amygdalo-cortical sprouting continues into early adulthood: Implications for the development of normal and abnormal function during adolescence. *The Journal of Comparative Neurology*, *453*(2), 116–130. https://doi.org/10.1002/cne.10376

Cunningham, M. G., Connor, C. M., Zhang, K., & Benes, F. M. (2005). Diminished serotonergic innervation of adult medial prefrontal cortex after 6-OHDA lesions in the newborn rat. *Developmental Brain Research*, *157*(2), 124–131. https://doi.org/10.1016/j.devbrainres.2005.02.020

Dana, H., Mohar, B., Sun, Y., Narayan, S., Gordus, A., Hasseman, J. P., Tsegaye, G., Holt, G. T., Hu, A., Walpita, D., Patel, R., Macklin, J. J., Bargmann, C. I., Ahrens, M. B., Schreiter, E. R., Jayaraman,

V., Looger, L. L., Svoboda, K., & Kim, D. S. (2016). Sensitive red protein calcium indicators for imaging neural activity. *ELife*, *5*, e12727. https://doi.org/10.7554/eLife.12727

Delevich, K., Jaaro-Peled, H., Penzo, M., Sawa, A., & Li, B. (2020). Parvalbumin Interneuron Dysfunction in a Thalamo-Prefrontal Cortical Circuit in *Disc1* Locus Impairment Mice. *Eneuro*, *7*(2), ENEURO.0496-19.2020. https://doi.org/10.1523/ENEURO.0496-19.2020

Delevich, K., Thomas, A. W., & Wilbrecht, L. (2018). Adolescence and "Late Blooming" Synapses of the Prefrontal Cortex. *Cold Spring Harbor Symposia on Quantitative Biology*, *83*, 37–43. https://doi.org/10.1101/sqb.2018.83.037507

Delgado, M. R. (2009). Avoiding negative outcomes: Tracking the mechanisms of avoidance learning in humans during fear conditioning. *Frontiers in Behavioral Neuroscience*, *3*. https://doi.org/10.3389/neuro.08.033.2009

DeNardo, L. A., Berns, D. S., DeLoach, K., & Luo, L. (2015). Connectivity of mouse somatosensory and prefrontal cortex examined with trans-synaptic tracing. *Nature Neuroscience*, *18*(11), 1687–1697. https://doi.org/10.1038/nn.4131

DeNardo, L. A., Liu, C. D., Allen, W. E., Adams, E. L., Friedmann, D., Fu, L., Guenthner, C. J., Tessier-Lavigne, M., & Luo, L. (2019). Temporal evolution of cortical ensembles promoting remote memory retrieval. *Nature Neuroscience*, *22*(3), 460–469. https://doi.org/10.1038/s41593-018-0318-7

DeNardo, L., & Luo, L. (2017). Genetic strategies to access activated neurons. *Current Opinion in Neurobiology*, *45*, 121–129. https://doi.org/10.1016/j.conb.2017.05.014

Dickson, C. R., Holmes, G. L., & Barry, J. M. (2022). Dynamic θ Frequency Coordination within and between the Prefrontal Cortex-Hippocampus Circuit during Learning of a Spatial Avoidance Task. *Eneuro*, *9*(2), ENEURO.0414-21.2022. https://doi.org/10.1523/ENEURO.0414-21.2022

Dickson, J. M., & MacLeod, A. K. (2006). Dysphoric adolescents' causal explanations and expectancies for approach and avoidance goals. *Journal of Adolescence*, *29*(2), 177–191. https://doi.org/10.1016/j.adolescence.2005.03.007

Diehl, M. M., Bravo-Rivera, C., & Quirk, G. J. (2019). The study of active avoidance: A platform for discussion. *Neuroscience & Biobehavioral Reviews*, *107*, 229–237. https://doi.org/10.1016/j.neubiorev.2019.09.010

Diehl, M. M., Bravo-Rivera, C., Rodriguez-Romaguera, J., Pagan-Rivera, P. A., Burgos-Robles, A., Roman-Ortiz, C., & Quirk, G. J. (2018). Active avoidance requires inhibitory signaling in the rodent prelimbic prefrontal cortex. *ELife*, *7*, e34657. https://doi.org/10.7554/eLife.34657

Diehl, M. M., Iravedra-García, J. M., Morán-Sierra, J., Rojas-Bowe, G., Gonzalez-Díaz, F., Valentín-Valentín, V., & Quirk, G. J. (2020). *Divergent projections of the prelimbic cortex bidirectionally regulate active avoidance* [Preprint]. Neuroscience. https://doi.org/10.1101/2020.05.28.120659

Dincheva, I., Drysdale, A. T., Hartley, C. A., Johnson, D. C., Jing, D., King, E. C., Ra, S., Gray, J. M., Yang, R., DeGruccio, A. M., Huang, C., Cravatt, B. F., Glatt, C. E., Hill, M. N., Casey, B. J., & Lee, F. S. (2015). FAAH genetic variation enhances fronto-amygdala function in mouse and human. *Nature Communications*, *6*(1), 6395. https://doi.org/10.1038/ncomms7395

Ding, D. C. D., Gabbott, P. L. A., & Totterdell, S. (2001). Differences in the laminar origin of projections from the medial prefrontal cortex to the nucleus accumbens shell and core regions in the rat. *Brain Research*, *917*(1), 81–89. https://doi.org/10.1016/S0006-8993(01)02912-2

Drzewiecki, C. M., Willing, J., & Juraska, J. M. (2016). Synaptic number changes in the medial prefrontal cortex across adolescence in male and female rats: A role for pubertal onset: Puberty and Synaptic Pruning in the MPFC. *Synapse*, *70*(9), 361–368. https://doi.org/10.1002/syn.21909

Du, X., Serena, K., Hwang, W. J., Grech, A. M., Wu, Y. W. C., Schroeder, A., & Hill, R. A. (2018). Prefrontal cortical parvalbumin and somatostatin expression and cell density increase during adolescence and are modified by BDNF and sex. *Molecular and Cellular Neuroscience*, *88*, 177–188. https://doi.org/10.1016/j.mcn.2018.02.001

Duff, G., Argaw, A., Cecyre, B., Cherif, H., Tea, N., Zabouri, N., Casanova, C., Ptito, M., & Bouchard, J.-F. (2013). Cannabinoid Receptor CB2 Modulates Axon Guidance. *PLoS ONE*, *8*(8), e70849. https://doi.org/10.1371/journal.pone.0070849

Duncan, G. E., Knapp, D. J., & Breese, G. R. (1996). Neuroanatomical characterization of Fos induction in rat behavioral models of anxiety. *Brain Research*, *713*(1–2), 79–91. https://doi.org/10.1016/0006-8993(95)01486-1

Durand, C. M., Betancur, C., Boeckers, T. M., Bockmann, J., Chaste, P., Fauchereau, F., Nygren, G., Rastam, M., Gillberg, I. C., Anckarsäter, H., Sponheim, E., Goubran-Botros, H., Delorme, R.,

Chabane, N., Mouren-Simeoni, M.-C., De Mas, P., Bieth, E., Rogé, B., Héron, D., … Bourgeron, T. (2007). Mutations in the gene encoding the synaptic scaffolding protein SHANK3 are associated with autism spectrum disorders. *Nature Genetics*, *39*(1), 25–27. https://doi.org/10.1038/ng1933

Economo, M. N., Viswanathan, S., Tasic, B., Bas, E., Winnubst, J., Menon, V., Graybuck, L. T., Nguyen, T. N., Smith, K. A., Yao, Z., Wang, L., Gerfen, C. R., Chandrashekar, J., Zeng, H., Looger, L. L., & Svoboda, K. (2018). Distinct descending motor cortex pathways and their roles in movement. *Nature*, *563*(7729), 79–84. https://doi.org/10.1038/s41586-018-0642-9

Edwards, A. C., Aliev, F., Bierut, L. J., Bucholz, K. K., Edenberg, H., Hesselbrock, V., Kramer, J., Kuperman, S., Nurnberger, J. I., Schuckit, M. A., Porjesz, B., & Dick, D. M. (2012). Genome-wide association study of comorbid depressive syndrome and alcohol dependence. *Psychiatric Genetics*, *22*(1), 31–41. https://doi.org/10.1097/YPG.0b013e32834acd07

Ellgren, M., Artmann, A., Tkalych, O., Gupta, A., Hansen, H. S., Hansen, S. H., Devi, L. A., & Hurd, Y. L. (2008). Dynamic changes of the endogenous cannabinoid and opioid mesocorticolimbic systems during adolescence: THC effects. *European Neuropsychopharmacology*, *18*(11), 826–834. https://doi.org/10.1016/j.euroneuro.2008.06.009

Elston, G. N., Oga, T., Okamoto, T., & Fujita, I. (2011). Spinogenesis and Pruning in the Anterior Ventral Inferotemporal Cortex of the Macaque Monkey: An Intracellular Injection Study of Layer III Pyramidal Cells. *Frontiers in Neuroanatomy*, *5*. https://doi.org/10.3389/fnana.2011.00042

Euston, D. R., Gruber, A. J., & McNaughton, B. L. (2012). The Role of Medial Prefrontal Cortex in Memory and Decision Making. *Neuron*, *76*(6), 1057–1070. https://doi.org/10.1016/j.neuron.2012.12.002

Fanselow, M. S. (2018). The role of learning in threat imminence and defensive behaviors. *Current Opinion in Behavioral Sciences*, *24*, 44–49. https://doi.org/10.1016/j.cobeha.2018.03.003

Farrell, M. R., Sengelaub, D. R., & Wellman, C. L. (2013). Sex differences and chronic stress effects on the neural circuitry underlying fear conditioning and extinction. *Physiology & Behavior*, *122*, 208–215. https://doi.org/10.1016/j.physbeh.2013.04.002

Feenstra, M. G. P., Teske, G., Botterblom, M. H. A., & De Bruin, J. P. C. (1999). Dopamine and noradrenaline release in the prefrontal cortex of rats during classical aversive and appetitive

conditioning to a contextual stimulus: Interference by novelty effects. *Neuroscience Letters*, *272*(3), 179–182. https://doi.org/10.1016/S0304-3940(99)00601-1

Fenno, L. E., Ramakrishnan, C., Kim, Y. S., Evans, K. E., Lo, M., Vesuna, S., Inoue, M., Cheung, K. Y. M., Yuen, E., Pichamoorthy, N., Hong, A. S. O., & Deisseroth, K. (2020). Comprehensive Dual- and Triple-Feature Intersectional Single-Vector Delivery of Diverse Functional Payloads to Cells of Behaving Mammals. *Neuron*, *107*(5), 836-853.e11. https://doi.org/10.1016/j.neuron.2020.06.003

Fenton, G. E., Halliday, D. M., Mason, R., Bredy, T. W., & Stevenson, C. W. (2016). Sex differences in learned fear expression and extinction involve altered gamma oscillations in medial prefrontal cortex. *Neurobiology of Learning and Memory*, *135*, 66–72. https://doi.org/10.1016/j.nlm.2016.06.019

Ferguson, B. R., & Gao, W.-J. (2015). Development of thalamocortical connections between the mediodorsal thalamus and the prefrontal cortex and its implication in cognition. *Frontiers in Human Neuroscience*, *8*. https://doi.org/10.3389/fnhum.2014.01027

File, S. E., Zangrossi, H., Sanders, F. L., & Mabbutt, P. S. (1994). Raised corticosterone in the rat after exposure to the elevated plus-maze. *Psychopharmacology*, *113*(3–4), 543–546. https://doi.org/10.1007/BF02245237

Fitzgerald, M. L., Chan, J., Mackie, K., Lupica, C. R., & Pickel, V. M. (2012). Altered dendritic distribution of dopamine D2 receptors and reduction in mitochondrial number in parvalbumin-containing interneurons in the medial prefrontal cortex of cannabinoid-1 (CB1) receptor knockout mice. *Journal of Comparative Neurology*, *520*(17), 4013–4031. https://doi.org/10.1002/cne.23141

Fitzgerald, M. L., Lupica, C. R., & Pickel, V. M. (2011). Decreased parvalbumin immunoreactivity in the cortex and striatum of mice lacking the CB1 receptor. *Synapse*, *65*(8), 827–831. https://doi.org/10.1002/syn.20911

Fitzgerald, M. L., Shobin, E., & Pickel, V. M. (2012). Cannabinoid modulation of the dopaminergic circuitry: Implications for limbic and striatal output. *Progress in Neuro-Psychopharmacology and Biological Psychiatry*, *38*(1), 21–29. https://doi.org/10.1016/j.pnpbp.2011.12.004

Floresco, S. B. (2015). The Nucleus Accumbens: An Interface Between Cognition, Emotion, and Action. *Annual Review of Psychology*, *66*(1), 25–52. https://doi.org/10.1146/annurev-psych-010213-115159

Floresco, S. B., Block, A. E., & Tse, M. T. L. (2008). Inactivation of the medial prefrontal cortex of the rat impairs strategy set-shifting, but not reversal learning, using a novel, automated procedure. *Behavioural Brain Research*, *190*(1), 85–96. https://doi.org/10.1016/j.bbr.2008.02.008

Fogaça, M. V., Aguiar, D. C., Moreira, F. A., & Guimarães, F. S. (2012). The endocannabinoid and endovanilloid systems interact in the rat prelimbic medial prefrontal cortex to control anxiety-like behavior. *Neuropharmacology*, *63*(2), 202–210. https://doi.org/10.1016/j.neuropharm.2012.03.007

Forero, A., Ku, H.-P., Malpartida, A. B., Wäldchen, S., Alhama-Riba, J., Kulka, C., Aboagye, B., Norton, W. H. J., Young, A. M. J., Ding, Y.-Q., Blum, R., Sauer, M., Rivero, O., & Lesch, K.-P. (2020). Serotonin (5-HT) neuron-specific inactivation of Cadherin-13 impacts 5-HT system formation and cognitive function. *Neuropharmacology*, *168*, 108018. https://doi.org/10.1016/j.neuropharm.2020.108018

Forero, A., Rivero, O., Wäldchen, S., Ku, H.-P., Kiser, D. P., Gärtner, Y., Pennington, L. S., Waider, J., Gaspar, P., Jansch, C., Edenhofer, F., Resink, T. J., Blum, R., Sauer, M., & Lesch, K.-P. (2017). Cadherin-13 Deficiency Increases Dorsal Raphe 5-HT Neuron Density and Prefrontal Cortex Innervation in the Mouse Brain. *Frontiers in Cellular Neuroscience*, *11*, 307. https://doi.org/10.3389/fncel.2017.00307

Franceschini, A., Costantini, I., Pavone, F. S., & Silvestri, L. (2020). Dissecting Neuronal Activation on a Brain-Wide Scale With Immediate Early Genes. *Frontiers in Neuroscience*, *14*, 569517. https://doi.org/10.3389/fnins.2020.569517

Friedmann, D., Pun, A., Adams, E. L., Lui, J. H., Kebschull, J. M., Grutzner, S. M., Castagnola, C., Tessier-Lavigne, M., & Luo, L. (2020). Mapping mesoscale axonal projections in the mouse brain using a 3D convolutional network. *Proceedings of the National Academy of Sciences*, *117*(20), 11068–11075. https://doi.org/10.1073/pnas.1918465117

Frye, C. A., Petralia, S. M., & Rhodes, M. E. (2000). Estrous cycle and sex differences in performance on anxiety tasks coincide with increases in hippocampal progesterone and 3α,5α-THP. *Pharmacology Biochemistry and Behavior*, *67*(3), 587–596. https://doi.org/10.1016/S0091-3057(00)00392-0

Fujisawa, S., & Buzsáki, G. (2011). A 4 Hz Oscillation Adaptively Synchronizes Prefrontal, VTA, and Hippocampal Activities. *Neuron*, *72*(1), 153–165. https://doi.org/10.1016/j.neuron.2011.08.018

Gabbott, P. L. A., Warner, T. A., Jays, P. R. L., Salway, P., & Busby, S. J. (2005). Prefrontal cortex in the rat: Projections to subcortical autonomic, motor, and limbic centers. *The Journal of Comparative Neurology*, *492*(2), 145–177. https://doi.org/10.1002/cne.20738

Gabriel, C. J., Zeidler, Z., Jin, B., Guo, C., Goodpaster, C. M., Kashay, A. Q., Wu, A., Delaney, M., Cheung, J., DiFazio, L. E., Sharpe, M. J., Aharoni, D., Wilke, S. A., & DeNardo, L. A. (2022). BehaviorDEPOT is a simple, flexible tool for automated behavioral detection based on markerless pose tracking. *ELife*, *11*, e74314. https://doi.org/10.7554/eLife.74314

Gale, G. D., Anagnostaras, S. G., Godsil, B. P., Mitchell, S., Nozawa, T., Sage, J. R., Wiltgen, B., & Fanselow, M. S. (2004). Role of the Basolateral Amygdala in the Storage of Fear Memories across the Adult Lifetime of Rats. *The Journal of Neuroscience*, *24*(15), 3810–3815. https://doi.org/10.1523/JNEUROSCI.4100-03.2004

Gao, L., Liu, S., Gou, L., Hu, Y., Liu, Y., Deng, L., Ma, D., Wang, H., Yang, Q., Chen, Z., Liu, D., Qiu, S., Wang, X., Wang, D., Wang, X., Ren, B., Liu, Q., Chen, T., Shi, X., … Yan, J. (2022). Single-neuron projectome of mouse prefrontal cortex. *Nature Neuroscience*, *25*(4), 515–529. https://doi.org/10.1038/s41593-022-01041-5

Garcia, L. P., Witteveen, J. S., Middelman, A., Van Hulten, J. A., Martens, G. J. M., Homberg, J. R., & Kolk, S. M. (2019). Perturbed Developmental Serotonin Signaling Affects Prefrontal Catecholaminergic Innervation and Cortical Integrity. *Molecular Neurobiology*, *56*(2), 1405–1420. https://doi.org/10.1007/s12035-018-1105-x

Gee, D. G., Fetcho, R. N., Jing, D., Li, A., Glatt, C. E., Drysdale, A. T., Cohen, A. O., Dellarco, D. V., Yang, R. R., Dale, A. M., Jernigan, T. L., Lee, F. S., Casey, B. J., the PING Consortium, Jernigan, T. L., San Diego, U., Co-PI of PING, Core PI, McCabe, C., San Diego, U., … Gruen, J. (2016). Individual differences in frontolimbic circuitry and anxiety emerge with adolescent changes in endocannabinoid signaling across species. *Proceedings of the National Academy of Sciences*, *113*(16), 4500–4505. https://doi.org/10.1073/pnas.1600013113

Gee, D. G., Humphreys, K. L., Flannery, J., Goff, B., Telzer, E. H., Shapiro, M., Hare, T. A., Bookheimer, S. Y., & Tottenham, N. (2013). A Developmental Shift from Positive to Negative Connectivity in

Human Amygdala–Prefrontal Circuitry. *The Journal of Neuroscience*, *33*(10), 4584–4593. https://doi.org/10.1523/JNEUROSCI.3446-12.2013

Gehrlach, D. A., Weiand, C., Gaitanos, T. N., Cho, E., Klein, A. S., Hennrich, A. A., Conzelmann, K.-K., & Gogolla, N. (2020). A whole-brain connectivity map of mouse insular cortex. *ELife*, *9*, e55585. https://doi.org/10.7554/eLife.55585

Gerhard, D. M., Meyer, H. C., & Lee, F. S. (2021). An Adolescent Sensitive Period for Threat Responding: Impacts of Stress and Sex. *Biological Psychiatry*, *89*(7), 651–658. https://doi.org/10.1016/j.biopsych.2020.10.003

Gildawie, K. R., Honeycutt, J. A., & Brenhouse, H. C. (2020). Region-specific Effects of Maternal Separation on Perineuronal Net and Parvalbumin-expressing Interneuron Formation in Male and Female Rats. *Neuroscience*, *428*, 23–37. https://doi.org/10.1016/j.neuroscience.2019.12.010

Gillan, C. M., Morein-Zamir, S., Urcelay, G. P., Sule, A., Voon, V., Apergis-Schoute, A. M., Fineberg, N. A., Sahakian, B. J., & Robbins, T. W. (2014). Enhanced Avoidance Habits in Obsessive-Compulsive Disorder. *Biological Psychiatry*, *75*(8), 631–638. https://doi.org/10.1016/j.biopsych.2013.02.002

Giustino, T. F., & Maren, S. (2015). The Role of the Medial Prefrontal Cortex in the Conditioning and Extinction of Fear. *Frontiers in Behavioral Neuroscience*, *9*. https://doi.org/10.3389/fnbeh.2015.00298

Gongwer, M. W., Klune, C. B., Couto, J., Jin, B., Enos, A. S., Chen, R., Friedmann, D., & DeNardo, L. A. (2023). Brain-wide projections and differential encoding of prefrontal neuronal classes underlying learned and innate threat avoidance. *The Journal of Neuroscience*, JN-RM-0697-23. https://doi.org/10.1523/JNEUROSCI.0697-23.2023

Gonzalez, M. C., Kramar, C. P., Tomaiuolo, M., Katche, C., Weisstaub, N., Cammarota, M., & Medina, J. H. (2014). Medial prefrontal cortex dopamine controls the persistent storage of aversive memories. *Frontiers in Behavioral Neuroscience*, *8*. https://doi.org/10.3389/fnbeh.2014.00408

Goodfellow, N. M., Benekareddy, M., Vaidya, V. A., & Lambe, E. K. (2009). Layer II/III of the Prefrontal Cortex: Inhibition by the Serotonin 5-HT $_{1A}$ Receptor in Development and Stress. *The Journal of Neuroscience*, *29*(32), 10094–10103. https://doi.org/10.1523/JNEUROSCI.1960-09.2009

Goosens, K. A. (2001). Contextual and Auditory Fear Conditioning are Mediated by the Lateral, Basal, and Central Amygdaloid Nuclei in Rats. *Learning & Memory*, *8*(3), 148–155. https://doi.org/10.1101/lm.37601

Grant, A., Fathalli, F., Rouleau, G., Joober, R., & Flores, C. (2012). Association between schizophrenia and genetic variation in DCC: A case–control study. *Schizophrenia Research*, *137*(1–3), 26–31. https://doi.org/10.1016/j.schres.2012.02.023

Green, M. F. (2006). Cognitive Impairment and Functional Outcome in Schizophrenia and Bipolar Disorder. *The Journal of Clinical Psychiatry*, *67*(10), e12. https://doi.org/10.4088/JCP.1006e12

Grewe, B. F., Gründemann, J., Kitch, L. J., Lecoq, J. A., Parker, J. G., Marshall, J. D., Larkin, M. C., Jercog, P. E., Grenier, F., Li, J. Z., Lüthi, A., & Schnitzer, M. J. (2017). Neural ensemble dynamics underlying a long-term associative memory. *Nature*, *543*(7647), 670–675. https://doi.org/10.1038/nature21682

Groman, S. M., Keistler, C., Keip, A. J., Hammarlund, E., DiLeone, R. J., Pittenger, C., Lee, D., & Taylor, J. R. (2019). Orbitofrontal Circuits Control Multiple Reinforcement-Learning Processes. *Neuron*, *103*(4), 734-746.e3. https://doi.org/10.1016/j.neuron.2019.05.042

Gründemann, J., & Lüthi, A. (2015). Ensemble coding in amygdala circuits for associative learning. *Current Opinion in Neurobiology*, *35*, 200–206. https://doi.org/10.1016/j.conb.2015.10.005

Guo, B., Chen, J., Chen, Q., Ren, K., Feng, D., Mao, H., Yao, H., Yang, J., Liu, H., Liu, Y., Jia, F., Qi, C., Lynn-Jones, T., Hu, H., Fu, Z., Feng, G., Wang, W., & Wu, S. (2019). Anterior cingulate cortex dysfunction underlies social deficits in Shank3 mutant mice. *Nature Neuroscience*, *22*(8), 1223–1234. https://doi.org/10.1038/s41593-019-0445-9

Guskjolen, A., Kenney, J. W., De La Parra, J., Yeung, B. A., Josselyn, S. A., & Frankland, P. W. (2018). Recovery of “Lost” Infant Memories in Mice. *Current Biology*, *28*(14), 2283-2290.e3. https://doi.org/10.1016/j.cub.2018.05.059

Haj-Dahmane, S., & Shen, R.-Y. (2011). Modulation of the serotonin system by endocannabinoid signaling. *Neuropharmacology*, *61*(3), 414–420. https://doi.org/10.1016/j.neuropharm.2011.02.016

Han, M.-H., & Nestler, E. J. (2017). Neural Substrates of Depression and Resilience. *Neurotherapeutics*, *14*(3), 677–686. https://doi.org/10.1007/s13311-017-0527-x

Hare, B. D., & Duman, R. S. (2020). Prefrontal cortex circuits in depression and anxiety: Contribution of discrete neuronal populations and target regions. *Molecular Psychiatry*. https://doi.org/10.1038/s41380-020-0685-9

Harris, K. D., & Shepherd, G. M. G. (2015). The neocortical circuit: Themes and variations. *Nature Neuroscience*, *18*(2), 170–181. https://doi.org/10.1038/nn.3917

Hartung, H., Brockmann, M. D., Pöschel, B., De Feo, V., & Hanganu-Opatz, I. L. (2016). Thalamic and Entorhinal Network Activity Differently Modulates the Functional Development of Prefrontal–Hippocampal Interactions. *The Journal of Neuroscience*, *36*(13), 3676–3690. https://doi.org/10.1523/JNEUROSCI.3232-15.2016

Hefner, K., & Holmes, A. (2007). Ontogeny of fear-, anxiety- and depression-related behavior across adolescence in C57BL/6J mice. *Behavioural Brain Research*, *176*(2), 210–215. https://doi.org/10.1016/j.bbr.2006.10.001

Heng, L., Beverley, J. A., Steiner, H., & Tseng, K. Y. (2011). Differential developmental trajectories for CB1 cannabinoid receptor expression in limbic/associative and sensorimotor cortical areas. *Synapse*, *65*(4), 278–286. https://doi.org/10.1002/syn.20844

Herrnstein, R. J. (1969). Method and theory in the study of avoidance. *Psychological Review*, *76*(1), 49–69. https://doi.org/10.1037/h0026786

Herry, C., & Johansen, J. P. (2014). Encoding of fear learning and memory in distributed neuronal circuits. *Nature Neuroscience*, *17*(12), 1644–1654. https://doi.org/10.1038/nn.3869

Hikida, T., Jaaro-Peled, H., Seshadri, S., Oishi, K., Hookway, C., Kong, S., Wu, D., Xue, R., Andradé, M., Tankou, S., Mori, S., Gallagher, M., Ishizuka, K., Pletnikov, M., Kida, S., & Sawa, A. (2007). Dominant-negative DISC1 transgenic mice display schizophrenia-associated phenotypes detected by measures translatable to humans. *Proceedings of the National Academy of Sciences*, *104*(36), 14501–14506. https://doi.org/10.1073/pnas.0704774104

Hill, M. N., McLaughlin, R. J., Pan, B., Fitzgerald, M. L., Roberts, C. J., Lee, T. T.-Y., Karatsoreos, I. N., Mackie, K., Viau, V., Pickel, V. M., McEwen, B. S., Liu, Q. -s., Gorzalka, B. B., & Hillard, C. J. (2011). Recruitment of Prefrontal Cortical Endocannabinoid Signaling by Glucocorticoids

Contributes to Termination of the Stress Response. *Journal of Neuroscience*, *31*(29), 10506–10515. https://doi.org/10.1523/JNEUROSCI.0496-11.2011

Hill, R. A., Kiss Von Soly, S., Ratnayake, U., Klug, M., Binder, M. D., Hannan, A. J., & Van Den Buuse, M. (2014). Long-term effects of combined neonatal and adolescent stress on brain-derived neurotrophic factor and dopamine receptor expression in the rat forebrain. *Biochimica et Biophysica Acta (BBA) - Molecular Basis of Disease*, *1842*(11), 2126–2135. https://doi.org/10.1016/j.bbadis.2014.08.009

Hinke, J. T., Watters, G. M., Reiss, C. S., Santora, J. A., & Santos, M. M. (2020). Acute bottlenecks to the survival of juvenile *Pygoscelis* penguins occur immediately after fledging. *Biology Letters*, *16*(12), 20200645. https://doi.org/10.1098/rsbl.2020.0645

Hiser, J., & Koenigs, M. (2018). The Multifaceted Role of the Ventromedial Prefrontal Cortex in Emotion, Decision Making, Social Cognition, and Psychopathology. *Biological Psychiatry*, *83*(8), 638–647. https://doi.org/10.1016/j.biopsych.2017.10.030

Holland, F. H., Ganguly, P., Potter, D. N., Chartoff, E. H., & Brenhouse, H. C. (2014). Early life stress disrupts social behavior and prefrontal cortex parvalbumin interneurons at an earlier time-point in females than in males. *Neuroscience Letters*, *566*, 131–136. https://doi.org/10.1016/j.neulet.2014.02.023

Holt, D. J., Coombs, G., Zeidan, M. A., Goff, D. C., & Milad, M. R. (2012). Failure of Neural Responses to Safety Cues in Schizophrenia. *Archives of General Psychiatry*, *69*(9), 893. https://doi.org/10.1001/archgenpsychiatry.2011.2310

Hoover, W. B., & Vertes, R. P. (2007). Anatomical analysis of afferent projections to the medial prefrontal cortex in the rat. *Brain Structure and Function*, *212*(2), 149–179. https://doi.org/10.1007/s00429-007-0150-4

Hormigo, S., Vega-Flores, G., & Castro-Alamancos, M. A. (2016). Basal Ganglia Output Controls Active Avoidance Behavior. *The Journal of Neuroscience*, *36*(40), 10274–10284. https://doi.org/10.1523/JNEUROSCI.1842-16.2016

Howes, O. D., McCutcheon, R., Owen, M. J., & Murray, R. M. (2017). The Role of Genes, Stress, and Dopamine in the Development of Schizophrenia. *Biological Psychiatry*, *81*(1), 9–20. https://doi.org/10.1016/j.biopsych.2016.07.014

Hu, H., Gan, J., & Jonas, P. (2014). Fast-spiking, parvalbumin $^{+}$ GABAergic interneurons: From cellular design to microcircuit function. *Science*, *345*(6196), 1255263. https://doi.org/10.1126/science.1255263

Hunter, W. S. (1917). Review of Studies in Animal Behavior. *Psychological Bulletin*, *14*(8), 291–293. https://doi.org/10.1037/h0064225

Hyman. (2010). Working memory performance correlates with prefrontal-hippocampal theta interactions but not with prefrontal neuron firing rates. *Frontiers in Integrative Neuroscience*. https://doi.org/10.3389/neuro.07.002.2010

Ibi, D., Nagai, T., Koike, H., Kitahara, Y., Mizoguchi, H., Niwa, M., Jaaro-Peled, H., Nitta, A., Yoneda, Y., & Nabeshima, T. (2010). Combined effect of neonatal immune activation and mutant DISC1 on phenotypic changes in adulthood. *Behavioural Brain Research*, *206*(1), 32–37. https://doi.org/10.1016/j.bbr.2009.08.027

Ironside, M., Amemori, K., McGrath, C. L., Pedersen, M. L., Kang, M. S., Amemori, S., Frank, M. J., Graybiel, A. M., & Pizzagalli, D. A. (2020). Approach-Avoidance Conflict in Major Depressive Disorder: Congruent Neural Findings in Humans and Nonhuman Primates. *Biological Psychiatry*, *87*(5), 399–408. https://doi.org/10.1016/j.biopsych.2019.08.022

Isaacson, J. S., & Scanziani, M. (2011). How Inhibition Shapes Cortical Activity. *Neuron*, *72*(2), 231–243. https://doi.org/10.1016/j.neuron.2011.09.027

Ishikawa, A., Ambroggi, F., Nicola, S. M., & Fields, H. L. (2008). Dorsomedial Prefrontal Cortex Contribution to Behavioral and Nucleus Accumbens Neuronal Responses to Incentive Cues. *The Journal of Neuroscience*, *28*(19), 5088–5098. https://doi.org/10.1523/JNEUROSCI.0253-08.2008

Ishikawa, A., & Nakamura, S. (2006). Ventral Hippocampal Neurons Project Axons Simultaneously to the Medial Prefrontal Cortex and Amygdala in the Rat. *Journal of Neurophysiology*, *96*(4), 2134–2138. https://doi.org/10.1152/jn.00069.2006

Izquierdo, A., Brigman, J. L., Radke, A. K., Rudebeck, P. H., & Holmes, A. (2017). The neural basis of reversal learning: An updated perspective. *Neuroscience*, *345*, 12–26. https://doi.org/10.1016/j.neuroscience.2016.03.021

Jayachandran, M., Linley, S. B., Schlecht, M., Mahler, S. V., Vertes, R. P., & Allen, T. A. (2019). Prefrontal Pathways Provide Top-Down Control of Memory for Sequences of Events. *Cell Reports*, *28*(3), 640-654.e6. https://doi.org/10.1016/j.celrep.2019.06.053

Jercog, D., Winke, N., Sung, K., Fernandez, M. M., Francioni, C., Rajot, D., Courtin, J., Chaudun, F., Jercog, P. E., Valerio, S., & Herry, C. (2021). Dynamical prefrontal population coding during defensive behaviours. *Nature*, *595*(7869), 690–694. https://doi.org/10.1038/s41586-021-03726-6

Jia, M., Travaglia, A., Pollonini, G., Fedele, G., & Alberini, C. M. (2018). Developmental changes in plasticity, synaptic, glia, and connectivity protein levels in rat medial prefrontal cortex. *Learning & Memory*, *25*(10), 533–543. https://doi.org/10.1101/lm.047753.118

Johnson, C. M., Loucks, F. A., Peckler, H., Thomas, A. W., Janak, P. H., & Wilbrecht, L. (2016). Long-range orbitofrontal and amygdala axons show divergent patterns of maturation in the frontal cortex across adolescence. *Developmental Cognitive Neuroscience*, *18*, 113–120. https://doi.org/10.1016/j.dcn.2016.01.005

Johnson, C., & Wilbrecht, L. (2011). Juvenile mice show greater flexibility in multiple choice reversal learning than adults. *Developmental Cognitive Neuroscience*, *1*(4), 540–551. https://doi.org/10.1016/j.dcn.2011.05.008

Kajs, B. L., Loewke, A. C., Dorsch, J. M., Vinson, L. T., & Gunaydin, L. A. (2022). Divergent encoding of active avoidance behavior in corticostriatal and corticolimbic projections. *Scientific Reports*, *12*(1), 10731. https://doi.org/10.1038/s41598-022-14930-3

Kalsbeek, A., Voorn, P., Buijs, R. M., Pool, C. W., & Uylings, H. B. M. (1988). Development of the dopaminergic innervation in the prefrontal cortex of the rat. *The Journal of Comparative Neurology*, *269*(1), 58–72. https://doi.org/10.1002/cne.902690105

Kawaguchi, Y. (1997). GABAergic cell subtypes and their synaptic connections in rat frontal cortex. *Cerebral Cortex*, *7*(6), 476–486. https://doi.org/10.1093/cercor/7.6.476

Kebschull, J. M., Garcia Da Silva, P., Reid, A. P., Peikon, I. D., Albeanu, D. F., & Zador, A. M. (2016). High-Throughput Mapping of Single-Neuron Projections by Sequencing of Barcoded RNA. *Neuron*, *91*(5), 975–987. https://doi.org/10.1016/j.neuron.2016.07.036

Kim, C. K., Yang, S. J., Pichamoorthy, N., Young, N. P., Kauvar, I., Jennings, J. H., Lerner, T. N., Berndt, A., Lee, S. Y., Ramakrishnan, C., Davidson, T. J., Inoue, M., Bito, H., & Deisseroth, K. (2016). Simultaneous fast measurement of circuit dynamics at multiple sites across the mammalian brain. *Nature Methods*, *13*(4), 325–328. https://doi.org/10.1038/nmeth.3770

Kim, C. K., Ye, L., Jennings, J. H., Pichamoorthy, N., Tang, D. D., Yoo, A.-C. W., Ramakrishnan, C., & Deisseroth, K. (2017). Molecular and Circuit-Dynamical Identification of Top-Down Neural Mechanisms for Restraint of Reward Seeking. *Cell*, *170*(5), 1013-1027.e14. https://doi.org/10.1016/j.cell.2017.07.020

Kim, Y., Venkataraju, K. U., Pradhan, K., Mende, C., Taranda, J., Turaga, S. C., Arganda-Carreras, I., Ng, L., Hawrylycz, M. J., Rockland, K. S., Seung, H. S., & Osten, P. (2015). Mapping Social Behavior-Induced Brain Activation at Cellular Resolution in the Mouse. *Cell Reports*, *10*(2), 292–305. https://doi.org/10.1016/j.celrep.2014.12.014

Klein, S., Staring, M., Murphy, K., Viergever, M. A., & Pluim, J. (2010). elastix: A Toolbox for Intensity-Based Medical Image Registration. *IEEE Transactions on Medical Imaging*, *29*(1), 196–205. https://doi.org/10.1109/TMI.2009.2035616

Klune, C. B., Jin, B., & DeNardo, L. A. (2021). Linking mPFC circuit maturation to the developmental regulation of emotional memory and cognitive flexibility. *ELife*, *10*, e64567. https://doi.org/10.7554/eLife.64567

Knowland, D., & Lim, B. K. (2018). Circuit-based frameworks of depressive behaviors: The role of reward circuitry and beyond. *Pharmacology Biochemistry and Behavior*, *174*, 42–52. https://doi.org/10.1016/j.pbb.2017.12.010

Koike, H., Arguello, P. A., Kvajo, M., Karayiorgou, M., & Gogos, J. A. (2006). *Disc1* is mutated in the 129S6/SvEv strain and modulates working memory in mice. *Proceedings of the National Academy of Sciences*, *103*(10), 3693–3697. https://doi.org/10.1073/pnas.0511189103

Kolb, B., Mychasiuk, R., Muhammad, A., Li, Y., Frost, D. O., & Gibb, R. (2012). Experience and the developing prefrontal cortex. *Proceedings of the National Academy of Sciences*, *109*(Supplement_2), 17186–17193. https://doi.org/10.1073/pnas.1121251109

Kolb, B., & Nonneman, A. J. (1978). Sparing of function in rats with early prefrontal cortex lesions. *Brain Research*, *151*(1), 135–148. https://doi.org/10.1016/0006-8993(78)90956-3

Kolb, B., Nonneman, A. J., & Singh, R. K. (1974). Double dissociation of spatial impairments and perseveration following selective prefrontal lesions in rats. *Journal of Comparative and Physiological Psychology*, *87*(4), 772–780. https://doi.org/10.1037/h0036970

Kopec, A. M., Smith, C. J., Ayre, N. R., Sweat, S. C., & Bilbo, S. D. (2018). Microglial dopamine receptor elimination defines sex-specific nucleus accumbens development and social behavior in adolescent rats. *Nature Communications*, *9*(1), 3769. https://doi.org/10.1038/s41467-018-06118-z

Kosaki, Y., & Watanabe, S. (2012). Dissociable roles of the medial prefrontal cortex, the anterior cingulate cortex, and the hippocampus in behavioural flexibility revealed by serial reversal of three-choice discrimination in rats. *Behavioural Brain Research*, *227*(1), 81–90. https://doi.org/10.1016/j.bbr.2011.10.039

Koss, W. A., Belden, C. E., Hristov, A. D., & Juraska, J. M. (2014). Dendritic remodeling in the adolescent medial prefrontal cortex and the basolateral amygdala of male and female rats: Dendritic Remodeling in the Adolescent Rat. *Synapse*, *68*(2), 61–72. https://doi.org/10.1002/syn.21716

Kramer, D. J., Aisenberg, E. E., Kosillo, P., Friedmann, D., Stafford, D. A., Lee, A. Y.-F., Luo, L., Hockemeyer, D., Ngai, J., & Bateup, H. S. (2021). Generation of a DAT-P2A-Flpo mouse line for intersectional genetic targeting of dopamine neuron subpopulations. *Cell Reports*, *35*(6), 109123. https://doi.org/10.1016/j.celrep.2021.109123

Kroon, T., van Hugte, E., van Linge, L., Mansvelder, H. D., & Meredith, R. M. (2019). Early postnatal development of pyramidal neurons across layers of the mouse medial prefrontal cortex. *Scientific Reports*, *9*(1), 5037. https://doi.org/10.1038/s41598-019-41661-9

Krypotos, A.-M. (2015). Avoidance learning: A review of theoretical models and recent developments. *Frontiers in Behavioral Neuroscience*, *9*. https://doi.org/10.3389/fnbeh.2015.00189

Kulesskaya, N., & Voikar, V. (2014). Assessment of mouse anxiety-like behavior in the light–dark box and open-field arena: Role of equipment and procedure. *Physiology & Behavior*, *133*, 30–38. https://doi.org/10.1016/j.physbeh.2014.05.006

Kvajo, M., McKellar, H., Arguello, P. A., Drew, L. J., Moore, H., MacDermott, A. B., Karayiorgou, M., & Gogos, J. A. (2008). A mutation in mouse *Disc1* that models a schizophrenia risk allele leads to specific alterations in neuronal architecture and cognition. *Proceedings of the National Academy of Sciences*, *105*(19), 7076–7081. https://doi.org/10.1073/pnas.0802615105

Lak, A., Okun, M., Moss, M. M., Gurnani, H., Farrell, K., Wells, M. J., Reddy, C. B., Kepecs, A., Harris, K. D., & Carandini, M. (2020). Dopaminergic and Prefrontal Basis of Learning from Sensory Confidence and Reward Value. *Neuron*, *105*(4), 700-711.e6. https://doi.org/10.1016/j.neuron.2019.11.018

Latagliata, E. C., Patrono, E., Puglisi-Allegra, S., & Ventura, R. (2010). Food seeking in spite of harmful consequences is under prefrontal cortical noradrenergic control. *BMC Neuroscience*, *11*(1), 15. https://doi.org/10.1186/1471-2202-11-15

Lauzon, N. M., Bishop, S. F., & Laviolette, S. R. (2009). Dopamine D $_1$ versus D $_4$ Receptors Differentially Modulate the Encoding of Salient versus Nonsalient Emotional Information in the Medial Prefrontal Cortex. *The Journal of Neuroscience*, *29*(15), 4836–4845. https://doi.org/10.1523/JNEUROSCI.0178-09.2009

Laviola, G., Macrì, S., Morley-Fletcher, S., & Adriani, W. (2003). Risk-taking behavior in adolescent mice: Psychobiological determinants and early epigenetic influence. *Neuroscience & Biobehavioral Reviews*, *27*(1–2), 19–31. https://doi.org/10.1016/S0149-7634(03)00006-X

La-Vu, M., Tobias, B. C., Schuette, P. J., & Adhikari, A. (2020). To Approach or Avoid: An Introductory Overview of the Study of Anxiety Using Rodent Assays. *Frontiers in Behavioral Neuroscience*, *14*, 145. https://doi.org/10.3389/fnbeh.2020.00145

Lazaro, M. T., Taxidis, J., Shuman, T., Bachmutsky, I., Ikrar, T., Santos, R., Marcello, G. M., Mylavarapu, A., Chandra, S., Foreman, A., Goli, R., Tran, D., Sharma, N., Azhdam, M., Dong, H., Choe, K. Y., Peñagarikano, O., Masmanidis, S. C., Rácz, B., … Golshani, P. (2019). Reduced Prefrontal

Synaptic Connectivity and Disturbed Oscillatory Population Dynamics in the CNTNAP2 Model of Autism. *Cell Reports*, *27*(9), 2567-2578.e6. https://doi.org/10.1016/j.celrep.2019.05.006

LeDoux, J. E. (2009). Emotion Circuits in the Brain. *FOCUS*, *7*(2), 274–274. https://doi.org/10.1176/foc.7.2.foc274

LeDoux, J. E., Moscarello, J., Sears, R., & Campese, V. (2017). The birth, death and resurrection of avoidance: A reconceptualization of a troubled paradigm. *Molecular Psychiatry*, *22*(1), 24–36. https://doi.org/10.1038/mp.2016.166

Lee, A. T., Vogt, D., Rubenstein, J. L., & Sohal, V. S. (2014). A Class of GABAergic Neurons in the Prefrontal Cortex Sends Long-Range Projections to the Nucleus Accumbens and Elicits Acute Avoidance Behavior. *The Journal of Neuroscience*, *34*(35), 11519–11525. https://doi.org/10.1523/JNEUROSCI.1157-14.2014

Lee, E., Hong, J., Park, Y.-G., Chae, S., Kim, Y., & Kim, D. (2015). Left brain cortical activity modulates stress effects on social behavior. *Scientific Reports*, *5*(1), 13342. https://doi.org/10.1038/srep13342

Lee, F. H., Zai, C. C., Cordes, S. P., Roder, J. C., & Wong, A. H. (2013). Abnormal interneuron development in disrupted-in-schizophrenia-1 L100P mutant mice. *Molecular Brain*, *6*(1), 20. https://doi.org/10.1186/1756-6606-6-20

Lee, T. T.-Y., Hill, M. N., & Lee, F. S. (2016). Developmental regulation of fear learning and anxiety behavior by endocannabinoids: Endocannabinoids, development and anxiety. *Genes, Brain and Behavior*, *15*(1), 108–124. https://doi.org/10.1111/gbb.12253

Legaria, A. A., Matikainen-Ankney, B. A., Yang, B., Ahanonu, B., Licholai, J. A., Parker, J. G., & Kravitz, A. V. (2022). Fiber photometry in striatum reflects primarily nonsomatic changes in calcium. *Nature Neuroscience*, *25*(9), 1124–1128. https://doi.org/10.1038/s41593-022-01152-z

Leow, Y. N., Zhou, B., Sullivan, H. A., Barlowe, A. R., Wickersham, I. R., & Sur, M. (2022). Brain-wide mapping of inputs to the mouse lateral posterior (LP/Pulvinar) thalamus–anterior cingulate cortex network. *Journal of Comparative Neurology*, *530*(11), 1992–2013. https://doi.org/10.1002/cne.25317

Leslie, C. A., Robertson, M. W., Cutler, A. J., & Bennett, J. P. (1991). Postnatal development of D 1 dopamine receptors in the medial prefrontal cortex, striatum and nucleus accumbens of normal and

neonatal 6-hydroxydopamine treated rats: A quantitative autoradiographic analysis. *Developmental Brain Research*, *62*(1), 109–114. https://doi.org/10.1016/0165-3806(91)90195-O

Lesting, J., Daldrup, T., Narayanan, V., Himpe, C., Seidenbecher, T., & Pape, H.-C. (2013). Directional Theta Coherence in Prefrontal Cortical to Amygdalo-Hippocampal Pathways Signals Fear Extinction. *PLoS ONE*, *8*(10), e77707. https://doi.org/10.1371/journal.pone.0077707

Levitt, P., & Moore, R. Y. (1979). Development of the noradrenergic innervation of neocortex. *Brain Research*, *162*(2), 243–259. https://doi.org/10.1016/0006-8993(79)90287-7

Lewis, D. (1997). Development of the Prefrontal Cortex during Adolescence: Insights into Vulnerable Neural Circuits in Schizophrenia. *Neuropsychopharmacology*, *16*(6), 385–398. https://doi.org/10.1016/S0893-133X(96)00277-1

Lewis, E. M., Barnett, J. F., Freshwater, L., Hoberman, A. M., & Christian, M. S. (2002). SEXUAL MATURATION DATA FOR CRL SPRAGUE-DAWLEY RATS: CRITERIA AND CONFOUNDING FACTORS. *Drug and Chemical Toxicology*, *25*(4), 437–458. https://doi.org/10.1081/DCT-120014794

Lezak, K. R., Missig, G., & Carlezon Jr, W. A. (2017). Behavioral methods to study anxiety in rodents. *Dialogues in Clinical Neuroscience*, *19*(2), 181–191. https://doi.org/10.31887/DCNS.2017.19.2/wcarlezon

Li, L., & Shao, J. (1998). Restricted lesions to ventral prefrontal subareas block reversal learning but not visual discrimination learning in rats. *Physiology & Behavior*, *65*(2), 371–379. https://doi.org/10.1016/S0031-9384(98)00216-9

Li, S., Kim, J. H., & Richardson, R. (2012). Updating memories: Changing the involvement of the prelimbic cortex in the expression of an infant fear memory. *Neuroscience*, *222*, 316–325. https://doi.org/10.1016/j.neuroscience.2012.06.038

Li, W., Zhou, Y., Jentsch, J. D., Brown, R. A. M., Tian, X., Ehninger, D., Hennah, W., Peltonen, L., Lönnqvist, J., Huttunen, M. O., Kaprio, J., Trachtenberg, J. T., Silva, A. J., & Cannon, T. D. (2007). Specific developmental disruption of disrupted-in-schizophrenia-1 function results in schizophrenia-related phenotypes in mice. *Proceedings of the National Academy of Sciences*, *104*(46), 18280–18285. https://doi.org/10.1073/pnas.0706900104

Likhtik, E., Stujenske, J. M., A Topiwala, M., Harris, A. Z., & Gordon, J. A. (2014). Prefrontal entrainment of amygdala activity signals safety in learned fear and innate anxiety. *Nature Neuroscience*, *17*(1), 106–113. https://doi.org/10.1038/nn.3582

Lin, H.-C., Mao, S.-C., Su, C.-L., & Gean, P.-W. (2009). The Role of Prefrontal Cortex CB1 Receptors in the Modulation of Fear Memory. *Cerebral Cortex*, *19*(1), 165–175. https://doi.org/10.1093/cercor/bhn075

Liska, A., Bertero, A., Gomolka, R., Sabbioni, M., Galbusera, A., Barsotti, N., Panzeri, S., Scattoni, M. L., Pasqualetti, M., & Gozzi, A. (2018). Homozygous Loss of Autism-Risk Gene CNTNAP2 Results in Reduced Local and Long-Range Prefrontal Functional Connectivity. *Cerebral Cortex*, *28*(4), 1141–1153. https://doi.org/10.1093/cercor/bhx022

Little, J. P., & Carter, A. G. (2013). Synaptic Mechanisms Underlying Strong Reciprocal Connectivity between the Medial Prefrontal Cortex and Basolateral Amygdala. *The Journal of Neuroscience*, *33*(39), 15333–15342. https://doi.org/10.1523/JNEUROSCI.2385-13.2013

Llorente-Berzal, A., Terzian, A. L. B., Di Marzo, V., Micale, V., Viveros, M. P., & Wotjak, C. T. (2015). 2-AG promotes the expression of conditioned fear via cannabinoid receptor type 1 on GABAergic neurons. *Psychopharmacology*, *232*(15), 2811–2825. https://doi.org/10.1007/s00213-015-3917-y

Loewke, A. C., Minerva, A. R., Nelson, A. B., Kreitzer, A. C., & Gunaydin, L. A. (2021). Frontostriatal Projections Regulate Innate Avoidance Behavior. *The Journal of Neuroscience*, *41*(25), 5487–5501. https://doi.org/10.1523/JNEUROSCI.2581-20.2021

Lovelace, J. W., Vieira, P. A., Corches, A., Mackie, K., & Korzus, E. (2014). Impaired Fear Memory Specificity Associated with Deficient Endocannabinoid-Dependent Long-Term Plasticity. *Neuropsychopharmacology*, *39*(7), 1685–1693. https://doi.org/10.1038/npp.2014.15

Lovibond, P. F., Mitchell, C. J., Minard, E., Brady, A., & Menzies, R. G. (2009). Safety behaviours preserve threat beliefs: Protection from extinction of human fear conditioning by an avoidance response. *Behaviour Research and Therapy*, *47*(8), 716–720. https://doi.org/10.1016/j.brat.2009.04.013

Lui, J. H., Nguyen, N. D., Grutzner, S. M., Darmanis, S., Peixoto, D., Wagner, M. J., Allen, W. E., Kebschull, J. M., Richman, E. B., Ren, J., Newsome, W. T., Quake, S. R., & Luo, L. (2021).

Differential encoding in prefrontal cortex projection neuron classes across cognitive tasks. *Cell*, *184*(2), 489-506.e26. https://doi.org/10.1016/j.cell.2020.11.046

Luo, L., Callaway, E. M., & Svoboda, K. (2018). Genetic Dissection of Neural Circuits: A Decade of Progress. *Neuron*, *98*(4), 865. https://doi.org/10.1016/j.neuron.2018.05.004

Lüthi, A., & Lüscher, C. (2014). Pathological circuit function underlying addiction and anxiety disorders. *Nature Neuroscience*, *17*(12), 1635–1643. https://doi.org/10.1038/nn.3849

Lynn, D. A., & Brown, G. R. (2009). The ontogeny of exploratory behavior in male and female adolescent rats (Rattus norvegicus). *Developmental Psychobiology*, *51*(6), 513–520. https://doi.org/10.1002/dev.20386

Maddaloni, G., Bertero, A., Pratelli, M., Barsotti, N., Boonstra, A., Giorgi, A., Migliarini, S., & Pasqualetti, M. (2017). Development of Serotonergic Fibers in the Post-Natal Mouse Brain. *Frontiers in Cellular Neuroscience*, *11*, 202. https://doi.org/10.3389/fncel.2017.00202

Madisen, L., Zwingman, T. A., Sunkin, S. M., Oh, S. W., Zariwala, H. A., Gu, H., Ng, L. L., Palmiter, R. D., Hawrylycz, M. J., Jones, A. R., Lein, E. S., & Zeng, H. (2010). A robust and high-throughput Cre reporting and characterization system for the whole mouse brain. *Nature Neuroscience*, *13*(1), 133–140. https://doi.org/10.1038/nn.2467

Maestripieri, D., Tomaszycki, M., & Carroll, K. A. (1999). Consistency and change in the behavior of rhesus macaque abusive mothers with successive infants. *Developmental Psychobiology*, *34*(1), 29–35. https://doi.org/10.1002/(SICI)1098-2302(199901)34:1<29::AID-DEV5>3.0.CO;2-U

Maner, J. K., & Schmidt, N. B. (2006). The Role of Risk Avoidance in Anxiety. *Behavior Therapy*, *37*(2), 181–189. https://doi.org/10.1016/j.beth.2005.11.003

Manitt, C., Eng, C., Pokinko, M., Ryan, R. T., Torres-Berrío, A., Lopez, J. P., Yogendran, S. V., Daubaras, M. J. J., Grant, A., Schmidt, E. R. E., Tronche, F., Krimpenfort, P., Cooper, H. M., Pasterkamp, R. J., Kolb, B., Turecki, G., Wong, T. P., Nestler, E. J., Giros, B., & Flores, C. (2013). Dcc orchestrates the development of the prefrontal cortex during adolescence and is altered in psychiatric patients. *Translational Psychiatry*, *3*(12), e338–e338. https://doi.org/10.1038/tp.2013.105

Maren, S. (2005). Synaptic Mechanisms of Associative Memory in the Amygdala. *Neuron*, *47*(6), 783–786. https://doi.org/10.1016/j.neuron.2005.08.009

Maren, S., De Oca, B., & Fanselow, M. S. (1994). Sex differences in hippocampal long-term potentiation (LTP) and Pavlovian fear conditioning in rats: Positive correlation between LTP and contextual learning. *Brain Research*, *661*(1–2), 25–34. https://doi.org/10.1016/0006-8993(94)91176-2

Martínez-Rivera, F. J., Bravo-Rivera, C., Velázquez-Díaz, C. D., Montesinos-Cartagena, M., & Quirk, G. J. (2019). Prefrontal circuits signaling active avoidance retrieval and extinction. *Psychopharmacology*, *236*(1), 399–406. https://doi.org/10.1007/s00213-018-5012-7

Mathis, A., Mamidanna, P., Cury, K. M., Abe, T., Murthy, V. N., Mathis, M. W., & Bethge, M. (2018). DeepLabCut: Markerless pose estimation of user-defined body parts with deep learning. *Nature Neuroscience*, *21*(9), 1281–1289. https://doi.org/10.1038/s41593-018-0209-y

Mathis, V. P., Williams, M., Fillinger, C., & Kenny, P. J. (2021). Networks of habenula-projecting cortical neurons regulate cocaine seeking. *Science Advances*, *7*(45), eabj2225. https://doi.org/10.1126/sciadv.abj2225

McCutcheon, J. E., White, F. J., & Marinelli, M. (2009). Individual Differences in Dopamine Cell Neuroadaptations Following Cocaine Self-Administration. *Biological Psychiatry*, *66*(8), 801–803. https://doi.org/10.1016/j.biopsych.2009.04.018

McEwen, B. S., & Morrison, J. H. (2013). The Brain on Stress: Vulnerability and Plasticity of the Prefrontal Cortex over the Life Course. *Neuron*, *79*(1), 16–29. https://doi.org/10.1016/j.neuron.2013.06.028

McGarry, L. M., & Carter, A. G. (2016). Inhibitory Gating of Basolateral Amygdala Inputs to the Prefrontal Cortex. *The Journal of Neuroscience*, *36*(36), 9391–9406. https://doi.org/10.1523/JNEUROSCI.0874-16.2016

McLaughlin, R. J., Hill, M. N., Bambico, F. R., Stuhr, K. L., Gobbi, G., Hillard, C. J., & Gorzalka, B. B. (2012). Prefrontal cortical anandamide signaling coordinates coping responses to stress through a serotonergic pathway. *European Neuropsychopharmacology*, *22*(9), 664–671. https://doi.org/10.1016/j.euroneuro.2012.01.004

Meyer, P. M., & Alberts, J. R. (2016). Non-nutritive, thermotactile cues induce odor preference in infant mice (Mus musculus). *Journal of Comparative Psychology*, *130*(4), 369–379. https://doi.org/10.1037/com0000044

Millar, J. K. (2000). Disruption of two novel genes by a translocation co-segregating with schizophrenia. *Human Molecular Genetics*, *9*(9), 1415–1423. https://doi.org/10.1093/hmg/9.9.1415

Minatohara, K., Akiyoshi, M., & Okuno, H. (2016). Role of Immediate-Early Genes in Synaptic Plasticity and Neuronal Ensembles Underlying the Memory Trace. *Frontiers in Molecular Neuroscience*, *8*. https://doi.org/10.3389/fnmol.2015.00078

Mingote, S., De Bruin, J. P. C., & Feenstra, M. G. P. (2004). Noradrenaline and Dopamine Efflux in the Prefrontal Cortex in Relation to Appetitive Classical Conditioning. *The Journal of Neuroscience*, *24*(10), 2475–2480. https://doi.org/10.1523/JNEUROSCI.4547-03.2004

Miyamae, T., Chen, K., Lewis, D. A., & Gonzalez-Burgos, G. (2017). Distinct Physiological Maturation of Parvalbumin-Positive Neuron Subtypes in Mouse Prefrontal Cortex. *The Journal of Neuroscience*, *37*(19), 4883–4902. https://doi.org/10.1523/JNEUROSCI.3325-16.2017

Modaresi, H. A. (1978). Facilitating effects of a safe platform on two-way avoidance learning. *Journal of Experimental Psychology: Animal Behavior Processes*, *4*(1), 83–94. https://doi.org/10.1037/0097-7403.4.1.83

Moin Afshar, N., Keip, A. J., Taylor, J. R., Lee, D., & Groman, S. M. (2020). Reinforcement Learning during Adolescence in Rats. *The Journal of Neuroscience*, *40*(30), 5857–5870. https://doi.org/10.1523/JNEUROSCI.0910-20.2020

Monteiro, P., & Feng, G. (2017). SHANK proteins: Roles at the synapse and in autism spectrum disorder. *Nature Reviews Neuroscience*, *18*(3), 147–157. https://doi.org/10.1038/nrn.2016.183

Morilak, D. A. (2012). Modulating the modulators: Interaction of brain norepinephrine and cannabinoids in stress. *Experimental Neurology*, *238*(2), 145–148. https://doi.org/10.1016/j.expneurol.2012.08.016

Moscarello, J. M., & LeDoux, J. E. (2013). Active Avoidance Learning Requires Prefrontal Suppression of Amygdala-Mediated Defensive Reactions. *The Journal of Neuroscience*, *33*(9), 3815–3823. https://doi.org/10.1523/JNEUROSCI.2596-12.2013

Moulds, M. L., Kandris, E., Starr, S., & Wong, A. C. M. (2007). The relationship between rumination, avoidance and depression in a non-clinical sample. *Behaviour Research and Therapy*, *45*(2), 251–261. https://doi.org/10.1016/j.brat.2006.03.003

Mowrer, O. H., & Lamoreaux, R. R. (1946). Fear as an intervening variable in avoidance conditioning. *Journal of Comparative Psychology*, *39*(1), 29–50. https://doi.org/10.1037/h0060150

Mulder, J., Aguado, T., Keimpema, E., Barabás, K., Ballester Rosado, C. J., Nguyen, L., Monory, K., Marsicano, G., Di Marzo, V., Hurd, Y. L., Guillemot, F., Mackie, K., Lutz, B., Guzmán, M., Lu, H.-C., Galve-Roperh, I., & Harkany, T. (2008). Endocannabinoid signaling controls pyramidal cell specification and long-range axon patterning. *Proceedings of the National Academy of Sciences*, *105*(25), 8760–8765. https://doi.org/10.1073/pnas.0803545105

Murugan, M., Jang, H. J., Park, M., Miller, E. M., Cox, J., Taliaferro, J. P., Parker, N. F., Bhave, V., Hur, H., Liang, Y., Nectow, A. R., Pillow, J. W., & Witten, I. B. (2017). Combined Social and Spatial Coding in a Descending Projection from the Prefrontal Cortex. *Cell*, *171*(7), 1663-1677.e16. https://doi.org/10.1016/j.cell.2017.11.002

Naisbitt, S., Kim, E., Tu, J. C., Xiao, B., Sala, C., Valtschanoff, J., Weinberg, R. J., Worley, P. F., & Sheng, M. (1999). Shank, a Novel Family of Postsynaptic Density Proteins that Binds to the NMDA Receptor/PSD-95/GKAP Complex and Cortactin. *Neuron*, *23*(3), 569–582. https://doi.org/10.1016/S0896-6273(00)80809-0

Naneix, F., Marchand, A. R., Di Scala, G., Pape, J.-R., & Coutureau, E. (2012). Parallel Maturation of Goal-Directed Behavior and Dopaminergic Systems during Adolescence. *The Journal of Neuroscience*, *32*(46), 16223–16232. https://doi.org/10.1523/JNEUROSCI.3080-12.2012

Negrón-Oyarzo, I., Pérez, M. Á., Terreros, G., Muñoz, P., & Dagnino-Subiabre, A. (2014). Effects of chronic stress in adolescence on learned fear, anxiety, and synaptic transmission in the rat prelimbic cortex. *Behavioural Brain Research*, *259*, 342–353. https://doi.org/10.1016/j.bbr.2013.11.001

Nestler, E. J., & Hyman, S. E. (2010). Animal models of neuropsychiatric disorders. *Nature Neuroscience*, *13*(10), 1161–1169. https://doi.org/10.1038/nn.2647

Nikolaev, E., Werka, T., & Kaczmarek, L. (1992). C-fos protooncogene expression in rat brain after long-term training of two-way active avoidance reaction. *Behavioural Brain Research*, *48*(1), 91–94. https://doi.org/10.1016/S0166-4328(05)80143-3

Nishida, M., Pearsall, J., Buckner, R. L., & Walker, M. P. (2009). REM Sleep, Prefrontal Theta, and the Consolidation of Human Emotional Memory. *Cerebral Cortex*, *19*(5), 1158–1166. https://doi.org/10.1093/cercor/bhn155

Niwa, M., Kamiya, A., Murai, R., Kubo, K., Gruber, A. J., Tomita, K., Lu, L., Tomisato, S., Jaaro-Peled, H., Seshadri, S., Hiyama, H., Huang, B., Kohda, K., Noda, Y., O'Donnell, P., Nakajima, K., Sawa, A., & Nabeshima, T. (2010). Knockdown of DISC1 by In Utero Gene Transfer Disturbs Postnatal Dopaminergic Maturation in the Frontal Cortex and Leads to Adult Behavioral Deficits. *Neuron*, *65*(4), 480–489. https://doi.org/10.1016/j.neuron.2010.01.019

Nonaka, A., Toyoda, T., Miura, Y., Hitora-Imamura, N., Naka, M., Eguchi, M., Yamaguchi, S., Ikegaya, Y., Matsuki, N., & Nomura, H. (2014). Synaptic Plasticity Associated with a Memory Engram in the Basolateral Amygdala. *Journal of Neuroscience*, *34*(28), 9305–9309. https://doi.org/10.1523/JNEUROSCI.4233-13.2014

Nonneman, A. J., Voigt, J., & Kolb, B. E. (1974). Comparisons of behavioral effects of hippocampal and prefrontal cortex lesions in the rat. *Journal of Comparative and Physiological Psychology*, *87*(2), 249–260. https://doi.org/10.1037/h0036864

Nussenbaum, K., & Hartley, C. A. (2019). Reinforcement learning across development: What insights can we draw from a decade of research? *Developmental Cognitive Neuroscience*, *40*, 100733. https://doi.org/10.1016/j.dcn.2019.100733

Oh, S. W., Harris, J. A., Ng, L., Winslow, B., Cain, N., Mihalas, S., Wang, Q., Lau, C., Kuan, L., Henry, A. M., Mortrud, M. T., Ouellette, B., Nguyen, T. N., Sorensen, S. A., Slaughterbeck, C. R., Wakeman, W., Li, Y., Feng, D., Ho, A., … Zeng, H. (2014). A mesoscale connectome of the mouse brain. *Nature*, *508*(7495), 207–214. https://doi.org/10.1038/nature13186

Ohta, K., Miki, T., Warita, K., Suzuki, S., Kusaka, T., Yakura, T., Liu, J., Tamai, M., & Takeuchi, Y. (2014). Prolonged maternal separation disturbs the serotonergic system during early brain development. *International Journal of Developmental Neuroscience*, *33*(1), 15–21. https://doi.org/10.1016/j.ijdevneu.2013.10.007

Otis, J. M., Namboodiri, V. M. K., Matan, A. M., Voets, E. S., Mohorn, E. P., Kosyk, O., McHenry, J. A., Robinson, J. E., Resendez, S. L., Rossi, M. A., & Stuber, G. D. (2017). Prefrontal cortex output

circuits guide reward seeking through divergent cue encoding. *Nature*, *543*(7643), 103–107. https://doi.org/10.1038/nature21376

Otsuka, I., Watanabe, Y., Hishimoto, A., Boku, S., Mouri, K., Shiroiwa, K., Okazaki, S., Nunokawa, A., Shirakawa, O., Someya, T., & Sora, I. (2015). Association analysis of the Cadherin13 gene with schizophrenia in the Japanese population. *Neuropsychiatric Disease and Treatment*, 1381. https://doi.org/10.2147/NDT.S84736

Overskaug, K., Bolstad, J. P., & Sunde, P. (1999). Fledgling Behavior and Survival in Northern Tawny Owls. *The Condor*, *101*(1), 169–174. https://doi.org/10.2307/1370460

Park, J., Wood, J., Bondi, C., Del Arco, A., & Moghaddam, B. (2016). Anxiety Evokes Hypofrontality and Disrupts Rule-Relevant Encoding by Dorsomedial Prefrontal Cortex Neurons. *Journal of Neuroscience*, *36*(11), 3322–3335. https://doi.org/10.1523/JNEUROSCI.4250-15.2016

Parolaro, D., Realini, N., Vigano, D., Guidali, C., & Rubino, T. (2010). The endocannabinoid system and psychiatric disorders. *Experimental Neurology*, *224*(1), 3–14. https://doi.org/10.1016/j.expneurol.2010.03.018

Pattwell, S. S., Bath, K. G., Casey, B. J., Ninan, I., & Lee, F. S. (2011). Selective early-acquired fear memories undergo temporary suppression during adolescence. *Proceedings of the National Academy of Sciences*, *108*(3), 1182–1187. https://doi.org/10.1073/pnas.1012975108

Peckford, G., Dwyer, J. A., Snow, A. C., Thorpe, C. M., Martin, G. M., & Skinner, D. M. (2014). The effects of lesions to the postsubiculum or the anterior dorsal nucleus of the thalamus on spatial learning in rats. *Behavioral Neuroscience*, *128*(6), 654–665. https://doi.org/10.1037/bne0000019

Pellow, S., & File, S. E. (1986). Anxiolytic and anxiogenic drug effects on exploratory activity in an elevated plus-maze: A novel test of anxiety in the rat. *Pharmacology Biochemistry and Behavior*, *24*(3), 525–529. https://doi.org/10.1016/0091-3057(86)90552-6

Peñagarikano, O., Abrahams, B. S., Herman, E. I., Winden, K. D., Gdalyahu, A., Dong, H., Sonnenblick, L. I., Gruver, R., Almajano, J., Bragin, A., Golshani, P., Trachtenberg, J. T., Peles, E., & Geschwind, D. H. (2011). Absence of CNTNAP2 Leads to Epilepsy, Neuronal Migration Abnormalities, and Core Autism-Related Deficits. *Cell*, *147*(1), 235–246. https://doi.org/10.1016/j.cell.2011.08.040

Perens, J., Salinas, C. G., Skytte, J. L., Roostalu, U., Dahl, A. B., Dyrby, T. B., Wichern, F., Barkholt, P., Vrang, N., Jelsing, J., & Hecksher-Sørensen, J. (2021). An Optimized Mouse Brain Atlas for Automated Mapping and Quantification of Neuronal Activity Using iDISCO+ and Light Sheet Fluorescence Microscopy. *Neuroinformatics*, *19*(3), 433–446. https://doi.org/10.1007/s12021-020-09490-8

Petanjek, Z., Judaš, M., Šimić, G., Rašin, M. R., Uylings, H. B. M., Rakic, P., & Kostović, I. (2011). Extraordinary neoteny of synaptic spines in the human prefrontal cortex. *Proceedings of the National Academy of Sciences*, *108*(32), 13281–13286. https://doi.org/10.1073/pnas.1105108108

Petreanu, L., Huber, D., Sobczyk, A., & Svoboda, K. (2007). Channelrhodopsin-2–assisted circuit mapping of long-range callosal projections. *Nature Neuroscience*, *10*(5), 663–668. https://doi.org/10.1038/nn1891

Phelan, K., & McDermid, H. E. (2011). The 22q13.3 Deletion Syndrome (Phelan-McDermid Syndrome). *Molecular Syndromology*, *2*(3–5), 186–201. https://doi.org/10.1159/000334260

Phillips, A. G., Ahn, S., & Floresco, S. B. (2004). Magnitude of Dopamine Release in Medial Prefrontal Cortex Predicts Accuracy of Memory on a Delayed Response Task. *The Journal of Neuroscience*, *24*(2), 547–553. https://doi.org/10.1523/JNEUROSCI.4653-03.2004

Piantadosi, P. T., Yeates, D. C. M., & Floresco, S. B. (2020). Prefrontal cortical and nucleus accumbens contributions to discriminative conditioned suppression of reward-seeking. *Learning & Memory*, *27*(10), 429–440. https://doi.org/10.1101/lm.051912.120

Piekarski, D. J., Boivin, J. R., & Wilbrecht, L. (2017). Ovarian Hormones Organize the Maturation of Inhibitory Neurotransmission in the Frontal Cortex at Puberty Onset in Female Mice. *Current Biology*, *27*(12), 1735-1745.e3. https://doi.org/10.1016/j.cub.2017.05.027

Piekarski, D. J., Johnson, C. M., Boivin, J. R., Thomas, A. W., Lin, W. C., Delevich, K., M. Galarce, E., & Wilbrecht, L. (2017). Does puberty mark a transition in sensitive periods for plasticity in the associative neocortex? *Brain Research*, *1654*, 123–144. https://doi.org/10.1016/j.brainres.2016.08.042

Pinzón-Parra, C., Vidal-Jiménez, B., Camacho-Abrego, I., Flores-Gómez, A. A., Rodríguez-Moreno, A., & Flores, G. (2019). Juvenile stress causes reduced locomotor behavior and dendritic spine density in

the prefrontal cortex and basolateral amygdala in Sprague-Dawley rats: XXXX. *Synapse*, *73*(1), e22066. https://doi.org/10.1002/syn.22066

Pirone, A., Alexander, J. M., Koenig, J. B., Cook-Snyder, D. R., Palnati, M., Wickham, R. J., Eden, L., Shrestha, N., Reijmers, L., Biederer, T., Miczek, K. A., Dulla, C. G., & Jacob, M. H. (2018). Social Stimulus Causes Aberrant Activation of the Medial Prefrontal Cortex in a Mouse Model With Autism-Like Behaviors. *Frontiers in Synaptic Neuroscience*, *10*, 35. https://doi.org/10.3389/fnsyn.2018.00035

Pokinko, M., Grant, A., Shahabi, F., Dumont, Y., Manitt, C., & Flores, C. (2017). Dcc haploinsufficiency regulates dopamine receptor expression across postnatal lifespan. *Neuroscience*, *346*, 182–189. https://doi.org/10.1016/j.neuroscience.2017.01.009

Poliak, S., Gollan, L., Martinez, R., Custer, A., Einheber, S., Salzer, J. L., Trimmer, J. S., Shrager, P., & Peles, E. (1999). Caspr2, a New Member of the Neurexin Superfamily, Is Localized at the Juxtaparanodes of Myelinated Axons and Associates with K+ Channels. *Neuron*, *24*(4), 1037–1047. https://doi.org/10.1016/S0896-6273(00)81049-1

Poo, C., Agarwal, G., Bonacchi, N., & Mainen, Z. F. (2022). Spatial maps in piriform cortex during olfactory navigation. *Nature*, *601*(7894), 595–599. https://doi.org/10.1038/s41586-021-04242-3

Puig, M. V., Antzoulatos, E. G., & Miller, E. K. (2014). Prefrontal dopamine in associative learning and memory. *Neuroscience*, *282*, 217–229. https://doi.org/10.1016/j.neuroscience.2014.09.026

Radnikow, G., & Feldmeyer, D. (2018). Layer- and Cell Type-Specific Modulation of Excitatory Neuronal Activity in the Neocortex. *Frontiers in Neuroanatomy*, *12*, 1. https://doi.org/10.3389/fnana.2018.00001

Ramirez, F., Moscarello, J. M., LeDoux, J. E., & Sears, R. M. (2015). Active Avoidance Requires a Serial Basal Amygdala to Nucleus Accumbens Shell Circuit. *Journal of Neuroscience*, *35*(8), 3470–3477. https://doi.org/10.1523/JNEUROSCI.1331-14.2015

Ramsaran, A. I., Schlichting, M. L., & Frankland, P. W. (2019). The ontogeny of memory persistence and specificity. *Developmental Cognitive Neuroscience*, *36*, 100591. https://doi.org/10.1016/j.dcn.2018.09.002

Rao, N., Northoff, G., Tagore, A., Rusjan, P., Kenk, M., Wilson, A., Houle, S., Strafella, A., Remington, G., & Mizrahi, R. (2019). Impaired Prefrontal Cortical Dopamine Release in Schizophrenia During a Cognitive Task: A [11C]FLB 457 Positron Emission Tomography Study. *Schizophrenia Bulletin*, *45*(3), 670–679. https://doi.org/10.1093/schbul/sby076

Rapanelli, M., Frick, L. R., & Pittenger, C. (2017). The Role of Interneurons in Autism and Tourette Syndrome. *Trends in Neurosciences*, *40*(7), 397–407. https://doi.org/10.1016/j.tins.2017.05.004

Rebello, T. J., Yu, Q., Goodfellow, N. M., Caffrey Cagliostro, M. K., Teissier, A., Morelli, E., Demireva, E. Y., Chemiakine, A., Rosoklija, G. B., Dwork, A. J., Lambe, E. K., Gingrich, J. A., & Ansorge, M. S. (2014). Postnatal Day 2 to 11 Constitutes a 5-HT-Sensitive Period Impacting Adult mPFC Function. *The Journal of Neuroscience*, *34*(37), 12379–12393. https://doi.org/10.1523/JNEUROSCI.1020-13.2014

Renard, J., Szkudlarek, H. J., Kramar, C. P., Jobson, C. E. L., Moura, K., Rushlow, W. J., & Laviolette, S. R. (2017). Adolescent THC Exposure Causes Enduring Prefrontal Cortical Disruption of GABAergic Inhibition and Dysregulation of Sub-Cortical Dopamine Function. *Scientific Reports*, *7*(1), 11420. https://doi.org/10.1038/s41598-017-11645-8

Renier, N., Adams, E. L., Kirst, C., Wu, Z., Azevedo, R., Kohl, J., Autry, A. E., Kadiri, L., Umadevi Venkataraju, K., Zhou, Y., Wang, V. X., Tang, C. Y., Olsen, O., Dulac, C., Osten, P., & Tessier-Lavigne, M. (2016). Mapping of Brain Activity by Automated Volume Analysis of Immediate Early Genes. *Cell*, *165*(7), 1789–1802. https://doi.org/10.1016/j.cell.2016.05.007

Reyes, B. A. S., Szot, P., Sikkema, C., Cathel, A. M., Kirby, L. G., & Van Bockstaele, E. J. (2012). Stress-induced sensitization of cortical adrenergic receptors following a history of cannabinoid exposure. *Experimental Neurology*, *236*(2), 327–335. https://doi.org/10.1016/j.expneurol.2012.05.016

Reynolds, L. M., Makowski, C. S., Yogendran, S. V., Kiessling, S., Cermakian, N., & Flores, C. (2015). Amphetamine in Adolescence Disrupts the Development of Medial Prefrontal Cortex Dopamine Connectivity in a dcc-Dependent Manner. *Neuropsychopharmacology*, *40*(5), 1101–1112. https://doi.org/10.1038/npp.2014.287

Reynolds, L. M., Pokinko, M., Torres-Berrío, A., Cuesta, S., Lambert, L. C., Del Cid Pellitero, E., Wodzinski, M., Manitt, C., Krimpenfort, P., Kolb, B., & Flores, C. (2018). DCC Receptors Drive

Prefrontal Cortex Maturation by Determining Dopamine Axon Targeting in Adolescence. *Biological Psychiatry*, *83*(2), 181–192. https://doi.org/10.1016/j.biopsych.2017.06.009

Riga, D., Matos, M. R., Glas, A., Smit, A. B., Spijker, S., & Van den Oever, M. C. (2014). Optogenetic dissection of medial prefrontal cortex circuitry. *Frontiers in Systems Neuroscience*, *8*. https://doi.org/10.3389/fnsys.2014.00230

Rinetti-Vargas, G., Phamluong, K., Ron, D., & Bender, K. J. (2017). Periadolescent Maturation of GABAergic Hyperpolarization at the Axon Initial Segment. *Cell Reports*, *20*(1), 21–29. https://doi.org/10.1016/j.celrep.2017.06.030

Rivero, O., Selten, M. M., Sich, S., Popp, S., Bacmeister, L., Amendola, E., Negwer, M., Schubert, D., Proft, F., Kiser, D., Schmitt, A. G., Gross, C., Kolk, S. M., Strekalova, T., Van Den Hove, D., Resink, T. J., Nadif Kasri, N., & Lesch, K. P. (2015). Cadherin-13, a risk gene for ADHD and comorbid disorders, impacts GABAergic function in hippocampus and cognition. *Translational Psychiatry*, *5*(10), e655–e655. https://doi.org/10.1038/tp.2015.152

Rivero, O., Sich, S., Popp, S., Schmitt, A., Franke, B., & Lesch, K.-P. (2013). Impact of the ADHD-susceptibility gene CDH13 on development and function of brain networks. *European Neuropsychopharmacology*, *23*(6), 492–507. https://doi.org/10.1016/j.euroneuro.2012.06.009

Rockland, K. S. (2018). Axon Collaterals and Brain States. *Frontiers in Systems Neuroscience*, *12*, 32. https://doi.org/10.3389/fnsys.2018.00032

Rodgers, R. J., Boullier, E., Chatzimichalaki, P., Cooper, G. D., & Shorten, A. (2002). Contrasting phenotypes of C57BL/6JOlaHsd, 129S2/SvHsd and 129/SvEv mice in two exploration-based tests of anxiety-related behaviour. *Physiology & Behavior*, *77*(2–3), 301–310. https://doi.org/10.1016/S0031-9384(02)00856-9

Rodriguez-Romaguera, J., Greenberg, B. D., Rasmussen, S. A., & Quirk, G. J. (2016). An Avoidance-Based Rodent Model of Exposure With Response Prevention Therapy for Obsessive-Compulsive Disorder. *Biological Psychiatry*, *80*(7), 534–540. https://doi.org/10.1016/j.biopsych.2016.02.012

Romer, D., & Hennessy, M. (2007). A Biosocial-Affect Model of Adolescent Sensation Seeking: The Role of Affect Evaluation and Peer-Group Influence in Adolescent Drug Use. *Prevention Science*, *8*(2), 89. https://doi.org/10.1007/s11121-007-0064-7

Rosas-Vidal, L. E., Lozada-Miranda, V., Cantres-Rosario, Y., Vega-Medina, A., Melendez, L., & Quirk, G. J. (2018). Alteration of BDNF in the medial prefrontal cortex and the ventral hippocampus impairs extinction of avoidance. *Neuropsychopharmacology*, *43*(13), 2636–2644. https://doi.org/10.1038/s41386-018-0176-8

Roth, B. L. (2016). DREADDs for Neuroscientists. *Neuron*, *89*(4), 683–694. https://doi.org/10.1016/j.neuron.2016.01.040

Rubinow, M. J., & Juraska, J. M. (2009). Neuron and glia numbers in the basolateral nucleus of the amygdala from preweaning through old age in male and female rats: A stereological study. *The Journal of Comparative Neurology*, *512*(6), 717–725. https://doi.org/10.1002/cne.21924

Rudaz, M., Ledermann, T., Margraf, J., Becker, E. S., & Craske, M. G. (2017). The moderating role of avoidance behavior on anxiety over time: Is there a difference between social anxiety disorder and specific phobia? *PLOS ONE*, *12*(7), e0180298. https://doi.org/10.1371/journal.pone.0180298

Sacco, T., & Sacchetti, B. (2010). Role of Secondary Sensory Cortices in Emotional Memory Storage and Retrieval in Rats. *Science*, *329*(5992), 649–656. https://doi.org/10.1126/science.1183165

Sala, C., Piëch, V., Wilson, N. R., Passafaro, M., Liu, G., & Sheng, M. (2001). Regulation of Dendritic Spine Morphology and Synaptic Function by Shank and Homer. *Neuron*, *31*(1), 115–130. https://doi.org/10.1016/S0896-6273(01)00339-7

Schipper, P., Brivio, P., De Leest, D., Madder, L., Asrar, B., Rebuglio, F., Verheij, M. M. M., Kozicz, T., Riva, M. A., Calabrese, F., Henckens, M. J. A. G., & Homberg, J. R. (2019). Impaired Fear Extinction Recall in Serotonin Transporter Knockout Rats Is Transiently Alleviated during Adolescence. *Brain Sciences*, *9*(5), 118. https://doi.org/10.3390/brainsci9050118

Schlosberg, H. (1937). The relationship between success and the laws of conditioning. *Psychological Review*, *44*(5), 379–394. https://doi.org/10.1037/h0062249

Schofield, C. M., Hsu, R., Barker, A. J., Gertz, C. C., Blelloch, R., & Ullian, E. M. (2011). Monoallelic deletion of the microRNA biogenesis gene Dgcr8 produces deficits in the development of excitatory synaptic transmission in the prefrontal cortex. *Neural Development*, *6*(1), 11. https://doi.org/10.1186/1749-8104-6-11

Schubert, D., Martens, G. J. M., & Kolk, S. M. (2015). Molecular underpinnings of prefrontal cortex development in rodents provide insights into the etiology of neurodevelopmental disorders. *Molecular Psychiatry*, *20*(7), 795–809. https://doi.org/10.1038/mp.2014.147

Schwarz, L. A., Miyamichi, K., Gao, X. J., Beier, K. T., Weissbourd, B., DeLoach, K. E., Ren, J., Ibanes, S., Malenka, R. C., Kremer, E. J., & Luo, L. (2015). Viral-genetic tracing of the input–output organization of a central noradrenaline circuit. *Nature*, *524*(7563), 88–92. https://doi.org/10.1038/nature14600

Sesack, S. R., Deutch, A. Y., Roth, R. H., & Bunney, B. S. (1989). Topographical organization of the efferent projections of the medial prefrontal cortex in the rat: An anterograde tract-tracing study withPhaseolus vulgaris leucoagglutinin. *The Journal of Comparative Neurology*, *290*(2), 213–242. https://doi.org/10.1002/cne.902900205

Shah, A. A., Sjovold, T., & Treit, D. (2004). Inactivation of the medial prefrontal cortex with the GABAA receptor agonist muscimol increases open-arm activity in the elevated plus-maze and attenuates shock-probe burying in rats. *Brain Research*, *1028*(1), 112–115. https://doi.org/10.1016/j.brainres.2004.08.061

Shapiro, L. P., Parsons, R. G., Koleske, A. J., & Gourley, S. L. (2017). Differential expression of cytoskeletal regulatory factors in the adolescent prefrontal cortex: Implications for cortical development: Cytoskeletal Regulatory Factors in Adolescent PFC. *Journal of Neuroscience Research*, *95*(5), 1123–1143. https://doi.org/10.1002/jnr.23960

Shen, S., Lang, B., Nakamoto, C., Zhang, F., Pu, J., Kuan, S.-L., Chatzi, C., He, S., Mackie, I., Brandon, N. J., Marquis, K. L., Day, M., Hurko, O., McCaig, C. D., Riedel, G., & St Clair, D. (2008). Schizophrenia-Related Neural and Behavioral Phenotypes in Transgenic Mice Expressing Truncated *Disc1*. *The Journal of Neuroscience*, *28*(43), 10893–10904. https://doi.org/10.1523/JNEUROSCI.3299-08.2008

Sheng, M., & Greenberg, M. E. (1990). The regulation and function of c-fos and other immediate early genes in the nervous system. *Neuron*, *4*(4), 477–485. https://doi.org/10.1016/0896-6273(90)90106-P

Shepard, R., Heslin, K., & Coutellier, L. (2017). The transcription factor Npas4 contributes to adolescent development of prefrontal inhibitory circuits, and to cognitive and emotional functions: Implications for neuropsychiatric disorders. *Neurobiology of Disease*, *99*, 36–46. https://doi.org/10.1016/j.nbd.2016.12.012

Shepherd, J. K., Grewal, S. S., Fletcher, A., Bill, D. J., & Dourish, C. T. (1994). Behavioural and pharmacological characterisation of the elevated "zero-maze" as an animal model of anxiety. *Psychopharmacology*, *116*(1), 56–64. https://doi.org/10.1007/BF02244871

Shumake, J., Ilango, A., Scheich, H., Wetzel, W., & Ohl, F. W. (2010). Differential Neuromodulation of Acquisition and Retrieval of Avoidance Learning by the Lateral Habenula and Ventral Tegmental Area. *The Journal of Neuroscience*, *30*(17), 5876–5883. https://doi.org/10.1523/JNEUROSCI.3604-09.2010

Siciliano, C. A., Noamany, H., Chang, C.-J., Brown, A. R., Chen, X., Leible, D., Lee, J. J., Wang, J., Vernon, A. N., Vander Weele, C. M., Kimchi, E. Y., Heiman, M., & Tye, K. M. (2019). A cortical-brainstem circuit predicts and governs compulsive alcohol drinking. *Science*, *366*(6468), 1008–1012. https://doi.org/10.1126/science.aay1186

Simon, N. W., & Moghaddam, B. (2015). Neural processing of reward in adolescent rodents. *Developmental Cognitive Neuroscience*, *11*, 145–154. https://doi.org/10.1016/j.dcn.2014.11.001

Simon, P., Dupuis, R., & Costentin, J. (1994). Thigmotaxis as an index of anxiety in mice. Influence of dopaminergic transmissions. *Behavioural Brain Research*, *61*(1), 59–64. https://doi.org/10.1016/0166-4328(94)90008-6

Skyberg, A. M., Newman, B. T., Graves, A. J., Goldstein, A. M., Brindley, S. R., Kim, M., Druzgal, T. J., Connelly, J. J., & Morris, J. P. (2023). An epigenetic mechanism for differential maturation of amygdala–prefrontal connectivity in childhood socio-emotional development. *Translational Psychiatry*, *13*(1), 91. https://doi.org/10.1038/s41398-023-02380-y

Sohal, V. S., & Rubenstein, J. L. R. (2019). Excitation-inhibition balance as a framework for investigating mechanisms in neuropsychiatric disorders. *Molecular Psychiatry*, *24*(9), 1248–1257. https://doi.org/10.1038/s41380-019-0426-0

Sohal, V. S., Zhang, F., Yizhar, O., & Deisseroth, K. (2009). Parvalbumin neurons and gamma rhythms enhance cortical circuit performance. *Nature*, *459*(7247), 698–702. https://doi.org/10.1038/nature07991

Soiza-Reilly, M., Meye, F. J., Olusakin, J., Telley, L., Petit, E., Chen, X., Mameli, M., Jabaudon, D., Sze, J.-Y., & Gaspar, P. (2019). SSRIs target prefrontal to raphe circuits during development modulating synaptic connectivity and emotional behavior. *Molecular Psychiatry*, *24*(5), 726–745. https://doi.org/10.1038/s41380-018-0260-9

Solmi, M., Radua, J., Olivola, M., Croce, E., Soardo, L., Salazar De Pablo, G., Il Shin, J., Kirkbride, J. B., Jones, P., Kim, J. H., Kim, J. Y., Carvalho, A. F., Seeman, M. V., Correll, C. U., & Fusar-Poli, P. (2022). Age at onset of mental disorders worldwide: Large-scale meta-analysis of 192 epidemiological studies. *Molecular Psychiatry*, *27*(1), 281–295. https://doi.org/10.1038/s41380-021-01161-7

Solomon, R. L., & Wynne, L. C. (1953). Traumatic avoidance learning: Acquisition in normal dogs. *Psychological Monographs: General and Applied*, *67*(4), 1–19. https://doi.org/10.1037/h0093649

Somogyi, P., Freund, T. F., & Cowey, A. (1982). The axo-axonic interneuron in the cerebral cortex of the rat, cat and monkey. *Neuroscience*, *7*(11), 2577–2607. https://doi.org/10.1016/0306-4522(82)90086-0

Spear, L. P. (2000). The adolescent brain and age-related behavioral manifestations. *Neuroscience & Biobehavioral Reviews*, *24*(4), 417–463. https://doi.org/10.1016/S0149-7634(00)00014-2

Stanley, W. C., & Elliot, O. (1962). Differential Human Handling as Reinforcing Events and as Treatments Influencing Later Social Behavior in Basenji Puppies. *Psychological Reports*, *10*(3), 775–788. https://doi.org/10.2466/pr0.1962.10.3.775

Stern, C. A. J., Do Monte, F. H. M., Gazarini, L., Carobrez, A. P., & Bertoglio, L. J. (2010). Activity in prelimbic cortex is required for adjusting the anxiety response level during the elevated plus-maze retest. *Neuroscience*, *170*(1), 214–222. https://doi.org/10.1016/j.neuroscience.2010.06.080

Stevenson, C. W., Halliday, D. M., Marsden, C. A., & Mason, R. (2008). Early life programming of hemispheric lateralization and synchronization in the adult medial prefrontal cortex. *Neuroscience*, *155*(3), 852–863. https://doi.org/10.1016/j.neuroscience.2008.06.013

Stoya, G., Redies, C., & Schmid-Hertel, N. (2014). Inversion of layer-specific cadherin expression profiles and maintenance of cytoarchitectonic areas in the allocortex of the reeler mutant mouse: Cadherins in allocortex of reeler mouse. *Journal of Comparative Neurology*, *522*(13), 3106–3119. https://doi.org/10.1002/cne.23572

Strauss, K. A., Puffenberger, E. G., Huentelman, M. J., Gottlieb, S., Dobrin, S. E., Parod, J. M., Stephan, D. A., & Morton, D. H. (2006). Recessive Symptomatic Focal Epilepsy and Mutant Contactin-Associated Protein-like 2. *New England Journal of Medicine*, *354*(13), 1370–1377. https://doi.org/10.1056/NEJMoa052773

Sullivan, R. M., & Gratton, A. (1999). Lateralized Effects of Medial Prefrontal Cortex Lesions on Neuroendocrine and Autonomic Stress Responses in Rats. *The Journal of Neuroscience*, *19*(7), 2834–2840. https://doi.org/10.1523/JNEUROSCI.19-07-02834.1999

Sullivan, R. M., Wilson, D. A., & Leon, M. (1989). Associative processes in early olfactory preference acquisition: Neural and behavioral consequences. *Psychobiology*, *17*(1), 29–33. https://doi.org/10.3758/BF03337814

Sun, Q., Li, X., Ren, M., Zhao, M., Zhong, Q., Ren, Y., Luo, P., Ni, H., Zhang, X., Zhang, C., Yuan, J., Li, A., Luo, M., Gong, H., & Luo, Q. (2019). A whole-brain map of long-range inputs to GABAergic interneurons in the mouse medial prefrontal cortex. *Nature Neuroscience*, *22*(8), 1357–1370. https://doi.org/10.1038/s41593-019-0429-9

Tan, H., Lauzon, N. M., Bishop, S. F., Bechard, M. A., & Laviolette, S. R. (2010). Integrated Cannabinoid CB1 Receptor Transmission within the Amygdala-Prefrontal Cortical Pathway Modulates Neuronal Plasticity and Emotional Memory Encoding. *Cerebral Cortex*, *20*(6), 1486–1496. https://doi.org/10.1093/cercor/bhp210

Tarazi, F. I., & Baldessarini, R. J. (2000). Comparative postnatal development of dopamine D_1, D_2 and D_4 receptors in rat forebrain. *International Journal of Developmental Neuroscience*, *18*(1), 29–37. https://doi.org/10.1016/S0736-5748(99)00108-2

Teicher, M. H., Andersen, S. L., & Hostetter, J. C. (1995). Evidence for dopamine receptor pruning between adolescence and adulthood in striatum but not nucleus accumbens. *Developmental Brain Research*, *89*(2), 167–172. https://doi.org/10.1016/0165-3806(95)00109-Q

Tervo, D. G. R., Hwang, B.-Y., Viswanathan, S., Gaj, T., Lavzin, M., Ritola, K. D., Lindo, S., Michael, S., Kuleshova, E., Ojala, D., Huang, C.-C., Gerfen, C. R., Schiller, J., Dudman, J. T., Hantman, A. W., Looger, L. L., Schaffer, D. V., & Karpova, A. Y. (2016). A Designer AAV Variant Permits Efficient Retrograde Access to Projection Neurons. *Neuron*, *92*(2), 372–382. https://doi.org/10.1016/j.neuron.2016.09.021

Tottenham, N., & Galván, A. (2016). Stress and the adolescent brain. *Neuroscience & Biobehavioral Reviews*, *70*, 217–227. https://doi.org/10.1016/j.neubiorev.2016.07.030

Tovote, P., Fadok, J. P., & Lüthi, A. (2015). Neuronal circuits for fear and anxiety. *Nature Reviews Neuroscience*, *16*(6), 317–331. https://doi.org/10.1038/nrn3945

Travaglia, A., Bisaz, R., Sweet, E. S., Blitzer, R. D., & Alberini, C. M. (2016). Infantile amnesia reflects a developmental critical period for hippocampal learning. *Nature Neuroscience*, *19*(9), 1225–1233. https://doi.org/10.1038/nn.4348

Trew, J. L. (2011). Exploring the roles of approach and avoidance in depression: An integrative model. *Clinical Psychology Review*, *31*(7), 1156–1168. https://doi.org/10.1016/j.cpr.2011.07.007

Tymula, A., Rosenberg Belmaker, L. A., Roy, A. K., Ruderman, L., Manson, K., Glimcher, P. W., & Levy, I. (2012). Adolescents' risk-taking behavior is driven by tolerance to ambiguity. *Proceedings of the National Academy of Sciences*, *109*(42), 17135–17140. https://doi.org/10.1073/pnas.1207144109

Uhlhaas, P. J., & Singer, W. (2010). Abnormal neural oscillations and synchrony in schizophrenia. *Nature Reviews Neuroscience*, *11*(2), 100–113. https://doi.org/10.1038/nrn2774

Van Eden, C. G., & Uylings, H. B. M. (1985). Cytoarchitectonic development of the prefrontal cortex in the rat. *The Journal of Comparative Neurology*, *241*(3), 253–267. https://doi.org/10.1002/cne.902410302

Vander Weele, C. M., Siciliano, C. A., Matthews, G. A., Namburi, P., Izadmehr, E. M., Espinel, I. C., Nieh, E. H., Schut, E. H. S., Padilla-Coreano, N., Burgos-Robles, A., Chang, C.-J., Kimchi, E. Y., Beyeler, A., Wichmann, R., Wildes, C. P., & Tye, K. M. (2018). Dopamine enhances signal-to-noise ratio in cortical-brainstem encoding of aversive stimuli. *Nature*, *563*(7731), 397–401. https://doi.org/10.1038/s41586-018-0682-1

Ventura, R., Alcaro, A., & Puglisi-Allegra, S. (2005). Prefrontal Cortical Norepinephrine Release Is Critical for Morphine-induced Reward, Reinstatement and Dopamine Release in the Nucleus Accumbens. *Cerebral Cortex*, *15*(12), 1877–1886. https://doi.org/10.1093/cercor/bhi066

Ventura, R., Cabib, S., Alcaro, A., Orsini, C., & Puglisi-Allegra, S. (2003). Norepinephrine in the Prefrontal Cortex Is Critical for Amphetamine-Induced Reward and Mesoaccumbens Dopamine Release. *The Journal of Neuroscience*, *23*(5), 1879–1885. https://doi.org/10.1523/JNEUROSCI.23-05-01879.2003

Ventura, R., Coccurello, R., Andolina, D., Latagliata, E. C., Zanettini, C., Lampis, V., Battaglia, M., D'Amato, F. R., & Moles, A. (2013). Postnatal Aversive Experience Impairs Sensitivity to Natural Rewards and Increases Susceptibility to Negative Events in Adult Life. *Cerebral Cortex*, *23*(7), 1606–1617. https://doi.org/10.1093/cercor/bhs145

Ventura, R., Latagliata, E. C., Morrone, C., La Mela, I., & Puglisi-Allegra, S. (2008). Prefrontal Norepinephrine Determines Attribution of "High" Motivational Salience. *PLoS ONE*, *3*(8), e3044. https://doi.org/10.1371/journal.pone.0003044

Vertes, R. P. (2004). Differential projections of the infralimbic and prelimbic cortex in the rat. *Synapse*, *51*(1), 32–58. https://doi.org/10.1002/syn.10279

Vetere, G., Kenney, J. W., Tran, L. M., Xia, F., Steadman, P. E., Parkinson, J., Josselyn, S. A., & Frankland, P. W. (2017). Chemogenetic Interrogation of a Brain-wide Fear Memory Network in Mice. *Neuron*, *94*(2), 363-374.e4. https://doi.org/10.1016/j.neuron.2017.03.037

Vizi, E. S., Zsilla, G., Caron, M. G., & Kiss, J. P. (2004). Uptake and Release of Norepinephrine by Serotonergic Terminals in Norepinephrine Transporter Knock-Out Mice: Implications for the Action of Selective Serotonin Reuptake Inhibitors. *The Journal of Neuroscience*, *24*(36), 7888–7894. https://doi.org/10.1523/JNEUROSCI.1506-04.2004

Vogt, D., Cho, K. K. A., Shelton, S. M., Paul, A., Huang, Z. J., Sohal, V. S., & Rubenstein, J. L. R. (2018). Mouse *Cntnap2* and Human *CNTNAP2* ASD Alleles Cell Autonomously Regulate PV+ Cortical Interneurons. *Cerebral Cortex*, *28*(11), 3868–3879. https://doi.org/10.1093/cercor/bhx248

Volk, D. W., & Lewis, D. A. (2013). Prenatal ontogeny as a susceptibility period for cortical GABA neuron disturbances in schizophrenia. *Neuroscience*, *248*, 154–164. https://doi.org/10.1016/j.neuroscience.2013.06.008

Walf, A. A., & Frye, C. A. (2007). The use of the elevated plus maze as an assay of anxiety-related behavior in rodents. *Nature Protocols*, *2*(2), 322–328. https://doi.org/10.1038/nprot.2007.44

Wang, Q., Ding, S.-L., Li, Y., Royall, J., Feng, D., Lesnar, P., Graddis, N., Naeemi, M., Facer, B., Ho, A., Dolbeare, T., Blanchard, B., Dee, N., Wakeman, W., Hirokawa, K. E., Szafer, A., Sunkin, S. M., Oh, S. W., Bernard, A., … Ng, L. (2020). The Allen Mouse Brain Common Coordinate Framework: A 3D Reference Atlas. *Cell*, *181*(4), 936-953.e20. https://doi.org/10.1016/j.cell.2020.04.007

Wang, Y., Dye, C. A., Sohal, V., Long, J. E., Estrada, R. C., Roztocil, T., Lufkin, T., Deisseroth, K., Baraban, S. C., & Rubenstein, J. L. R. (2010). *Dlx5* and *Dlx6* Regulate the Development of Parvalbumin-Expressing Cortical Interneurons. *The Journal of Neuroscience*, *30*(15), 5334–5345. https://doi.org/10.1523/JNEUROSCI.5963-09.2010

Warden, M. R., Selimbeyoglu, A., Mirzabekov, J. J., Lo, M., Thompson, K. R., Kim, S.-Y., Adhikari, A., Tye, K. M., Frank, L. M., & Deisseroth, K. (2012). A prefrontal cortex–brainstem neuronal projection that controls response to behavioural challenge. *Nature*, *492*(7429), 428–432. https://doi.org/10.1038/nature11617

Warkentin, K. M. (1999). The development of behavioral defenses: A mechanistic analysis of vulnerability in red-eyed tree frog hatchlings. *Behavioral Ecology*, *10*(3), 251–262. https://doi.org/10.1093/beheco/10.3.251

Watt, M. J., Roberts, C. L., Scholl, J. L., Meyer, D. L., Miiller, L. C., Barr, J. L., Novick, A. M., Renner, K. J., & Forster, G. L. (2014). Decreased prefrontal cortex dopamine activity following adolescent social defeat in male rats: Role of dopamine D2 receptors. *Psychopharmacology*, *231*(8), 1627–1636. https://doi.org/10.1007/s00213-013-3353-9

Wellman, C. L., Izquierdo, A., Garrett, J. E., Martin, K. P., Carroll, J., Millstein, R., Lesch, K.-P., Murphy, D. L., & Holmes, A. (2007). Impaired Stress-Coping and Fear Extinction and Abnormal Corticolimbic Morphology in Serotonin Transporter Knock-Out Mice. *The Journal of Neuroscience*, *27*(3), 684–691. https://doi.org/10.1523/JNEUROSCI.4595-06.2007

Wheeler, A. L., Teixeira, C. M., Wang, A. H., Xiong, X., Kovacevic, N., Lerch, J. P., McIntosh, A. R., Parkinson, J., & Frankland, P. W. (2013). Identification of a Functional Connectome for Long-Term

Fear Memory in Mice. *PLoS Computational Biology*, *9*(1), e1002853. https://doi.org/10.1371/journal.pcbi.1002853

Willing, J., Cortes, L. R., Brodsky, J. M., Kim, T., & Juraska, J. M. (2017). Innervation of the medial prefrontal cortex by tyrosine hydroxylase immunoreactive fibers during adolescence in male and female rats. *Developmental Psychobiology*, *59*(5), 583–589. https://doi.org/10.1002/dev.21525

Wiltgen, B. J., Sanders, M. J., Behne, N. S., & Fanselow, M. S. (2001). Sex differences, context preexposure, and the immediate shock deficit in Pavlovian context conditioning with mice. *Behavioral Neuroscience*, *115*(1), 26–32. https://doi.org/10.1037/0735-7044.115.1.26

Winnubst, J., Bas, E., Ferreira, T. A., Wu, Z., Economo, M. N., Edson, P., Arthur, B. J., Bruns, C., Rokicki, K., Schauder, D., Olbris, D. J., Murphy, S. D., Ackerman, D. G., Arshadi, C., Baldwin, P., Blake, R., Elsayed, A., Hasan, M., Ramirez, D., … Chandrashekar, J. (2019). Reconstruction of 1,000 Projection Neurons Reveals New Cell Types and Organization of Long-Range Connectivity in the Mouse Brain. *Cell*, *179*(1), 268-281.e13. https://doi.org/10.1016/j.cell.2019.07.042

Xu, S., Jiang, M., Liu, X., Sun, Y., Yang, L., Yang, Q., & Bai, Z. (2021). Neural Circuits for Social Interactions: From Microcircuits to Input-Output Circuits. *Frontiers in Neural Circuits*, *15*, 768294. https://doi.org/10.3389/fncir.2021.768294

Ye, L., Allen, W. E., Thompson, K. R., Tian, Q., Hsueh, B., Ramakrishnan, C., Wang, A.-C., Jennings, J. H., Adhikari, A., Halpern, C. H., Witten, I. B., Barth, A. L., Luo, L., McNab, J. A., & Deisseroth, K. (2016). Wiring and Molecular Features of Prefrontal Ensembles Representing Distinct Experiences. *Cell*, *165*(7), 1776–1788. https://doi.org/10.1016/j.cell.2016.05.010

Yizhar, O., Fenno, L. E., Prigge, M., Schneider, F., Davidson, T. J., O'Shea, D. J., Sohal, V. S., Goshen, I., Finkelstein, J., Paz, J. T., Stehfest, K., Fudim, R., Ramakrishnan, C., Huguenard, J. R., Hegemann, P., & Deisseroth, K. (2011). Neocortical excitation/inhibition balance in information processing and social dysfunction. *Nature*, *477*(7363), 171–178. https://doi.org/10.1038/nature10360

Yu, Q., Liu, Y.-Z., Zhu, Y.-B., Wang, Y.-Y., Li, Q., & Yin, D.-M. (2019). Genetic labeling reveals temporal and spatial expression pattern of D2 dopamine receptor in rat forebrain. *Brain Structure and Function*, *224*(3), 1035–1049. https://doi.org/10.1007/s00429-018-01824-2

Yue, S., Moccia, R. D., & Duncan, I. J. H. (2004). Investigating fear in domestic rainbow trout, Oncorhynchus mykiss, using an avoidance learning task. *Applied Animal Behaviour Science*, *87*(3–4), 343–354. https://doi.org/10.1016/j.applanim.2004.01.004

Yuen, E. Y., Wei, J., Liu, W., Zhong, P., Li, X., & Yan, Z. (2012). Repeated Stress Causes Cognitive Impairment by Suppressing Glutamate Receptor Expression and Function in Prefrontal Cortex. *Neuron*, *73*(5), 962–977. https://doi.org/10.1016/j.neuron.2011.12.033

Zhang, F., Vierock, J., Yizhar, O., Fenno, L. E., Tsunoda, S., Kianianmomeni, A., Prigge, M., Berndt, A., Cushman, J., Polle, J., Magnuson, J., Hegemann, P., & Deisseroth, K. (2011). The Microbial Opsin Family of Optogenetic Tools. *Cell*, *147*(7), 1446–1457. https://doi.org/10.1016/j.cell.2011.12.004